Calhoun
Institutional Archive of the Naval Postgraduate School

Calhoun: The NPS Institutional Archive

DSpace Repository

Theses and Dissertations 1. Thesis and Dissertation Collection, all items

1990

Outside the Hull Electric Propulsion for a submarine

Amy, John Victor

http://hdl.handle.net/10945/28436

This publication is a work of the U.S. Government as defined in Title 17, United States Code, Section 101. Copyright protection is not available for this work in the United States.

Downloaded from NPS Archive: Calhoun

DUDLEY KNOX LIBRARY

Calhoun is the Naval Postgraduate School's public access digital repository for research materials and institutional publications created by the NPS community. Calhoun is named for Professor of Mathematics Guy K. Calhoun, NPS's first appointed -- and published -- scholarly author.

Dudley Knox Library / Naval Postgraduate School
411 Dyer Road / 1 University Circle
Monterey, California USA 93943

http://www.nps.edu/library

DUDLEY KNOX LIBRARY
NAVAL POSTGRADUATE SCHOOL
MONTEREY, CALIFORNIA 93943-5002

DUDL
NAVA
MONT

OUTSIDE THE HULL ELECTRIC PROPULSION FOR A SUBMARINE

by
JOHN VICTOR AMY JR.

B.S., Electrical Engineering
United States Naval Academy
(1983)

SUBMITTED TO THE DEPARTMENT OF
OCEAN ENGINEERING
IN PARTIAL FULFILLMENT OF THE REQUIREMENTS
FOR THE DEGREES OF

NAVAL ENGINEER
and
MASTER OF SCIENCE
in
ELECTRICAL ENGINEERING AND COMPUTER SCIENCE

at the
MASSACHUSETTS INSTITUTE OF TECHNOLOGY
May, 1990

(c) copyright John V. Amy Jr., 1990. All rights reserved.
The author hereby grants to MIT permission to reproduce and to
distribute copies of this thesis document in whole or in part.

DU
NA
MO

Thesis
A43855
C.1

DUDLEY KNOX LIBRARY
NAVAL POSTGRADUATE SCHOOL
MONTEREY, CALIFORNIA 93943-500

OUTSIDE THE HULL ELECTRIC PROPULSION FOR A SUBMARINE

by
JOHN VICTOR AMY JR.

Submitted on May 10, 1990 in partial fulfillment of the requirements for the degrees of Naval Engineer and Master of Science in Electrical Engineering and Computer Science.

ABSTRACT

Advances by all nations in ship silencing, passive sonar detection and active sonar target strength reduction have made significant improvements in the acoustic performance of conventional submarine designs excessively difficult and expensive. An unconventional propulsion system located outside of the pressure hull offers potential acoustic improvements, improved arrangement flexibility, and possible increases in hydrodynamic performance, among other improvements. Outside The Hull Electric Propulsion (OTHEP) uses an inverted geometry, squirrel-cage induction motor to drive a large hub-to-diameter ratio propeller. A quantitative means to predict radiated sound power levels is needed to assess the relative acoustic merit of OTHEP.

To determine the feasibility of OTHEP, a single iteration submarine design is performed. The propulsion induction motor configuration from the design is used to develop a relationship which describes the forces of electromagnetic origin which act on the induction motor core. An estimate of the structureborne noise source levels, in Transfer Function Analysis (TFA) form, is made based upon the description of the forces of electromagnetic origin. A TFA acoustic model, which is used for shipboard airborne noise prediction, is adapted to describe the noise which is radiated into the sea. With the estimated induction motor source level and the TFA model, the OTHEP radiated sound power level is compared with radiated sound power levels from an electric drive variant and a geared, turbine drive variant.

The OTHEP submarine design is a feasible submarine design. The inverted geometry, squirrel-cage induction motor appears to be adaptable to the marine environment and can provide the required power to the propeller. Further, the OTHEP submarine design offers several naval architectural benefits. The estimated structureborne noise source level of the inverted geometry, induction motor is plausible given the simplifying assumptions that are made. The results of the radiated sound power level comparison indicate a lack of accurate structureborne noise source level information for electric machines with ratings in the tens of megaWatts.

Thesis Supervisor: James L. Kirtley Jr.
Title: Associate Professor of Electrical Engineering

DU
NA
MO

My heartfelt gratitude to

Professor James L. Kirtley Jr.
CAPT B.F. Tibbitts
CAPT Harry A. Jackson

Rebecca
John
my parents

and everyone else who helped to make this possible.
I could not have done it without you.

DU
NA
MO

Table of Contents

1 Introduction 11
  1.1 Objectives 11
  1.2 Advantages of Outside the Hull Electric Propulsion 14
  1.3 Selection of Motor Type 16
  1.4 Comparison of Propellers 18
  1.5 Selection of Acoustic Model Type 19
  1.6 How the Research Will Proceed 20

2 Background 22
  2.1 Overview 22
  2.2 Twin Propeller System 24
    2.2.1 Configuration 24
    2.2.2 Associated Research Effort 24
    2.2.3 Research Results 25
    2.2.4 Conclusions 25
  2.3 Novel Electric Power Propulsion System 26
    2.3.1 Configuration 26
    2.3.2 Associated Research Effort 26
    2.3.3 Research Results 26
    2.3.4 Conclusions 26
  2.4 Outside the Hull Electric Propulsion 27
    2.4.1 Configuration 27
    2.4.2 Associated Research Effort 27
    2.4.3 Research Results 27
    2.4.4 Conclusions 27
  2.5 Discussion 28

3 Baseline Design 29
  3.1 Submarine Design 29
    3.1.1 Baseline Submarine Requirements 29
    3.1.2 Baseline Submarine Design Philosophy 30
    3.1.3 Hull Shape 31
    3.1.4 Weight Breakdown 32
    3.1.5 Pressure Hull Design 35
    3.1.6 MBT/Control Surface Feasibility 38
    3.1.7 Appendage Sizing 40
    3.1.8 Development of a Power versus Speed Relationship 41
  3.2 Propulsion Motor Design 48
    3.2.1 Impacts on the Motor Design 48
    3.2.2 Motor Design Calculations 49
      3.2.2.1 Rough Sizing 50
      3.2.2.2 Geometric Scaling 53
      3.2.2.3 Determination of Circuit Parameters 56
      3.2.2.4 Equivalent Circuit Analysis 66
      3.2.2.5 Additional Power Losses 69
        3.2.2.5.1 Eddy Current and Hysteresis Losses 70

DU
NA
MO

3.2.2.5.2 Windage Losses 70
3.2.2.5.3 Electromagnetic 'Air'-Gap Losses 71
3.2.2.5.4 Thrust Bearing Losses 72
3.2.2.6 Core Thickness 73
3.2.2.7 Space Required 73
3.2.3 Impacts on the Submarine Design 74
3.3 Tentative Motor Controller Design 76
3.4 Thrust and Journal Bearing Design 78
3.4.1 Thrust Bearing Design 78
3.4.2 Journal Bearing Design 81
3.5 Structural Support Design 83
3.5.1 Determination of Forces 87
3.5.1.1 Gravitational Forces 87
3.5.1.2 Pressure Forces 87
3.5.1.3 Normal Electromagnetic Forces 87
3.5.1.4 Electromagnetic Torque Forces 88
3.5.2 Core Pins 89
3.5.3 Tilters 90
3.5.4 Ring Pins 91
3.5.5 Stator Rings 92
3.5.6 Axial Beam 93
3.5.7 Torque Reactors 94
3.5.8 Integration of Components 94
3.6 Sea-Water and the Baseline Design 95
3.7 Baseline Design Closure 97
3.7.1 Refined Weight Estimates 97
3.7.2 Arrangements 100
3.7.3 Baseline Submarine Balance 102
3.7.4 MBT Sizing and Location 102
3.7.5 Equilibrium Polygon and Stability 103
3.8 Conclusion 104

4 Acoustic Model 105
4.1 Introduction 105
4.1.1 Applications of the Acoustic Model 105
4.1.2 Discussion of Dominant Noise Sources for Baseline Design 106
4.1.3 Acoustic Model of OTHEP 109
4.1.3.1 Determination of Forces of EM Origin 109
4.1.3.2 Development of a Simplified Overall Model for Comparisons 109
4.2 Description of Forces of Electromagnetic Origin .. 110
4.2.1 Derivation of 'Air'-Gap MMF, Including Harmonics 110
4.2.1.1 Stator Winding MMF 110
4.2.1.2 Rotor Cage MMF 117
4.2.1.3 'Air'-Gap MMF 122
4.2.2 The 'Air'-Gap Magnetic Field Intensity and Maxwell's Stress Tensor 123

DU
NA
MO

4.2.3 Using the Forces as Input to Acoustic Analysis 127
4.2.4 Estimated Baseline Propulsion Motor Source Level 128
4.3 Description of the Simplified Comparison Model ... 136
4.3.1 Development of the Model Sources 138
4.3.1.1 Propulsion Steam Turbine Source Levels .. 139
4.3.1.2 Reduction Gear Source Levels 140
4.3.1.3 Ship Service Turbo-Generators Source Levels 141
4.3.1.4 Pump Source Levels 142
4.3.1.5 Electric Motor and Generator Source Levels 144
4.3.1.5.1 Generator Source Levels 144
4.3.1.5.2 Motor Source Levels 145
4.3.2 Transmission Path Models 147
4.3.2.1 Structureborne Noise Transmission 147
4.3.2.1.1 Machinery Attachments 148
4.3.2.1.2 Foundations 152
4.3.2.1.3 Ship Hull Structures 153
4.3.2.1.4 Radiation into the Sea 158
4.3.2.2 Airborne to Structureborne Noise Transmission 166
4.3.3 Overview of the Models That Will be Compared 167

5 Comparative Acoustic Analysis 168
5.1 Overview of Process 168
5.1.1 The Acoustic Model 169
5.1.2 The Comparison 170
5.1.3 The Method 170
5.1.4 The Results 171
5.2 Description of the Alternate Propulsion Systems, Acoustic Sources and Paths 172
5.2.1 OTHEP 172
5.2.1.1 System Configuration 172
5.2.1.2 Acoustic Sources 173
5.2.1.3 Acoustic Paths 173
5.2.2 Electric Drive With Conventional Propeller ... 175
5.2.2.1 System Configuration 175
5.2.2.2 Acoustic Sources 176
5.2.2.3 Acoustic Paths 177
5.2.3 Geared, Steam Turbine Drive 177
5.2.3.1 System Configuration 177
5.2.3.2 Acoustic Sources 179
5.2.3.3 Acoustic Paths 180
5.3 Discussion of Results 180
5.3.1 Sources That Were Not Considered 180
5.3.2 Interpretation of Findings 181

6 Conclusion 183
- 6.1 Interpretation of Results 183
  - 6.1.1 Feasibility Design 183
  - 6.1.2 Forces of Electromagnetic Origin 183
  - 6.1.3 Source Level Estimation 183
  - 6.1.4 Acoustic Model Comparative Analysis 184
- 6.2 Fulfillment of Objectives 185
- 6.3 Recommendations for Further Research 185
  - 6.3.1 Continue Design Process of OTHEP 185
  - 6.3.2 Validation of Expression for Electromagnetic Force 186
  - 6.3.3 Validation of Source Level Estimation 186
  - 6.3.4 Validation of Acoustic Model 186
- 6.4 Recommendations for Supporting Research 186
  - 6.4.1 Determination of Propulsive Coefficient of OTHEP Design 186
  - 6.4.2 Design an Optimal Propeller for OTHEP 187

7 References 188

8 Nomenclature 192

A Submarine Design Calculations 201
- 1.1 Table 1 - Baseline Submarine Design Hull Envelope Offsets 201
- 1.2 Table 2 - Combined Structural Design Worksheet .. 203
- 1.3 Table 3 - Program Output, P_HULL 225
- 1.4 Figure 1 - Pressure Hull Design Showing Frames and Bulkheads 226
- 1.5 Table 4 - MBT Size and Location Calculations, Initial Estimate 227
- 1.6 Table 5 - Hull Envelope Wetted Surface Calculations, Program Output, SHAPE 1.6 232
- 1.7 Table 6 - Power versus Speed Calculations 233
- 1.8 Table 7 - Forward Thrust Bearing Calculation, Wilcock Analysis 236
- 1.9 Table 8 - Forward Thrust Bearing Calculation, Constantinescu et al Analysis 241
- 1.10 Table 9 - Astern Thrust Bearing Calculation, Wilcock Analysis 252
- 1.11 Table 10 - Astern Thrust Bearing Calculation, Constantinescu et al Analysis 254
- 1.12 Table 11 - Journal Bearing Calculation, Wilcock Analysis 256
- 1.13 Table 12 - Journal Bearing Calculation, Constantinescu et al Analysis 258
- 1.14 Table 13 - ‘Air’-Gap Pressure Force Calculations 260
- 1.15 Table 14 - Stator Ring Force and Moment Calculations 264

1.16 Figure 2 - Stator Ring Shear Diagram 270
1.17 Figure 3 - Stator Ring Bending Moment Diagram .. 271
1.18 Table 15 - Combined Stator Support Structure Calculations 272
1.19 Figure 4 - Arrangement Drawings, Deck Plans 286
1.20 Table 16 - Weight Report and Weight Balancing Calculations 287
1.21 Figure 5 - Inboard Profile, Showing Some External Features 297
1.22 Table 17 - MBT Size and Location Calculations, Refined Solution 298

B Comparative Acoustic Analysis Calculations 300
- 2.1 OTHEP 300
  - 2.1.1 OTHEP Sources 300
    - 2.1.1.1 Rotor Source 300
    - 2.1.1.2 Stator Source 301
    - 2.1.1.3 Generator Steam Turbine Sources 301
    - 2.1.1.4 Generator Sources 302
    - 2.1.1.5 Sea-Water Cooling/Lubrication Pump 303
  - 2.1.2 OTHEP Paths 305
    - 2.1.2.1 Structureborne Noise Excited by Airborne Noise 305
    - 2.1.2.2 Rotor Source Structureborne Noise 308
    - 2.1.2.3 Stator Source Structureborne Noise 309
    - 2.1.2.4 Turbine-Generator Structureborne Noise .. 310
    - 2.1.2.5 Sea-Water Cooling/Lubrication Pump Structureborne Noise 311
  - 2.1.3 OTHEP Radiation 312
- 2.2 Electric Drive With Conventional Propeller 317
  - 2.2.1 Electric Drive Sources 317
    - 2.2.1.1 Propulsion Motor Source 317
    - 2.2.1.2 Generator Steam Turbine Sources 318
    - 2.2.1.3 Generator Sources 318
    - 2.2.1.4 Propulsion Motor Cooling Water Pump 319
    - 2.2.1.5 Propulsion Motor Lubrication Oil Pump ... 322
  - 2.2.2 Electric Drive Paths and Radiation 325
    - 2.2.2.1 Airborne Noise-Excited Structureborne Noise 325
    - 2.2.2.2 Propulsion Motor Structureborne Noise ... 328
    - 2.2.2.3 Turbine-Generator Structureborne Noise .. 329
    - 2.2.2.4 Propulsion Motor Cooling Water Pump Unit Structureborne Noise 330
    - 2.2.2.5 Propulsion Motor Lubrication Oil Pump Unit Structureborne Noise 331
  - 2.2.3 Electric Drive Total Radiated Sound Power Level 332
- 2.3 Geared, Steam Turbine Drive 333
  - 2.3.1 Geared Drive Sources 333
    - 2.3.1.1 Propulsion Steam Turbine 333

2.3.1.2 Reduction Gear 334
2.3.1.3 Turbine-Generator Source Level 335
2.3.1.4 Turbine-Generator Generator Source Levels 336
2.3.1.5 Reduction Gear Lubrication Oil Pump 337
2.3.2 Geared Turbine Drive Paths and Radiation 339
2.3.2.1 Airborne Noise-Excited Structureborne Noise 339
2.3.2.2 Reduction Gear Structureborne Noise 343
2.3.2.3 Turbine-Generator Structureborne Noise .. 344
2.3.2.4 Reduction Gear Lubrication Oil Pump Unit Structureborne Noise 345
2.3.3 Geared Turbine Drive Total Radiated Sound Power Level 346

Table of Figures

Outboard Profile of OTHEP Submarine 12
Side View of OTHEP Motor 13
Body of Revolution Variables 32
Power versus Speed Relationship 47
Stator Slot Geometry 54
Rotor Slot Geometry 54
Induction Motor Equivalent Circuit 56
Baseline Motor Torque versus Speed Curve 68
Baseline Motor Power versus Speed Curve 69
Motor Power Factors 75
Induction Motor Power Factor versus Speed 75
Thrust Bearing Geometry 79
Journal Bearing Geometry 82
Stator Support Structure Geometry 85
Stator Support Structure Geometry (Radial Detail) 86
Core Pin Geometry 89
Tilter Geometry 90
Ring Pin Geometry 91
Stator Ring Geometry 92
Axial Beam Geometry 93
Torque Reactor Geometry 94
Equilibrium Polygon 104
MMF Integral Contour 112
Stator Winding a-Phase MMF 113
Current Distortion Waveform 115
.... 116
Surface of Integration for Evaluation of the Stress Tensor 126
Structural Model of Motor Core 133
"T" Junctions in Ship Structure 155
Cross Junctions in Ship Structure 157
OTHEP Propulsion Motor Structureborne Noise Paths 174
Source, Mounting, Foundation, Hull Acoustic Path 175
Electric Drive Engineroom Arrangement 176
Geared Turbine Drive Engineroom Arrangement 179
Pressure Hull Design Showing Frames and Bulkheads 226
Stator Ring Shear Diagram 270
Stator Ring Bending Moment Diagram 271
Arrangement Drawings, Deck Plans 286
Inboard Profile, Showing Some External Features 297

U.
A
O.

1 Introduction

1.1 Objectives

The principal goal of this research is to develop a method to assess the relative merit of acoustic emissions from Outside the Hull Electric Propulsion, OTHEP. Two secondary goals support this principal goal. First, this research will endeavor to provide a description of the forces of electromagnetic origin, within the propulsion motor that is a component of OTHEP, which excite vibrations in the propulsion motor core. Such a description of the forces of electromagnetic origin could be used in a sophisticated structural acoustic analysis of an OTHEP submarine. Second, an approximate comparison of OTHEP with other submarine propulsion systems will be attempted using an acoustic transfer function analysis.

U
A
O

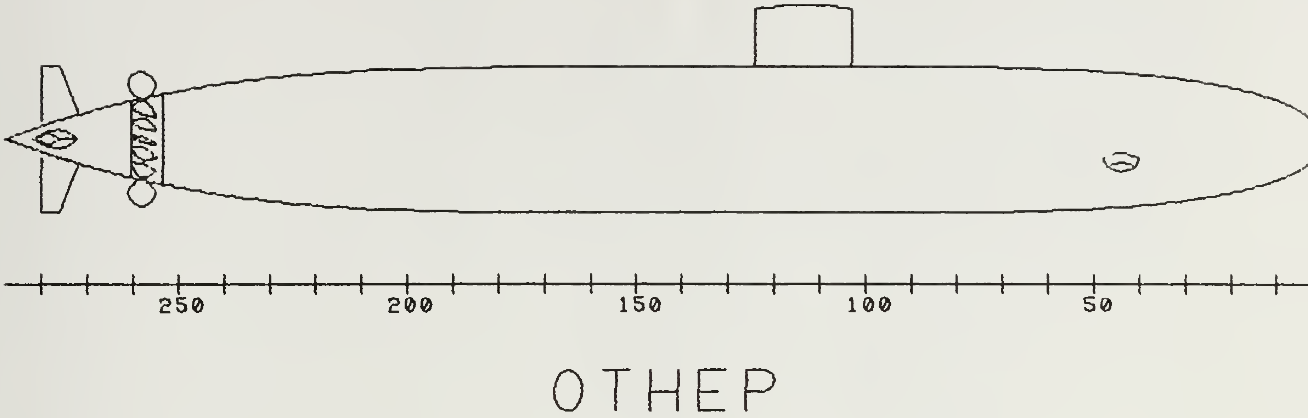

Figure 1 - Outboard Profile of OTHEP Submarine

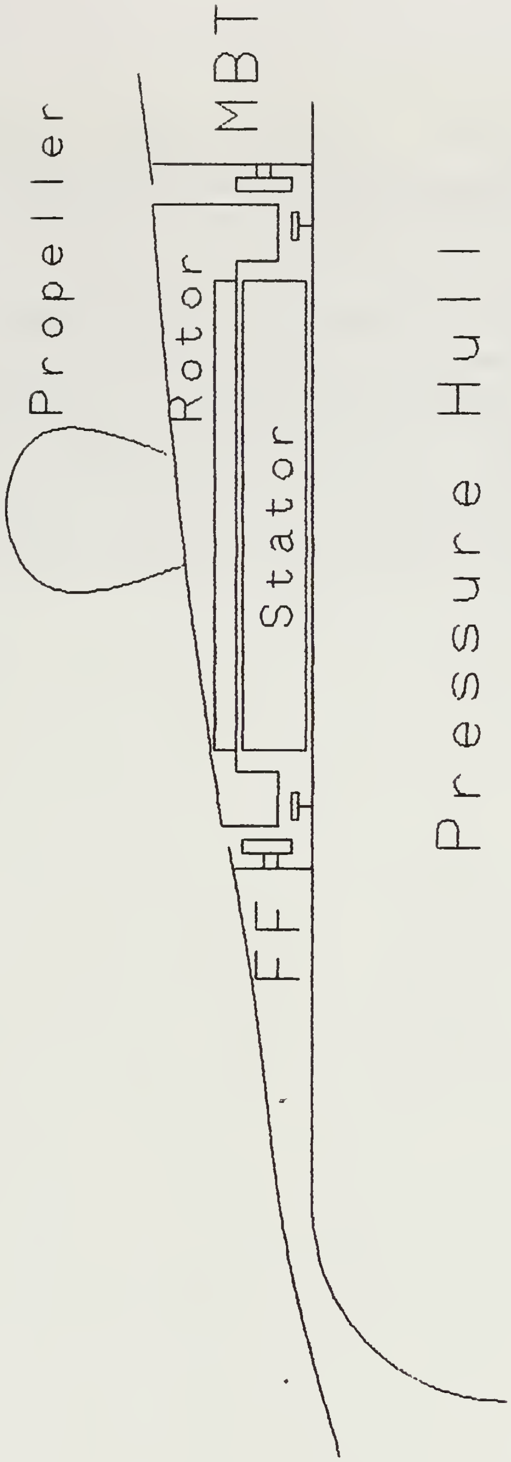

Figure 2 - Side View of OTHEP Motor

OTHEP uses a large hub-to-diameter ratio propeller. This propeller is located on the after-body paraboloid of the submarine's hull, forward of the control surfaces. This is shown in Figure 1. The propeller hub is rigidly connected to the rotor

U
A
O.

of an inverted-geometry induction motor. The propulsion motor's stator is rigidly affixed to the pressure hull of the submarine. The propulsion motor's rotor is a squirrel-cage rotor.

1.2 Advantages of Outside the Hull Electric Propulsion

The motivation behind this research arises from the advantages which OTHEP presents to submarine designers, submarine repair activities and submarine operators. OTHEP offers several benefits which could greatly improve the effectiveness of submarine designs as a whole. The advantages of OTHEP relative to other submarine propulsion systems are shown below.

Advantage	Remark
No Rotating Shaft	The shaft can excite low frequency hull modes. The shaft seal is a low impedance acoustic path to the sea as well as a maintenance concern. Reduction gears, a significant acoustic source, are eliminated.
Arrangement Flexibility	The traditional stack length of the propulsion system can be reduced as well as providing more efficient arrangements. OTHEP also provides a large payload space aft, on the submarine's axis.
Propulsive Efficiency	The location along the hull of the large hub-to-diameter ratio propeller used in OTHEP may increase the propulsive coefficient of the submarine, indicating improved efficiency.
Acoustic Advantages	The large hub-to-diameter propeller offers the possibility of reduced propeller noise. (See section 1.4.) The location of the propeller is forward of the control surfaces, which means that incident flow at the propeller is more uniform, thus reducing components of blade passage noise.
Simplified Towing	The aft end of the submarine is clear of the propeller and rotating shaft. This permits much easier and quicker deployment and retrieval of towed sensor arrays.

OTHEP has disadvantages as well. Some of these are discussed below.

Disadvantage	Remark
Sea-Water Flooded Motor	The propulsion motor is flooded in sea-water which can be considered a hostile environment. The motor requires close clearances and relative movement between some components, making corrosion prevention difficult.
External Motor	The propulsion motor is outside of the pressure hull. Hence, inspection of the motor by the operators themselves during operation is not possible.
Tight Clearances	The motor requires close clearances, particularly at the 'air'-gap, and relative movement between some components, both of which tend to decrease the ability of the structure to withstand shock.

1.3 Selection of Motor Type

In the brief description of OTHEP in section 1.1, the type of motor that will be used for the OTHEP propulsion motor is given as an induction motor. Induction motors possess characteristics which make the induction motors the prime candidates when considering several important requirements for submarine propulsion motors. These requirements and the corresponding induction motor characteristics are discussed below.

Electric motors will be grouped into three broad groups for the purposes of this discussion. The three groups are DC motors, synchronous motors, and induction motors. These are the only types of motors that will be considered.

Essential to OTHEP is the fact that the propulsion motor is outside of the pressure hull. The implication of this requirement is that the propulsion motor must be either free-flooded or protected by rotating seals. Given the size of OTHEP for a modern attack submarine, a rotating shaft seal that could keep all water out of the motor area would be extremely difficult to construct. An alternative would be to design a seal, which operates with a low pressure differential, to keep the motor flooded with fresh water or oil or some other benign liquid. In view of the requirement for the liquid to cool the propul-

sion motor and the necessity for circulating and filtering the flooding liquid, such a scheme would be very complex. Hence, the OTHEP motor must be free-flooded.

A consequence of the requirement that the motor be free-flooded arises when considering possible electrical connections to the rotor. Such connections are usually implemented using slip rings and brushes. Use of slip rings and brushes would require that the slip rings and brushes be isolated from the sea-water. This would impose a requirement for rotating seals. Consequently, the propulsion motor must not require any electrical connections to the rotor. This requirement leaves two alternatives. The first is a permanent magnet synchronous motor. The second is an induction motor.

It is vital that the OTHEP propulsion motor be a continuously variable speed motor. This requirement is readily fulfilled by DC motors, synchronous motors, and now, thanks to power electronics, induction motors. Speed control of induction motors is discussed in detail in section 3.3.

These two requirements leave two alternatives for the propulsion motor, a permanent magnet synchronous motor and an induction motor. In view of past experience in construction of permanent magnet motors, the induction motor provides a better choice with regards to manufacturability. From the two alternatives, the type of motor that is used is the induction motor.

Several types of induction motor need to be considered prior to proceeding. Two basic types of induction motor are wound rotor and squirrel-cage motors. Once again, one type must be selected. In view of the hostile environment in which this motor will operate, the squirrel-cage motor appears to be the more rugged, more easily protected alternative. After considering the possibility of using pole-changing for acoustic deception, see section 3.3, the use of a wound rotor would preclude the possibility of pole-changing. Hence, in light of the two preceding considerations, the squirrel-cage motor is the motor that will be designed.

Whereas submarines put a premium on space and weight, the electrical power that is used to supply the propulsion induction motor should be capable of supplying other shipboard loads as well. Hence, three-phase, 60Hz, $4000V_{l-l}$ power is the input power to the propulsion motor system.

1.4 Comparison of Propellers

As discussed briefly in section 1.2, OTHEP possesses some potential acoustic advantages over conventional hub-to-diameter ratio propeller systems. This discussion will point out qualitatively the acoustic advantages that should be realisable with OTHEP's large hub-to-diameter ratio propeller. A quantitative discussion of propeller and propeller-excited acoustics is well beyond the scope of this research.

Propellers cause acoustic emissions through several mechanisms. First, unsteady forces on the propeller blades can be radiated directly into the water or transmitted through structure into the hull. Second, non-uniformities in the incident flow at the propeller can cause broadband blade passage noise. Third, the pressure field in the propeller wake can excite hull structure vibrations. Lastly, cavitation causes significant acoustic emissions.

The OTHEP propeller is not connected to a rotating shaft which penetrates the pressure hull. Hence, this low-impedance acoustic path does not exist in the OTHEP design. Propeller vibrations due to unsteady forces must travel via other paths before being radiated.

Since the recent past, propellers are the dominant noise source for deep, fast submarines [13]. One of the dominant propeller noise sources is turbulence at the inflow to the propeller. The OTHEP propeller is forward of the control surfaces. In fact, the sail is the only significant turbulence stimulator forward of the propeller in the OTHEP design. Further, it may be that the pressure field produced by the OTHEP propeller will delay the inception of the turbulent boundary layer so that it occurs further aft than on current submarines. This would reduce the thickness of the turbulent boundary layer at the propeller's location. Hence, it is very

likely that the incident flow at the OTHEP propeller will be very uniform, which will greatly improve the acoustic characteristics at speed and depth.

The increased diameter of the OTHEP propeller, its relatively slow rotation rate, the increased number of blades, and uniform incident flow all conspire to reduce the disc-loading of the propeller. This, in turn, greatly improves the cavitation performance of the OTHEP propeller relative to conventional propellers.

Of the four sources of propeller noise, OTHEP's large hub-to-diameter ratio propeller offers significant improvements in the reduction of three of the noise sources relative to conventional propellers. Regrettably, this research will not seek to quantify this assertion. Hence, determining the true acoustic merit of OTHEP as a whole cannot be accomplished without further research into the acoustics of propellers.

1.5 Selection of Acoustic Model Type

In order to construct a means to compare propulsion plants, an acoustic model is developed. This model offers a means to compare the acoustic emissions of the propulsion plant, specifically the propulsion motor and its principal auxiliaries. Given different types of acoustic models, the selected model must be appropriate.

Three methods are being used in acoustic modelling. These three methods of progressively increasing difficulty and precision are typically used during different stages in ship design. This is understandable because more complex models require progressively more detailed information about the particulars of a design. These particulars typically are not established until later stages in a design. As for its design maturity, OTHEP can be considered to be in a very early feasibility design stage.

The first acoustic method is a transfer function analysis, TFA. This method is also known as "empirical analysis". A low level of detail is required for this method. Hence, it is only approximate. TFA is usually performed in early feasibility design stages. TFA predictions are usually in agreement with

U
A
O.

actual acoustic emissions. This is not surprising because TFA is empirical rather than theoretical. Where empirical support is scant, TFA should be viewed with a critical eye.

A second acoustic modelling method is a statistical energy analysis, SEA. This method requires a moderate degree of detail in the description of the design. Hence, SEA is typically used in post-feasibility design stages. (This stage is mid-way along the design timeline.) The moderate detail requirements makes SEA less expensive than finite element methods. The results of SEA, though, are most accurate in the high-frequency range.

The third acoustic modelling method is a finite element method, FEM. This method most closely approaches a complete characterisation of structural stiffness and damping. It requires that a high level of detail be included; therefore, it is typically used in the detail design stage. (This stage is very far along in the design timeline.) The level of detail necessarily makes this an expensive, time-consuming method. FEM requires discretising the entire hull structure. The displacements between the nodes of the discretised structure are found by interpolating between the two adjacent nodes' displacements. Such interpolation does not provide sufficient resolution to accurately describe high frequency characteristics. FEM is very accurate for low frequencies only.

TFA uses results of measurements of existing systems to develop transfer functions for proposed systems. Consequently, to describe a new system, similarities with existing systems must be developed so that use of the empirical data will be justified. This research seeks to develop a TFA model of the structural details of OTHEP. The TFA model should describe how the forces of electromagnetic origin are transformed to far-field pressure waves. Such a model would permit prediction of OTHEP acoustic emissions and assessment of its acoustic merit.

1.6 How the Research Will Proceed

This research proceeds in three steps. The first step is to carry out a feasibility design of an OTHEP submarine. The second step is to develop a TFA model that can be used to predict the radiated sound power levels of the OTHEP design.

The third step is to use the TFA model developed in step two to predict the radiated sound power level from the design of step one and compare that radiated sound power level with predicted radiated sound power levels of two alternate propulsion systems.

Chapter 2 describes the research into OTHEP through the present. Chapter 3 is the baseline submarine design which uses OTHEP. Chapter 3, taken in combination with Appendix A, can be considered as a complete, first iteration feasibility design. Chapter 4 deals with developing of the acoustic model. In the first portion of Chapter 4, the forces of electromagnetic origin which act on the OTHEP propulsion motor's core are calculated and an estimate of the structureborne noise source level of the propulsion motor is made. The second portion of Chapter 4 modifies the TFA method presented by reference [7] so that it will predict radiated noise. Chapter 5 presents the results of the comparison of OTHEP propulsion plant emissions with two alternate propulsion systems' emissions. Appendix B presents the calculations which yield the results given in Chapter 5.

2 Background

2.1 Overview

Early submarines were essentially submersible surface craft. Due to limited battery technology, these vessels could remain submerged for relatively short periods of time. Their maximum submerged speed was very low. These vessels operated on the surface much of the time. Consequently, their designers sought to optimise surfaced performance while retaining the ability to submerge.

The requirement to operate efficiently on the surface had a major impact on the hull form of early submarines. For a relatively short vessel to reach high speeds on the surface, a "fine", or slender, hull form was necessary. Freeboard was required to provide a platform for deck guns. Additionally, for intact transverse stability on the surface, early submarines were configured with saddle tanks, which provided adequate waterplane area to ensure sufficient righting moments. Operating in head seas required a raised bow. Hence, early submarines' hulls had much in common with surface ship hulls.

The propulsion systems of early submarines resembled surface ship propulsion systems as well. Propellers were located underneath the submarine. Since twin propeller shafts were used, the propellers were not located on the centerline of the submarine. This limited the possible diameter of the propellers. Early submarines' propellers operated in the wake created by the hull, which is where surface ship propellers operated. The rudder and stern planes were located aft of the propellers.

The principal difference between surface ship and early submarine propulsion systems was found in the machinery that was used to drive the propeller. At the time, surface ship propellers were typically driven by a shaft which was connected to reduction gears that were driven by steam turbines. Submarines, on the other hand, had to operate submerged. This precluded the use of an engine which required air for combustion. Hence, electric motors were used to turn the shaft which turned the propeller. The electric motors received electric power

J
A
0

from storage batteries that were charged by diesel-driven generators while the submarine was operating on the surface, or near the surface in the case of snorkel submarines.

Nuclear power provided the capability for submarines to operate submerged indefinitely. Hence, on the eve of the introduction of nuclear power to submarine propulsion systems, the U.S. Navy realised that it was necessary to design a submarine that was optimised for submerged performance. This design goal was realised in **USS Albacore**.

USS Albacore's hull form was a body of revolution. Its shape was designed to reduce hydrodynamic drag. The propeller(s) (At different periods in her service life, **USS Albacore** had either a single propeller or contra-rotating propellers.) were located on the longitudinal axis of the submarine. In her first configuration, **USS Albacore**'s control surfaces were located aft of her propeller(s). Later, **USS Albacore** tested locating the control surfaces forward of the propeller(s). Diesel engines were used to charge the storage batteries which provided power for the electric motors which turned the propeller(s). History has proven **USS Albacore** to be a truly revolutionary submarine.

Several aspects of **USS Albacore**'s design are worthy of note. First, because the propeller was on the longitudinal axis of the submarine, the incident flow at the propeller improved the propeller's performance relative to that of the early submarines and surface ships. Second, because the propeller was at the aft end of the boat, the propeller diameter was not constrained. Third, the control surfaces were quite effective without having to be in the propeller wash. Last, although the location of the propeller on the longitudinal axis improved propeller performance, the propeller still operated in a flow field that was disturbed by the sail and the control surfaces.

A tribute to her designers, many of **USS Albacore**'s features are the standard for today's submarines throughout the world. Propellers are located on the longitudinal axis of a body of revolution, aft of the control surfaces. This design is optimised for submerged performance. A fact of modern submarine

warfare, though, is acoustic quieting. Hence, a submarine design that is optimised for quiet submerged performance is now necessary.

This research builds on three previous designs. All three are based on a submarine propulsion concept patented in 1963 by (then) LCDR F.R. Haselton, USN. The three designs are subsequently described in some detail. Hamner describes the results of the Twin Propeller System (TPS) design and the Novel Electric Power Propulsion System (NEPPS) design research in greater detail, reference [1]. He goes on to offer a design of his own, which will be referred to as Outside-the-Hull Electric Propulsion (OTHEP). References [1], [3] and [4] describe OTHEP, TPS and NEPPS in much greater detail. The intent of this chapter is not to review all of the results of the research that has been performed, but, rather, to glean results that are pertinent to the goals of this research.

It is important to note that TPS, NEPPS and OTHEP were not initially considered for their acoustic characteristics. They possessed other advantages that motivated their being pursued. All three would provide much improved submarine arrangement flexibility. All three would eliminate the need for a rotating shaft seal. TPS would eliminate the need for control surfaces.

2.2 Twin Propeller System

2.2.1 Configuration

TPS used two large hub-to-diameter ratio propellers. One was located forward, the other aft. The pitch of the propeller blades on both propellers could be controlled collectively and cyclically. Hydraulic systems were to provide for the pitch control. The two propellers rotated in opposite directions. An electric motor provided the power to rotate the propeller. The combination of the location of two, fore and aft, contra-rotating, controllable pitch propellers allows for the generation of thrusts and torques in any direction, obviating the need for control surfaces.

2.2.2 Associated Research Effort

The research on the TPS concept took place between 1961 and 1965, and was carried out under the guidance of the Office of Naval Research by Electric Boat Division of General Dyna-

mics, General Electric Company, Elliott Company, Honeywell, David Taylor Naval Ship Research and Development Center, Cornell Aeronautical Laboratory, and Netherlands Ship Model Basin, references [2], [3], [20], [21], [22], and [23]. Research included hydrodynamic tests using a 13.5 foot model. The research focused on the hydrodynamic efficiency of large hub-to-diameter ratio propellers and the issue of manoeuverability and controllability.

2.2.3 Research Results

Research into TPS yielded the following, pertinent results.

* The maximum propulsive efficiency of large hub-to-diameter ratio propellers is roughly equivalent to that of small hub propellers, references [3], and [20].
* The maximum propulsive efficiency of the fore and aft propeller combination is less than that of a single, large hub-to-diameter propeller which is located aft, references [3], and [20].
* The forward propeller and its fairing are turbulent flow promoters, references [3], and [20].
* Electric motor efficiency estimated for the TPS design is roughly only 0.78, reference [3].
* TPS is dynamically unstable while maintaining a straight course at constant depth, reference [23].
* Rudders would provide better turning moments at high speeds than the controllable pitch propellers, reference [23].

2.2.4 Conclusions

The results of the research into TPS led to the following conclusions.

* The hydraulic system necessary to provide the type of pitch control envisioned for TPS would be ponderous, probably requiring frequent maintenance.
* The propulsion system would be heavy, bulky and difficult to build.
* TPS would be less manoeuverable at high speed than a conventional submarine.

In light of these conclusions and the contemporary success of steam turbine driven reduction gears, whose propulsive efficiency was much greater than the electric motors of the time, TPS never passed beyond a feasibility design stage.

2.3 Novel Electric Power Propulsion System

2.3.1 Configuration

NEPPS used two large hub-to-diameter ratio, contra-rotating, fixed pitch propellers which were located aft. The propellers' inner diameters were integrated with two rotors of a pair of inverted geometry, free flooding AC motors. The propellers were shrouded.

2.3.2 Associated Research Effort

The Electric Boat Division of General Dynamics carried out the research into NEPPS at roughly the same time that the research into TPS was underway, reference [4], [24], and [25]. The results of the electrical and mechanical studies were not available because of their proprietary nature. However, the conclusions drawn from the hydrodynamic research were available. A 10.7 foot model was the basis for the hydrodynamic research.

2.3.3 Research Results

Research into NEPPS yielded the following results.

* Reverse thrust was 78% of forward thrust.
* The propulsive coefficient was 0.90.
* The cavitation performance of the propellers was excellent.

2.3.4 Conclusions

The following conclusions are based on the results of the research into NEPPS.

* NEPPS would be more manoeuverable that a submarine with a conventional propulsion system.
* The large hub-to-diameter ratio propeller was characterised as a better overall performer than the conventional small hub propeller.
* The propulsive coefficient of NEPPS was just as good as the best conventional small hub propeller drives.
* The motor design was not optimal.

The low efficiency and power density of the AC motor was probably the reason why NEPPS could not compete with the mechanical drives of the time. Although, the exact reason why it has never been implemented is not known.

2.4 Outside the Hull Electric Propulsion

2.4.1 Configuration

OTHEP uses a single, fixed pitch, large hub-to-diameter ratio propeller located forward of the control surfaces. The rotor of an inverted geometry induction motor is integrated with the inner diameter of the propeller hub. The induction motor which turns the propeller is free-flooding.

2.4.2 Associated Research Effort

Hamner's research, conducted from 1982 to 1983 at MIT, focuses on three issues concerning OTHEP, reference [1]. First, he develops an analytical heat flow model of the induction motor. Second, he performs a first order propeller design. Last, Hamner estimates the component weights of OTHEP so that it may be compared with existing propulsion systems.

2.4.3 Research Results

Hamner's research yields the following results.

* The analytical heat flow model of the induction motor indicates that heat can be adequately removed by conduction to the sea water which free floods the motor.

* The efficiency of the propeller can be expected to be greater than 0.75. This minimum efficiency is slightly less than or equal to the propeller efficiencies of small hub propellers.

* Cavitation characteristics of the propeller can be very good.

* Some weight reduction is possible relative to typical nuclear power propulsion systems.

* Motor efficiency at rated speed is 0.939.

2.4.4 Conclusions

The following conclusions are based on the results of Hamner's research.

* Heat removal by convection, due to sea water flooding, would improve heat removal characteristics and motor performance.

* The propulsive efficiency of the entire propulsion system cannot be determined until it is possible to calculate the thrust deduction factor that accounts for the propeller being both forward of the control surfaces and further forward than conventional hub-to-diameter ratio propellers.

* Cavitation characteristics and propeller performance depend heavily on propeller design. An optimal propeller design must be developed, which is not a trivial matter.

* The induction motor design appears to be very feasible.

2.5 Discussion

The conclusions from TPS, NEPPS and OTHEP research indicate that large hub-to-diameter propellers are comparable in efficiency to small hub propellers. The effect of having the propeller forward of the control surfaces has not yet been quantified. Overall propulsive efficiency should, though, be roughly equal to or greater than existing propulsion systems. Cavitation performance can be improved relative to small hub propellers. Use of twin, controllable pitch propellers to generate manoeuvering forces does not appear to be feasible.

Since 1961, the development of motor designs has provided a motor whose efficiency can compete with the efficiency of mechanical drives. Given the shift in the relative importance of acoustic quieting since 1961, a slight decrease in efficiency may be a justifiable compromise if improved acoustic performance is obtained. TPS, NEPPS and OTHEP indicate that a propulsion system with a large hub-to-diameter ratio propeller will have roughly equivalent or slightly improved performance characteristics as existing propulsion systems. The potential for increasing arrangement flexibility, removing a rotating seal, and improving acoustic emissions provides the impetus for pursuing this research even further.

3 Baseline Design

3.1 Submarine Design

Submarine designs seek to fulfill requirements which are established by the prospective operators of the submarines. The goal of this research is to find a means to evaluate the performance of an induction motor drive located outside the pressure hull of a submarine. To this end, a submarine design which incorporates the induction motor drive will be developed.

It is necessary to establish a baseline submarine design for several reasons. First, a baseline submarine design determines the fundamental feasibility of a new propulsion system concept. Second, to examine the acoustic characteristics of any propulsion system requires knowing many details of the candidate design. Third, a baseline submarine design is useful in comparing a proposed system with an existing system.

3.1.1 Baseline Submarine Requirements

To determine feasibility and to provide a justification for comparison, the only novel feature of the baseline submarine should be the propulsion drive. Thus, the baseline submarine must closely resemble existing submarines. Design details should follow from current design practices. The table shown below provides specific design requirements based on the characteristics of existing U.S. Navy submarines, as described in Jane's, reference [26].

Table 1 - Baseline Submarine Required Design Characteristics

Design Characteristic	**Maximum**	**Minimum**
Submerged Displacement	6000 TONS	3000 TONS
Length	350 FT	200 FT
Diameter	40 FT	30 FT
Operating Depth	400m	300m
Submerged Speed	32 KTS	30 KTS

To ensure structural comparability with U.S. Navy submarines, HY-80, a high strength steel with a yield stress of 80KSI, will be the structural material used in design calculations. Internal arrangement and the size of the sail and appendages should also be similar to current submarines'.

3.1.2 Baseline Submarine Design Philosophy

The baseline submarine design incorporates the following list of design priorities.

1) The baseline submarine must be similar to current submarines.

2) The baseline submarine must have characteristics similar to the submarine developed by Hamner, reference [1], so that essential elements of his analysis can be applied directly to the baseline submarine design.

3) Despite the fact that it is not an optimal design, the propeller for the baseline submarine will be the propeller analysed by Hamner. Insofar as the acoustic performance of the large hub-to-diameter ratio propeller is concerned, it is easy to make a noisy propeller regardless of the configuration. The OTHEP propeller has some inherent acoustic advantages. However, a detailed acoustic assessment of the propeller itself would require a detailed propeller design, which is not within the scope of this research.

4) Standard design practices and factors of safety will be used in the baseline submarine.

Before consideration of the propulsion system, the baseline submarine design will provide important parameters for the propulsion system design. The baseline submarine design, specifically the hull shape and appendage size and shape, will dictate the required rating of the propulsion motor. The baseline submarine design also provides the structure to which the motor must be connected and to which the thrust and reaction torque are applied. In this instance, the motor cooling water system is also dictated to a degree by the baseline hull form.

The baseline submarine design proceeds in the following steps.

A) A hull size and shape is selected.

B) With the displacement arising from A), a typical weight breakdown is developed for the baseline submarine. This breakdown specifies the pressure hull size and the main ballast tank (MBT) size.

C) With the pressure hull size from B), a first iteration pressure hull structure is designed. The diameter of the motor in Hamner's design is used to place the motor on the tapered end of the baseline submarine.

D) With location constraints arising from the pressure hull design, C), tentative MBT size and location, and control surface mechanism arrangement yields a check of the baseline submarine design's feasibility.

E) Sail and control surface sizes are selected.

F) A propulsive coefficient is developed.

G) Using A), E) and F), a power versus speed relationship for the baseline submarine is calculated.

H) Design a propulsion motor based on the results of G).

I) Design the components necessary to support the motor design of H).

J) Integrate the impacts of the motor design from H) and I) into the entire submarine design.

K) Re-estimate weights and balance the submarine design.

3.1.3 Hull Shape

To directly apply Hamner's propeller design to the baseline submarine requires that the diameter of the baseline submarine be equal to 32 feet. A typical length to diameter ratio, L/D, for modern submarines is roughly 9. L represents the length of the submarine and D, its diameter. This will make the length of the baseline submarine 288 feet, somewhat longer than Hamner's submarine.

Submarine hulls are typically bodies of revolution. An optimal hydrodynamic hull will have a length-to-diameter ratio approximately equal to 6, reference [27]. The length of the forward body ellipsoid is usually 2.4 times the diameter of the hull. The length of the aft body paraboloid is usually 3.6 times the diameter of the hull. When a longer hull is

necessary, a cylindrical midsection (parallel mid-body) is added between the forward section ellipsoid and the aft section paraboloid.

The equations of the radius of the body of revolution for the different hull sections are shown below, reference [27]. The exponents determine the fullness of the hull form. For hydrodynamic reasons, let $n_f=2.25$ and $n_a=2.75$. n_f and n_a are the exponents of the polynomial expressions which define the body of revolution.

$$r_{aft}=\frac{D}{2}\times\left[1-\left(\frac{x_a}{L_A}\right)^{n_a}\right] \qquad \#1$$

$$r_{forward}=\frac{D}{2}\times\left[1-\left(\frac{x_f}{L_F}\right)^{n_f}\right]^{\frac{1}{n_f}} \qquad \#2$$

The significance of each of the terms in these two expressions is shown in the figure below.

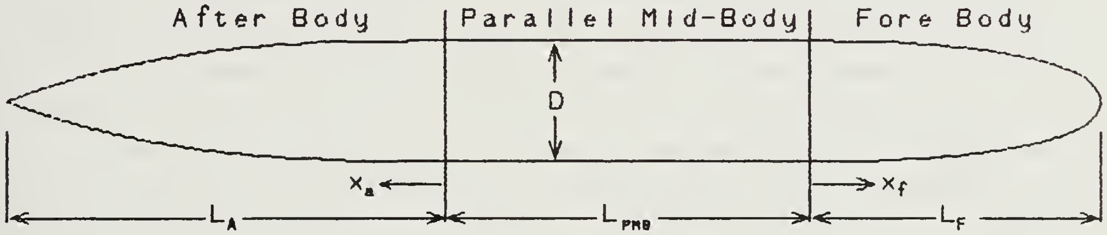

Figure 1 - Body of Revolution Variables

With the stated length, diameter and exponents, the offsets for the hull are given in Table 1 in Appendix A. The offsets were generated by a computer program named SHAPE 1.6, reference [28].

3.1.4 Weight Breakdown

The hull shape that the offsets which were developed above describe displaces a specific amount of seawater. In the context of this discussion, displacement refers to the weight of the sea-water displaced by the cited volume. The displacement of this entire shape is known as the envelope displacement. A

certain amount of the volume within the hull envelope is free flooded space. The free flooded space is in open communication with the sea. In a feasibility study such as this, the amount of free flood water is usually assumed to be a certain percentage of the envelope displacement. This research will assume a free flood displacement equal to seven percent of the envelope displacement. Subtracting the free flood displacement from the envelope displacement yields the submerged displacement.

The submerged displacement is comprised of two components. The first is the main ballast tank displacement (MBT). The second is the group of weights which make up what is known as the "normal surface condition" displacement (NSC). Typically, MBT is required to be a specified percentage of NSC, ten to fifteen percent in modern nuclear attack submarines, reference [27]. MBT allows the submarine to submerge and subsequently surface. This research will require MBT to be twelve and one-half percent of NSC.

Once MBT is subtracted from the submerged displacement, NSC remains. NSC is comprised of items which exist both outside of the pressure hull and inside of the pressure hull. The items which exist outside of the pressure hull and are not MBT or free flood water are a small percentage of NSC weight, typically about seven percent, reference [27]. Hence, the pressure hull should displace or weigh ninety-three percent of NSC. Knowing the pressure hull displacement will allow the pressure hull geometry to be designed.

The NSC items inside the pressure hull are broken into two components, variable load weight and condition A-1 weight. Variable load weight is made up of those items which are consumed or used in the course of submarine operations. Hence, their weight will vary over time. Condition A-1 weight is a fixed weight.

Condition A-1 weight has two components itself, lead ballast (LEAD) and condition A weight. LEAD is used to provide stability and margin. Condition A weight is made up of all of the structures, equipment and furnishings that will be the submarine.

LEAD is broken down into stability lead and margin lead. Stability lead is placed low in the submarine, at a position fore and aft, in a location port or starboard, which ensures that the submarine's centers of gravity and buoyancy lie in a vertical line and provide a restoring moment when the submarine's trim and/or heel is perturbed. Margin lead is placed on the axis of the body of revolution at the longitudinal center of gravity of the submerged displacement. Margin lead is meant to provide a buffer against the uncertainties associated with calculated and estimated weights and to provide for future growth.

Condition A weight can be broken down in any way which suits the submarine designer. This baseline submarine design will break down condition A weights according to the Ship's Work Breakdown System (SWBS), which is the system that the U.S. Navy uses. Use of this system permits comparison of this baseline submarine design's weights with the weights of existing submarine designs. SWBS groups all shipboard equipment into seven groups which are distinguished by their functions.

The table below presents the foregoing discussion of the weight breakdown of the baseline submarine design in a tabular format. The table also contains a description of the functions of the seven SWBS categories. The specific weights for SWBS groups 1 through 7 are determined using SUBLAB, reference [29], a computer program which bases its weight estimation on past U.S. Navy submarine designs. As the baseline submarine design proceeds, more accurate and appropriate weight estimates are developed. Of note, submarine design is an iterative process. The baseline submarine design developed for this research will be a single iteration design.

Table 1 - Baseline Submarine Initial Weight Estimates

Weight Component	Symbol	Long Tons	Comment
Envelope Displacement	Δ_{env}	5106	Weight % from SUBLAB
Free Flood	FF	357	7% of Δ_{env}
Submerged Displacement	Δ_{sub}	4749	Δ_{env} - FF
Main Ballast Tanks	MBT	528	12.5% of NSC
Normal Surface Cond.	NSC	4221	Δ_{sub} = NSC + MBT
Variable Loads	VL	245	NSC = VL + A
Condition A	A	3976	A = LEAD + A1
Lead Ballast	LEAD	361	10% of A-1
Condition A-1	A1	3614	Sum of W1 - W7
Group 1	W1	1608	Structures
Group 2	W2	933	Propulsion Equipment
Group 3	W3	160	Electrical Equipment
Group 4	W4	155	Command and Surveillance
Group 5	W5	421	Auxiliary Equipment
Group 6	W6	206	Outfit and Furnishings
Group 7	W7	130	Armament

Note, throughout this paper, unless specifically stated otherwise, tons will mean long-tons.

3.1.5 Pressure Hull Design

The table in the preceding section provides a departure point from which the design of the pressure hull will proceed. The structural details of the pressure hull are important for

two reasons. First, the pressure hull is a major portion of SWBS weight group 1. Knowing the pressure hull design will provide a much better estimate of SWBS weight group 1 than the one in the table in the preceding section. Second, acoustic transmission through the pressure hull is heavily dependent upon its structure.

The procedure used to design the pressure hull structure, a combined design worksheet, is based upon the structural design worksheet presented in Chapter 7 of reference [27]. That structural design worksheet treats the design of shell thickness, standard frame scantlings and deep frame scantlings. The design process used in the combined design worksheet for structural bulkheads, transitions, and end closures is taken from the notes presented in sections of Chapter 7, but are not addressed in the structural design worksheet. Table 2 in Appendix A contains a spreadsheet representation of the combined design worksheet calculations.

The approach taken in the combined design worksheet uses the operating depth, hull diameter and hull material characteristics as input data. The user provides tentative structural dimensions; subsequently, the user evaluates the suitability of those tentative dimensions based on the spreadsheet calculations. Acceptable solutions provide a pressure hull of sufficient strength. The desired solution is the lightest structure.

The combined design worksheet treats the pressure hull as a ring stiffened cylinder. This is a good approximation in light of the fore and after body shapes and the amount of parallel midbody. Further, the pressure hull occupies the center portion of the submarine, far from the ends where the diameter rapidly changes.

The combined design worksheet begins by calculating a shell thickness based upon the static pressure at operating depth. A factor of safety is applied. The shell thickness is meant to resist general yield due to hydrostatic-pressure-induced hoop stress in the shell. The standard frames are meant to resist shell buckling. The deep frames are meant to resist general instability of the cylinder as a whole.

The shell thickness calculations are straightforward and simple. The standard frame and deep frame buckling and instability calculations are not as simple. The standard frames and deep frames (or King frames) are likened to Euler columns. A bending stress analysis is used to compute stresses in both types of frame; additionally, mode-number calculations are made based upon any eccentricity-induced transverse displacement. The first through fourth modes are considered. The design is dictated by the mode with the smallest critical pressure.

Once the shell thickness and frame scantlings have been developed, the combined design worksheet presents bulkhead design. The bulkhead dimensions are intended to withstand the hydrostatic pressure at a specified depth, in this case the operating depth. The bulkhead and shear girder dimensions are based upon a simple flexure analysis of a bending beam under a distributed loading.

The final pressure hull element to be analysed is the end closures. In this submarine design, hemispheres are used. The principal design choice is the shell thickness of the hemisphere. Given the geometry, this is simple to compute.

Once the structural dimensions have been calculated, the remaining task is to determine the position of the pressure hull within the envelope. The correct pressure hull displacement must also be ensured. P_HULL , reference [30], is used to calculate the volume of the pressure hull as well as its longitudinal center of buoyancy (LCB) and the longitudinal center of gravity of the structure (LCG).

Using the requirements in section 3.1.1, the combined design worksheet, and P_HULL, a tentative pressure hull design is developed. See Table 3 in Appendix A. A drawing of the pressure hull design, which locates it within the hull envelope and shows pressure hull plating, frames, bulkheads, and end closures, is shown in Figure 1, Appendix A. This is the structure which will be used in the calculations involving acoustic transmission paths.

The weight of the pressure hull and envelope plating, which is not part of the pressure hull, designed using the above methods and shown in Appendix A, is approximately 1135tons. The pressure hull and hull envelope plating typically constitute approximately 67% of SWBS group 1. This yields a relatively accurate estimate for W1, W1 = 1687tons.

3.1.6 MBT/Control Surface Feasibility

Several important components of the submarine are located outside of the pressure hull. Their precise location within the hull envelope and outside of the pressure hull will dictate the feasibility of the pressure hull location within the hull envelope and the feasibility of the submarine design as a whole.

The MBT's provide the ability of the submarine to submerge and surface. Flooding these tanks removes buoyancy causing submergence. Blowing the water out of these tanks using compressed air restores buoyancy, allowing the submarine to surface. As discussed in the second paragraph of section 3.1.4, the MBT's should displace a certain percentage of the NSC displacement. From Table 1 of section 3.1.4, this is taken to be 528tons. Hence, the MBT's must have a corresponding volume of 18,470 cubic feet. This volume must be found outside of the pressure hull and within the hull envelope.

Perhaps just as important as the displacement of the MBT's is the longitudinal location of the MBT's. To ensure that the submarine operates with an even trim both surfaced and submerged, the combined longitudinal centers of gravity (LCG's) of the MBT and NSC must be located at the same longitudinal position as the Δ_{sub} longitudinal center of buoyancy (LCB). SUBLAB provides values for these LCG's and LCB's that are typical for modern nuclear submarines. These values will be used for initial MBT sizing and location. The initial location of the MBT LCG will be 131 feet aft of the forward perpendicular (FP, the forward end of the submarine) according to SUBLAB calculations.

Two MBT's are found in modern submarines, one forward and one aft. The forward MBT in this case surrounds the sonar dome access tunnel and the aft MBT the aft pressure hull cylinder. The aft MBT can have a volume of 9449 cubic feet. The forward MBT must then have a volume of 9018 cubic feet. These sizes and locations provide the necessary MBT displacement and location. See Table 4 in Appendix A. Hence, the MBT arrangement is feasible.

The control surfaces of the submarine design, the rudder and the stern planes, are located outside the hull envelope. However, these control surfaces must be capable of being deflected to produce the desired control forces. Due to the large forces that must be generated by the actuating mechanism of the control surfaces, hydraulic systems are usually used. Further, the connection between the hydraulic actuator and the shaft which is connected to the control surface is located outside of the pressure hull and within the hull envelope.

The location of the control surface actuating mechanism must be aft of the propulsion motor and outside of the pressure hull. It is usually placed in what in known as the "mud tank". The mud tank is a free flooding space at the after-most end of the hull envelope. This space must be on the order of 11 feet long to enclose the control surface actuators.

Examining the drawing of the pressure hull and hull envelope in Figure 1 of Appendix A. It is readily apparent that there is plenty of space in the mud tank for the control surface actuators. It is also true that the actuators for this submarine design will not be as bulky as those for conventional submarine designs. Conventional submarine designs have a rotating shaft that runs through the center of the mud tank. To permit both stern planes to be moved by one actuator requires a very large, forged yoke. The same is true of the rudder. Whereas this submarine design has no shaft, such large, cumbersome yokes will not be necessary. This will save weight and space. The space saved could be dedicated to such equipments as towed sonar arrays or other towed devices.

The arrangement of the pressure hull within in the hull envelope allows feasible MBT sizes and locations and ample mud tank space. Further, there is some flexibility remaining in the design should the centers of gravity shift somewhat.

3.1.7 Appendage Sizing

The size, shape and location of the external appendages to the hull envelope have a large impact on the submarine design's performance. The size and shape of the appendages greatly affect the resistance of the submarine, which impacts the rating of the propulsion plant. The location of the control surfaces affects the hydrodynamic characteristics of the hull and the ability to generate moments to control the path of the submarine.

A complete analysis of the equations of motion of the submarine and an optimisation of the control surface design is far beyond the scope of this research. Hence, the control surface design for this submarine will be based on a previous successful design scaled by the ratio of the hull volumes to the two-thirds power. This procedure is recommended reference [27] for feasibility studies.

Using the hull envelope's volume to the two-thirds power is effectively using an area to scale the appendage size. Both the lift and drag forces associated with the hull are calculated using coefficients of lift and drag, C_L and C_D. In such a formulation, the lift or drag force is non-dimensionalised using fluid density, ρ_{SW}, velocity squared, V_{sub}^2, and a surface area. The force of interest here is the lift force, F_L, generated by the control surface. This force is directly proportional to the area of the control surface, W_{sa}.

$$F_L=\left(\frac{1}{2}\rho_{SW}V_{sub}^{2}W_{sa}\right)\cdot C_L \qquad \#1$$

Using hull volume, ∇, to the two-thirds power assumes the following relationship.

$$W_{sa}\propto\nabla^{\frac{2}{3}} \qquad \#2$$

Taking the planar area of the control surfaces of a submarine which had a satisfactory control surface design and scaling that design provides a starting point for a detailed control surface design. It also provides a reasonable estimate of what the resistance characteristics of the final control surface design will be. The same approach is used for the design of the sail. Standard coefficients of drag are used for the control surfaces and sail.

Table 1 - Appendage Drag Parameters

Surface	Wetted Surface Area (ft^2)	Drag Coefficient
Sail	589	0.0090
Bow Planes	192	0.0062
Stern Planes	422	0.0060
Rudder	305	0.0060

The preceding table shows a summary of the appendage sizes and drag coefficients. These will be used in the development of a power versus speed relationship.

3.1.8 Development of a Power versus Speed Relationship

Once the baseline submarine is sized and appendage sizes are known, a power versus speed relationship can be calculated. The development of this relationship, that is, the shaft horsepower required to propel the submarine at any given speed, is a very important factor in the design of the propulsion plant. Submarines operate in two distinct fashions, fully submerged or on the surface. The submarine's power versus speed relationship is different in each of these situations. Whereas modern nuclear submarines rarely operate on the surface, the most important operating condition is submerged.

Development of a power versus speed relationship is a relatively common procedure for ship and submarine designs. Hence, a detailed discussion is not warranted. However, two items peculiar to the propulsion system of the baseline submarine do warrant discussion. These items concern open-water

propeller efficiency and thrust deduction factor. These two quantities have a significant impact on the propulsive coefficient (PC), which is a fundamental indicator of the combined efficiency of the hull and the propulsion system. To understand the effect of these two peculiarities, some discussion of the power versus speed calculation is necessary.

The calculation of the submerged resistance of the submarine is based on the well known coefficient of drag.

$$F_R = \frac{1}{2}\rho_{SW} V_{sub}^2 W_{sa} C_D \qquad \#1$$

Knowing the resistive force, F_R, at a given speed allows calculation of the power needed to overcome this force at that given speed.

$$EHP = F_R V_{sub} = \frac{1}{2}\rho_{SW} V_{sub}^3 W_{sa} C_D \qquad \#2$$

The power needed to overcome the resistance of the submarine's hull and appendages for a given speed, V_{sub}, is known as the effective horsepower (EHP). Hence, to calculate the EHP for a given V_{sub} , the density of sea-water, ρ_{SW}, the wetted surface area, W_{sa}, and the coefficient of drag, C_D, must be known. The density of sea-water is known. The wetted surface area of the hull envelope and all of the appendages must be calculated. The coefficient of drag for the hull envelope and all of the appendages must be determined.

The wetted surface area of the hull envelope is a simple integration of the equations for the hull radius, equations 3.1.3.1 and 3.1.3.2. This calculation is performed by SHAPE 1.6, reference [28]. The results are shown in Table 5 of Appendix A. The wetted surface areas of all of the appendages is known from Table 1 in section 3.1.7. Therefore, all of the wetted surface areas are known.

The coefficients of drag for each of the appendages is known and is shown in Table 1 in section 3.1.7. The appendages are NACA, reference [31], sections, whose coefficients of drag are well documented. Hence, only the coefficient of drag of the hull envelope must be calculated. This is not as straightforward as the case of the appendages.

Determination of the coefficient of drag for the hull envelope builds on the method of Froude, reference [32]. The resistance due to the pressure distribution about the hull and the resistance due to skin friction are each assumed to be independent of the other and are calculated separately. C_r represents the resistance due to the pressure distribution about the hull. This is called residual resistance or form drag. C_f represents the frictional resistance.

The residual resistance is typically found by model tests. To bring experimental and actual values into agreement a correlation factor is applied to the residual resistance from the model test, C_{rm}. For the baseline submarine design, the standard correlation allowance is used, $\Delta C_f = 0.0004$. The hull envelope that has been selected is fairly conventional. In light of this, it is possible to use previous model test results to determine C_{rm}.

Reference [27] contains a compilation of residual resistance data in Chapter 6. Based upon this information, reference [27]'s figure 6-10, and the hull shape chosen for the baseline submarine design, $C_{rm} = 0.000134$. Now that C_{rm} and ΔC_f are known, C_r for the hull envelope can be calculated.

$$C_r = C_{rm} + \Delta C_f = 0.000534 \qquad \#3$$

The International Towing Tank Conference (ITTC) offers the preferred method for computing the second component of the hull envelope's coefficient of drag, reference [32]. The frictional resistance is a function of Reynolds' number. Hence, the frictional resistance coefficient will vary with speed. The equation below describes the values used for C_f.

$$C_f = \frac{0.075}{[\log Re - 2]^2} \qquad \#4$$

Reynolds' number is described as the ratio of viscous to inertial forces. The usual expression for Reynolds' number of a submarine is shown below. ν is the kinematic viscosity of the fluid in which the submarine is moving.

$$Re = \frac{V_{sub} L}{\nu} \qquad \#5$$

The overall drag coefficient of the hull envelope is simply the sum of the frictional drag coefficient and the residual drag coefficient.

$$C_D=C_F+C_R \qquad \#6$$

To find the power required to overcome the resistance of the entire hull, the coefficient of drag of each component must be multiplied by the wetted surface area of each component. These products are then summed and multiplied by the sea-water density and the cube of the speed. This summing and multiplication must be carried out for each speed. The result of these calculations is an effective horsepower corresponding to a specific speed.

While it is important to know the power required to overcome the resistance of the hull and appendages, it is more important to know how much power the propulsion machinery must supply to the propeller. This power which is supplied to the propeller is called shaft horsepower (SHP). EHP and SHP are related by a term known as the propulsive coefficient (PC).

$$SHP=\frac{EHP}{PC} \qquad \#7$$

The propulsive coefficient is, therefore, a very important term which contains a lot of complicated information. Its components are the efficiency of the mechanical transmission and shafting, η_s, the open-water efficiency of the propeller, η_o, the effect of the hull shape as it causes swirling flow into the plane of the propeller, η_{rr}, and the effect that the wake and the hull's boundary layer has on the incident velocity field at the propeller, η_h. For the propulsion system being researched here, there is no mechanical transmission.--Hence, its efficiency will be taken to be one. Each of the other components of the PC will be discussed briefly.

$$PC=\eta_S\cdot\eta_O\cdot\eta_H\cdot\eta_{RR} \qquad \#8$$

The propeller efficiency, η_O, essentially describes how well the propeller converts torque to thrust. This is highly dependent on the propeller geometry. It is usually determined by model tests in a propeller tunnel. Whereas the propeller

geometry suggested by TPS and Hamner is somewhat novel, very little propeller tunnel data exists for large hub-to-diameter ratio propellers. (See the discussion of research in Chapter 2.) In his research, Hamner does an analysis of a non-optimal propeller and reaches the conclusion that, at worst, large hub-to-diameter ratio propellers can be just as, or slightly less, efficient as small hub-to-diameter ratio propellers. His estimation takes the following form.

$$\frac{\eta_O \cdot \eta_{RR}}{1-w} \geq 0.75 \qquad \#9$$

Values of the relative rotative efficiency, η_{RR}, range from 1.0 to 1.1 for modern submarines, reference [27]. The relative rotative efficiency is a strong function of the incident flow at the propellers. Whereas the control surfaces will be located aft of the propeller on the baseline submarine design and the sail is relatively small, then the incident flow at the propeller will be much less affected than on other modern submarines. Hence, an appropriate value for η_{RR} would be closer to 1.0. This value of η_{RR} will be used in subsequent calculations.

The hull efficiency, η_H, consists of the ratio of two factors.

$$\eta_H = \frac{1-t}{1-w} \qquad \#10$$

The first term, 1 - t, is the thrust-deduction factor. This is a measure of the velocity field at the propeller. Of all of the characterizations of this propulsion system, the thrust-deduction coefficient, t, is the most uncertain. This coefficient is best determined experimentally. Given the dearth of test data on modern hull shapes with control surfaces aft of the propeller, little confidence should be placed in the standard means of determining t. Although, intuitively, drastic differences do not seem likely. Nonetheless, the following empirical relationship, taken from Chapter 6 of reference [27], will be used to develop an estimate of the thrust-deduction factor. D_{prop} is the propeller diameter.

$$1-t=0.632+2.44\times\frac{D_{prop}}{\sqrt{W_{SA}}} \qquad \#11$$

The second term, 1 - w, depends upon the wake fraction, w. In light of equation 9, assuming that it's correct, there is no need to explicitly determine w.--This is usually experimentally determined just as t is determined.

Based on the foregoing discussion, the propulsive coefficient can be expressed as follows.

$$PC=[1-t]\frac{\eta_O\cdot\eta_{RR}}{1-w} \qquad \#12$$

In light of the 30'10" diameter propeller used both by Hamner and this baseline submarine design and the wetted surface area calculated by SHAPE 1.6 for the selected hull envelope, a conservative PC would be 0.83. This allows computation of a SHP versus speed relationship. For the required speed of 32 knots submerged, this relationship will yield the required motor rating. With the data in Table 1 in section 3.1.7, the coefficient of drag developed in this section, and equations 2 and 7, a spreadsheet is used to develop the graph shown below. See Table 6 of Appendix A.

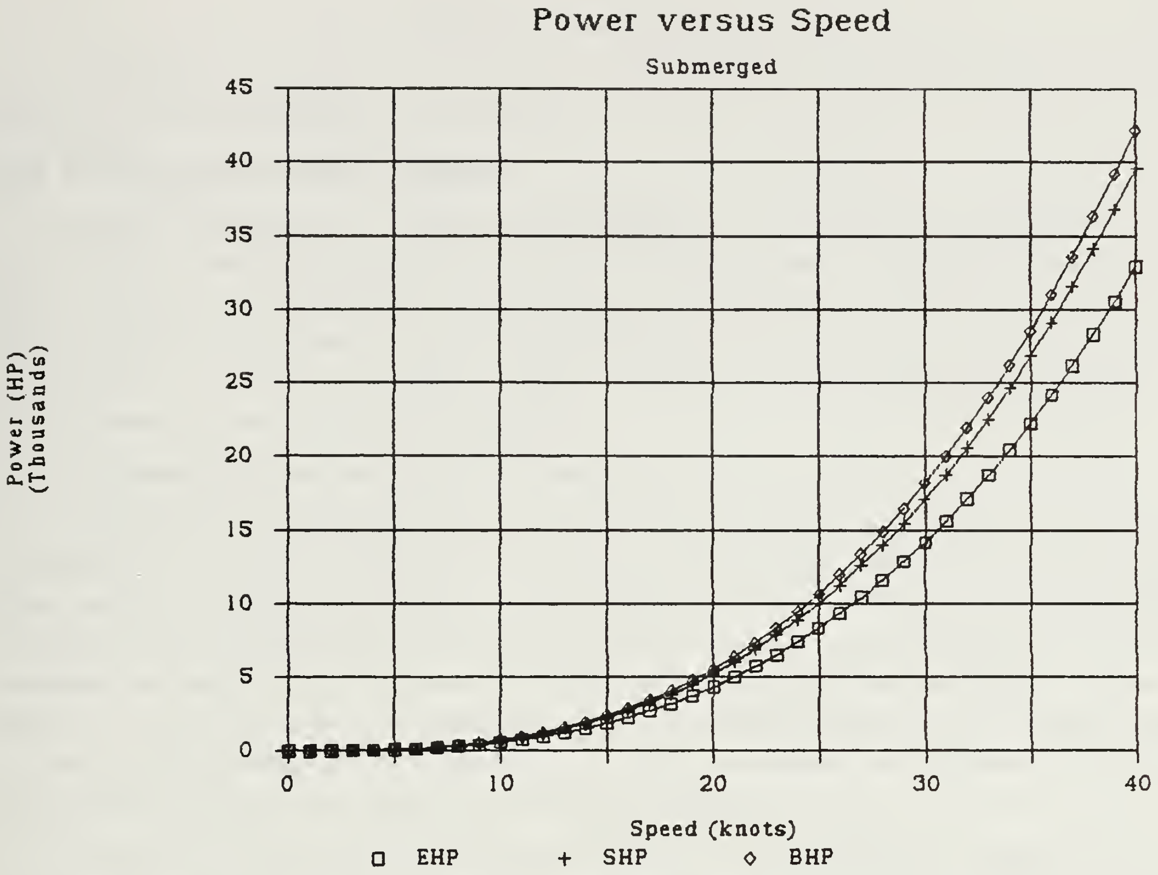

Figure 1 - Power versus Speed Relationship

The curve representing BHP is the required brake horsepower. This is the power which the electrical distribution system must supply to the propulsion motor. Hence, BHP is the real electrical power, P_{in}, drawn by the propulsion motor. The propulsion motor's efficiency is represented by η_M.

$$P_{in} = BHP = \frac{SHP}{\eta_M} \qquad \#13$$

The power versus speed curve indicates that 17,120HP (12.8MW) is necessary to propel the submarine through the water at 32 knots. The propulsion motor must provide 20,620HP (15.4MW) to the propeller to accomplish this. In determining the rating of the propulsion motor, it is practice to apply a margin to the power output of the motor to provide for the uncertainty which exists in the design. A factor of 1.25 is used, reference [33].

$$SHP_{installed} = 1.25 \times SHP_{required} \qquad \#14$$

Therefore, the propulsion motor will be required to have a rating of 25,780HP (19.2 MW).

3.2 Propulsion Motor Design

Within Chapter 1, the advantages of using an induction motor for the propulsion motor are discussed. Hence, this propulsion motor design will concentrate on the details of the motor design rather than including a discussion of motor type selection. First, though, the explicit and implicit design requirements will be collected.

3.2.1 Impacts on the Motor Design

Section 3.1 concludes by giving a required SHP which the propulsion motor must provide. Hence, this will be taken as the motor rating, 19.2MW. A second set of motor requirements arises from the explicit requirement that the propeller from Hamner's analysis be used. Use of that propeller specifies where along the hull the motor will be located. It also specifies the speed of the motor. To a degree, an upper limit on the radius of the motor is established.

Several implicit requirements arise from the need to locate the motor outside of the pressure hull and within the hull envelope. The shape of the hull provides a limit on how far aft the aft end of the motor can be located. Placement of the aft MBT imposes restrictions on the size and forward location of the motor. The table below summarizes these requirements.

Table 1 - Motor Design Requirements

Rating	19.2MW (25,780HP)
Speed	58.8RPM (synchronous-60RPM)
Radius	propeller hub-2.758m (9.05ft) pressure hull-2.134m (7ft)
Core Length	same order as Hamner's design 2.591m (102inches)
Motor Cooling	strained, flowing sea-water
Lubrication	strained, flowing sea-water

The rating requirement is taken from the power versus speed relationships developed in section 3.1.8. The speed requirement refers to the rotor's mechanical speed. This speed is dependent upon the propeller design.--Propellers are designed typically for optimal performance at a specific speed. Whereas Hamner's propeller is assumed for this design, the same speed will be used.

The radius and core length requirements are based upon being able to use the same propeller and fitting the motor within the hull envelope. To assume that heat flow will be satisfactory, the size of the motor should be close to that of Hamner's design. The motor cooling and lubrication requirements reflect an assumption in Hamner's heat flow analysis. In that analysis, Hamner assumes that the water surrounding the motor is flowing at a speed of 1knot (1.688 ft/s). To prevent clogging and consequent hot spots, the sea-water will have to be strained to prevent large marine life from getting caught within the motor and obstructing sea-water flow.

3.2.2 Motor Design Calculations

Hamner's motor's rating is 17.8MW (23,900HP). The baseline submarine's motor design must provide 8% greater power than Hamner's motor design. Hamner's motor design will be

used as a base which will be modified to provide the increased power rating. Therefore, the goal is to develop a motor design which is as similar as possible to Hamner's design.

The assumption here is that Hamner's heat flow analysis results will be generalisable to a derivative machine of very similar dimensions. Furthermore, the same materials will be proposed for the baseline propulsion motor. Additionally, the fact of a common propeller requires that the baseline motor operate at the same speed as Hamner's motor. Consequently, the stator electrical frequency, number of phases, number of poles and rated slip will be the same as Hamner's.

Expressions for the rated torque, T_{rated}, and rated power, P_{rated}, for a multi-phase (3) induction motor are shown below. In order to use these expressions, it is necessary to be able to describe the motor in terms of equivalent circuit parameters, reference [34]. Development of equivalent circuit parameters is somewhat complicated and is certainly approximate. The computer program which Hamner uses develops equivalent circuit parameters from machine geometry and construction materials. This research will calculate circuit parameters from the basic machine flux relationships. The circuit parameters describe the stator, R_1 and X_1, the air-gap, X_ϕ, and the rotor, R_2 and X_2.

$$T_{rated} = \frac{1}{\omega_{syn}} q I_2^2 \frac{R_2}{s_{rated}} \qquad \#1$$

$$P_{rated} = q I_2^2 R_2 \frac{1 - s_{rated}}{s_{rated}} \qquad \#2$$

Of the terms in equations 1 and 2, the required speed, from the Table 1 in section 3.2.1, dictates both the synchronous frequency, ω_{syn}, and rated slip, s_{rated}. The number of stator phases, q, will also remain the same as in Hamner's motor design, 3. Therefore, increases in the rated power must arise from changes in the referred rotor current, I_2, or R_2 or both.

3.2.2.1 Rough Sizing

Torque is generated through a shear stress, τ_{ij}, on the stator and rotor surfaces, reference [35]. It is caused by

the perpendicular magnetic field intensities, H_i, due to the air-gap flux density, in the radial direction, and the flux density due to the stator and rotor currents, in the tangential direction.

$$\tau_{r\theta} = \mu_0 H_r \cdot H_\theta \qquad \#1$$

This is the appropriate shear stress. It is a force per unit area. To find the torque, T_z, multiply the shear stress by the appropriate area to obtain a force. Then, multiply that force by a moment arm to obtain the torque. Here, R_{ag} is the air-gap radius and L the air-gap length.

$$T_z = \tau_{r\theta} \cdot (2\pi R_{ag} L) \cdot R_{ag} \qquad \#2$$

Knowing the torque, the power output, P_{out}, can be determined by multiplying the torque by the mechanical speed, Ω_m.

$$P_{out} = T \cdot \Omega_m \qquad \#3$$

Now, the shear stress for a particular machine can be developed. Consider first the radial air-gap flux density, B_r. This can be considered to be limited to a value of 1T.

$$\mu_0 \cdot H_r \sim B_r \sim 1T \qquad \#4$$

The tangential field intensity, H_θ, is a function of the current density in the stator or rotor. Hence, it is limited by the current density limit of the conductors. This is reasonably well established for machines with various types of conductors and various cooling schemes. Nevertheless, an empirical relationship will be used to find the shear stress.

$$\tau_{r\theta} = \alpha \times \frac{B_{sat}}{2 \cdot \mu_0} \qquad \#5$$

Alpha is an empirical machine constant which equals approximately 0.1 for large machines and 0.01 for small machines, references [34] and [35]. The propulsion motor under consideration certainly qualifies as a large motor. However, due to uncertainty arising from a sea-water filled 'air-gap', alpha will be taken to be 0.05.

Table 1 - Established Motor Parameters

Known Quantities	
$P_{out}=$	19.2MW
$\Omega_m=$	$6.1575s^{-1}$
$B_{sat}=$	1.6T (taken from data for M-19 machine steel)
$B_r=$	1T
$\alpha=$	0.05
$\mu_o=$	$4\cdot\pi\times10^{-7}$ H/m

Table 2 - Unknown Motor Parameters

Unknown Quantities
R_{ag}
L
t_s

With regard to the known quantities, B_{sat} and B_r are related through the machine geometry, specifically the stator tooth width. B_{sat} is the saturation flux density. The stator teeth must provide a path for all of the air-gap flux. Hence, the stator teeth, which present a much smaller surface area than the air-gap surface, will saturate long before the backing material. The relationship between B_{sat} and B_r is shown below. λ_p is the ratio of the aggregate stator slot width to the air-gap circumference.

$$B_r=(1-\lambda_p)B_{sat} \qquad \#6$$

The quantities shown for B_{sat} and B_r in the table above indicate that the machine must possess an aggregate stator slot width to air-gap circumference ratio close to 0.38.

The known quantities from the table above will be substituted into equations 1 through 5 to gain acceptable values for the unknown quantities. The magnetic backing material thickness, t_B, is discussed later.

$$P_{out} = 2\pi \cdot R_{ag}^2 \cdot L \cdot \tau_{r\theta} \cdot \Omega_m \qquad \#7$$

$$R_{ag}^2 \cdot L = \frac{P_{out}}{2\pi \cdot \tau_{r\theta} \cdot \Omega_m} \qquad \#8$$

$$R_{ag}^2 \cdot L = \frac{19.2 \times 10^6 W}{2\pi \cdot \tau_{r\theta} \cdot 6.1575 s^{-1}} \qquad \#9$$

$$\tau_{r\theta} = 0.05 \times \frac{1.6T}{2 \cdot 4\pi \times 10^{-7} \frac{Tm}{A}} = 31.8 \times 10^3 Pa \qquad \#10$$

$$\therefore R_{ag}^2 \cdot L = 16.5 \qquad \#11$$

Based on the pressure hull calculations, a reasonable value for R_{ag} would be 2.51m. This would yield a core length of 2.614m (103 inches). This is a reasonable length. In fact, it is only 0.9 inches greater than the length of Hamner's motor design.

3.2.2.2 Geometric Scaling

So that the results of Hamner's heat flow analysis can be assumed to be applicable to the baseline motor, the geometry of the baseline motor will be made similar to Hamner's. Having determined the radius and length of the baseline submarine propulsion motor, the other motor design details can be scaled up from Hamner's motor design by an appropriate amount. The dimensions that will be altered will be 'air'-gap radius, core length, and slot depth and width. The two following figures show the geometry and appropriate dimensional variables of the rotor and stator slots.

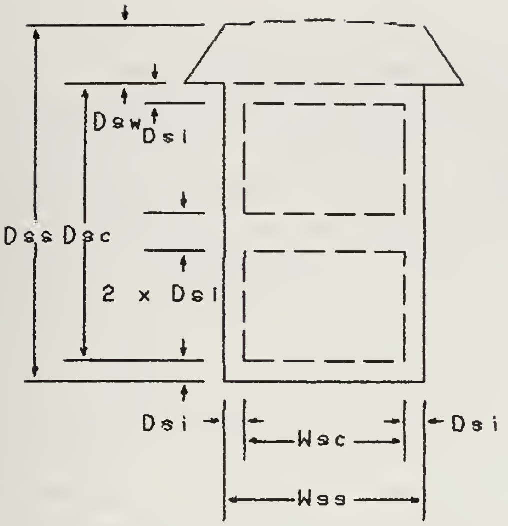

Figure 1-Stator Slot Geometry

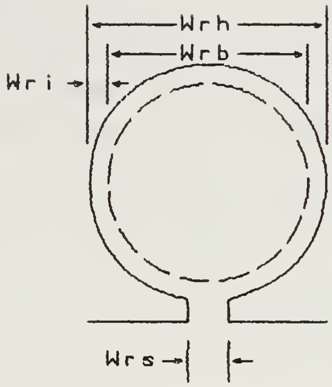

Figure 2-Rotor Bar Geometry

The circumference of Hamner's stator is 15.249m. The stator slot width of Hamner's motor is 0.041m. Their ratio is 0.002689. The circumference of the baseline submarine motor is 15.771m. If the same ratio is to exist, then the stator slot width of the baseline submarine motor will be 0.042m.

The radius of Hamner's stator is 2.427m. The stator slot depth is 0.064m. Their ratio is 0.02637. The radius of the baseline submarine motor is 2.510m. Using the same ratio, the baseline motor slot depth will be 0.066m.

Increasing the dimensions of the conductor in the stator slots will permit more current to be carried by the stator conductors. Hence, for the same current density, the armature current may be increased from 4843A, in Hamner's motor, to 5262A in the baseline motor. Adjusting the motor to yield appropriate equivalent circuit parameters will provide a motor which could use the higher current to produce the higher output power. It is important to note that the insulation thickness will change if the voltage level is changed. If insulation thickness increases, for the same slot size, then a smaller conductor cross-section will be available for current conduction.

The rotor circumference in Hamner's motor is 15.281m. The diameter of the holes punched in the rotor core laminations, which hold the rotor bars in Hamner's rotor, is 0.041m. The ratio of these two dimensions is 0.002683. The circumference of the baseline rotor is 15.802m. For the same ratio, the baseline rotor bar diameter must be 0.042m. The rotor bar slot width will be kept the same size.

The following table contains all of the stator and rotor slot and conductor dimensions. The baseline dimensions represent a scaled version of Hamner's design.

Table 1 - Motor Geometry Details

	Symbol	Hamner's Design	Baseline Design
Stator Slot Depth	D_{ss}	0.064m	0.066m
Stator Conductor Depth	D_{sc}	0.055m	0.057m
Stator Insulation Thickness	D_{si}	0.002m	0.002m
Stator Wedge Depth	D_{sw}	0.007m	0.007m
Stator Slot Width	W_{ss}	0.041m	0.042m
Stator Conductor Width	W_{sc}	0.037m	0.038m
Rotor Hole Diameter	W_{rh}	0.041m	0.042m
Rotor Bar Diameter	W_{rb}	0.041m	0.042m
Rotor Bar Slot Width	W_{rs}	0.010m	0.010m
Rotor Bar Slot Gap	D_{sg}	0.0006m	0.0006m
Stator Conductor Area	A_{sc}	0.00185m^2	0.00196m^2
Rotor Conductor Area	A_{rc}	0.00132m^2	0.00139m^2
Stator Slots	N_{ss}	180	180
Rotor Bars	N_R	206	206

3.2.2.3 Determination of Circuit Parameters

Changing the size of the motor and its geometric details will certainly alter the value of the equivalent circuit parameters. A classic equivalent circuit representation of an induction motor is used.

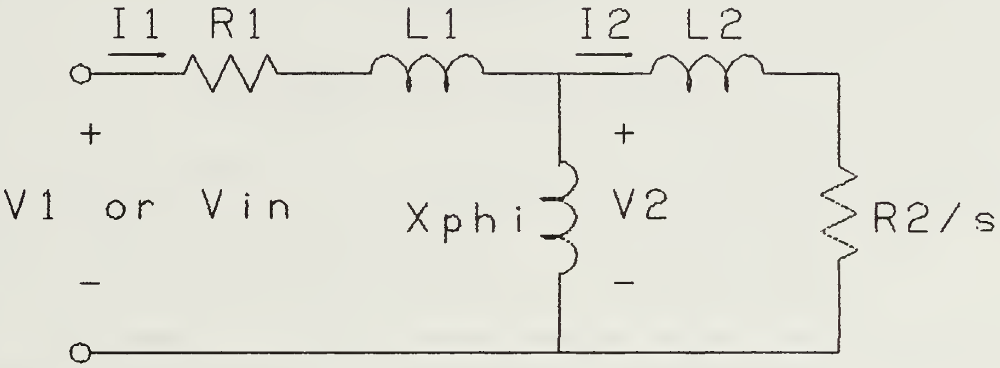

Figure 1 - Induction Motor Equivalent Circuit

In this section, the principal equivalent circuit parameters of the baseline motor design will be calculated from first principles.

In the development of the circuit parameters the "classical" approach will be taken with its concomitant assumptions, reference [34]. The first assumption is that the rotor and stator can each be modelled as balanced, identical, three-phase windings. Although the rotor of the baseline motor is actually a squirrel-cage rotor, modelling it as a three-phase wound rotor serves as an initial approximation in calculating the magnetising, or air-gap, reactance. The second assumption is that there are no saliency effects. The third assumption is that the three-phase windings, both rotor and stator, are identical. In this treatment, only the effects of the space fundamental component of the travelling flux wave will be considered.

Using a Fourier series to describe the square-wave MMF, reference [34] goes on to determine the synchronous inductance, L_{syn}, of a three-phase winding and the mutual inductance, M_{ag}, between windings linked across the air-gap. Both of these terms are for the space-fundamental term of the Fourier expansion. The stator mechanical angular displacement is given as θ.

$$L_{syn} = \frac{3}{2}\frac{4\mu_0 RL}{\pi p^2 g} N_s^2 k_s^2 \qquad \#1$$

$$M_{ag} = \frac{4\mu_0 RL}{\pi p^2 g} N_s k_s N_r k_r \cos(p\theta) = M\cos(p\theta) \qquad \#2$$

The air-gap width is g. The number of pole-pairs is p. The air-gap radius is R. The stator and rotor winding factors are k_s and k_r, respectively. The stator and rotor series-turns per phase are N_s and N_r, respectively.

Flux linkages, λ, for a three-phase induction machine are described by the series of equations shown below.

$$\begin{bmatrix} \lambda_{sa} \\ \lambda_{sb} \\ \lambda_{sc} \\ \lambda_{ra} \\ \lambda_{rb} \\ \lambda_{rc} \end{bmatrix} = \begin{bmatrix} \underline{\mathbf{L}}_s & \underline{\mathbf{M}}_{ag} \\ \underline{\mathbf{M}}_{ag}^T & \underline{\mathbf{L}}_r \end{bmatrix} \cdot \begin{bmatrix} i_{sa} \\ i_{sb} \\ i_{sc} \\ i_{ra} \\ i_{rb} \\ i_{rc} \end{bmatrix} \qquad \#3$$

The three sub-matrices which comprise the inductance matrix in equation 3 above follow. $\underline{\mathbf{L}}_s$ represents the stator winding induction matrix, $\underline{\mathbf{L}}_r$ the rotor winding inductance matrix, and $\underline{\mathbf{M}}_{ag}$ the air-gap mutual inductance matrix.

$$\underline{\mathbf{L}}_s = \begin{bmatrix} L_{sa} & L_{sab} & L_{sac} \\ L_{sba} & L_{sb} & L_{sbc} \\ L_{sca} & L_{scb} & L_{sc} \end{bmatrix} \qquad \#4$$

Whereas the windings are identical, the non-diagonal terms of the $\underline{\mathbf{L}}_s$ matrix are all equal.

$$\underline{\mathbf{L}}_s = \begin{bmatrix} L_{sa} & L_{sab} & L_{sab} \\ L_{sab} & L_{sa} & L_{sab} \\ L_{sab} & L_{sab} & L_{sa} \end{bmatrix} \qquad \#5$$

$$\underline{L}_r = \begin{bmatrix} L_{ra} & L_{rab} & L_{rab} \\ L_{rab} & L_{ra} & L_{rab} \\ L_{rab} & L_{rab} & L_{ra} \end{bmatrix} \qquad \#6$$

The actual values of the elements in the matrices of equations 5 and 6 are determined by the analysis which led to equation 1. L_{sa} and L_{ra} represent the self inductance of the a-phase of each winding. L_{sab} and L_{rab} represent the mutual inductance between stator a- and b-phase windings and rotor a- and b-phase windings respectively. The mutual inductance which links the stator and rotor windings across the air-gap is shown below.

$$\underline{M}_{ag} = \begin{bmatrix} M\cos(p\theta) & M\cos\left(p\theta + \frac{2\pi}{3}\right) & M\cos\left(p\theta - \frac{2\pi}{3}\right) \\ M\cos\left(p\theta - \frac{2\pi}{3}\right) & M\cos(p\theta) & M\cos\left(p\theta + \frac{2\pi}{3}\right) \\ M\cos\left(p\theta + \frac{2\pi}{3}\right) & M\cos\left(p\theta - \frac{2\pi}{3}\right) & M\cos(p\theta) \end{bmatrix} \qquad \#7$$

The air-gap mutual inductances are determined by the analysis which led to equation 2.

The stator and rotor windings described by equation 3 are excited with balanced, three-phase currents, i_s. The rotor winding is also excited by three phase currents, i_r. These currents are shown below.

$$i_{sa} = I_s\cos(\omega t)$$

$$i_{sb} = I_s\cos\left(\omega t - \frac{2\pi}{3}\right)$$

$$i_{sc} = I_s\cos\left(\omega t + \frac{2\pi}{3}\right)$$

$$i_{ra} = I_r\cos(\omega_r t + \xi_r)$$

$$i_{rb} = I_r\cos\left(\omega_r t + \xi_r - \frac{2\pi}{3}\right)$$

$$i_{rc} = I_r\cos\left(\omega_r t + \xi_r + \frac{2\pi}{3}\right) \qquad \#8$$

The current subscripts indicate the rotor or stator and the respective phases. Since balanced currents are assumed, I_s is the magnitude of the three stator phase currents.

Likewise, I_r is the magnitude of the three rotor phase currents. ξ_r is the relative phase angle between stator and rotor currents.

A relationship is required that will relate the mechanical rotation of the rotor, ω_m, to the angular location, θ. θ_0 represents the angular displacement of the rotor at time zero. This relationship plays a key role in the air-gap mutual inductance.

$$\theta = \omega_m t + \theta_0 \qquad \#9$$

Substituting the currents in equation 8 and the angular location described by equation 9 into equation 3, and then solving for the a-phase stator and rotor flux linkages yields the following two expressions.

$$\lambda_{sa} = (L_{sa} - L_{sab}) I_s \cos(\omega t) + \frac{3}{2} M I_r \cos((p\omega_m + \omega_r)t + \xi_r + p\theta_0) \qquad \#10$$

$$\lambda_{ra} = \frac{3}{2} M I_s \cos((\omega - p\omega_m)t - p\theta_0) + (L_{ra} - L_{rab}) I_r \cos(\omega_r t + \xi_r) \qquad \#11$$

Now, the relationship between the stator frequency and mechanical speed of an induction motor, slip, is used to relate the stator frequency and the rotor frequency. ω is the stator electrical frequency, ω_r the rotor electrical frequency.

$$\omega_r = \omega - p\omega_m \qquad \#12$$

The goal of using this relationship is to describe the stator and rotor flux linkages using complex notation, which requires both quantities to have the same time dependence. The desired complex notation is shown below.

$$\lambda_{sa} = Re\left\{\underline{\Lambda}_{sa} e^{j\omega t}\right\} \quad i_{sa} = Re\left\{\underline{I}_{sa} e^{j\omega t}\right\} \qquad \#13$$

$$\lambda_{ra} = Re\left\{\underline{\Lambda}_{ra} e^{j\omega_r t}\right\} \quad i_{ra} = Re\left\{\underline{I}_{ra} e^{j\omega_r t}\right\} \qquad \#14$$

The expression for the stator flux linkage and current has a time dependence whose frequency is that of the stator current, while the rotor flux linkage and current has a time dependence whose frequency is the rotor's electrical frequency.

Substituting equation 12 into equation 10, then solving for the complex amplitude of the a-phase flux linkage of the stator, $\underline{\Lambda}_{sa}$, permits utilisation of the same time dependence and the use of complex notation. The complex amplitudes of the stator and rotor a-phase flux linkages are shown below in this notation.

$$\underline{\Lambda}_{sa} = L_s \underline{I}_{sa} + \frac{3}{2} M \underline{I}_{ra} e^{j(\xi_r - p\theta_o)} \qquad \#15$$

$$\underline{\Lambda}_{ra} = \frac{3}{2} M \underline{I}_{sa} e^{-jp\theta_o} + L_r \underline{I}_{ra} e^{j\xi_r} \qquad \#16$$

$$L_s = L_{sa} - L_{sab} \qquad L_r = L_{ra} - L_{rab} \qquad \#17$$

Now define a rotor a-phase flux linkage and current in terms of the stator phase angle. This definition seeks only to relate the rotor flux and rotor current phase angle to the stator phase angle.

$$\underline{\Lambda}_{ras} = \underline{\Lambda}_{ra} e^{jp\theta_o} \quad \underline{I}_{ras} = \underline{I}_{ra} e^{j(p\theta_o - \xi_r)} \qquad \#18$$

The stator and rotor a-phase flux linkages can now be expressed as shown below.

$$\begin{bmatrix} \underline{\Lambda}_{sa} \\ \underline{\Lambda}_{ras} \end{bmatrix} = \begin{bmatrix} L_s & \frac{3}{2}M \\ \frac{3}{2}M & L_r \end{bmatrix} \cdot \begin{bmatrix} \underline{I}_{sa} \\ \underline{I}_{ras} \end{bmatrix} \qquad \#19$$

These equations describing the a-phase stator and rotor flux linkages can now be converted into voltage equations. The ultimate goal in this case is to develop an equivalent circuit which possesses the same voltage relationships as that of the voltage equation derived from the induction motor flux linkage relationships. In these expressions, R_{sa} and R_{ra} are the resistances of the stator and rotor a-phase windings respectively. $\underline{V}_{sa}$ is the complex a-phase stator voltage.

$$\underline{V}_{sa} = R_{sa} \underline{I}_{sa} + j\omega \underline{\Lambda}_{sa} = (R_{sa} + j\omega L_s) \underline{I}_{sa} + j\omega \frac{3}{2} M \underline{I}_{ras} \qquad \#20$$

$$\underline{V}_{ras} = R_{ra} \underline{I}_{ras} + j\omega_r \underline{\Lambda}_{ras} = j\omega_r \frac{3}{2} M \underline{I}_{sa} + (R_{ra} + j\omega_r L_r) \underline{I}_{ras} \qquad \#21$$

Before proceeding, the following two expressions are needed to simplify the voltage equations. The first defines the air-gap permeance.

$$\rho_{ag} = \frac{4\mu_0 R L}{\pi p^2 g} \qquad \#22$$

$$\omega_r = s\omega \qquad \#23$$

Taking these two expressions, the analysis which yields equations 1 and 2, and substituting them into equation 17, the following three expressions are developed. These three expressions describe how the physical windings affect the voltage equations. Note, L_s and L_r contain two terms, the space fundamental inductance, which is the first term on the right-hand side of equations 24 and 25, and a leakage inductance, which is the second term.

$$L_s = \frac{3}{2}\rho_{ag} N_s^2 k_s^2 + L_{sl} \qquad \#24$$

$$L_r = \frac{3}{2}\rho_{ag} N_r^2 k_r^2 + L_{rl} \qquad \#25$$

$$M = \rho_{ag} N_s N_r k_s k_r \qquad \#26$$

These three expressions are all descriptions of the inductances that appear in equations 20 and 21. The leakage inductances, L_{sl} and L_{rl}, will be dealt with later. Hence, after substitution of these expressions into 20 and 21, the following voltage equations are obtained.

$$\underline{V}_{sa} = \left[R_{sa} + j\omega\left(\frac{3}{2}\rho_{ag} N_s^2 k_s^2 + L_{sl}\right)\right]\underline{I}_{sa} + j\omega\left(\frac{3}{2}\rho_{ag} N_s N_r k_s k_r\right)\underline{I}_{rac} \qquad \#27$$

$$\underline{V}_{rac} = j\omega\left(s\frac{3}{2}\rho_{ag} N_s N_r k_s k_r\right)\underline{I}_{sa} + \left[R_{ra} + j\omega\left(s\frac{3}{2}\rho_{ag} N_r^2 k_r^2 + sL_{rl}\right)\right]\underline{I}_{rac} \qquad \#28$$

Now, through the use of an effective turns ratio, the rotor current will be referred to the stator. The physical significance of this step is that the referred current is that which, if travelling through the stator winding, would give rise to the same flux wave as if it were flowing in the rotor winding. Hence, all of the air-gap MMF will arise from combined stator current and referred rotor current flowing in

the stator winding. This is what permits the use of a stationary equivalent circuit. Define I_2 as I_{ras} referred to the stator.

$$\underline{I}_2=\frac{N_r k_r}{N_s k_s}\underline{I}_{ras} \qquad \#29$$

Using this defined current, and assuming that V_{ras} is equal to zero because the rotor windings are shorted, the two voltage equations below result.

$$\underline{V}_{sa}=[R_1+j(X_\phi+X_1)]\underline{I}_{sa}+jX_\phi\underline{I}_2 \qquad \#30$$

$$0=jX_\phi\underline{I}_{ca}+\left[\frac{R_2}{s}+j(X_\phi+X_2)\right]\underline{I}_2 \qquad \#31$$

The parameters appearing in these two equations follow.

$$R_1=R_{sa} \qquad \#32$$

$$X_\phi=\omega\frac{3}{2}\rho_{ag}N_c^2k_c^2 \qquad \#33$$

Given the form of equations 30 and 31 above, and the equivalent circuit configuration shown in Figure 1 of this section, it is readily seen that equations 32-33 provide the descriptions of the values of two of the circuit elements in the induction motor equivalent circuit. What remains left to do in order that an equivalent circuit analysis of the baseline motor be performed is to determine values for the leakage reactances and the referred rotor resistance.

R_1 is the resistance of the stator winding.

$$R_1=p\left[\rho_{cond}\frac{(4\times L_{ag}+2\times\lambda_p)}{A_{cc}}\right]=6.1\,m\Omega \qquad \#34$$

The next step is to compute the magnetising inductance, X_ϕ. This requires knowing the number of stator turns, N_{s}, 60 in this case. The stator winding factor, k_{s}, must also be known. Reference [34] provides a method of computing k_{s}.

$$k_s=k_{sb}\cdot k_{sp}=\frac{\sin\left(\frac{nm\gamma}{2}\right)}{m\sin\left(\frac{n\gamma}{2}\right)}\cdot\sin\left(\frac{n\alpha}{2}\right) \qquad \#35$$

Using the expression above for the stator winding factor and considering the space fundamental harmonic only, yields the winding factor for the stator. γ is the electrical angle between the stator turns of a single phase, α the winding pitch angle, m the number of turns per phase, k_{wb} and k_{wp} the breadth and pitch factors of the stator winding. n is the harmonic index.

$$k_s = \frac{\sin(\gamma)}{2\sin\left(\frac{\gamma}{2}\right)} \cdot \sin\left(\frac{\alpha}{2}\right) = \frac{0.866}{1} \cdot 0.866 = 0.75 \qquad \#36$$

Using these two values in equation 33 will yield the magnetising inductance.

$$X_\phi = 188.50s^{-1} \cdot \frac{3}{2} \cdot 2.34 \times 10^{-6} H \cdot 60^2 0.75^2 = 1.337\Omega \qquad \#37$$

R_2 is calculated in a method totally analogous to R_1 but for inclusion of the effective turns ratio. The effective turns ratio is difficult in this sense only because the rotor turns and rotor winding factor are somewhat in question in the case of a squirrel cage rotor. Hence, reference [34] will be used to provide the relationship which describes the value of R_2 for a squirrel-cage rotor to be used in the induction motor equivalent circuit. The development of the squirrel-cage rotor model is discussed in section 4.2.1.2. The expression for R_2 is shown below.

$$R_2 = \frac{12 L_{ag}}{N_R} N_s^2 k_s^2 \cdot R_{bar} \qquad \#38$$

The actual resistance of a rotor bar, R_{bar}, is calculated just as that of the stator conductor in equation 34.

$$R_{bar} = \frac{\rho_{cond} L_{ag}}{A_{rc}} = 50.6\mu\Omega \qquad \#39$$

$$\therefore R_2 = \frac{12 \cdot 2.614m}{206} \cdot 60^2 \cdot 0.75^2 \cdot R_{bar} = 15.6m\Omega \qquad \#40$$

What is left is computation of the stator and rotor leakage reactances. This is difficult because the leakage flux paths are not well defined. Many references offer empirical relationships which provide estimated values for

the leakage reactances. Several sources of leakage reactance are usually accepted. These sources are slot, belt, zigzag, end winding and skew, references [17, 18, 34 and 36].

Reference [34] offers a derivation of a method for calculating the slot, belt and zigzag inductances for the stator winding of an induction motor. It also offers a method for the calculation of the leakage inductance of the rotor cage. This reference does not offer an analytical means of calculating the end winding and skew leakage inductances.

Reference [18] offers a qualitative discussion of leakage inductances in general, a discussion of slot leakage, and how to determine them from blocked rotor tests of actual machines. Reference [17] states that the stator leakage flux is usually 5 to 11 percent of the space fundamental inductance. Such a range is not offered for the rotor leakage inductances. Reference [36] indicates that the ratio of leakage inductance to magnetising inductance varies from 9 to 20 percent for conventional geometry cylindrical rotor machines. Hence, reference [34] will be used to calculate all but one of the leakage reactances.

The stator leakage inductance will be considered first. The slot, belt zigzag and skew leakage inductances will each be considered in turn.

The equation below shows the calculation of the stator slot leakage inductance. Reference [18], page 109, describes the method used here.

$$L_{s1slot} = 2 \cdot N_s \frac{\mu_0 L_{ag} \frac{1}{2}((D_{sw} + D_{s1}) + (D_{sw} + 3 \cdot D_{s1}))}{W_{ss}} = 103.2 \mu H \qquad \#41$$

At nominal stator frequency, 30Hz, this inductance becomes the reactance shown below.

$$X_{1slot} = \omega \cdot L_{s1slot} = 19.5 m\Omega \qquad \#42$$

The equation below shows the calculation of stator belt leakage inductance. Reference [34] describes the method used to develop this equation.

$$L_{s1belt6} = \frac{3}{2}\frac{4}{\pi}\frac{\mu_0 N_s^2 k_5^2 R_{ag} L_{ag}}{25 p} = 42.6 \mu H \qquad \#43$$

$$L_{slbelt7}=\frac{34}{2\pi}\frac{\mu_0 N_s^2 k_7^2 R_{ag} L_{ag}}{49p}=21.7\mu H \qquad \#44$$

These belt 'leakage' terms actually link with the rotor, as discussed in reference [34]; hence, the inductances above appear in parallel with the corresponding rotor harmonic terms shown below. The first expression develops the rotor slot inductance needed in the two subsequent expressions.

$$L_{rlslot}=\frac{\mu_0 L_{ag} D_{slotgap}}{W_{rs}}=0.2\mu H \qquad \#45$$

$$L_{rlbelt5}=\frac{12L_{ag}N_s^2k_5^2}{N_R}L_{rlslot}+\frac{6}{\pi}\frac{\mu_0 R_{ag} L_{ag} N_s^2 k_5^2}{g}\left(\frac{1}{(N_R+5p)^2}+\frac{1}{(N_R-5p)^2}\right)=2147.7\mu H \qquad \#46$$

$$L_{rlbelt7}=\frac{12L_{ag}N_s^2k_7^2}{N_R}L_{rlslot}+\frac{6}{\pi}\frac{\mu_0 R_{ag} L_{ag} N_s^2 k_7^2}{g}\left(\frac{1}{(N_R+7p)^2}+\frac{1}{(N_R-7p)^2}\right)=399.0\mu H \qquad \#47$$

The combined effect of these belt leakage terms is the parallel combination of the fifth and seventh order terms.

$$L_{sl5}=\frac{1}{\frac{1}{L_{slbelt5}}+\frac{1}{L_{rlbelt5}}}=41.8\mu H \qquad \#48$$

$$L_{sl7}=\frac{1}{\frac{1}{L_{slbelt7}}+\frac{1}{L_{rlbelt7}}}=20.6\mu H \qquad \#49$$

Reference [34] describes the stator zigzag leakage inductance using the equation shown below.

$$L_{slzz}=\frac{34}{2\pi}\frac{\mu_0 N_s^2 R_{ag} L_{ag}}{p}\left(\frac{1}{(N_{slots}+p)^2}+\frac{1}{(N_{slots}-p)^2}\right)=0.1\mu H \qquad \#50$$

Reference [36] provides a means to estimate the skew leakage inductance. This estimate is based upon a calculation describing the effect of skew on the magnetising inductance. The estimate of skew leakage inductance is shown below.

$$L_{slr}=(1-k_r)\cdot L_\phi \qquad \#51$$

k_r represents the "skew factor". It describes the effect of skew in a manner analogous to pitch and breadth winding factors. The key parameter is the skew angle, β_r; in most motors this is the pitch between one pair of slots given in electrical radians.

$$k_r = \frac{\sin\left(\frac{\beta_r}{2}\right)}{\left(\frac{\beta_r}{2}\right)} \qquad \#52$$

After evaluation of the preceding expression, the value of skew leakage inductance is found to be approximately 213 micro-Henries. This leads to a skew leakage reactance of 0.0401 Ohms.

The total leakage inductance is the sum of the foregoing inductances. The total stator leakage reactance is the leakage inductance multiplied by the stator electrical frequency.

$$X_1 = \omega L_{sl} = 188.5 s^{-1} \times (103.2 + 41.8 + 20.6 + 0.1 + 212.8) \times 10^{-6} H = 71.3 m\Omega \qquad \#53$$

X_2 can now be calculated. Reference [34] provides the expression for X_2 shown below.

$$L_2 = \frac{12 L_{ag} N_t^2 k_t^2}{N_R} L_{r1slot} + \frac{6}{\pi} \frac{\mu_0 R_{ag} L_{ag} N_t^2 k_t^2}{g} \left(\frac{1}{(N_R + p)^2} + \frac{1}{(N_R - p)^2} \right) = 382.4 \mu H \qquad \#54$$

$$X_2 = \omega L_2 = 72.1 mH \qquad \#55$$

The table below shows the values of the equivalent circuit parameters that were developed analytically.

Table 1 - Equivalent Circuit Parameters from Analytic Derivation

$R_1 = 0.0061\Omega$
$X_1 - 0.071\Omega$
$X_\phi = 1.337\Omega$
$X_2 = 0.072\Omega$
$R_2 = 0.0156\Omega$

3.2.2.4 Equivalent Circuit Analysis

In order to find the power rating of the motor, equation 3.2.2.2 must be used. To do this, I_2 must be found. Hence, a circuit analysis of the equivalent circuit, shown in Figure

1 of section 3.2.2.3, will be performed. As originally designed, Hamner's motor used an input voltage of $2309V_{l-n}$ at 30Hz. This same voltage will be used initially in hopes that it will provide adequate power given the equivalent circuit parameters developed in the foregoing section.

Calculations based on the equivalent circuit diagram indicate that, with the circuit element parameters of section 3.2.2.3 and the applied voltage level of $2309V_{l-n}$, the baseline motor will not provide the required power. If, however, the rotor resistance, R_2, could be reduced to a value of 0.0141Ohms, then the motor will provide the required 19.2MW. This decrease in resistance can be achieved by increasing the diameter of the rotor bars.

$$R_2=\frac{12L_{ag}}{N_R}N_s^2k_s^2\cdot R_{bar} \qquad \#1$$

The actual resistance of a rotor bar, R_{bar}, is shown below.

$$R_{bar}=\frac{\rho_{cond}L_{ag}}{A_{cc}} \qquad \#2$$

$$\therefore R_2=\frac{12\cdot 2.614m}{206}\cdot 60^2\cdot 0.75^2\cdot R_{bar} \qquad \#3$$

$$R_2=0.0141\Omega=308.35\cdot\frac{26.9\times 10^{-9}Ohm-m\cdot 2.614m}{A_{rc}} \qquad \#4$$

$$\therefore A_{rc}=0.00154m^2 \qquad \#5$$

To achieve this, the rotor bar diameter must be increased to 0.044m. This represents an increase in diameter of 2mm or almost 5 percent. The impact of this change on the rotor flux density is minimal, 3 percent; however, it does increase the rated power of the motor to 19.2MW, the design requirement.

The stator current, I_1, in the case of the baseline design, is equal to 3583A. The stator current in Hamner's motor is 4843A. Computing the Ohmic loss in the stator, P_{1ohm}, indicates that the heat which must be removed from the baseline design is slightly less than that of Hamner's

design. Hence, the heat flow conclusions made by Hamner should be just as true about the baseline design as his design.

$$P_{loss} = I^2 R_1 \qquad \#6$$

Hamner's Motor $$P_{loss} = (4842.7A)^2 \times 0.011\Omega = 258.0kW \qquad \#7$$

Baseline Motor $$P_{loss} = (3582.6A)^2 \times 0.0061\Omega = 78.3kW \qquad \#8$$

Standard analysis of the equivalent circuit model of the motor will yield a torque versus speed and output-power versus speed curves. These two figures are shown below.

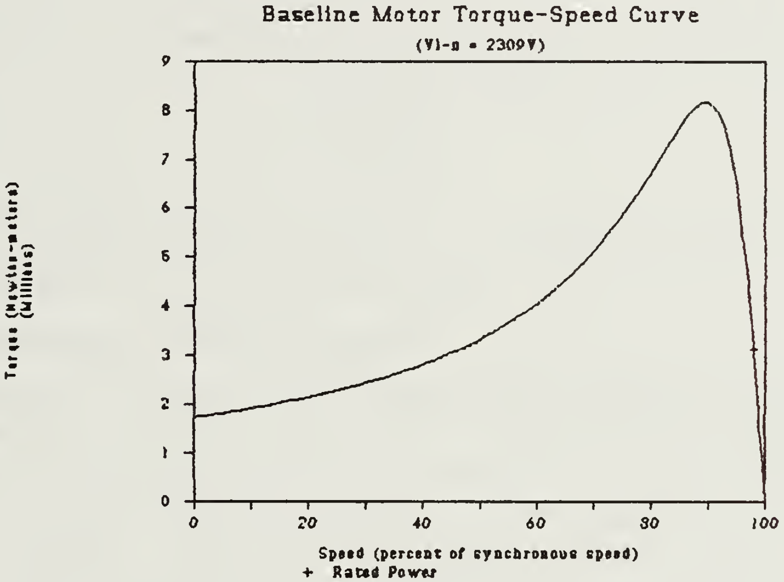

Figure 1

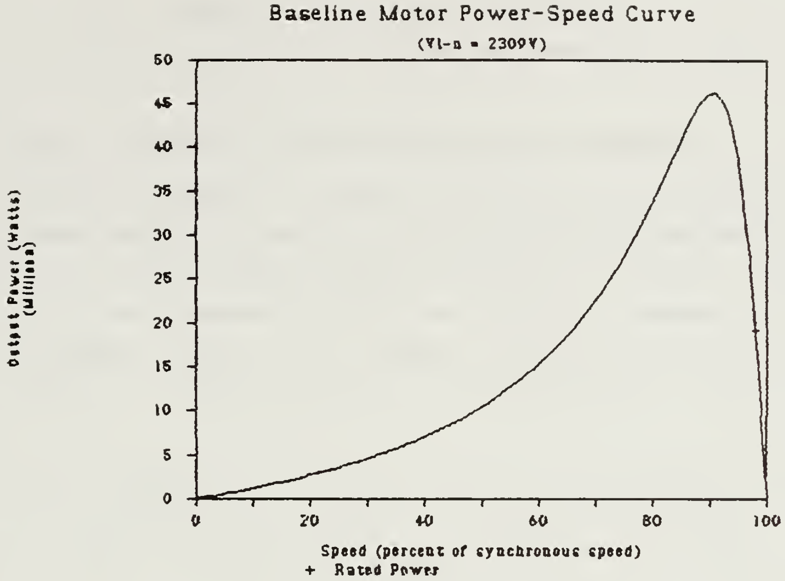

Figure 2

The equivalent circuit analysis indicates that the baseline design motor, as currently configured, will produce the required amount of shaft horsepower.

3.2.2.5 Additional Power Losses

The typical losses calculated using the equivalent circuit method are due to stator and rotor ohmic losses. In the simplified circuit used in this research, eddy current and hysteresis losses are neglected. This research also neglects 'windage' losses. The unique nature of the 'air'-gap in this particular motor adds another possible loss mechanism. Further losses involve energy dissipated in the thrust bearings.

Regarding losses, two important issues arise which are related to the presence of sea-water in the 'air'-gap. First, having a viscous liquid in the 'air'-gap will increase windage losses of the motor. Second, the sea-water in the 'air'-gap, being an electrical conductor (albeit a poor one), will be subjected to a time-varying magnetic field. This will induce currents in the sea-water, introducing another source of electromagnetic losses.

After going through all of these types of losses, the total sum of these losses, which will be neglected throughout

the rest of this research, is on the order of 100.4kW. This amounts to about one half of one percent of the motor's rating.

3.2.2.5.1 Eddy Current and Hysteresis Losses

The usual approach to eddy current and hysteresis losses is to use loss data from the information sheets for the magnetic material that comprises the motor core. For M19 steel, the material that Hamner and this design assume, the information sheet from U.S. Steel provides the core loss in Watts per pound. This loss is a function of flux density and frequency.

For a flux density of 1.6T and a frequency of 30Hz, the core loss is roughly 0.37W/lbf. The core weighs 71tons, 159,200lbf. This implies a core loss of 58.4kW. This represents 0.3 percent of the propulsion motor's rating.

3.2.2.5.2 Windage Losses

By virtue of the fact that there is a viscous fluid in the 'air'-gap, the windage losses of the propulsion motor will be significantly more than if there were air in the 'air'-gap. Some notion of whether or not this loss mechanism is significant compared to the motor's rating must be obtained.

The flow of fluid within the 'air'-gap is essentially a viscous "Couette" flow. The velocity gradient between the moving surface and the fixed surface gives rise to a shear stress, τ, reference [37]. This shear stress can be found at the outer stator surface around the entire circumference. The constant of proportionality between the velocity gradient and the shear stress is the absolute viscosity of the fluid.

$$\tau=\mu\frac{dv}{dr} \qquad \#1$$

The force due to this shear stress can be found by multiplying the shear stress by the 'air'-gap area.

$$F=\tau\cdot 2\pi R_{ag}\cdot L_{ag} \qquad \#2$$

The power dissipated in this way is found by multiplying this shear-induced force by the rotor's linear velocity, V.

$$P_{diss} = F \cdot V = F \cdot R_{ag} \omega \qquad \#3$$

Using this approach, the estimated power dissipation is on the order of 4kW. Compared to the rating of the motor, 19,200kW, the losses due to 'windage' are negligible in the context of this research. This result may appear to indicate that it is possible to make the 'air'-gap smaller from a 'windage' perspective; however, the 'air'-gap width is driven by machining tolerances.

3.2.2.5.3 Electromagnetic 'Air'-Gap Losses

Two relationships are used to determine the losses arising from the currents induced in the sea-water which is in the 'air'-gap. Faraday's Law describes the electric field intensity, **E**, arising from a time-varying flux density, **B**. This relationship is shown below in integral form, reference [19].

$$\oint_c \mathbf{E}' \cdot d\mathbf{l} = -\frac{d}{dt}\int_s \mathbf{B} \cdot \mathbf{n}\, da \qquad \#1$$

Once the electric field intensity is known, it is possible by using the constitutive relationship for sea-water conduction, Ohm's Law, to find the current density, **J**, induced in the sea-water.

$$\mathbf{E}' = \rho \cdot \mathbf{J} \qquad \#2$$

The path for the line integral in the first equation extends axially down the 'air'-gap, circumferentially half the way around the motor, then back up the 'air'-gap, and finally to the starting point by travelling circumferentially half the way around the motor a second time. Assume that the electric field intensity is zero along the circumferential-legs. This leaves the following relationship.

$$2(E \cdot L_{ag}) = -\frac{d}{dt}\int_s \mathbf{B} \cdot \mathbf{n}\, da \qquad \#3$$

Now, the flux density which passes through the surface bordered by the curve of the integral of the electric field intensity is time variant. Assume that it is a sinusoidal travelling wave.

$$\mathbf{B} = B_0 \exp j(m\phi - \omega_e t)\hat{i}_r \qquad \#4$$

Integrating this expression over the surface amounts to multiplying by one half of the 'air'-gap surface. The time derivative of this expression introduces a phase shift term. The exponential term will be dropped for ease of handling.

$$2\cdot(\hat{E}\cdot L_{ag})=-j\omega_s B_0\times\pi R_{ag}L_{ag} \qquad \#5$$

Whereas the concern here is solely with magnitudes, E and B_o, the phase relationships will be ignored. The electric field intensity will give rise to a voltage. This voltage appears along the length of the 'air'-gap.

$$V_{ag}=|\hat{E}|\cdot L_{ag}=\frac{1}{2}\omega_s B_0\times\pi R_{ag}L_{ag} \qquad \#6$$

The resistance of the 'air'-gap can now be computed. The resistance will be equal to the resistivity of sea-water, ρ_{SW}, divided by the cross-sectional area of the conducting region, A_{CS}, multiplied by the length of the conducting path.

$$R_{SW}=\frac{\rho_{SW}}{A_{CS}}L_{ag} \qquad \#7$$

The power dissipated will be equal to the voltage squared divided by the resistance computed above.

$$P_{diss}=\frac{\frac{1}{4}\omega_s^2 B_0^2\pi^3 R_{ag}^3 L_{ag} g}{\rho_{SW}} \qquad \#8$$

For a flux density of 1.6T, B_o, a five millimeter 'air'-gap, g, and saltwater resistivity of 0.25Ohm-m, the power dissipated in the sea-water is 650W.

3.2.2.5.4 Thrust Bearing Losses

Appendix A contains the thrust and journal bearing calculations. Included in those calculations is a determination of power loss due to the shear stresses generated within the sea-water which lubricates the bearings. The shear stress is proportional to the velocity gradient across the lubricant film. The velocity gradient is a function of the motor's speed. The power loss in the forward thrust bearing is 19.7kW. The power loss in the astern thrust bearing is 17.3kW. The power loss in the journal bearings is 17.6kW.

Hence, the largest operating power loss due to these bearings is 37.3kW. This loss, as the others, is small enough to neglect in an early feasibility study such as this.

3.2.2.6 Core Thickness

The remaining motor design calculation will address the question of the thickness of the magnetic core material. This item is important because it accounts for most of the motor weight. The sizing relationship that will be used is shown below, reference [35].

$$t_B = \frac{R}{p} \cdot \frac{B_r}{B_{sat}} \qquad \#1$$

The baseline machine has 30 pole pairs, a radius of 2.5125m, an air-gap flux density of 1T, and a saturation intensity of 1.6T. These attributes yield a backing thickness, t_B, equal to 5.3cm. With this backing thickness, the minimum stator core and rotor core thicknesses are 0.119m and 0.105m respectively. Using these thicknesses yields a motor core weight of roughly 71tons. This will be taken as the total motor weight. The additional equipment weights, supporting structure, propeller, bearings, controller, conductors and cooling equipment will be calculated subsequently.

3.2.2.7 Space Required

A vital issue asks whether or not the proposed motor design will fit into the space between the hull envelope and the pressure hull. First, the axial length of the motor is considered. Second, the radial extent of the motor is assessed.

The length of the motor by itself is determined by the core length and the end-turns of the stator conductors or conductor rings of the rotor. The core length is 2.614m for both rotor and stator. The stator end-turns will have a somewhat larger axial length than the rotor conductor ring. The thickness of the rotor ring will be on the order of 1cm. Hence, the stator provides the limiting length. The length of the end-turns extending beyond the stator core on each end of the stator core will be taken as 0.160m. This is the length offered by Hamner. The axial length of the motor is 2.934m.

The radial extent of the motor depends on the core thicknesses and the air-gap. The outer radius of the stator core is 2.510m. With a core thickness of 0.119m, the inner radius of the stator core would be 2.391m. The air-gap is 5mm wide. Hence, the rotor inner radius is 2.515m. This means that, for a rotor core thickness of 0.105m, the outer rotor radius is 2.620m. Hence, the motor extends radially from 2.391m to 2.620m. The pressure hull radius at the motor location is 2.134m. The propeller hub radius is 2.758m. Therefore, the motor will fit between the pressure hull and the hull envelope.

3.2.3 Impacts on the Submarine Design

The baseline propulsion motor produces requirements that the submarine design, as a whole, must accommodate. These requirements can be broken into four areas, electrical input power, motor control, structural support and force transmission, and lubrication and cooling auxiliaries.

The submarine design's electrical generating plant must provide sufficient power to the propulsion motor. Figure 1 in section 3.1.8 shows the real power required by the motor, P_{in}.--This must be supplied by the submarine design's generating plant. Furthermore, as the propulsion motor is an induction motor, the generating plant must supply this power, P_{in}, at a less-than-unity power factor. The effect of a lagging load on the electrical generation plant of the submarine must considered when determining the generation plant's capacity.

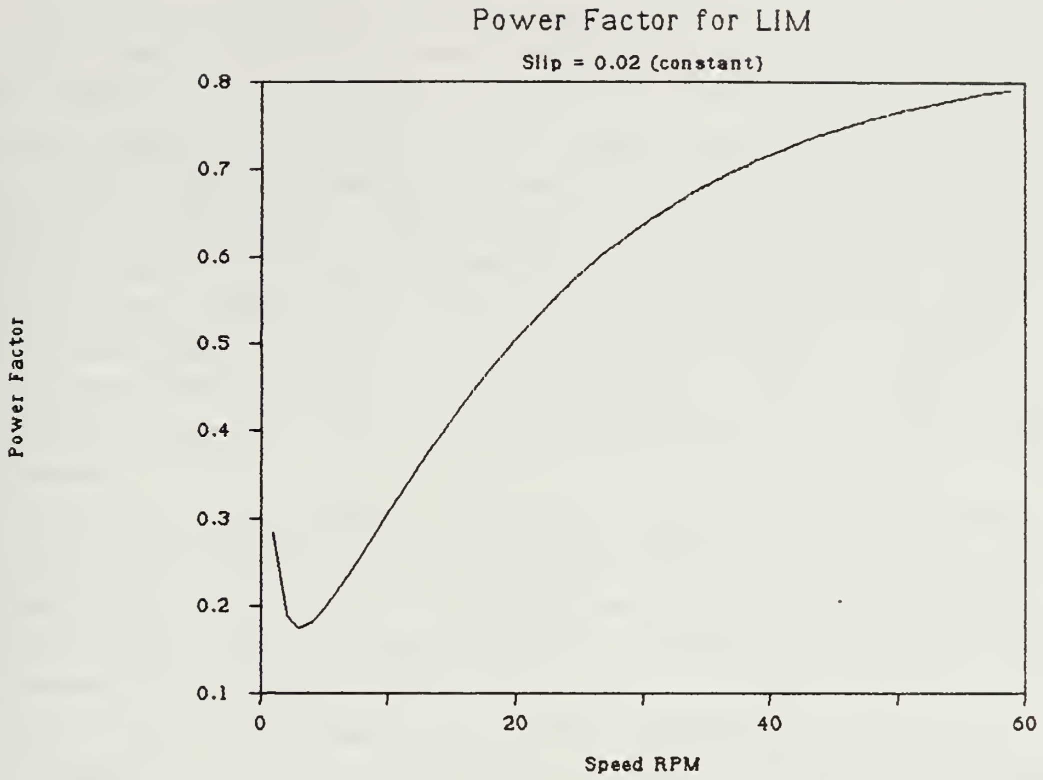

Figure 1 - Induction Motor Power Factor versus Speed

The figure above contains several assumptions. A control scheme for the motor is assumed to vary speed by varying input frequency and voltage. The slip at each frequency is assumed to be the same. Winding inductances are assumed to be constant over the frequency range.

When interpreting Figure 1, it is vital to recall the power versus speed relationship, Figure 3.1.8.1. Figure 1 may seem to indicate that motor operation at slow speeds places great demands upon the power generation plant. However, the power versus speed relationship shows that the propulsion motor has a low power factor for light loading only. Near rated power, its power factor is close to 0.8, which is not overly burdensome.

An implicit requirement for submarine propulsion is that the submarine's speed be continuously variable. In the case of the baseline motor design, this dictates a need for a motor controller and power conversion equipment. Given the rating

of the propulsion motor, this power conversion equipment will be relatively large and have relatively stringent cooling requirements.

The submarine design's hull must support the weight of the baseline propulsion motor as well as the dynamic forces created by the motor. The support structure, called the motor casing, motor frame and foundation in conventional electric motors, must react the forces of electromagnetic origin. Thrust bearings must be included in the design to react the thrust from the propeller on the rotor. Further, the rotor requires a journal bearing that will preserve the air-gap clearance.

Given the clearances involved, the cooling and lubricant requirements, and the dire consequences of overheating due to clogged flow, the 'free-flooding' space surrounding the propulsion motor must be supplied by forced-circulation, strained sea-water system.

The four requirements form the basis of the support that the submarine design must provide. They also are the impact that the propulsion motor has on the submarine design. These issues are addressed in subsequent sections.

3.3 Tentative Motor Controller Design

It is an absolute requirement that the baseline submarine have continuously variable speed. This requirement in any application usually puts induction motors at an immediate disadvantage. However, developments in power electronics have permitted induction motors to be competitive with other motor types in variable speed drives.

The speed of an induction motor can be varied by three different means, reference [18]. First, through switching windings, the number of poles that an induction machine has can be varied. Second, the stator frequency can be varied. Third, the motor's slip can be varied. The best method of speed control for the baseline submarine's propulsion motor is control of the stator frequency and voltage.

Using pole-changing by itself to control speed has several disadvantages. First of all, this scheme will only allow a discrete number of speeds. Rather than having continuously variable speed, only two or three distinct speeds could be possible. Second, changing the number of poles changes the flux density. Halving the number of poles doubles the required backing thickness. This increases weight. Pole-changing is very simple for squirrel-cage induction motors, though.

Pole-changing does offer an advantage when used in conjunction with variable stator frequency. This advantage comes in making it possible to travel at either of two speeds with a given stator frequency. The advantage of this is in acoustic deception.--An observer would not know for certain by monitoring the electrical supply frequency what speed the submarine was making.

Now that the method of speed control has been chosen, its implementation must be considered. Power must be supplied to the stator at varying frequency and voltage levels. Rotating frequency changers can be used or static (power electronic) frequency converters can be used. For acoustic reasons, the static frequency converters are somewhat more desirable than motor-generators.

Basically two schemes exist for creating a variable frequency stator voltage, reference [38]. First, a variable voltage level can be used in a bridge converter type of topology. Second, a constant voltage level can be used in conjunction with a pulse-width modulation scheme. Choosing which method is preferable will focus on generation of harmonics.

In the variable voltage bridge converter, square waves are made to approximate sinusoidal waveforms. Through harmonic elimination and cancellation techniques, usually the lowest harmonic is the 7th harmonic of the sinusoidal frequency. With the pulse width modulation scheme, the harmonics are harmonics of the switching frequency, which can be a high frequency. Hence, the pulse width modulation scheme produces harmonics that are most easily filtered out.

Therefore, the turbine-generators on the baseline submarine will supply 60Hz AC power. This power will feed a DC link converter. The DC link converter will supply variable frequency and variable voltage level AC power to the propulsion motor. The AC power supplied to the propulsion motor will be filtered, pulse width modulated, DC link voltage.

3.4 Thrust and Journal Bearing Design

Several characteristics of a motor usually have a large impact on which type of bearings to use. Two basic types of bearing are available, sliding bearings and roller bearings. These two types are broken down further. Prior to selecting a particular type of bearing, the characteristics of the motor which the bearings will support will be considered.

The results of the thrust and journal bearing designs show that the sea-water lubricated bearings are feasible. The designs also provide the dimensions of the bearings.

3.4.1 Thrust Bearing Design

The baseline propulsion motor can be characterised as a highly loaded, slow motor. The expected thrust which the thrust bearings must react is on the order of 1.2MN (270,000lbf or 120tons). The rated speed of the motor is 58.8rpm. At the air-gap radius, 2.510m, this translates into a linear velocity of 16.1m/s (52.8ft/s or 36mph). Of great importance to this thrust bearing design is the fact that it is necessary to be able to reverse the direction of rotation of the motor. Furthermore, the speed of rotation is continuously variable from 0 to 58.8rpm.

Additional constraints are placed on the thrust bearing design by the requirement that the motor be flooded. It would be very difficult to design a sea-water flooded thrust bearing that was not sea-water lubricated. To do so would require rotating seals, a great complication. Hence, the lubricant of choice is sea-water.

Based on the selection criteria offered by Harris, reference [14], by Wilcock, reference [15], and by Constantinescu et al, reference [16], the most suitable type of thrust bearing is a lenticulated, tilting, rectangular, tin-bronze pad sea-water flooded, sea-water lubricated, thrust bearing.

This type of thrust bearing has good load carrying capability at slow speeds and is also acoustically quieter than most of the alternative bearing types. Furthermore, its direction is reversible. (Lenticulated describes the fact that the active surface of the thrust bearing pad is not flat, but, rather, is convex in the longitudinal axis of the pad.)

The principle behind lenticulated, tilting pad thrust bearings is using the hydrodynamic characteristics of the flow of lubricant between the pad and the thrust surface to transmit thrust between two surfaces in relative motion with respect to each other. In this application, the thrust bearing pads are fixed to the hull. The thrust surface is the smooth forward, and aft, faces of the rotor. As the rotor starts to move, a thin film of sea-water forms between the thrust bearing pad and the thrust surface. This thin film of sea-water transmits the thrust from the rotor to the hull. See the figure shown below.

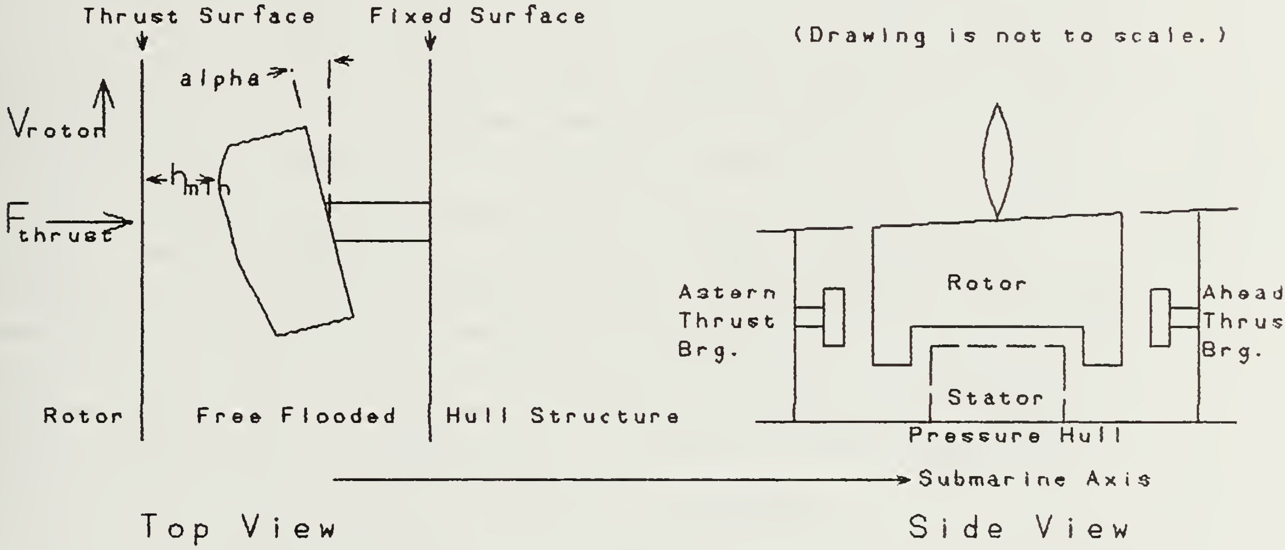

(Drawing is not to scale.)

Top View

Side View

Figure 1 - Thrust Bearing Geometry

In many thrust bearing applications, the lubricant is provided to the bearing at pressure by an external lubricant supply system. In this application, no need is seen at this point in the design to provide pressurised sea-water to each

bearing pad. This would represent an unnecessary complication to the design, increasing the weight and complexity of the propulsion motor auxiliary systems.

Whereas the motor and thrust bearings are flooded in sea-water, adequate lubricant flow is ensured by the flow of sea-water through the free-flooded space surrounding the motor. Rather than providing sea-water to each pad, a sea-water distribution system will be implemented to ensure a consistent flow of sea-water through the entire free-flooded space surrounding the motor and thrust bearing pads. The sea-water distribution system is discussed in more detail in section 3.6.

To this point, the geometry of the assembled bearing, speed, thrust, and lubricant for the thrust bearing are specified. Additionally, the type of thrust bearing pad is specified. Only selection of specific pad geometry, number of pads, and lubricant film thickness remains. Wilcock offers a thrust bearing design method. It is somewhat simplified and is only wholly correct for flat tilting pad thrust bearings. Constantinescu et al offers a more generalised thrust bearing design method. Both of these methods are used for the baseline propulsion motor thrust bearing design.

Both thrust bearing design methods are iterative. The critical design component is the lubricant temperature increase as it flows through the pad. The ambient lubricant temperature, lubricant kinematic viscosity as a function of temperature, lubricant density, and thrust bearing geometry must be specified. A maximum lubricant pressure level within the lubricant film is specified. Finally, the temperature of the lubricant as it exits the pad is guessed.

With the given geometry and lubricant, Wilcock's method provides pad size and the number of pads needed. This method also provides the pad tilt angle as well as the minimum film thickness. Additional information provided by this design method is stress within the lubricant film, power loss, required lubricant flow rate and the lubricant temperature rise. The calculated outlet temperature is compared with the assumed outlet temperature. Further iterations should bring the guessed and the calculated temperature rises into agree-

ment. The lubricant stress should also be less than the maximum allowable stress level. One final criteria that should be met is the minimum film thickness.

In addition to all of the inputs to Wilcock's method, the pad tilt angle, minimum film thickness, pad size, pad material and number of pads are inputs to Constantinescu's et al design method. This second design method is suitable for lenticulated pad designs and provides much more accurate characterisations of thrust bearing performance. The design method also provides a pad thickness.

Wilcock's and Constantinescu's et al design methods were cast into spreadsheet form. The forward and astern thrust bearing design spreadsheets are shown in Tables 7 through 10 in Appendix A. Wilcock's method provides the inputs to Contantinescu's et al more accurate design procedure.

Table 1 - Thrust Bearing Design Summary

Bearing Pad Length	0.305m
Bearing Pad Width	0.305m
Lenticular Height	19.1μm
Minimum Film Thickness	39.4μm
Number of Pads	42
Power Lost Due to Lubricant Shear Stresses	19.7kW
Lubricant Flow through Pad	112gpm
Temperature Rise Across Pad	1.2°F

3.4.2 Journal Bearing Design

After reviewing the design selection criteria in Harris, Wilcock and Constantinescu et al for journal bearings, the load, speed and reversibility requirements indicated that tilting pad journal bearings, much the same as the thrust bearing, would provide satisfactory performance.

The design method used for the thrust bearing is also used for the journal bearing. The spreadsheets appear in Tables 11 and 12 of Appendix A. The figure below shows the journal bearing relative to the rotor and stator.

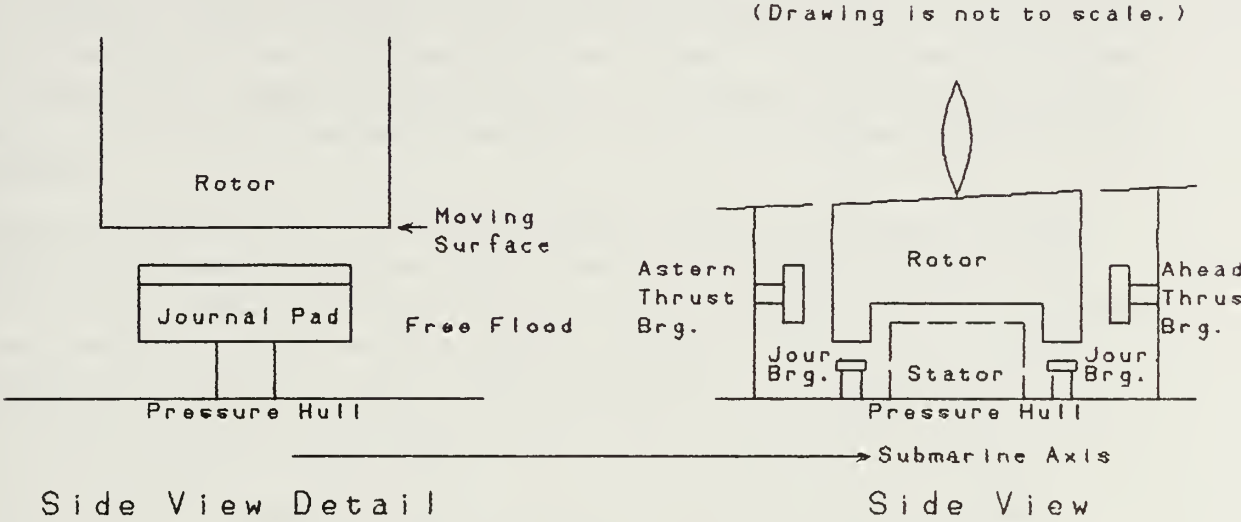

Figure 1 - Journal Bearing Geometry

Table 1 - Journal Bearing Design Summary

Bearing Pad Length	0.178m
Bearing Pad Width	0.178m
Lenticular Height	17.5μm
Minimum Film Thickness	36.0μm
Number of Pads	64
Power Lost Due to Lubricant Shear Stresses	8.8kW
Lubricant Flow through Pad	81gpm
Temperature Rise Across Pad	0.7°F

3.5 Structural Support Design

Having designed a baseline propulsion motor, the structure which attaches the motor to the hull and allows the motor to hold its shape must be considered. This task is divided into two areas. The structure which supports the motor and connects it to the hull has a vital role in the transmission of acoustic energy from the motor to the hull and then into the surrounding sea. The stator support structure is of vital interest to this research. The rotor support structure is of lesser interest at the moment.

Once the baseline propulsion motor and thrust and journal bearings have been designed, the remaining step is to design the structure needed to support the stator core. Three issues have an impact on the design of the support structure. First, the support structure must allow sea-water to flow past the stator core to allow cooling of the core. Second, prior to an acoustic analysis, unnecessary vibrations must be eliminated if just to avoid a time-varying 'air'-gap. Third, the support structure must adapt when the pressure hull is compressed at depth.

The forces with which the stator support structure will interact are forces of hydrodynamic origin (due to flow within the free flooded space), hydrostatic forces, forces of electromagnetic origin, forces due to the propeller, and forces due to the weight of all of the appropriate components. At this stage in the design, a detailed determination of all of these forces is not necessary nor is it desirable. Instead, an estimate of the maximum magnitude of each of these forces will be assumed. For a worst-case analysis, the magnitudes of these forces will be added appropriately.

The stator support structure is broken into six components. These components are envisioned to address the three issues mentioned previously. In view of the first issue, ensuring sea-water flow, the support structure must not be monolithic. To address the second issue, unnecessary vibrations, cantilever structures and excessive flexibility must be avoided. Addressing the final issue, pressure hull displacement, requires that the support structure be free to move in the radial direction, relative to the pressure hull.

Bearing in mind the guidelines expressed above, the stator support structure components will now be examined and the criteria for their design discussed. Each component will be designed separately; however, at the completion of the entire design, many of the components may be combined into larger pieces. The initial stator support structure configuration is shown in the figure below.

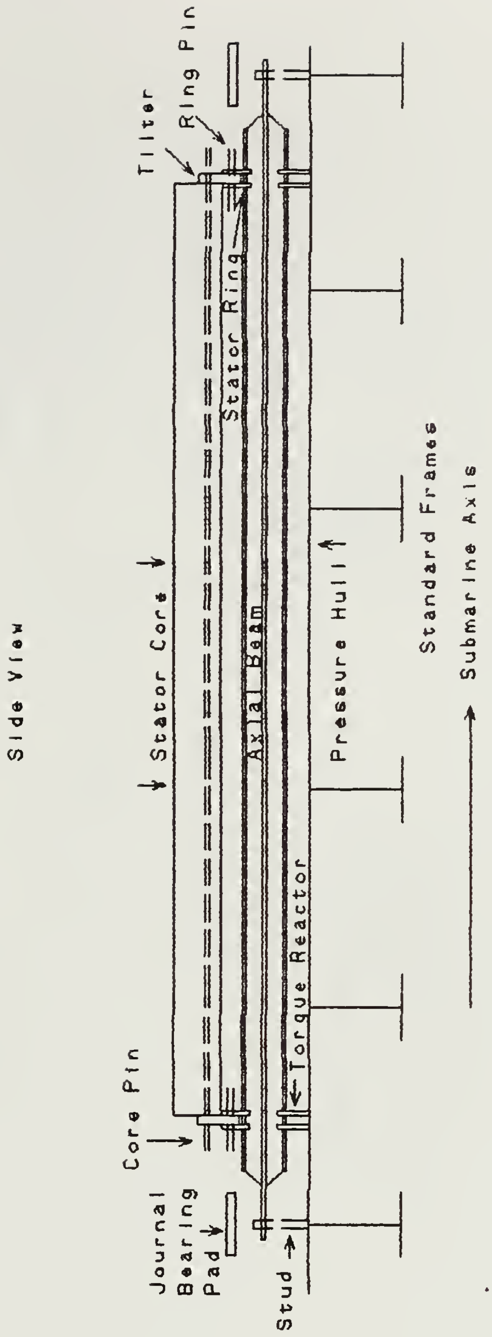

Figure 1 - Stator Support Structure Geometry

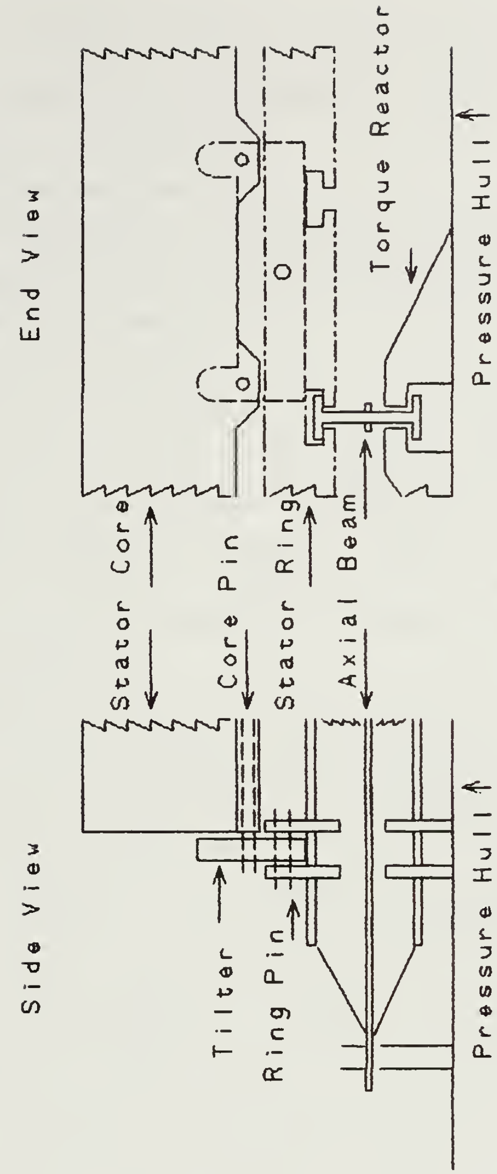

Figure 2 - Stator Support Structure Geometry (Radial Detail)

The material from which all of these components will be constructed is a high strength stainless steel with a yield stress of no less than 80kpsi. Whereas most of the forces involved are orthogonal, von Mises' criteria will be used to

determine design stress levels. For structures under axial and shearing loads, a factor of safety of 1.5 will be used. For structures under bending and possibly buckling loads, a factor of safety of 3.75 will be used.

3.5.1 Determination of Forces

Before beginning design calculations, some notion of the maximum magnitudes of the forces acting on the stator support structure must be developed.

3.5.1.1 Gravitational Forces

These forces are the weights of the various motor components. Since these components are being designed, their weights are unknown at present. However, the weight of the stator core, developed in section 3.2.2, is roughly 37tons. At the outset, it does not seem likely that the weight of the other components will come even close to this weight.

3.5.1.2 Pressure Forces

The sea-water inside the free-flooding area surrounding the stator will be supplied at some pressure slightly above the ambient pressure outside of the submarine. This is to ensure a flow of cooling water around the motor core. The pressure of the supplied sea-water would only need be on the order of 10psi greater than ambient pressure.

While intelligent distribution of the supply ports for this sea-water would greatly reduce a pressure differential at the two sides of the stator core, a worst case estimate of 10psi sea-water being supplied to the half-length location of the ‘air’-gap with the sea-water at the stator core back at ambient pressure will be used for design purposes. A linear pressure distribution is assumed in the force calculation. See Table 13 of Appendix A. The results indicate that, in a worst-case instance, an outward radial force of 141tons will be exerted over the entire stator.

3.5.1.3 Normal Electromagnetic Forces

In his thesis on linear induction motor transportation systems, reference [5], Weisman offers a derivation of the following equation which expresses the normal force of electromagnetic origin, F_N. This force acts normal to the stator surface.

$$F_N = -\frac{1}{2}\cdot\frac{1}{2\mu_0}\cdot[|b_p|^2 - (\mu_0 \cdot J_m)^2]\cdot L\lambda_p \qquad \#1$$

$$b_p = -iB_{sat} - B_{sat}\bar{k}_c \sin\psi' e^{-i\psi'} \qquad \#2$$

In these equations, J_m is the maximum linear current density along the stator outer diameter, 173,641A/m conservatively. λ_p is the wavelength of the stator or distance between like poles along the circumference, 0.526m. $\bar{k}_c$ relates the rotor current to its average value. In this case, a squirrel-cage rotor, it is assumed to be one. The most difficult term to determine is ψ'.

$$\psi' = \tan^{-1}\left(\frac{s\omega\mu_0 c_s}{k^2 \rho g}\right) \qquad \#3$$

The physical significance of ψ' is that it relates the phase of the rotating MMF wave to the phase of the induced potential in the rotor. c_{ms} is the rotor sheet conductor thickness in Weisman's work. In this research it will be estimated using the thickness of the rotor bars averaged over the entire rotor circumference, 0.018m. ρ is the resistivity of the rotor bars, 26.9 x 10^{-9}Ohm-m for aluminum. g is the 'air'-gap width, 5mm. k is the wavenumber associated with λ_p from above, 11.95m^{-1}. This makes $\psi' = 1.380$radians.

Using the values discussed, the normal force of electromagnetic origin is 12,280N (2760lbf) per slot or roughly 222tons over the entire stator. This value is based on assumptions involving maximum current values.

3.5.1.4 Electromagnetic Torque Forces

These forces arise from the fact that the stator must react the torque which drives the rotor. Hence, to find this force only the motor's torque and the stator's outer diameter need be considered. The maximum torque is 4.05 x 10^6N-m. The outside radius of the stator is 2.510m. Therefore, the force on the stator in the circumferential direction is equal to 1.612 x 10^6N (363,000lbf or 162tons).

3.5.2 Core Pins

The core pins have a relatively simple purpose. They are meant to hold the stator core, a stack of laminations, together and provide an attachment point for the rest of the structure. The core pin must withstand an axial load caused by the stacking pressure of the laminations. The other forces acting on the core pins will generate shear stress across the cross-section of the core pin. These other forces are the weight of the core, the normal electromagnetic force, the electromagnetic torque force, and a pressure force.

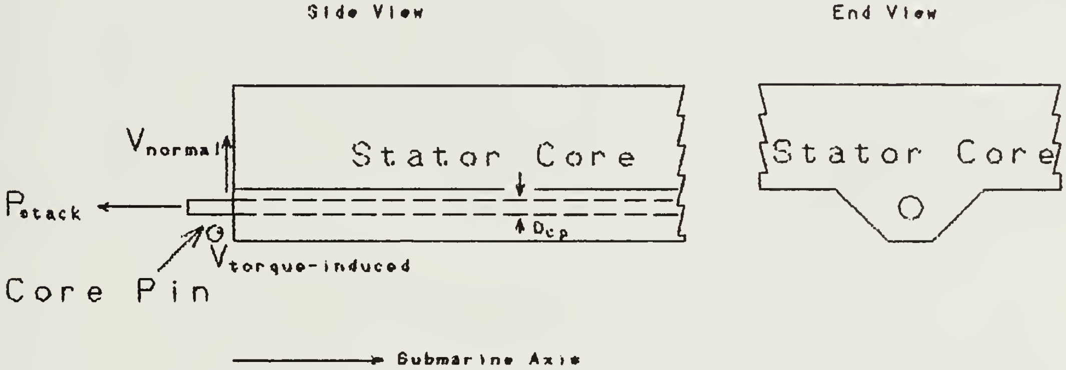

Figure 1 - Core Pin Geometry

All but the lamination stacking pressure have been specified. In his research, Hamner recommends using epoxy encapsulation to protect the stator core from sea-water. This requires compressing the stack of laminations. The pressure used to hold the epoxy encapsulated laminations together needs to be greater than the expected hydrostatic pressure at which the submarine expects to operate. A core stacking pressure of 670psi is used based on these requirements.

A core pin will be placed through the length of the stator at each pole location. This means that there will be 60 core pins.

3.5.3 Tilters

The tilters connect the stator core to the stator ring. The core pin will fit into a hole in the tilter arm. The core pin and tilter are free to rotate relative to each other. The tilters have two arms. Hence, they attach to two neighboring poles. The normal electromagnetic forces on the two neighboring poles should be equal and opposite. Hence, no net force due to normal electromagnetic forces should act on the tilter; however, a moment will act on the tilter.

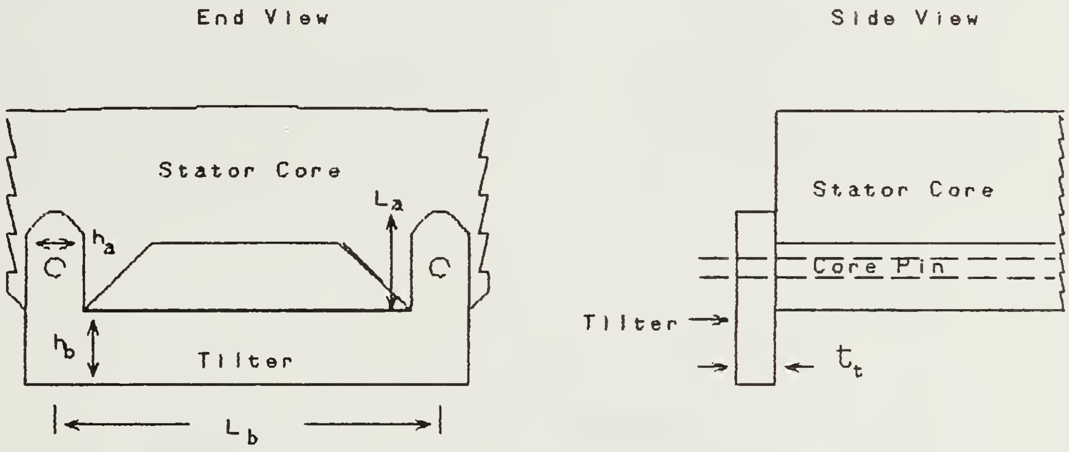

Figure 1 - Tilter Geometry

The tilter must withstand the force due to the weight of the core plus the normal pressure force. The tilter must also support the bending stress associated with the normal electromagnetic forces. The tilter will also have to transmit the electromagnetic torque-induced lateral force. There will be two tilters for each pole-pair, one on the forward end of the stator core and one on the aft end of the stator core, a total of 60 tilters.

3.5.4 Ring Pins

The ring pins form the connection between the base of the tilter and the stator ring. The tilter and stator ring are free to rotate relative to the ring pin. Ring pins are supported on either end by stator rings. The are loaded in the middle by the tilter.

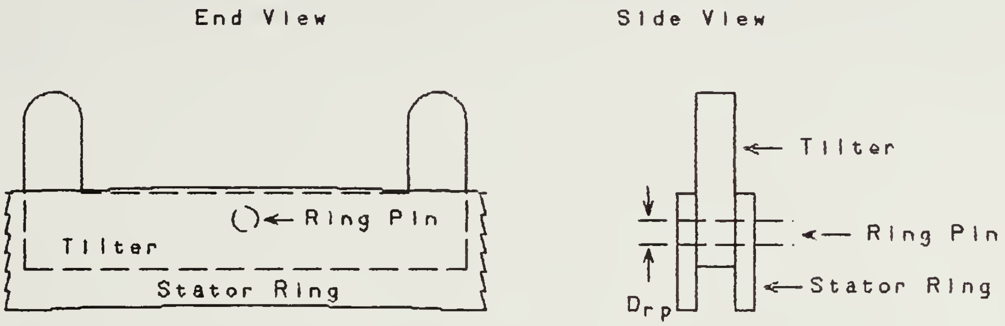

Figure 1 - Ring Pin Geometry

The ring pins must withstand a shear force caused by the weight of the core, the weight of the tilters, the normal pressure force, as well as the electromagnetic torque-induced force. There will be one ring pin for each tilter, a total of 60 ring pins.

3.5.5 Stator Rings

All of the tilters and, hence, all of the core pins are connected to the four stator rings. The stator rings are circumferentially continuous rings which serve to provide an attachment scheme for the axial beams used to connect the entire assembly to the hull. Tilters, located at the thirty stator pole-pairs, attach to the outer circumference of the stator rings. Axial beams, located at each of the 64 journal bearing pad supports, attach to the inner circumference of the stator rings.

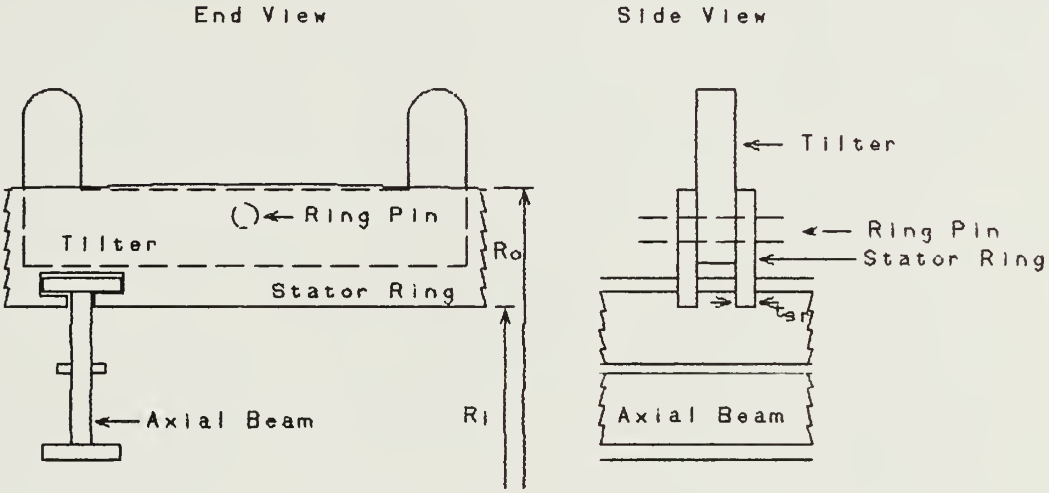

Figure 1 - Stator Ring Geometry

The stator rings must withstand a bending (or hoop) stress due to the weight of the core and tilters and the normal pressure force. The rings must also withstand a shear force in the circumferential plane that is due to the electromagnetic torque-induced force. Whereas the number of tilters and axial beams are not multiples of each other, the distribution of stresses will vary around the circumference of the stator rings. Prior to applying design criteria, a calculation of the maximum stresses within the stator ring is carried out. See Table 14 of Appendix A.

3.5.6 Axial Beam

The axial beam is perhaps the most interesting component of the entire stator support structure. It is essentially a supported beam which holds the stator core and other stator support structure components in place and attached to the hull. Its ends are attached to the journal bearing pad supports. These, in turn, are located on the pressure hull opposite an internal frame. This is done to minimize the impact of pressure hull deflections at depth and ties the stator radial location to the rotor's contact point with the pressure hull.

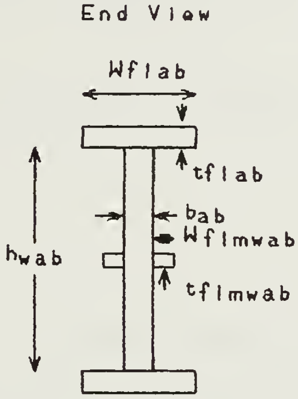

Figure 1 - Axial Beam Geometry

The axial beam should be stiff so that it does not tend to deflect much at midspan. This is to preserve the 'air'-gap width. It must support the bending stresses due to the weights and normal pressure forces. It must also react a torque which is created by the electromagnetic torque-induced forces and the torque reactor. The torque tends to twist the axial beam about its longitudinal axis. An in-depth look at the bending moment distribution is necessary.

3.5.7 Torque Reactors

The torque reactors are acted upon by the axial beams. Only the electromagnetic torque-induced force is transmitted to the torque reactors. The torque reactors are hard-mounted to the pressure hull. In this way, the electromagnetic torque is transmitted to the hull.

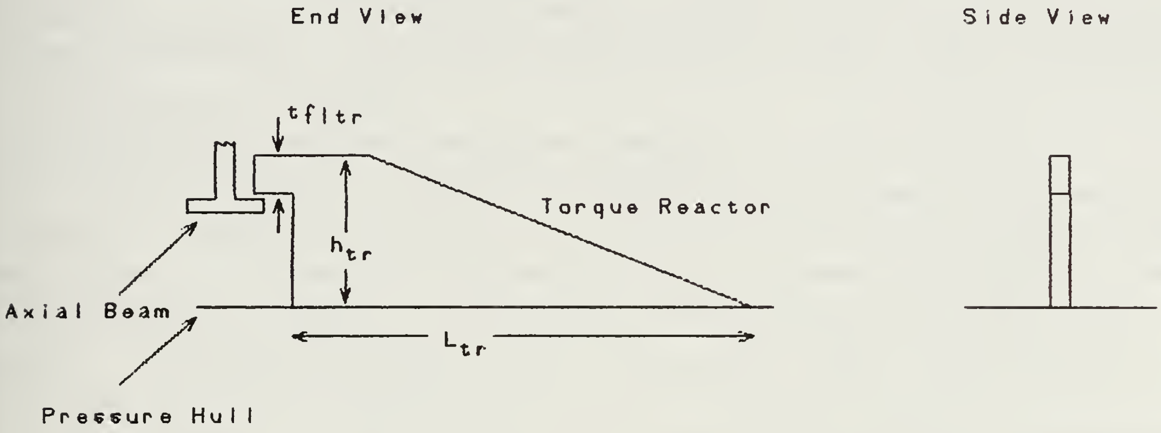

Figure 1 - Torque Reactor Geometry

The torque reactors must withstand a bending moment over their upper portion. Along the base of the torque reactor, the electromagnetic torque causes a shear stress at the connection to the pressure hull.

3.5.8 Integration of Components

The design criteria and forces for each of the components of the stator support structure is incorporated into a spreadsheet where the structural calculations are performed. A further check is made to ensure that all of the pieces fit together and fit within the space allotted. The spreadsheet appears in Table 15 of Appendix A. Included in the appendix are some of the appropriate bending moment and shear calculations.

No claim is made that the proposed structure is the optimal structure. In fact, many alternative structures are perhaps just as suitable. Initial calculations, though, indicate that this structure will serve the need.--That is, provide a structure to test acoustic properties of the propulsion motor.

The baseline structure can be taken to be that shown in Figures 1 and 2 in section 3.5. The dimensions of each of the components can be found in the spreadsheet of Table 15 in Appendix A. The estimated weight of the stator support structure is 8.5tons. The estimated weight of the rotor support structure is 7.2tons.

3.6 Sea-Water and the Baseline Design

A revolutionary feature of this entire baseline submarine design is the fact that the propulsion motor is immersed in sea-water. To design engineers, this represents a great simplification in cooling water provisions and gland seal concerns. To operating and repair persons, this represents a serious cause for concern.

The concerns with a sea-water immersed motor are threefold. First, the electrical conductors in both rotor and stator must be protected from being shorted by sea-water. Second, the baseline motor design consists of large pieces which are in motion relative to each other and which will be machined to very demanding tolerances. These large pieces are easily corroded in sea-water. Third, the cooling function of the sea-water would be lost if marine life or particulate matter clogged any of the sea-water channels surrounding the stator core.

The second and third concerns voiced above are equally valid for the thrust and journal bearings. The bearings must also have unobstructed flow to ensure lubrication as well as cooling.

Hamner offers an acceptable means of protecting the stator core and rotor core as well as the stator and rotor windings from the harmful effects of sea-water. The question now is how the support structure can be protected. The simple answer is to use materials which will not corrode. The suggested solution would combine a corrosion-resistant material such as the

most suitable of the various types of stainless steel (recognising that it too corrodes however slowly) and a protective coating.

In the past, when structural components of a submarine are located in a free-flooding space, the scantlings of those components are increased over their required value to provide for strength after material has been lost due to corrosion. This practice is recommended for this propulsion scheme. However, specific calculations of how much scantlings should be increased are beyond the scope of this research.

Increasing scantlings alone does not provide the most efficacious approach to mitigating the deleterious effects of corrosion. For example, the clearances involved in maintaining a 5mm ‘air’-gap on a 5.02m diameter structure do not allow much room for corrosion allowances in scantlings. Therefore, steps in addition to corrosion allowances in scantlings must be taken.

Hence, all of the support structure components will be fabricated from stainless steel, then coated with protective material similar to that proposed for core protection by Hamner. Doubtless, at locations where two pieces are in contact or can move relative to each other, the protective coating scheme must be modified. Where relative motion exists, cladding with a sacrificial metal may provide the solution. Eventually, though, the cladding metal must be replaced.

Additional anti-corrosion measures can be specified. An installed active cathodic protection system would provide protection, but with added weight and power requirements. Zincs could be installed throughout the free-flooding baseline propulsion motor space, which, if properly arranged, will mitigate corrosion as well.

While building in as much corrosion resistance as possible, it is vitally important during the manufacturing engineering phase of the construction of such a submarine design that allowances are made in the design for relatively simple removal of the rotor and getting ready access to all components of the motor, structure and bearings. Zincs must be replaced; corroded structural elements must be replaced; the structure must

be inspected to assess the precise degree of corrosion at the very least. All of these require easy and inexpensive access (in a dry-dock environment) to the propulsion motor internals. Access in this instance must include the ability to remove and restore any given structural component.

3.7 Baseline Design Closure

The remaining step left in the baseline submarine design is to check the feasibility of the design. The initial submarine design presented in section 3.1 is used to develop the requirements for the motor designed in section 3.2. The baseline propulsion motor design meets the power requirements. The controller for the propulsion motor is discussed in section 3.3 and found to be feasible. Thrust and journal bearings are found to be feasible and designed in section 3.4. Section 3.5 provides the design of the structure of the motor.

A calculated weight is provided for each of the structures that is designed. These weights will now be included with other weight estimates to determine if the required equipment can fit into the hull proposed in section 3.1. Additionally, some arrangements will be performed to obtain the center of gravity of the various equipments. Thus, the submarine design can be balanced.

3.7.1 Refined Weight Estimates

More accurate estimates of the weights of the seven weight groups will now be developed based on the baseline propulsion motor design. As mentioned earlier, the initial weight estimates, section 3.1.4, are based on SUBLAB. Now that $P_{s,m}$ is known, reference [27]'s empirical weight estimating relationships can be used to obtain relatively accurate weight estimates. (Table 1 in section 3.1.4 contains a description of the function of each of the weight groups.)

Weight Group 1

Based on the selected hull shape and NSC, the estimated weight from section 3.1.5 will be used. This weight includes the motor support structure and propeller hub as well.

Weight Group 2

This weight group can be broken into four groups, nuclear reactor weight, radiation shielding weight, propulsion machinery, and propulsion auxiliaries. The reactor and shielding weight is a function of the reactor's output power. As the baseline submarine design is an electric powered boat, the reactor plant capacity must be based on the combined propulsion input power, P_{in}, and the ship service electrical power. Consider the ship service load to be roughly 1.5MW. Hence, the required reactor output power is roughly 54,000HP (41.1MW).

Based on the relationships offered in section 3.2 of reference [27], the weight of the reactor is approximately 393tons. The weight of the shielding is approximately 238tons. The weight of the auxiliaries is approximately 67tons. Lastly, the weight of the propulsion machinery, which consists of the propulsion motor, bearings, and propeller blades, is 89tons. This weight is developed using the weights obtained during the motor and bearing designs. See section 3.2.2 for motor weights. The propeller weight is taken from Hamner's research, 5.3tons.

Weight Group 3

Finding an accurate weight estimate for the generating plant for the baseline submarine design is very difficult. However, after reviewing a number of studies, the research done by Greene et al, reference [39], provides accurate estimates. Recognising differences between submarine electrical requirements and surface ship electrical requirements, the weights from this study provide the basis for the estimate for the baseline submarine design. The electrical plant for the baseline submarine design has a capacity of 41.1MW. The generators of this plant, two 20.1MW generators, will have water-cooled stators and air-cooled rotors. This weight group must also include the steam turbines and condensers associated with electrical generation. The distribution system will have port and starboard (dual) power distribution switchboards.

Weight Group 4

This weight is somewhat arbitrary; however, it is very close to the absolute weight of the command and control equipment found on contemporary submarine designs.

Weight Group 5

This weight is taken to be a function of the pressure hull size and the complement. Reference [27] develops the function in its section 3.5.

Weight Group 6

This weight is based on mostly on the crew size. Whereas the baseline submarine design has only one engine room (and no forward auxiliary machinery room) and much less equipment within that engineroom, the number of engineering personnel assigned to the baseline submarine should be less than the number assigned to contemporary nuclear powered submarines. The complement of the baseline submarine is 102, 12 officers, 12 CPO's and 78 crew. This number combined with a stores endurance of 45 days provides an input to reference [27]'s section 3.6.

Weight Group 7

This essentially represents the weight of the torpedo launching and handling equipment. Whereas there has been little change in how this is done, a weight similar to the torpedo launch and handling weight from another past submarine will be used.

Table 1 - Revised Weight Estimates

Weight Component	Symbol	Long Tons	Comment
Envelope Displacement	Δ_{env}	5106	
Free Flood	FF	357	7% of Δ_{env}
Submerged Displacement	Δ_{sub}	4749	Δ_{env} - FF
Main Ballast Tanks	MBT	528	12.5% of NSC
Normal Surface Cond.	NSC	4221	Δ_{sub} = NSC + MBT
Variable Loads	VL	274	NSC = VL + A1
Condition A	A	3947	A = LEAD + A1
Lead Ballast	LEAD	359	10% of A
Condition A-1	A1	3588	Sum of W1 - W7
Group 1	W1	1687	Sections 3.1.5 and 3.5
Group 2	W2	787	Sections 3.2, 3.3, 3.4 and 3.7.1
Group 3	W3	237	Section 3.7.1
Group 4	W4	220	Section 3.7.1
Group 5	W5	421	Section 3.7.1
Group 6	W6	131	Section 3.7.1
Group 7	W7	105	Section 3.7.1

3.7.2 Arrangements

Given the above weights, the equipment will now be located so that some notion of the centers of gravity of the weight groups can be developed. Once these centers of gravity are known, the design can be balanced, that is, the LEAD can be

located. Arrangements in submarine designs require drawings to determine the feasibility of the pressure hull size. Hence, initial arrangement drawings are developed. These drawings are shown in Figure 4 of Appendix A.

From these drawings the centers of gravity of some of the weight groups are taken. Other weight groups, such as weight group 1, are calculated separately. Following the arrangement drawing is a spreadsheet that contains the centers of gravity of the different weight groups and their components. That spreadsheet is also used for the design balance discussed in the next section. See Table 16 of Appendix A.

The arrangement drawing has many similarities with modern submarine arrangements. It also has numerous, and significant, differences. The forward portion of the submarine is relatively conventional. The aft portion of the submarine is certainly the unorthodox portion of the design.

Locating the berthing compartment in the aft portion of the submarine is begging for criticism. However, due to the nearby location of the passageway through the reactor compartment, getting to general quarters stations should not take overly long, especially for the engineers. Further, the ventilation and equipment rooms forward of the berthing area and hard by the reactor compartment bulkhead will serve as desirable additional shielding. A valid concern will be the noise levels experienced above the engineroom. However, if the boat is well-quieted, as all good submarines should be, then this concern can be surmountable.

One of the potential advantages of the baseline submarine propulsion motor is that it may be possible to locate a large payload space aft. Installing advanced acoustic sensor array equipment is also possible back aft. Doubtless, the specifics of such systems are classified and, hence, are inappropriate for discussion. The flexibility of the arrangements back aft, though, would permit inclusion of such equipment.

Figure 5 of Appendix A contains an outboard profile of the baseline submarine design with the locations of the control surfaces included.

3.7.3 Baseline Submarine Balance

This step considers all of the weights and locations of weight groups 1 through 7. A lead solution is obtained using the classic approach. The LCG of the envelope displacement must be located at the exact same position as the LCB of the hull envelope. For acceptable submerged stability, the VCG of the envelope displacement must be located below the VCB. This will produce a righting moment if the submarine rolls to one side. Usually, the distance between these two points should be no less than one foot. Hence, the VCB is typically located very close to the submarine's axis. The VCG, then, should be no higher than 15.0ft. The weight balance sheet, Table 16 of Appendix A, shows that the VCG is at 14.98ft, which is acceptable.

The LEAD solution is also shown on the spreadsheet, Table 16 of Appendix A. Section 3.1.4 discusses the location of LEAD. Of some concern to the designer, the stability lead is a relatively large percentage of the total amount of lead, 30%. The implication is that less of the lead is available as insurance against uncertainty in construction and future growth potential. The LCG of the stability lead indicates that it is located rather far forward. This tells the designer that the boat is a bit heavy aft. If additional design iterations were to be performed, then this could be addressed. It is satisfactory for this stage of the design effort.

3.7.4 MBT Sizing and Location

Section 3.1.6 dealt with the sizing and location of the MBT's for the initial weights and centers of gravity locations. Whereas new values for the weights have been calculated and new locations of the centers of gravity have been taken from the arrangements, so too must the size and location of the MBT's be refined.

The outboard profile in Figure 5 of Appendix A shows the updated location of the refined MBT locations. A spreadsheet shows the updated MBT sizing calculations. See Table 17 of Appendix A. Based on these results, the pressure hull location is feasible.

3.7.5 Equilibrium Polygon and Stability

In addition to the MBT's, submarines also have trim-tanks. The role of trim-tanks is to maintain the trim and heel of the submarine. In effect, trim-tanks ensure that the LCG always lines up with the LCB and that the submarine is heavy enough to submerge. Developing an equilibrium polygon for the submarine design ensures that the trim-tank design is feasible.

The standard approach used by the U.S. Navy is used to determine which weights will be included in various load conditions. For example, one particular loading is called "heavy forward". In this loading, all variable load items located aft in the submarine are assumed to be consumed. Hence, the boat will have a trimming moment tending to push the bow down. To compensate for this trimming moment, the aft trim tank must be capable of being filled with enough water to bring the boat back to an even trim.

In this early feasibility study, five load conditions were used to test the trim tank and weight balance feasibility. These five conditions were, "heavy 2"-H2, "heavy forward 1"-HF1, "heavy aft"-HA, "light 2"-L2, and "normal"-N. These five conditions are explicitly described in reference [40]. On the figure below, the trimming moment caused by these five conditions are indicated by crosses.

The three trim tanks, forward, aft, and an auxiliary tank close to the LCG of the submarine, are capable of providing continuously variable trimming moments. The polygon on the figure below encloses all of the possible trimming moments that can be generated by the trim tanks. The goal of the trim tank system is to enclose all of the possible load conditions. If this is true, then the trim system will be capable of compensating for any conceivable changes in the variable loads on the submarine.

The variable load locations are derived using locations from the arrangement drawings and outboard profile. For each load condition, the requisite variable ballast weight and its LCG were computed. The trim-tanks shown in the outboard profile of Figure 5 in Appendix A provide the equilibrium polygon shown below.

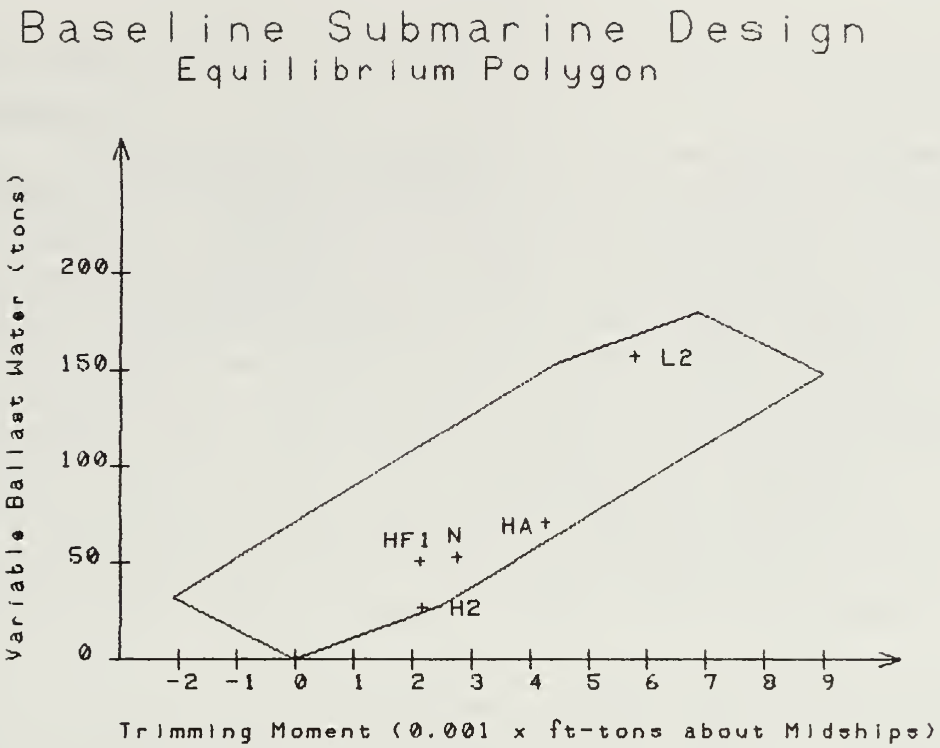

Figure 1 - Equilibrium Polygon

The equilibrium polygon shows that the trim-tank configuration shown on the baseline submarine design is feasible and stable.

3.8 Conclusion

The baseline submarine design presented in the preceding sections appears to be a feasible submarine design. This conclusion is based on a single iteration design. A real submarine design would go through many such design iterations before construction would begin.

The baseline submarine, as described in this chapter and Appendix A will be the subject of the acoustic analysis developed in the next chapter.

4 Acoustic Model

4.1 Introduction

Chapter 1 discusses the selection of an acoustic model that will be adapted to describe the acoustic emissions of the OTHEP propulsion system. The model selected is referred to as TFA (Transfer Function Analysis, or "empirical analysis"). This model must be modified to account for the unique aspects of OTHEP. This chapter develops the necessary adaptations.

Before discussing the modifications to TFA, the forces of electromagnetic (EM) origin that act on the propulsion motor's core, causing vibrations, will be described. Hopefully, this description of the EM forces could be used by structural acousticians as an excitation force in a more sophisticated acoustic model analysis than the adapted TFA model analysis used in this research.

The EM forces will also be used to estimate the structure-borne noise source level of the propulsion motor. This estimate will be extremely approximate. A more accurate model would involve acoustic modelling techniques which are well beyond the scope of this research.

After describing the forces of EM origin, the TFA model will be established. This model will be used in the next chapter to compare estimated noise emissions from the baseline submarine design propulsion system with estimated noise emissions from several other submarine propulsion systems.

4.1.1 Applications of the Acoustic Model

The baseline submarine design of this research, which features OTHEP, can be considered to be in the very early feasibility design stage. Hence, the description of OTHEP is not very detailed. The weights, structures, and arrangements presented in Chapter 3 and Appendix A are essentially an educated guess as to how an OTHEP submarine could be realised.

Referring here to structural features, discussion of the baseline design in greater detail than plating, framing, bulkheads and decks is not possible. Structural components such as stanchions, stringers and stiffeners have not been considered at all. Furthermore, equipment foundation designs and sound isolation mounting designs have not been developed.

These two items are very important to any detailed acoustic model of the baseline design. Structures are the predominant acoustic path within the submarine.

Regarding the equipment within the baseline submarine design, especially the major pieces of equipment such as generator steam turbines and condensers et cetera, much of the equipment is of a sort that is designed specifically for that particular application. Many pieces of equipment are not of the "off-the-shelf" variety. Hence, measured acoustic emissions data for those pieces of equipment will not exist until that piece of gear is designed and built. An accurate analytical estimate of the noise emissions for that piece of equipment would not be possible until a detailed design has been developed.

The foregoing discussion seeks to point out that the precise nature of the noise emissions from the source equipment is not known. Further, the precise nature of the path that that noise will take through the structure of the submarine is not known either. With these two facts in mind, the approximate nature of the assessment of noise emissions attempted in this research is manifest. Hence, an accurate assessment of the precise noise emission characteristics of the baseline submarine will probably not be developed. What this research can provide is twofold. First, it can provide an upper bound on the noise emission level. This indicates whether or not the acoustic design of the baseline submarine is "within the ball-park" in an absolute sense. Second, this research can also provide a rough comparison with other propulsion plant configurations.

4.1.2 Discussion of Dominant Noise Sources for Baseline Design

Virtually everything on a submarine, or any vessel for that matter, is capable of making noise.--Some sources of noise are more ‘important’ than others. Acoustic quietness is a desirable characteristic for a submarine for two reasons. First, in order to detect faint acoustic signals in the sea, a submarine must first be quiet herself. This is the issue of "self-noise". Second, in order not to be detected by other listeners, a submarine must not emit noise into the sea. This is the issue of "radiated-noise".

In the context of the two issues listed above, the principal concern is with noise that is transmitted into the sea, travels some distance through the water, then is observed by a listening device. In this context, noise that propagates some distance through sea-water can be considered to be 'important' noise.

The sea, as a medium, provides an upper limit on the frequency of noise that will propagate over the distances envisioned here (on the order of several kilometers). The dissolved chemicals within sea-water affect the absorption, or attenuation, of sound waves travelling through the water. This absorption can be roughly described as arising from a damped, visco-elastic response of the dissolved chemicals to the sound pressure waves. The absorption due to this mechanism increases as the frequency of the sound pressure wave increases.

The submarine, as emitter or receiver, provides a lower limit on the frequency of 'important' noise. Listening to low frequency signals requires a physically extensive listening array. If such an array is on the order of the size of the submarine, then the size of the submarine provides some clue as to the lowest frequency of interest.

For an indication of the upper limit on frequency, the following expression is taken from reference [41].

$$\alpha r_{lim} \sim 10dB \qquad \#1$$

Here, α represents the absorption coefficient for the sea-water. α is a function of frequency, temperature, salinity, acidity and pressure. r_{lim} represents the maximum propagation distance. For 'nominal' sea-water, which has a salinity of 35ppt, a temperature of 4C, a pH of 8.0 and a pressure of 300ATM, the α corresponding to a range, r_{lim}, of 10km is roughly equal to 1, reference [41] figure 3.5. The frequency that corresponds to this alpha is roughly 11kHz. This, then, is the upper limit to the frequencies that will be examined in this research.

For an indication of the lower limit on frequency, the following expression is also taken from reference [41].

$$\lambda_{max} \sim \frac{c_{sw}}{f_{min}} \sim L_{array} \qquad \#2$$

Here λ_{max} represents the wavelength of the lowest frequency sound, f_{min}, that can be detected on array of length L_{array}. The speed of sound in sea-water is a function of temperature, pressure, and salinity. It varies continuously over a wide range of values; however, an 'average' value of the speed of sound in sea-water, c_{sw}, is taken to be 1500m/s. For a submarine whose length is that of the baseline design's, the maximum array length would be approximately 67m (220ft). This yields a minimum frequency of roughly 22.4Hz.

Based on the discussion above, the frequency range of 'important' noise extends from roughly 22Hz to 11,000Hz. This is not to say that all other emissions are unimportant. Rather, for a submarine whose size is on the order of the baseline design, emitting and observing noise, this is the frequency range of greatest interest to this research.

Noises whose frequency lies within the range shown above can come from a myriad of sources. If one is comparing two different propulsion schemes, perhaps OTHEP and an electric motor driven conventional propeller system, then many different acoustic emitters will have to be considered. For example, the control surfaces of the baseline submarine are aft of the propeller. For a shaft-driven propeller on the axis of the submarine, the control surfaces are forward of the propeller. These two configurations will have different radiated noise levels for noise that originates from flow variations across the control surfaces and noise that originates from flow variations at incidence with the propeller. For the rotational speed of the propellers, the number of propeller blades, and number of control surfaces for both propulsion systems, the noise due to the flow variations will lie within the range of 'important' noise.

Needless to say, it would be very difficult indeed to compare all of these potential noise sources. Hence, this research will be limited specifically to the noises arising from the forces of electromagnetic origin that lie within the frequency range developed above. In the comparison study,

only the propulsion train noises will be considered for comparison. Issues pertaining to structural acoustics will be ignored.

4.1.3 Acoustic Model of OTHEP

4.1.3.1 Determination of Forces of EM Origin

This task is based on the assumption that harmonics in the 'air'-gap magneto-motive force (MMF) of the propulsion motor will cause time varying forces to act on the motor core. Any MMF wave will generate normal forces on the motor's core, harmonics or not. These forces are then transmitted to the motor's mounting and then on to the hull. The harmonics in the 'air'-gap MMF will be attributable to winding space-harmonics of the stator, rotor-bar space harmonics of the squirrel-cage rotor, and time harmonics in the stator current due to pulse width modulation of the stator current.

The approach will be to compute the MMF for the stator winding and rotor cage without explicitly solving for the currents. The currents will then be determined and subsequently substituted into the respective expressions for MMF. Once the MMF is known, the radial magnetic field intensity can easily be found. Knowing the magnetic field intensity, the Maxwell stress tensor can be used to find the radial force on the motor.

The description of the MMF will be based on the baseline propulsion motor design of Chapter 3, as will be the description of the stator currents. Once the MMF and currents are specified, forces on the motor can be found. These forces can be converted into acceleration levels. This will permit the calculation of source levels for use in the simplified model discussed in the next section.

4.1.3.2 Development of a Simplified Overall Model for Comparisons

The method of predicting the radiated noise level for the baseline submarine is a modified version of the TFA model analysis developed in reference [7]. Reference [7] provides a method for calculating predictions of airborne noise levels within the ship design under consideration. Reference [7]'s

principal use is to assess compliance with various airborne noise level regulations, which are meant to either protect human operators in equipment spaces or ensure crew and passenger comfort outside of the machinery spaces.

The method developed by reference [7] has to be modified to predict waterborne noise levels. Instead of airborne noise levels within the submarine, the chief interest of this research is an assessment of the noise levels radiated into the sea. Hence, some of the transfer functions used in reference [7] must be adapted to describe radiation into the sea.

Only the noise sources from the propulsion train that will be compared in the comparative analysis will be considered here. The goal is not to develop an absolute noise prediction, but, rather, to assess comparative merit.

4.2 Description of Forces of Electromagnetic Origin

The objective of this section is to provide a description of the acceleration levels within the propulsion motor. These acceleration levels are the structureborne noise source level inputs used by the TFA model.

Finding the acceleration levels requires knowing the ‘air’-gap MMF, which requires knowing the winding geometry and currents of the stator and rotor. These two issues are treated in the next section.

4.2.1 Derivation of ‘Air’-Gap MMF, Including Harmonics

4.2.1.1 Stator Winding MMF

The first task in determining the forces of electromagnetic origin that act on the motor is to determine the MMF that is created by the stator winding. Many texts on the subject treat this in the general sense. This research concentrates on the specific configuration of the baseline propulsion motor.

Table 1 - Propulsion Motor Winding Characteristics

Motor Characteristic	
Stator Slots	180
Conductors per Slot	2
Phases	3
Pitch	2/3
Pole Pairs	30
Slots per Pole Pair	6
Nominal Stator Frequency	30Hz

The number of slots and the number of pole-pairs dictate the slots per pole-pair. The slots per pole-pair and pitch, taken together, yield the winding pattern of a single pole, which is shown below.

Table 2 - Propulsion Motor Winding Pattern

Outer Slot	a	c'	b	a'	c	b'
Inner Slot	b'	a	c'	b	a'	c

The effect of the width of each conductor is included in this MMF derivation. Let α' represent the conductor width in mechanical degrees. The equation below shows α' in terms of electrical degrees; this will be called α. (It is assumed here that the insulation thickness is not important in MMF calculations.)

$$\alpha = p \cdot \alpha' = p \cdot \frac{W_{cc}}{R_{OD}} \qquad \#1$$

MMF is defined to be the current intersected by the area integral of the integral form of Ampere's Law. The integral form of Ampere's Law is shown below, reference [19].

$$\oint_C \mathbf{H} \cdot d\mathbf{l} = \int_S \mathbf{J} \cdot \mathbf{n}\, da \qquad \#2$$

In equation 2, **H** is the magnetic field intensity vector. **J** is the current density vector.

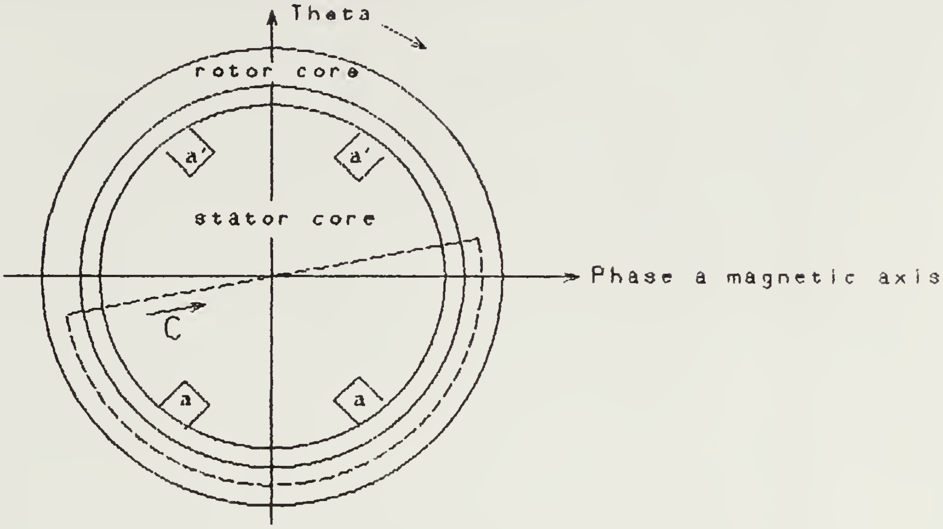

Figure 1 - MMF Integral Contour and Winding Geometry

The path of the closed line integral is shown in Figure 1 above. The surface circumscribed by that line integral is the surface of the area integral on the right hand side of equation 2. This second integral is simply the current intersected by the area circumscribed by the closed line integral's path. Hence, MMF is described in the following equation.

$$MMF = \int_S \mathbf{J} \cdot \mathbf{n}\, da \qquad \#3$$

The winding pattern shown above taken in combination with the angular conductor width and Ampere's Law yield the MMF distribution for a single pole-pair shown below.

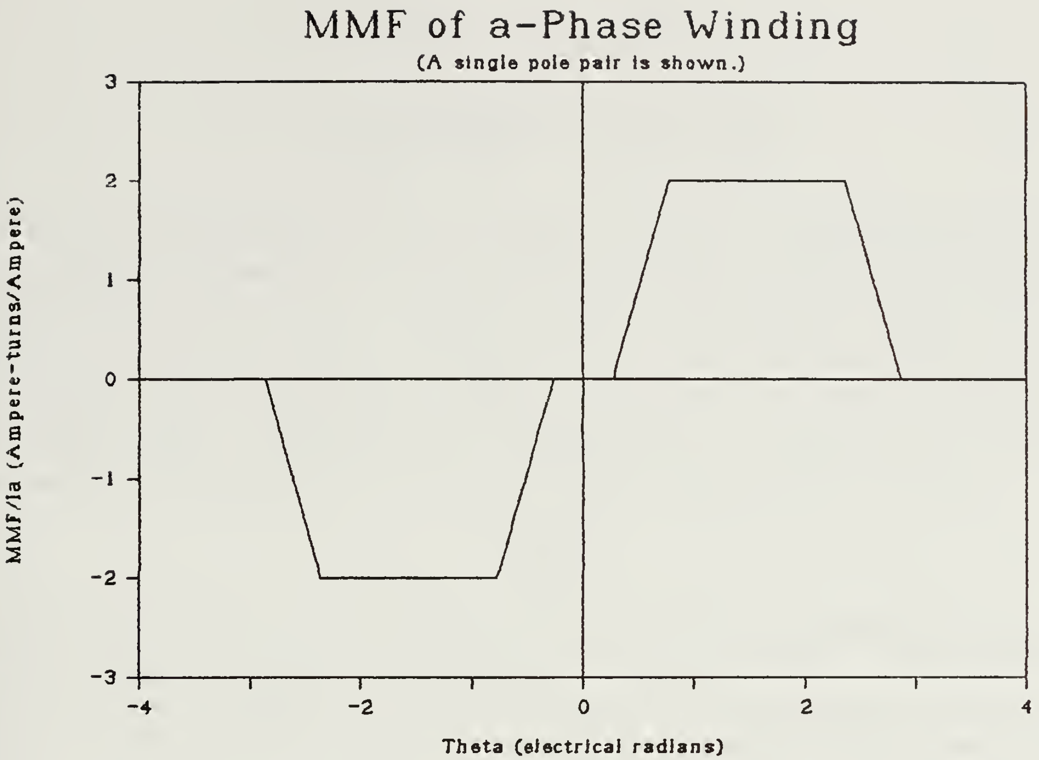

Figure 2 - Stator Winding a-Phase MMF

This MMF distribution can also be described using a Fourier sine series. A sine series is chosen because, with the reference axis shown in Figure 1, the MMF distribution is an odd function. The Fourier representation of this MMF is shown below.

$$MMF_a(\theta_e) = \sum_{n=1}^{\infty} a_n \sin(n\theta_e) \qquad \#4$$

$$a_n = \frac{2}{\pi}\int_0^{\pi} MMF_a \sin(n\theta_e)\, d\theta_e \qquad \#5$$

Evaluating a_n using the MMF distribution in the figure above, yields the following expression for the Fourier coefficients of the a-phase MMF.

$$a_n = \frac{8 i_a}{\pi n}\,\frac{\sin\left(\frac{n\alpha}{2}\right)}{\frac{n\alpha}{2}}\sin\left(\frac{n\pi}{3}\right)\sin\left(\frac{n\pi}{2}\right) \qquad \#6$$

Before considering the role of current, i_a, in this expression, the a-phase MMF will be rewritten as follows.

$$MMF_a = \sum_{n=1}^{\infty} A_n i_a \sin(n\theta_s) \qquad \#7$$

$$A_n = \frac{8}{\pi n}\left(\frac{\sin\left(\frac{n\alpha}{2}\right)}{\frac{n\alpha}{2}}\right)\sin\left(\frac{n\pi}{3}\right)\sin\left(\frac{n\pi}{2}\right) \qquad \#8$$

This derivation of the effect of slot and winding geometry closely agrees with the classic derivation of winding MMF's, reference [18]. According to reference [18], equation B-22, for point conductors ($\alpha = 0$), and using winding factors for the winding geometry shown in Figure 1, and considering only the space fundamental frequency, n=1, the coefficient of the space fundamental term of the a-phase MMF follows.

$$A_1 = \frac{6}{\pi} \qquad \#9$$

The value of A_1 arising from the use of equation 8 is shown below. The difference is roughly 15.5%. The difference is attributable to the effect of the width of the conductor on the MMF. The method of reference [18] does not account for this effect. The propulsion motor does, in fact, have conductors of very finite width.

$$A_1 = \frac{6.9282}{\pi} \qquad \#10$$

The expression developed here for A_n, equation 8, accurately conveys the effect of winding geometry on the MMF generated by the stator winding. Equation 7 also includes a current term, i_a, which must now be developed.

As discussed in Chapter 3, the propulsion motor armature will be supplied by a variable frequency, variable voltage level, pulse-width-modulation (PWM) power converter. The current from this converter will contain the time-fundamental stator frequency and harmonics of the PWM converter switching frequency, ω_p. Hence, the current should be representable in such a form as follows.

$$i_a(t) = I_p\cos(\omega_s t) + \sum_{m=1}^{\infty}(a_{pwm}\cos m(\omega_p t) + b_{pwm}\sin m(\omega_p t)) \qquad \#11$$

As a worst-case approximation, the shape of the distortion can be approximated by a square wave of one-half duty cycle, with a magnitude called I_{max}, added to the time fundamental component. Hence the coefficients of the Fourier series representation of the current waveform can be reduced somewhat. Shown in the figure below is a representation of the square wave addition to the current waveform. An odd-function square wave is assumed. (Note, this is a very conservative description of the distortion. A square wave of one-half duty cycle can carry a lot of energy.)

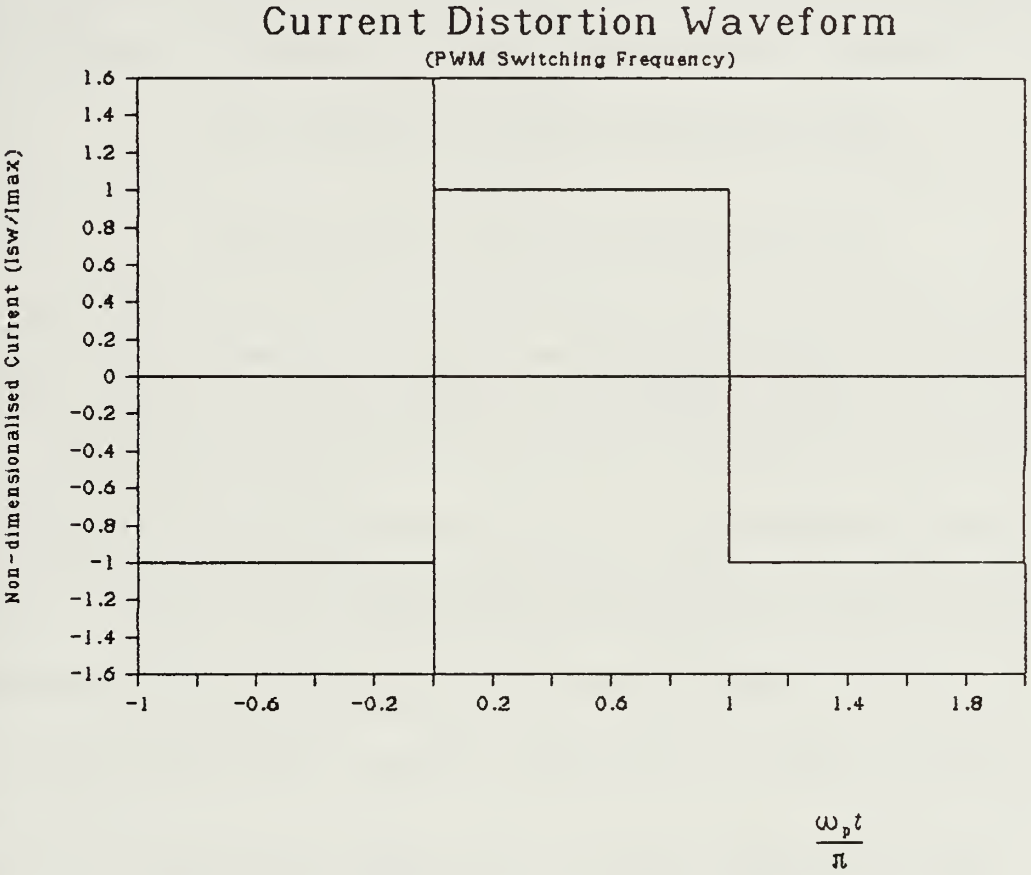

Figure 3 - Current Distortion Waveform

The following is the Fourier sine series description of the distortion waveform.

$$i_{sw} = \sum_{m=1}^{\infty} \frac{2I_{max}}{m\pi}(1-\cos m\pi)\sin m\omega_p t \qquad \#12$$

The total current will be taken as the sum of the fundamental component of the current and the distortion component shown above. The coefficient, A_m, eliminates even time harmonics of the PWM switching frequency.

$$i_a(t) = I_p \cos \omega_e t + \sum_{m=1}^{\infty} A_m I_{max} \sin m(\omega_p t) \qquad \#13$$

$$\text{where} \quad A_m = \frac{2(1-\cos m\pi)}{m\pi} \qquad \#14$$

Whereas the propulsion motor is a three phase machine, the other two phases of the stator current can be described as follows. A balanced three phase system is implied here.

$$i_b(t) = I_p \cos\left(\omega_e t - \frac{2\pi}{3}\right) + \sum_{m=1}^{\infty} A_m I_{max} \sin m\left(\omega_p t - \frac{2\pi}{3}\right) \qquad \#15$$

$$i_c(t) = I_p \cos\left(\omega_e t + \frac{2\pi}{3}\right) + \sum_{m=1}^{\infty} A_m I_{max} \sin m\left(\omega_p t + \frac{2\pi}{3}\right) \qquad \#16$$

In equations 13-16, ω_e represents the fundamental stator electrical frequency. ω_p is the PWM switching frequency. I_p is the stator's time-fundamental frequency peak line current. I_{max} represents the amplitude of the square-wave distortion of the stator current.

Substituting the expression for the a-phase current, equation 13, into the expression for the a-phase MMF, equation 7, gives a more complete description of the a-phase MMF.

$$MMF_{sa}(\theta_e, t) = \sum_{n=1}^{\infty} A_n \left(I_p \cos(\omega_e t) + \sum_{m=1}^{\infty} A_m I_{max} \sin m(\omega_p t) \right) \sin(n\theta_e) \qquad \#17$$

The b-phase and c-phase components of MMF will take similar forms.

$$MMF_{sb}(\theta_e, t) = \sum_{n=1}^{\infty} A_n \left(I_p \cos\left(\omega_e t - \frac{2\pi}{3}\right) + \sum_{m=1}^{\infty} A_m I_{max} \sin m\left(\omega_p t - \frac{2\pi}{3}\right)\right) \sin n\left(\theta_e - \frac{2\pi}{3}\right) \qquad \#18$$

$$MMF_{sc}(\theta_e, t) = \sum_{n=1}^{\infty} A_n \left(I_p \cos\left(\omega_e t + \frac{2\pi}{3}\right) + \sum_{m=1}^{\infty} A_m I_{max} \sin m\left(\omega_p t + \frac{2\pi}{3}\right)\right) \sin n\left(\theta_e + \frac{2\pi}{3}\right) \qquad \#19$$

The preceding three expressions for the MMF of the three phases represent travelling waves. Combining the three sets of travelling waves yields the MMF due to the entire stator winding. The results of the combination are shown below.

$$MMF_s(\theta_e,t)=\sum_{n=1}^{\infty}\Bigg\{\Bigg[\frac{3}{2}A_n I_p \sin\Bigg(n\theta_e-\Bigg[\frac{2}{\sqrt{3}}\sin\frac{n2\pi}{3}\Bigg]\omega_s t\Bigg)\Bigg]$$
$$+A_n\Bigg[\sum_{m=1}^{\infty}A_m I_{max}\Bigg(2\sin\frac{m2\pi}{3}\sin\frac{n2\pi}{3}\Bigg)\cos(n\theta_e-m\omega_p t)\Bigg]$$
$$+A_n\Bigg[\sum_{m=1}^{\infty}A_m I_{max}\Bigg(1+2\cos\frac{(m+n)2\pi}{3}\Bigg)\cos(n\theta_e+m\omega_p t)\Bigg]$$
$$+A_n\Bigg[\sum_{m=1}^{\infty}A_m I_{max}\Bigg(1+2\cos\frac{(m+n)2\pi}{3}\Bigg)\cos n\theta_e \cos m\omega_p t\Bigg]\Bigg\} \qquad \#20$$

Although somewhat complex, equation 20 contains a familiar result. The first term on the right-hand side of equation 20 is a travelling, synchronous speed, sinusoidal MMF wave. This first term includes the non-even, non-triplen space harmonics. The remaining terms on the right-hand side of equation 20 represents the effect of the time harmonics of the stator currents.

The first of the PWM switching frequency harmonic terms is a forward-travelling wave. The second is a reverse-travelling wave. The third is a standing wave. The coefficients of the wave expressions dictate which of the PWM switching frequency harmonics will participate in the various travelling waves.

4.2.1.2 Rotor Cage MMF

The first step in determining the MMF which arises from the current in the rotor bars is to find the magnitude of the current in each of the rotor bars. Reference [34] discusses the relationship between the results of the equivalent circuit analysis and an actual description of currents in squirrel-cage rotor bars. A vital result is the relationship between the referred rotor current of the equivalent circuit, i_2, and the current in the reference rotor bar, i_{bref}, reference [34] equation 35.

$$i_2=\frac{N_R}{6N_s k_s}i_{bref} \qquad \#1$$

Based on circuit analysis of the equivalent circuit, the following two terms describe the referred rotor current, i_2, in terms of the stator line current, i_{ph}.

$$Z^2_{split} = \frac{(\omega_s L_\phi)^2}{\left(\left(\frac{R_2}{s}\right)^2 + (\omega_s(L_2 + L_\phi))^2\right)} \qquad \#2$$

$$\psi_{split} = \tan^{-1}\left[\frac{\frac{R_2}{s}\tan\beta - \omega_s(L_2 + L_\phi)}{\frac{R_2}{s} + \omega_s(L_2 + L_\phi)\tan\beta}\right] \qquad \#3$$

The expressions above describe how the time-fundamental frequency component of the stator current divides between the magnetising inductance, L_ϕ, and the rotor impedance. β is the phase angle of the stator line current. For the a-phase current, β is zero. For the b-phase and c-phase currents, β is $-\frac{2\pi}{3}$ and $\frac{2\pi}{3}$ respectively. The stator time-fundamental frequency is not the only frequency which contributes to the stator current. Hence, the time harmonics of the PWM switching frequency must also be included. This requires defining two more terms.

$$Z'^2_{msplit} = \frac{(m\omega_p L_\phi)^2}{\left(\left(\frac{R_2}{s}\right)^2 + (m\omega_p(L_2 + L_\phi))^2\right)} \qquad \#4$$

$$\psi'_{msplit} = \tan^{-1}\left[\frac{\frac{R_2}{s}\tan\left(\beta + \frac{\pi}{2}\right) - m\omega_p(L_2 + L_\phi)}{\frac{R_2}{s} + m\omega_p(L_2 + L_\phi)\tan\left(\beta + \frac{\pi}{2}\right)}\right] \qquad \#5$$

Hence, if the current described by equation 4.2.1.1.13 is the input current in an equivalent circuit analysis, then the current shown below represents the current in the reference rotor bar.

$$i_2 = (Z^2_{split} I^2_p)^{\frac{1}{2}} \sin(s\omega_s t + \psi_{split}) + \sum_{m=1}^{\infty} A_m I_{max} (Z'^2_{msplit})^{\frac{1}{2}} \sin m(s\omega_p t + \psi'_{msplit}) \qquad \#6$$

$$\therefore i_{bref} = \frac{N_R}{6N_s k_s}\left[(Z^2_{split} I^2_p)^{\frac{1}{2}} \sin(s\omega_s t + \psi_{split}) + \sum_{m=1}^{\infty} A_m I_{max} (Z'^2_{msplit})^{\frac{1}{2}} \sin m(s\omega_p t + \psi'_{msplit})\right]$$

#7

Hence, the current in the reference rotor bar is known. Now the current in the other rotor bars must be found. In a derivation similar to that of reference [34], the current in each rotor bar will be phase retarded relative to the reference rotor bar by an amount equal to the spatial displacement between the rotor bars. Let the reference rotor bar be bar number 1. The current in the j^{th} bar is shown below.

$$i_{bj}=\frac{N_R}{6N_s k_s}\left[(Z^2_{split}I^2_p)^{\frac{1}{2}}\sin\left(s\omega_s t+\psi_{split}-(j-1)\frac{2\pi p}{N_R}\right)\right.$$

$$\left.+\sum_{m=1}^{\infty}A_m I_{max}(Z'^2_{msplit})^{\frac{1}{2}}\sin\left(ms\omega_p t+\psi'_{msplit}-(j-1)\frac{2\pi p}{N_R}\right)\right] \qquad \#8$$

The goal of the following steps is to develop a relationship which describes the rotor currents as a series of travelling waves. To expedite this, complex notation will be adopted to ease the manipulations. Additionally, only the time fundamental frequencies will be considered. The current in the j^{th} bar is shown below in complex notation.

$$\tilde{i}_{bj}=\underline{I}_{bj}e^{-j(s\omega_s t)}+\sum_{m=1}^{\infty}\underline{I}^m_{bbj}e^{-jm(s\omega_p t)} \qquad \#9$$

where $$\underline{I}_{bj}=\underline{I}_b e^{j\left((j-1)\frac{2\pi p}{N_R}+\frac{\pi}{2}\right)} \qquad \#10$$

$$\underline{I}_b=\left[\frac{N_R}{6N_s k_s}(Z^2_{split}I^2_p)^{\frac{1}{2}}\right]e^{-j\psi_{split}}=I_b e^{-j\psi_{split}} \qquad \#11$$

and $$\underline{I}^m_{bbj}=\underline{I}^m_{bb}e^{j\left((j-1)\frac{2\pi p}{N_R}+\frac{\pi}{2}\right)} \qquad \#12$$

$$\underline{I}^m_{bb}=\left[\frac{N_R}{6N_s k_s}A_m I_{max}(Z'^2_{msplit})^{\frac{1}{2}}\right]e^{-j\psi'_{msplit}}=I^m_{bb}e^{-j\psi'_{msplit}} \qquad \#13$$

To find the surface current density due to the current in each of the N_R bars, the current in each bar will be summed and divided by the circumferential distance corresponding to one rotor slot.

$$K_r(\theta')=\frac{1}{R_r}\left[\sum_{j=1}^{N_R}\underline{I}_{bj}e^{-j(s\omega_s t)}\delta\left(\theta'-\frac{2\pi(j-1)}{N_R}\right)+\sum_{j=1}^{N_R}\sum_{m=1}^{\infty}\underline{I}^m_{bbj}e^{-jm(s\omega_p t)}\delta\left(\theta'-\frac{2\pi(j-1)}{N_R}\right)\right] \qquad \#14$$

This surface current density, which is composed of N_R impulses, will be described using a Fourier series. The Fourier series that will be used is shown below.

$$\tilde{K}_r^f = \sum_{n=-\infty}^{\infty}\left\{\underline{K}_n e^{j(np\theta' - s\omega_s t)} + \sum_{m=1}^{\infty}\underline{K}_{bn}^m e^{j(np\theta' - ms\omega_p t)}\right\} \qquad \#15$$

$$\underline{K}_n = \frac{1}{2\pi}\int_{-\pi}^{\pi}\frac{1}{R_r}\sum_{j=1}^{N_R}\underline{I}_{bj} e^{-j(s\omega_s t)}\delta\left(\theta' - \frac{2\pi(j-1)}{N_R}\right)e^{-j(np\theta' - s\omega_s t)}d\theta' \qquad \#16$$

$$\underline{K}_{bn}^m = \frac{1}{2\pi}\int_{-\pi}^{\pi}\frac{1}{R_r}\sum_{j=1}^{N_R}\sum_{m=1}^{\infty}\underline{I}_{bbj}^m e^{-jm(s\omega_p t)}\delta\left(\theta' - \frac{2\pi(j-1)}{N_R}\right)e^{-j(np\theta' - ms\omega_p t)}d\theta' \qquad \#17$$

As mentioned earlier, this series should include space and time harmonics. However, as will become apparent in the evaluation of an approximate source level, it is very desirable to avoid excessively complex descriptions of the 'air'-gap MMF. Hence, the time harmonics will be forsaken.

The Fourier coefficients are evaluated next. The delta functions, upon integration, simply yield an evaluation of the integrand at the points where the impulse function is non-zero.

$$\underline{K}_n = \frac{1}{2\pi R_r}\underline{I}_b e^{j\frac{\pi}{2}}\sum_{j=1}^{N_R} e^{j\left((j-1)\frac{2\pi p}{N_R}(1-n)\right)} \qquad \#18$$

$$\underline{K}_{bn}^m = \frac{1}{2\pi R_r}\underline{I}_{bb}^m e^{j\frac{\pi}{2}}\sum_{j=1}^{N_R} e^{j\left((j-1)\frac{2\pi p}{N_R}(1-n)\right)} \qquad \#19$$

$$\therefore\ \tilde{K}_r^f = \sum_{n=-\infty}^{\infty}\left\{\frac{1}{2\pi R_r}\underline{I}_b e^{j\frac{\pi}{2}}\left(\sum_{j=1}^{N_R} e^{j\left((j-1)\frac{2\pi p}{N_R}(1-n)\right)}\right)e^{j(np\theta' - s\omega_s t)} + \right.$$

$$\left.\sum_{m=1}^{\infty}\frac{1}{2\pi R_r}\underline{I}_{bb}^m e^{j\frac{\pi}{2}}\left(\sum_{j=1}^{N_R} e^{j\left((j-1)\frac{2\pi p}{N_R}(1-n)\right)}\right)e^{j(np\theta' - ms\omega_p t)}\right\} \qquad \#20$$

This series will now be altered to contain only positive indices. This is done by adding to the summed expression the same expression with the signs of the indices changed. The case of n=0 is considered independently. This is done to simplify visualisation of the travelling waves.

$$\tilde{K}_r^f = \sum_{n=1}^{\infty}\left\{\frac{1}{2\pi R_r}\underline{I}_b e^{j\frac{\pi}{2}}\left[\left(\sum_{j=1}^{N_R} e^{j\left((j-1)\frac{2\pi p}{N_R}(1-n)\right)}\right)e^{j(np\theta' - s\omega_s t)} + \left(\sum_{j=1}^{N_R} e^{j\left((j-1)\frac{2\pi p}{N_R}(1+n)\right)}\right)e^{-j(np\theta' + s\omega_s t)}\right] + \right.$$

$$\left.\frac{1}{2\pi R_r}\left(\sum_{m=1}^{\infty}\underline{I}_{bb}^m e^{j\frac{\pi}{2}}\left[\left(\sum_{j=1}^{N_R} e^{j\left((j-1)\frac{2\pi p}{N_R}(1-n)\right)}\right)e^{j(np\theta' - ms\omega_p t)} + \left(\sum_{j=1}^{N_R} e^{j\left((j-1)\frac{2\pi p}{N_R}(1+n)\right)}\right)e^{-j(np\theta' + ms\omega_p t)}\right]\right)\right\}$$

#21

One particular issue warrants discussion at this point. In the equation above, the series expression which represents the sum over the number of rotor bars has only two distinct values, N_R and 0. Whether the series expression equals N_R or 0 depends upon the expression shown below.

$$\frac{(1-n)p}{N_R}=\text{integer} \qquad \frac{(1+n)p}{N_R}=\text{integer} \qquad \#22$$

If equation 22 is true, then the sum over the number of rotor bars equals N_R for the two different cases. The first corresponds to a forward travelling wave, the second a reverse travelling wave. These expressions act as a 'filter' which permits only harmonics that coincide with the rotor bar frequency, which seems intuitively correct. These terms will be examined later during the development of an approximate source level for the propulsion motor.

Now that the surface current density due to the current in each of the rotor bars has been described as a function of rotor angle, the rotor MMF may now be developed. The method used here is the same as was used to determine the stator MMF in section 4.2.1.1.

$$M\hat{M}F_r(\theta'_e,t)=\int_{\theta'_e}^{\theta'_e+\pi} K_r^r R_r \, d\bar{\theta}'_e \qquad \#23$$

After evaluation of the integral and some simplification, the expression below for the rotor MMF results.

$$\begin{aligned} M\hat{M}F_r = & -\frac{N_R}{\pi}\underline{I}_b e^{j\frac{\pi}{2}} e^{j(\theta'_e - s\omega_e t)} - \sum_{m=1}^{\infty}\frac{N_R}{\pi}\underline{I}_{bb}^{m} e^{j(\theta'_e - ms\omega_p t)} \\ & + \sum_{m=1}^{\infty}\underline{I}_{bb}^{m}\left(\sum_{j=1}^{N_R} e^{j\left((j-1)\frac{2\pi p}{N_R}\right)}\right)\cos m(s\omega_p t) \\ & + \sum_{n=2}^{\infty}\frac{1}{\pi n}\Bigg\{\underline{I}_b e^{j\frac{\pi}{2}}\left(\sum_{j=1}^{N_R} e^{j\left((j-1)\frac{2\pi p}{N_R}(1-n)\right)}\right)e^{-j(n\theta'_e - s\omega_e t)} \\ & \quad - \sum_{m=1}^{\infty}\underline{I}_{bb}^{m}\Bigg[\left(\sum_{j=1}^{N_R} e^{j\left((j-1)\frac{2\pi p}{N_R}(1-n)\right)}\right)e^{j(n\theta'_e - ms\omega_p t)} \\ & \quad\quad - \left(\sum_{j=1}^{N_R} e^{j\left((j-1)\frac{2\pi p}{N_R}(1+n)\right)}\right)e^{j(n\theta'_e + ms\omega_p t)}\Bigg]\Bigg\} \end{aligned} \qquad \#24$$

The expression above for the rotor MMF is a complex expression. The real component of the expression above follows.

$$
\begin{aligned}
MMF_r = {} & \frac{N_R}{\pi} I_b \sin(\theta'_e - s\omega_s t - \psi_{split}) + \sum_{m=1}^{\infty} \frac{N_R}{\pi} I_{bb}^{m} \sin(\theta'_e - ms\omega_p t - \psi'_{msplit}) \\
& + \sum_{m=1}^{\infty} I_{bb}^{m} \left(\sum_{j=1}^{N_R} e^{j\left((j-1)\frac{2\pi p}{N_R}\right)} \right) \sin\psi'_{msplit} \cos m(s\omega_p t) \\
& + \sum_{n=2}^{\infty} \frac{1}{\pi n} \left\{ I_b \left(\sum_{j=1}^{N_R} e^{j\left((j-1)\frac{2\pi p}{N_R}(1+n)\right)} \right) \sin(n\theta'_e + s\omega_s t + \psi_{split}) \right. \\
& \qquad - \sum_{m=1}^{\infty} I_{bb}^{m} \left[\left(\sum_{j=1}^{N_R} e^{j\left((j-1)\frac{2\pi p}{N_R}(1-n)\right)} \right) \cos(n\theta'_e - ms\omega_p t - \psi'_{msplit}) \right. \\
& \qquad\qquad \left.\left. - \left(\sum_{j=1}^{N_R} e^{j\left((j-1)\frac{2\pi p}{N_R}(1+n)\right)} \right) \cos(n\theta'_e + ms\omega_p t - \psi'_{-msplit}) \right] \right\}
\end{aligned}
\qquad \#25
$$

4.2.1.3 'Air'-Gap MMF

The resultant 'air'-gap MMF is simply the sum of the stator and rotor MMF's. The only obstacle, at this point, is the variables used to describe the spatial distribution of the MMF. The stator MMF is given in terms of θ_e and the rotor MMF in terms of θ'_e. It is now necessary to relate these two variables. This is done through the "slip" relationship shown below.

$$\theta' = \theta - \omega_m t \qquad \#1$$

$$p\theta' = \theta'_e = \theta_e - p\omega_m t \qquad \#2$$

$$\theta'_e = \theta_e - p(1-s)\omega_{syn} t \qquad \#3$$

$$\theta'_e = \theta_e - (1-s)\omega_e t \qquad \#4$$

When equation 4 is substituted into the expression for rotor MMF, equation 4.2.1.2.25, the rotor MMF and the stator MMF, equation 4.2.1.1.20, can be combined to yield the 'air'-gap MMF. After combination and some simplification the 'air'-gap MMF appears as below.

$$
\begin{aligned}
MMF_{air\text{-}gap} = \sum_{n=1}^{\infty}\Bigg\{ & \frac{3}{2}A_n I_p\left[\frac{1}{3}\left(1+2\cos\frac{(n-1)2\pi}{3}\right)\sin(n\theta_s-\omega_s t)+\frac{1}{3}\left(1+2\cos\frac{(n+1)2\pi}{3}\right)\sin(n\theta_s+\omega_s t)\right] \\
& +I_b\left(\frac{\cos n\pi-1}{2\pi pn}\right)N_R\Bigg[\frac{1}{N_R}\left(\sum_{j=1}^{N_R} e^{j\left((j-1)\frac{2\pi p}{N_R}(1-n)\right)}\right)\sin(n\theta_s-(n(1-s)+s)\omega_s t-\psi_{split}) \\
& \qquad +\frac{1}{N_R}\left(\sum_{j=1}^{N_R} e^{j\left((j-1)\frac{2\pi p}{N_R}(1-n)\right)}\right)\sin(n\theta_s-(n(1-s)-s)\omega_s t+\psi_{split})\Bigg] \\
& +\sum_{m=1}^{\infty}\Bigg[A_n A_m I_{max}\Bigg(\left(1+2\cos\frac{(m+n)2\pi}{3}\right)\cos(n\theta_s+m\omega_p t) \\
& \qquad -\left(1+2\cos\frac{(m-n)2\pi}{3}\right)\cos(n\theta_s-m\omega_p t)\Bigg) \\
& +I_{bb}^{m}\left(\frac{\cos n\pi-1}{2\pi pn}\right)N_R\Bigg[\frac{1}{N_R}\left(\sum_{j=1}^{N_R} e^{j\left((j-1)\frac{2\pi p}{N_R}(1-n)\right)}\right)\Big(\cos(n\theta_s-(n(1-s)\omega_s+ms\omega_p)t-\psi'_{msplit}) \\
& \qquad -\cos(n\theta_s-(n(1-s)\omega_s-ms\omega_p)t-\psi'_{-msplit})\Big) \\
& \qquad +\frac{1}{N_R}\left(\sum_{j=1}^{N_R} e^{j\left((j-1)\frac{2\pi p}{N_R}(1-n)\right)}\right)\Big(\cos(n\theta_s-(n(1-s)\omega_s+ms\omega_p)t+\psi'_{-msplit}) \\
& \qquad -\cos(n\theta_s-(n(1-s)\omega_s-ms\omega_p)t+\psi'_{msplit})\Big)\Bigg]\Bigg]\Bigg\}
\end{aligned}
\qquad \#5
$$

4.2.2 The 'Air'-Gap Magnetic Field Intensity and Maxwell's Stress Tensor

Equation 4.2.1.3.5 describes the 'air'-gap magneto-motive force that is developed by the stator winding and rotor cage of the propulsion motor. Using this MMF, the radial force on the motor core can be calculated. This radial force will comprise the basis of the structureborne noise source level estimates for the propulsion motor. Tangential, or circumferential, forces act on the conductors of the rotor and stator; however, the transmission of these forces to the motor core is not simple to analyse. Consequently, only radial forces on the motor core are considered. This is not an overly restrictive assumption given the nature of the propulsion motor. The stator and rotor of the propulsion motor are thin cylindrical shells. Hence, it is not entirely inaccurate to be chiefly concerned with radial forces. As a consequence, the circumferential, or "thrust", forces are ignored.

To find the force on the motor core due to the 'air'-gap MMF, the description of the electromechanical stress tensor given in Chapter 3 of reference [19] will be used. Einstein's summation notation is used in these equations. The electromechanical stress tensor follows.

$$T_{ij}=H_iB_j-\frac{1}{2}\delta_{ij}\mu_0H_kH_k \qquad \#1$$

The force arising from this stress tensor is described by the following integral equation.

$$\int_V F_i dV=\oint_S T_{ij}n_j da \qquad \#2$$

In the preceding equations, F_i represents the component of force density in the i^{th} direction. T_{ij} is the component of the stress tensor in the i^{th} direction on the component of the face of the closed surface perpendicular to the j^{th} axis. H_n and B_n represent the components of the magnetic field intensity and magnetic flux intensity, respectively, in the n^{th} direction. δ_{ij} represents the Kronecker delta function. Lastly, n_j and da correspond to the component of the normal to the closed surface of integration in the j^{th} and the area of the closed surface of integration respectively.

For the present, chief interest will be in the force density, F_i. To examine this force density, the stress tensor must be evaluated within the motor core and the 'air'-gap. To simplify this process, two assumptions will be made. The first assumption is that, compared to the 'air'-gap, the motor core is infinitely permeable; therefore, the magnetic field intensity within the motor core is zero. The second assumption is that the magnetic field intensity within the 'air'-gap is entirely oriented in the radial direction. Using these two assumptions and cylindrical coordinates, the components of the resultant stress tensor follow.

$$T_{rr}=H_rB_r-\frac{1}{2}\delta_{rr}\mu_0(H_rH_r+H_\theta H_\theta+H_zH_z) \qquad \#3$$

$$T_{r\theta}=H_rB_\theta-\frac{1}{2}\delta_{r\theta}\mu_0(H_rH_r+H_\theta H_\theta+H_zH_z) \qquad \#4$$

$$T_{rz} = H_r B_z - \frac{1}{2}\delta_{rz}\mu_0 (H_r H_r + H_\theta H_\theta + H_z H_z) \qquad \#5$$

In light of the second assumption made regarding the 'air'-gap magnetic field intensity, only T_{rr} is significant. Furthermore, the linear relationship between the magnetic field intensity and magnetic flux density will be used to simplify the expression for T_{rr}. This expression is shown below.

$$\int_V F_r dV = \oint_S T_{rr} n_r da = \oint_S \frac{1}{2}\mu_0 H_r H_r da \qquad \#6$$

The surface over which this integration will be performed must now be specified. Figure 1, below, shows the surface of this integration. Two surfaces are actually shown, one from within the rotor, the other from within the stator. The resultant force on the motor will be the same.

In subsequent calculations, equations 15, 16, and 17, a surface force density is actually what is found.

$$F_{Az} = \lim_{\Delta x \to 0 \ \Delta y \to 0} \frac{f_z}{\Delta x \Delta y} \qquad \#7$$

Here, F_{Az} is the surface force density. f_z is a z-directed force. Δx Δy represents a vanishingly small area.

$$F_{Az} = \lim_{\Delta x \to 0 \ \Delta y \to 0} \frac{1}{\Delta x \Delta y} \int_V F_z dV \qquad \#8$$

$$F_{Az} = \lim_{\Delta x \to 0 \ \Delta y \to 0} \frac{1}{\Delta x \Delta y} \oint_S \underline{T} \cdot \underline{n} da \qquad \#9$$

This relationship is true for strictly orthogonal coordinate systems. Hence, it would seem that use of cylindrical coordinates would be inappropriate. However, two considerations mitigate this. First, use of cylindrical coordinates will yield the correct result because Δx and Δy are taken in a limit that approaches zero.--The dimension vanishes. Second, the ratio of motor radius to pole-length in the case of the propulsion motor is so large that it approximates strictly orthogonal coordinates over the length of one pole.

$$F_{Ar} = \lim_{\Delta \theta \to 0 \ \Delta z \to 0} \oint_S T_{rr} n_r da \qquad \#10$$

$$\therefore\ f_r = \int_3 F_{Ar}\,da = \int_3 \left(\lim_{\Delta\theta \to 0\ \Delta z \to 0} \frac{1}{\Delta\theta \Delta z} \oint_S T_{rr} n\ da \right) R\,d\theta\,dz \qquad \#11$$

$$f_r = \int_3 T_{rr} n_r\,da \qquad \#12$$

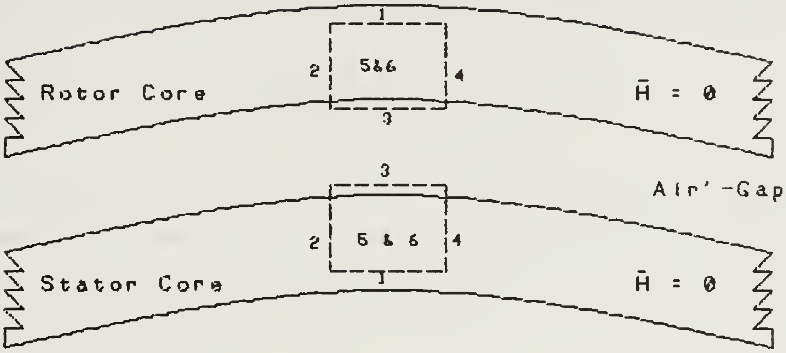

(Numerals denote surfaces. 5 & 6 are at ends of core.)

End View

(Not to scale)

Figure 1 - Surface of Integration for Evaluation of the Stress Tensor

To evaluate equation 6, or 12, now requires knowing H_r. This, though, has already been computed. Equations 4.2.1.1.2 and 4.2.1.1.3 provide the means to calculate H_r.

$$H_r \cdot (2g) = MMF_{\text{air-gap}} \qquad \#13$$

Evaluation of this expression is simple because the 'air'-gap MMF was calculated in the preceding section, equation 4.2.1.3.5.

$$H_r = \frac{MMF_{\text{air-gap}}}{2g} \qquad \#14$$

Substitution of this expression into equation 6 provides the integral which must be evaluated to determine the radial force acting on the motor core.

$$\int_V F_r\,dV = \oint_S \frac{1}{2}\mu_0 \left(\frac{MMF_{\text{air-gap}}}{2g} \right) \cdot \left(\frac{MMF_{\text{air-gap}}}{2g} \right) da \qquad \#15$$

From Figure 1, da is simply the surface area of surface number 3. An expression for the differential area is shown below.

$$da = L_{ag} R d\theta_e \qquad \#16$$

$$\therefore\ f_r = \int_V F_r dV = \int_3 \frac{1}{2}\mu_0 \left(\frac{MMF_{air\text{-}gap}}{2g}\right) \cdot \left(\frac{MMF_{air\text{-}gap}}{2g}\right) L_{ag} R d\theta_e \qquad \#17$$

$$f_r = \frac{\mu_0 L_{ag} R}{8g^2} \int_0^{\pi} (MMF_{air\text{-}gap})^2 d\theta_e \qquad \#18$$

This is the desired result.--The radially directed force on a segment of the motor core can be calculated as a function of time. f_r represents the radially directed force on the segment of the motor core taken in the surface integral shown in Figure 1.

4.2.3 Using the Forces as Input to Acoustic Analysis

Equation 4.2.2.18 describes the force on a segment of the motor core as a function of the 'air'-gap MMF. Hence, this expression provides the required input to a very sophisticated acoustic analysis model. Evaluation of equation 4.2.2.18 provides the force on the motor core as a function of time.--Included in the resultant description of excitation forces are magnitude and phase relationships.

Equation 4.2.2.18, though correct given the underlying assumptions, is not very practical to use. The expression for the 'air'-gap MMF, equation 4.2.1.3.5, is an infinite series. Equation 4.2.2.18 involves squaring an infinite series. Through judicious selection of the circumferential extent of surface number 3 in Figure 4.2.2.1, orthogonality of the spatial harmonics will reduce some of the cross terms resulting from squaring the expression for the 'air'-gap MMF. Nonetheless, all of the cross terms involving the time harmonics in the expression for the 'air'-gap MMF will remain.

In the next section, an estimated structureborne noise source level for the propulsion motor will be developed. This estimation is meant only to provide a quick, simple survey of the dominant noise sources. Hence, many of the cross terms arising from the squaring of the infinite series can be

ignored. If the results of equation 4.2.2.18 are to be used in a sophisticated acoustic analysis, then more terms will have to be retained than will be in the next section.

Two criteria will be used to eliminate terms so that 4.2.2.18 can be evaluated. The first criteria is to eliminate any terms from the expression for the 'air'-gap MMF whose temporal frequency lies outside of the frequency range of "important" noise discussed at the beginning of this chapter. This criteria ignores the effect that multiplying sinusoidal functions has on frequency. Namely, the product of two sinusoidal functions is the sum of a sinusoidal function, whose frequency is equal to the sum of the frequencies of the terms being multiplied, and another sinusoidal function, whose frequency is equal to the difference of the frequencies of the terms being multiplied. In a more accurate analysis, this criteria should be modified.

The second criteria that will be applied will involve the magnitude of the harmonic terms. All terms of a series following the last term which is greater than or equal to one-half of one percent of the fundamental term will be neglected. This criteria may not seem to be too judicious; however, in squaring the magnitudes, the error involved in neglecting such small terms grows even smaller. Once again, in a more accurate analysis, this criteria should be modified.

When considering which terms from equation 4.2.2.18 to keep and which to discard, many different considerations arise. Namely, what are the frequencies for which the acoustic analysis is most accurate? What is the range of "important" frequencies? These are just two of many concerns.

4.2.4 Estimated Baseline Propulsion Motor Source Level

The two criteria discussed in the preceding section are applied to the expression for 'air'-gap MMF, equation 4.2.1.3.5. The first criteria eliminates the time harmonics which lie outside the range of "important" noise developed in section 4.1.2, that is, greater than 11kHz. Any terms whose time dependence is described by $n\omega_e$ will only be considered up to the term corresponding to n equal to 367 because any term with a frequency greater than 367 times 30Hz is beyond the

11kHz upper bound. While this may not seem to be much help in eliminating the number of terms to be carried around, the term including the sum over the number of rotor bars multiplies the terms with the stated time dependence.--Only five terms could possibly be included.

Any terms whose time dependence is described by $m\omega_p$ will be considered through the term with m equal to 4. Any terms whose time dependence is described by $ms\omega_p$ will only be considered up to the term corresponding to m equal to 219. As in the preceding paragraph, the terms with the $ms\omega_p$ time dependence are multiplied by the rotor bar "filter" term, thus reducing the number of terms to be considered.

When the second criteria from the preceding section is applied, the number of terms which must be carried around is decreased even more. Terms multiplied by A_n drop to less than one-half of one percent of A_1 for n greater than 19. (Do not forget than A_n is zero for even and triplen terms.) Terms multiplied by A_m, which is zero for even values of m, drop to less than one-half of one percent of A_{1m} for m greater than 199. Terms multiplied by $I_{bm}^{m}\left(\frac{\cos n\pi - 1}{2\pi p n}\right)N_R$ drop to less than one-half of one percent of the value corresponding to n equal to one for n greater than 23.

After imposing all of these constraints on the indices, the following expression for 'significant' 'air'-gap MMF results. It contains 34 terms.

$$
\begin{aligned}
MMF_{\text{air-gap}} \approx \frac{3}{2} I_p \Big[& A_1 \sin(\theta_e - \omega_s t) + A_5 \sin(5\theta_e + \omega_s t) \\
& + A_7 \sin(7\theta_e - \omega_s t) + A_{11} \sin(11\theta_e + \omega_s t) \\
& + A_{17} \sin(17\theta_e + \omega_s t) + A_{19} \sin(19\theta_e - \omega_s t) \Big] \\
& - I_b \frac{N_R}{\pi p} \cos(\theta_e - \omega_s t - \psi_{\text{split}}) \\
& + 3 I_{\max} C_{1m} \Big[- A_1 \cos(\theta_e - \omega_p t) + A_6 \cos(5\theta_e + \omega_p t) \\
& - A_7 \cos(7\theta_e - \omega_p t) + A_{11} \cos(11\theta_e + \omega_p t) \\
& + A_{17} \cos(17\theta_e + \omega_p t) - A_{19} \cos(19\theta_e - \omega_p t) \Big] \\
& + \frac{N_R}{\pi p} \sum_{m=1}^{21} I_{bb}^{m} \Big[\cos(\theta_e - ((1-s)\omega_s + ms\omega_p)t + \psi'_{-\text{msplit}}) \\
& - \cos(\theta_e - ((1-s)\omega_s - ms\omega_p)t - \psi'_{\text{msplit}}) \Big] \qquad \#1
\end{aligned}
$$

Whereas the method of the TFA model is principally concerned with describing forces within a frequency spectrum, the ‘air’-gap MMF described above is averaged over one pole. The resultant ‘averaged’ MMF can then be squared and subsequently multiplied by the ‘air’-gap surface corresponding to one pole to yield the force on one pole of the motor core.

After taking the spatial average of the ‘air’-gap MMF over one pole, only time-dependence remains. Taking the average of equation 1 yields 24 terms with distinct frequencies. These terms are shown in the table below. To square the ‘air’-gap MMF, these terms are multiplied as in a nested summation. See the expressions which follow the table.

Table 1 - MMF Terms Included in Source Level Estimate

Frequency (Hz)	Magnitude (A-turns)	Description
30	5574	Stator Fundamental
2500	4686	PWM Switching Freq.
21	1180	Rotor Bar/PWM Harmonics
79	1180	
121	393	
179	393	
221	236	
279	236	
321	169	
379	169	
421	131	
479	131	
521	107	
579	107	
621	91	
679	91	
721	79	
779	79	
821	69	
879	69	
921	62	
979	62	
1021	56	

1079	56	

$$<MMF_{air\text{-}gap}> = \sum_{k=1}^{24} C_k \sin(\omega_k t + \zeta_k) \qquad \#2$$

$$(<MMF_{air\text{-}gap}>)^2 = \sum_{k=1}^{24} \left[C_k \cdot \sin(\omega_k t + \zeta_k) \cdot \left(\sum_{q=1}^{24} C_q \cdot \sin(\omega_q t + \zeta_p) \right) \right] \qquad \#3$$

When this expression is evaluated, some 576 terms result. Taking the magnitudes of the resultant sinusoidal functions and grouping them into the octave bands used in the TFA model described by reference [7] and subsequently multiplying those summed magnitudes by the appropriate parameters shown in equation 4.2.2.18 yields a force spectrum. This force spectrum must then be converted into an acceleration level in the motor core in order to provide the structureborne noise source level required for the TFA model.

Converting force levels into acceleration levels requires being able to describe to some degree how the motor core structurally responds to the forces applied to it. Hence, a structural model of the motor core is used to provide the acceleration response to the force level.

The structural model used to determine the acceleration levels of the propulsion model is a simple model. The motor core is considered to be a simply supported flexural beam. The mid-span displacements are taken to provide the acceleration levels. Furthermore, to account for the sea-water which surrounds the motor core the mid-span of the flexural beam is supported by a spring whose spring constant is based on the bulk modulus of sea-water. Additionally, the added-mass effect of the motor core accelerating sea-water is included. The figure shown below represents the model used to determine the acceleration response of the motor core.

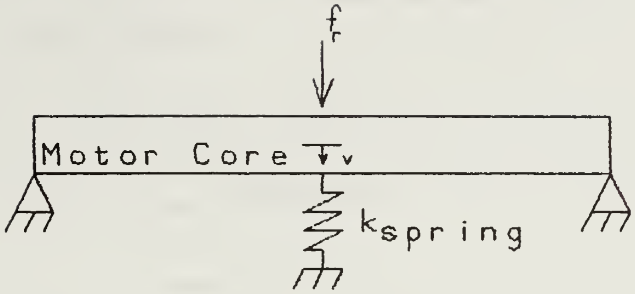

Figure 1 - Structural Model of Motor Core

The equation of motion for the mid-span of the structural model is shown below. The equation ignores damping.--It assumes small deflections so that rotational inertia can be neglected. Only the displacement at mid-span is considered.

$$f_r = (M + m_a)\ddot{v} + (k_{flex} + k_{spring})v \qquad \#4$$

Whereas harmonic functions are being considered here, the expression above can be solved for the acceleration at mid-span. Magnitudes of the response are of chief interest in this stage. Hence, phase information is forsaken.

$$\ddot{v} = -\omega^2 v \qquad \#5$$

$$\ddot{v} = \left(\frac{f_r}{(M + m_a) + \frac{1}{\omega^2}(k_{flex} + k_{spring})}\right) \qquad \#6$$

The mass, M, represents the mass of one-half the circumference of the motor core. The added mass, m_a, is calculated using methods from reference [31].--Using the slender body assumption, the two-dimensional added mass coefficient for a rectangular shape is multiplied by its length. The relationship between force and the displacement due to flexure of the motor core, k_{flex}, is described by reference [42]. The spring

constant of the sea-water is taken to be a linear function of the bulk modulus of elasticity of sea water, k_{spring}. These relationships are shown below.

$$m_a = 4.754\rho_{sw}\left(\frac{1}{2}L_{ag}\right)^2 L_{pole} \qquad \#7$$

$$k_{flex} \sim \frac{384 E_{steel} I_{core}}{5L^3} \qquad \#8$$

$$k_{spring} = E_{sw}\cdot 2L_{ag} \qquad \#9$$

In the expressions above, E represents the modulus of elasticity. I_{core} represents the moment of inertia of the motor core. L_{pole} represents the circumferential length corresponding to one pole.

The fact that one pole of the motor core is immediately adjacent to another pole, which is vibrating with opposite phase, will have an effect on the radiated sound power level. This effect is due to cancellation. By computing, in the far field, the radiated sound power level of a vibrating sphere and comparing it with the radiated sound power level of two spheres, in close proximity, with opposite phase angles, the amount of energy lost through cancellation can be found.

When this calculation is carried out using the relationships developed in Chapter 2 of reference [41], the differences in the radiated sound power level are obvious. There is a pronounced frequency dependence on the difference in sound power levels. In fact, the distance between the spheres will determine at which frequency the sound power levels of the spheres will be additive.

Since the effect of having poles with opposite phase angles in not purely a source level effect, the cancellation effect described above will be added to the source levels. The sum is called the effective source level, L_{eff}.

Table 2 - Dipole Cancellation Effect
(dB)

Octave Band Center Frequency (Hz)

31.5	63	125	250	500	1000	2000	4000	8000
-34	-28	-22	-16	-10	-4	2	8	14

Computing expressions 7, 8, and 9 above, then substituting them into equation 6 yields the estimated acceleration level of the motor core. Once the acceleration level is known, the structureborne source level for the propulsion motor can be calculated. See equation 4.3.1.2 in the next section of this chapter for a discussion. The table below shows the resultant structureborne noise source level for the propulsion motor.

Table 3 - Structureborne Noise Source Level for the Propulsion Motor

(dB re $10^{-3}cm/s^{2}$)

Octave Band Center Frequency (Hz)

Description	31.5	63	125	250	500	1000	2000	4000	8000
EM Noise	14	61	74	89	104	111	144	137	0

The shape of this spectrum of source levels appears to be plausible. The sharp spike in the 2000Hz octave bank is due to the very conservative evaluation of the harmonic content of the stator current.--The magnitude of the square wave distortion is very large in this instance. While this motor may seem noisy compared to the levels given in reference [7], it is a very large motor. Furthermore, no design features have been included for the purpose of reducing noise. Consequently, the source levels shown above can be interpreted to represent something of the very worst case analysis.

A small factor to account for the damping of vibrations in the motor due to the epoxy encapsulation between laminations is included. Any reduction in magnitude due to phase relationships is ignored except for the adjacent pole cancellation effect. The fact that no noise is radiated in the 8000Hz octave band represents the effect of eliminating harmonics prior to calculation of the square of the 'air'-gap MMF. Bearing in mind that the source levels shown above are very approximate, those source levels are used in the comparative analysis. Hence, any results arising from the use of these source levels should be viewed with some degree of skepticism.

4.3 Description of the Simplified Comparison Model

Reference [7] is a design guide which seeks to compute airborne noise levels at various locations throughout a ship. The ultimate goal is the determination of whether or not various noise criteria are met throughout the ship. To accomplish this prediction, reference [7] uses transfer function analysis to relate noise source levels to radiated, airborne noise levels.

The method of TFA used by reference [7] is simplified in the sense that it ignores phase relationships. When discussing transfer functions what is usually meant is a function, which when multiplied by some input, yields an output. Generally, transfer functions contain a phase shift as well as a magnitude amplification factor. TFA ignores the phase relationships. TFA uses decibels in manipulations. Hence, where using transfer functions usually involves complex multiplication, TFA involves addition and subtraction of decibels.

The TFA described by reference [7] distinguishes between airborne and structureborne noise. Airborne noise sources are characterised by a sound power level, L_w. See equation 4.3.1.1. A vibrating machine, an airborne noise source, radiates sound through the generation of pressure waves. The airborne noise level inside of a space depends upon several factors, the strength of the noise sources, the relative locations of the sources, and the acoustic characteristics of the boundaries of the space. Hence, it would be difficult to characterise an airborne noise source in terms of a "loudness", or sound pressure level, independent of the space into which it radiates. Instead, airborne noise sources are described by the rate at which they transmit acoustic energy, the sound power level.

Structureborne noise sources are characterised by acceleration levels, L_m. See equation 4.3.1.2. A vibrating machine will cause vibrations in the structure to which it is attached. It is easier to measure the accelerations set up by vibrating machinery than it is to measure the acoustic energy transmitted into the structure to which the structureborne noise source is attached. Hence, TFA describes airborne noise sources in terms of sound power level and structureborne noise sources in terms of acceleration level.

This research is chiefly concerned with sound that is radiated into the sea. Characterisation of airborne noise sources by a sound power level obviates the need to describe how machinery vibrations are converted into sound radiated into the air. A relationship between structureborne noise and radiated sound must be developed, though, because acceleration levels within a structure reveal nothing of loudness without consideration of geometry and medium.

Noise is not transmitted directly from a noise source into the sea. It must travel from the noise source, within the submarine, to the sea, which, hopefully, is outside of the submarine's hull. Airborne noise within the engineroom, caused by all of the equipment which operates in the engineroom, is transmitted to the hull and then into the sea. Transfer functions which describe the attenuation, or amplification, of the airborne acoustic noise must be used to relate the sound pressure level in the engineroom to the acceleration level in the hull structure and then on to the sound power radiated into the sea.

Structureborne noise must travel from its source, a piece of machinery, through the machinery's mounting, to its foundation, through hull structure, to the location where the sound is radiated into the sea. Hence, transfer functions which describe the transmission of vibration 1) through the machinery mounting, 2) through the machinery foundation, 3) through hull structure, and 4) into the sea, are needed. See equation 4.3.1.

The prediction of radiated noise is arrived at by using the following relationship. It is based on both empirical data and analytic analyses of hypothetical structures.

$$L_W = L_a - TF_{\mathrm{mount}} - TF_{\mathrm{foundation}} - TF_{\mathrm{structure}} + TF_{\mathrm{radiation}} \qquad \#1$$

In this expression, L_w represents the radiated sound power level. L_a represents the acceleration source level for a particular piece of equipment. The transfer functions of the various acoustic transmission path components tell of the effect of the path on noise propagation. This expression is slanted towards an analysis of structureborne noise, which is the principal interest of this research.

Since reference [7] is principally concerned with airborne noise, the transfer function relating the hull acceleration level to sound radiated into the sea is not considered. This transfer function, $TF_{radiation}$, is developed in section 4.3.2.1.4. The development of that transfer function provides a good description of the relationship of TFA to actual pressure fields and structural dynamics. It also points out the nature of the sound pressure level and acceleration level and how phase information is ignored.

Reference [7] provides noise source levels that are based on empirical relationships which are derived from acoustic measurements of existing equipment. The transfer functions describing mountings, namely isolation mountings, and foundations deal with very generalised descriptions of those components of the acoustic transmission path. Here too, empirical data is used. The transfer functions are based on characteristics of isolation mounts and foundations that have been built and tested. The transfer functions describing the transmission of acoustic noise through the ship's structure are based on typical ship construction features.

Reference [7] breaks the frequency spectrum into 9 frequency bands. These bands are called octave bands. They are identified by their center frequency. The different bands are used to provide the description of noise emissions with some notion, however rough, of frequency content.

All of the reference quantities and nomenclature of reference [7] are used in the following adaptation of the TFA model. All of the calculations involved with the TFA model are logarithmic operations.

4.3.1 Development of the Model Sources

The model from reference [7] distinguishes between airborne and structureborne noise sources in its characterisation of the source's strength. Airborne sources are characterised by sound power levels. Structureborne sources are characterised by acceleration levels. Sound power level and acceleration level are described below.

$$L_W = 10\log\left(\frac{W}{W_0}\right) \quad dB \ \ re \ \ W_0 \qquad \#1$$

W represents the sound power generated by the source in Watts. For reference [7], W_o is taken to be $10^{-12}W$.

$$L_a = 20\log\left(\frac{a}{a_o}\right) \quad dB \ re \ a_o \qquad \#2$$

a represents the acceleration level of the structureborne noise source in cm/s^2. For reference [7], a_o is taken to be $10^{-3}cm/s^2$.

The only sources of noise that will be considered during this comparative analysis will be those noise sources which are present in each of the alternative designs and not in the others. This limits the scope of the noise sources to be considered to propulsion system sources. Whereas all of the variants for the comparative study will be nuclear powered with identical nuclear steam generation plants, this source of noise will not be examined.

4.3.1.1 Propulsion Steam Turbine Source Levels

One of the variants in the comparative analysis will be the standard steam turbine driven propulsion plant. Reference [7], sections 6.2.2 and 6.3.2, offers airborne and structureborne emission characteristics of propulsion steam turbines. These are shown below.

The airborne noise characteristics of propulsion steam turbines are shown in the table below. Reference [7] indicates that propulsion steam turbines emit roughly the same noise independent of power rating.

Table 1 - Airborne Noise Source Levels
for Propulsion Steam Turbines
(in dB re $10^{-12}W$)
This table is taken from reference [7]
page 6-10.

Octave Band Center Frequency (Hz)

Description	31.5	63	125	250	500	1000	2000	4000	8000
Airborne Noise	90	95	97	93	93	93	91	90	87

According to reference [7], the structureborne noise characteristics of the propulsion steam turbines are dominated by the reduction gear that it drives. Hence, the reduction gear structureborne noise source level will be taken as the structureborne noise source for the steam turbine/reduction gear combination.

4.3.1.2 Reduction Gear Source Levels

The steam turbine-driven variant for the comparative analysis will use reduction gears to drive the propeller shaft. Hence, its noise source level characteristics will be given.

The baseline airborne noise source level for reduction gears is a function of the power and speed of the reduction gears. The expression for this baseline airborne noise level is shown below, reference [7] equation 6-13.

$$L_{WB} = 69 + 3.4\log(hp) + 3.4\log(rpm) \quad dB \;\; re \;\; 10^{-12} W \qquad \#1$$

To this baseline noise source level are added octave band adjustments to account for variations in source level over the frequency spectrum. The octave band adjustments are shown in the table below.

Table 1 - Octave Band Adjustment (in dB) for
Baseline Reduction Gear Source
Airborne Noise Source Level
This table is taken from reference [7]
page 6-17.

Octave Band Center Frequency (Hz)

Description	31.5	63	125	250	500	1000	2000	4000	8000
Add to Eqn.1	8	9	10	12	14	15	16	12	0

The baseline structureborne noise source level for reduction gears is a function of the rated power of the reduction gears. The expression for this baseline structureborne noise level is shown below, reference [7] equation 6-28.

$$L_{aB} = 47 + 10\log(hp) \quad dB \;\; re \;\; 10^{-3}\frac{cm}{s^2} \qquad \#2$$

To this baseline noise source level are added octave band adjustments to account for variations in source level over the frequency spectrum. The octave band adjustments are shown in the table below.

Table 2 - Octave Band Adjustment (in dB) for
Baseline Reduction Gear Source
Structureborne Noise Source Level
This table is taken from reference [7]
page 6-40.

Octave Band Center Frequency (Hz)

Description	31.5	63	125	250	500	1000	2000	4000	8000
Add to Eqn.2	0	9	3	8	23	33	33	28	18

4.3.1.3 Ship Service Turbo-Generators Source Levels

All of the variants for the comparative analysis will use ship service turbo-generators (SSTG's). The ratings of the SSTG's, though, will change between variants. The electric drive variants will have SSTG's that are capable of generating power on the order of the propulsion load. The steam turbine-driven variant will have SSTG's large enough for the service load only.

The baseline airborne noise source level for SSTG's is a function of the power rating. The expression for this baseline airborne noise level is shown below, reference [7] equation 6-14.

$$L_{WB} = 60 + 10\log(kW) \quad dB \ re \ 10^{-12} W \qquad \#1$$

To this baseline noise source level are added octave band adjustments to account for variations in source level over the frequency spectrum. The octave band adjustments are shown in the table below.

Table 1 - Octave Band Adjustment (in dB) for Baseline SSTG Source Airborne Noise Source Level
This table is taken from reference [7] page 6-18.

Octave Band Center Frequency (Hz)

Description Add to Eqn.1	31.5	63	125	250	500	1000	2000	4000	8000
Static Exciter	2	7	8	12	10	10	11	6	5
Dynamic Exciter	14	10	8	12	10	13	11	7	8

The structureborne noise source level for SSTG's is dominated by the electrical generator that is driven by the steam turbine, reference [7]. Hence, the structureborne noise of an SSTG set will be calculated by computing the structureborne source level for the generator. The generator's structureborne source level will be developed later.

4.3.1.4 Pump Source Levels

The OTHEP propulsion system requires that a large volume of sea-water be circulated through the free-flooding space surrounding the motor. While the pressure differential that the pump which supplies this sea-water must overcome is not great, the capacity is large. Hence, this pump will be included in the acoustic comparison. In addition to the pump itself, the motor or turbine that drives the pump must be included, reference [7] page 6-18. The other variants of the comparative analysis will require that pumps for cooling and lubrication be included in the radiated noise prediction calculations.

The baseline airborne noise source level for pumps is a function of the power rating of the drive motor and the speed of the pump. The expression for this baseline airborne noise level is shown below, reference [7] equation 6-15.

$$L_{WB} = 15 + 10\log(hp) + 15\log(rpm) \quad dB \ \ re \ \ 10^{-12} W \qquad \#1$$

To this baseline noise source level are added octave band adjustments to account for variations in source level over the frequency spectrum. The octave band adjustments are shown in the table below.

Table 1 - Octave Band Adjustment (in dB) for
Baseline Pump Source Airborne
Noise Source Level
This table is taken from reference [7]
page 6-19.

Octave Band Center Frequency (Hz)

Description Add to Eqn.1	31.5	63	125	250	500	1000	2000	4000	8000
Centrifugal Pump	25	25	26	26	27	29	26	23	18
Gear Pump	35	35	36	36	37	39	36	33	28
Cavitating Pump	0	0	0	1	3	6	10	13	5

The baseline structureborne noise source level for pumps is a function of the rated power of the drive motor. The expression for this baseline structureborne noise level is shown below, reference [7] equation 6-29.

$$L_{aB} = 60 + 10\log(hp) \quad dB \;\; re \;\; 10^{-3}\frac{cm}{s^2} \qquad \#2$$

To this baseline noise source level are added octave band adjustments to account for variations in source level over the frequency spectrum. The octave band adjustments are shown in the table below.

Table 2 - Octave Band Adjustment (in dB) for Baseline Pump Source Structureborne Noise Source Level
This table is taken from reference [7] page 6-41.

Octave Band Center Frequency (Hz)

Description Add to Eqn.2	31.5	63	125	250	500	1000	2000	4000	8000
Centrifugal Pump	0	8	21	19	23	24	20	24	23
Gear Pump	10	21	34	32	37	38	34	44	45

4.3.1.5 Electric Motor and Generator Source Levels

All of the variants for the comparative study will use generators. The electric drive variants will also have large propulsion motors. Additionally, the drive motor for the sea-water circulation pump for the OTHEP free-flooding space, as well as all of the other pump drive motors, will be taken to be an electric motor. The source levels for the electric machinery are developed here. The source level for the OTHEP propulsion motor is developed in the preceding section, section 4.2.4.

4.3.1.5.1 Generator Source Levels

The baseline airborne noise source level for electrical generators is a function of the power rating and the speed. Static excitation is assumed here. The expression for this baseline airborne noise level is shown below, reference [7] equation 6-17.

$$L_{WB} = 34 + 10\log(kW) + 7\log(rpm) \quad dB \ \ re \ \ 10^{-12}W \qquad \#1$$

To this baseline noise source level are added octave band adjustments to account for variations in source level over the frequency spectrum. The octave band adjustments are shown in the table below.

Table 1 - Octave Band Adjustment (in dB) for
Baseline Generator Source Airborne
Noise Source Level
This table is taken from reference [7]
page 6-24.

Octave Band Center Frequency (Hz)

Description	31.5	63	125	250	500	1000	2000	4000	8000
Add to Eqn.1	8	11	12	13	13	10	8	5	0

For dynamic exciters, an additional 5 dB must be added to the octave band which will contain the exciter slot frequency, reference [7] page 6-24.

The baseline structureborne noise source level for electrical generators is a function of the rated power and speed of the generator. The expression for this baseline structureborne noise level is shown below, reference [7] equation 6-32.

$$L_{aB} = 42 + 10\log(kW) + 7\log(rpm) \quad dB \ re \ 10^{-3}\frac{cm}{s^2} \qquad \#2$$

To this baseline noise source level are added octave band adjustments to account for variations in source level over the frequency spectrum. The octave band adjustments are shown in the table below.

Table 2 - Octave Band Adjustment (in dB) for
Baseline Generator Source
Structureborne Noise Source Level
This table is taken from reference [7]
page 6-44.

Octave Band Center Frequency (Hz)

Description	31.5	63	125	250	500	1000	2000	4000	8000
Add to Eqn.2	0	11	14	14	16	17	18	18	18

4.3.1.5.2 Motor Source Levels

The baseline airborne noise source level for electrical motors is a function of the power rating and the speed.

Drip-proof, totally enclosed motors are assumed here. The expression for this baseline airborne noise level is shown below, reference [7] equation 6-18.

$$L_{WB} = 5 + 13\log(hp) + 15\log(rpm) \quad dB\ re\ 10^{-12} W \qquad \#1$$

To this baseline noise source level are added octave band adjustments to account for variations in source level over the frequency spectrum. The octave band adjustments are shown in the table below. The allowance for drip-proof enclosures, reference [7] page 6-25, has been included.

Table 1 - Octave Band Adjustment (in dB) for
Baseline Motor Source Airborne
Noise Source Level
This table is taken from reference [7]
page 6-24.

Octave Band Center Frequency (Hz)

Description	31.5	63	125	250	500	1000	2000	4000	8000
Add to Eqn.1									
AC Motor	-5	-4	0	4	5	5	4	-2	-9
DC Motor	-10	-10	-5	0	5	5	4	-2	-9

The baseline structureborne noise source level for electrical motors is more easily given in the form of an envelope which the motor is not likely to exceed. The table showing the limit of this baseline structureborne noise level is shown below, reference [7] table 6-41 and 6-42.

Table 2 - AC and DC Electric Motor
Structureborne Noise Source Levels
(dB re 10^{-3}cm/s^{2})
This table is taken from reference [7]
page 6-44.

Octave Band Center Frequency (Hz)

Description	31.5	63	125	250	500	1000	2000	4000	8000
AC Motor	92	92	92	92	92	92	92	92	92
DC Motor	74	75	76	80	83	84	80	81	82

4.3.2 Transmission Path Models

Reference [7] was developed principally to determine airborne noise levels in an effort to detect spaces where noise was a problem from the perspective of concern for the hearing of humans in those spaces. Hence, reference [7] spends a lot of effort discussing airborne noise paths. The comparative analysis being developed in this research is not so concerned with airborne noise paths.

Two noise paths will be considered in the comparative acoustic analysis. The first path is the airborne to structureborne path. In this path, airborne noise is transferred to the structure. The second path is a wholly structureborne path.

Each of these paths involves transfer functions which account for losses differently. Hence, the effect of the paths on the transmitted noise will be developed separately.

The goal for each path will be to develop a transfer function which when subtracted from the structureborne source level provides an acceleration level at the radiation location. The transfer function (or transmission loss) for each portion of the path is added arithmetically, then the sum is subtracted from the source level.

4.3.2.1 Structureborne Noise Transmission

The source levels given in section 4.3.1 are for the respective pieces of equipment independent of the foundations or mountings upon which they sit. Here the path that the noise takes, from the piece of equipment through the attachments, the foundation, the ship's structures and to the location of hull radiation, will be characterised.

The path from a noise source to its point of radiation must be considered for each noise source. Since the path corresponding to each source can be different, the means to calculate a transfer function which describes a particular path must include provisions for all of the possible segments of that path. Hence, this section considers separately the transfer functions for the different path components.

Consider the following example. Suppose the structureborne noise from a motor travels 1) through the mount which attaches the motor to its foundation, 2) through the motor's foundation, 3) along a segment of deck plating, 4) around a 90° joint into bulkhead plating, 5) along the bulkhead plating, and 6) to the hull plating where it is radiated into the sea. In this instance, the transfer function of the entire structureborne path will be the sum of the six given path components. Accordingly, this section offers the transfer functions for mountings, foundations, hull structures (plating, stanchions, and junctions) and radiation into the sea.

4.3.2.1.1 Machinery Attachments

These components comprise how the piece of equipment in question is attached to its foundation. The attachments can amount to hard mounting or can include different types of sound isolation. The desired transfer function relates the acceleration level of the source equipment to the vibration level it produces in the top of the foundation.

Prior to discussion of the transfer function for the different mounting methods, reference [7] discusses how equipment is categorised according to weight. Class I includes equipment that weighs less than 0.45tons (1000lbs). Class II equipment weighs between 0.45 (1000lbs) and 4.46tons (10,000lbs). Class III equipment weighs more than 4.46tons (10,000lbs). The weight of a piece of equipment, in large part, dictates the type of mounting that can be used.

Reference [7] also discusses the two categories of foundations. Type A foundations are relatively light, pipe foundations. Type B foundations are heavier, plate foundations.

The class of equipment will invariably have an effect on which type of foundation is used. The table shown below gives the transfer function for hard mounted machinery.

Table 1 - Transfer Function for
Hard Mounted Machinery (in dB)
This table is taken from reference [7]
page 7-47.

Octave Band Center Frequency (Hz)

Description FT / MC		31.5	63	125	250	500	1000	2000	4000	8000
A	I	6	6	6	6	6	6	6	6	6
A	II	5	4	4	4	4	4	4	4	4
B	I	13	10	8	6	6	6	6	6	6
B	II	9	7	6	5	5	5	5	5	5
B	III	5	4	3	3	3	3	3	3	3

FT = Foundation Type MC = Machinery Weight Class

Machinery in submarines is rarely hard mounted to the hull. Reference [7] discusses three types of isolation mountings. The first type is high-frequency isolation mountings. The second type is low-frequency isolation mountings. The third type is two-stage isolation systems. Each type of mounting has its transfer function developed separately.

High frequency isolation mountings are usually distributed mountings. That is, the equipment rests on pads of material that has flexibility and damping appropriate to reduction of high frequency vibrations. These mountings are called distributed isolation material (DIM) pads. Their transfer function is shown in the table below.

Table 2 - Transfer Function for
Distributed Isolation Material Mounts (in dB)
This table is taken from reference [7]
page 7-48.

Octave Band Center Frequency (Hz)

Description FT / MC		31.5	63	125	250	500	1000	2000	4000	8000
A	I	6	6	6	7	8	9	10	10	10
A	II	5	4	4	4	4	4	5	6	8
B	I	13	11	9	8	10	15	15	15	15
B	II	9	7	7	6	8	8	9	10	10
B	III	5	4	3	2	3	3	4	5	8

FT = Foundation Type MC = Machinery Weight Class

Low frequency isolation mountings are sometimes called resilient mounts. These mounts are designed to isolate the vibrations of a specific piece of equipment. The isolation mount design takes into account the weight of the mounted system and the stiffness of the mounts.

These low frequency isolation mounts are essentially oscillatory systems described by second order equations of motion. Hence, they possess a natural frequency. Were the mount to be excited by vibrations at a frequency close to the natural frequency of the mount, then the mount may very well amplify the vibrations. Hence, it is vital to know the frequencies of vibration of the piece of equipment to be mounted and the natural frequency (or resonance frequency) of the total system before a transfer function can be developed.

It is possible, though, to characterise low frequency isolation mountings. Reference [7], section 7.3.1.3, indicates that for typical shipboard systems, the resonance frequencies of the mounted systems are less than 15Hz. Hence, the table shown below will provide transfer functions for low frequency isolation mounts.

Table 3 - Transfer Function for
Low-Frequency Mounts (in dB)
This table is taken from reference [7]
page 7-49.

Octave Band Center Frequency (Hz)

Description FT / MC		31.5	63	125	250	500	1000	2000	4000	8000
A	I	9	14	20	23	25	25	25	25	25
A	II	4	8	12	14	17	20	20	20	20
B	I	20	25	30	30	30	30	30	30	30
B	II	12	16	20	23	25	25	25	25	25
B	III	8	12	13	14	15	18	20	20	20

FT = Foundation Type MC = Machinery Weight Class

The two-stage isolation mounting is essentially two low frequency isolation mounts in series. It consists of the source machinery being resiliently mounted to an intermediate plate. The intermediate plate is itself mounted to the foundation by means of low frequency isolation mounts.

The two-stage isolation mounts have resonance frequencies just as did the low frequency mounts. In the case of two-stage isolation mounts though, the machinery connected to the intermediate plate will have a resonance frequency of its own, above the resonance frequency of the intermediate plate mounting system. This tends to increase the natural frequency of the entire mounting system.

Just as with the low frequency mounts it is possible, though, to characterise two-stage isolation mountings. Reference [7], section 7.3.1.4, indicates that for typical shipboard systems, the resonance frequencies of the entire two-stage systems are less than 30Hz. Hence, the table shown below will provide transfer functions for two-stage isolation mounts.

Table 4 - Transfer Function for
Two-Stage Mounting Systems (in dB)
This table is taken from reference [7]
page 7-51.

Octave Band Center Frequency (Hz)

Description FT / MC		31.5	63	125	250	500	1000	2000	4000	8000
A	I	20	25	30	35	40	45	45	45	45
A	II	15	22	27	32	35	40	45	45	45
B	I	25	33	40	45	50	50	50	50	50
B	II	22	30	35	40	45	48	50	50	50
B	III	20	25	30	35	40	45	50	50	50

FT = Foundation Type MC = Machinery Weight Class

4.3.2.1.2 Foundations

Transfer functions for a foundation relate the vibration level at the point of attachment of the mounting at the top of the foundation to the vibration level at the ship structure at the bottom of the foundation. The types of foundation that are considered are the two types described in the beginning of the preceding section.

It is important to note that if a piece of machinery is directly mounted to the ship's structure, then there is no transfer function (TF = 0) related to the foundation, reference [7] page 7-51.

The transfer function, or transmission loss in this instance, for the two types of foundation are shown in the table below. Negative transmission loss values are interpreted to mean that the foundation is excited at a resonant frequency.

Table 1 - Transmission Losses for Foundations
(in dB)
This table is taken from reference [7]
page 7-53.

Octave Band Center Frequency (Hz)

Description	31.5	63	125	250	500	1000	2000	4000	8000
Found. Type									
A	-8	-11	-11	-8	-5	-5	-5	-1	-1
B	-13	-16	-16	-13	-10	-8	-5	-2	0

4.3.2.1.3 Ship Hull Structures

Reference [7] breaks ship structures into three groups. The first group consists of the structures that lie within an area derived from the area of the "footprint" of the exciting equipment. The second group consists of the structure through which the vibrations must be transmitted. The third group consists of intersections of structure through which the vibrations must be transmitted. Each of these three groups will be discussed in turn.

A transfer function describing the transmission losses within what is called the "effective source area" is not developed. Here it is assumed that the vibrations are equal to the vibrations at the bottom of the foundation. Instead, though, it is necessary to develop a measure of the "effective source area".

Reference [7] develops the "effective source area" in the following way. Consider the "footprint" of the machinery that is the noise source. The "footprint" is the area covered by the base of the foundation. To get the "effective source area", reference [7] includes three feet beyond each side of the "footprint" in its computation of the "effective source area". Presumably this is an empirically observed effect in typical ship installations. The measured area of the expanded "footprint" is called the "effective source area" and represented by A_s.

The transfer function for ship structures through which vibrations are transmitted depends upon the location of the source equipment and whether or not the structure is wetted, that is, in contact with the sea. Equation 1 below describes the transfer function for transmission through structures within the compartment where the source is located. Equation 2 below describes the transfer function for transmission through structures outside of the source compartment. Both equations are taken from reference [7] page 7-56.

$$TF = 10\log\left(\frac{r}{r_f}\right) + \beta(r - r_f) \quad dB \qquad \#1$$

$$TF = \beta \times l \quad dB \qquad \#2$$

r_f is the distance from the center of the "footprint" to the edge of the source compartment, in feet. r is the distance from the center of the "footprint", in feet. l is the path length in spaces outside of the source compartment, in feet. β is the dissipative loss coefficient, in dB per foot. β can be increased, thus reducing transmitted noise, by applying damping materials to the ship's structure. This will not be considered in the comparative study. β does depend on whether or not the ship's structure is wetted. Shown below is a table describing β.

Table 1 - Dissipative Loss Coefficient β for
Undamped Ship Structures
(in dB per foot)
This table is taken from reference [7]
page 7-56.

Octave Band Center Frequency (Hz)

Description	31.5	63	125	250	500	1000	2000	4000	8000
Unwetted Deck	0.4	0.4	0.4	0.4	0.4	0.4	0.4	0.4	0.4
Wetted Hull	0.3	0.3	0.3	0.3	0.3	0.3	0.3	0.3	0.3

Transmission of vibrations through stanchions is somewhat different from the paths through plating. Transverse and compressive wave propagation are present. The table below shows the transfer function, that is transmission loss, for transmission of vibration through stanchions.

Table 2 - Transmission Loss for Stanchions
(in dB)
This table is taken from reference [7]
page 7-60.

Octave Band Center Frequency (Hz)

Description	31.5	63	125	250	500	1000	2000	4000	8000
TF	0	0	1	1	1	1	2	2	2

Transmission of vibrations around a right angle in the ship structure or through an intersection at a right angle is discontinuous. Hence, transmission losses are associated with intersections of the ship structure. Reference [7] describes these transmission losses for "T" junctions and cross junctions. These transmission losses are shown in the figures and tables below.

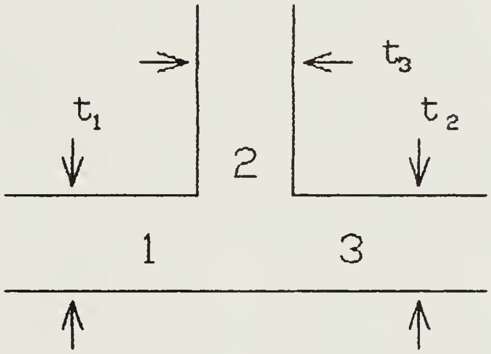

Figure 1 - "T" Junctions in Ship Structure

Table 3 - Structureborne Noise Transmission Loss for "T"-Junctions of Steel of Aluminum of Various Thicknesses (in dB)
This table is taken from reference [7] page 7-58.

Straight-Through Vibration Transmission Loss (dB)

Plate 2 Thickness (in.)

		1/4	3/8	1/2	5/8	3/4	1
	1/4	7	11	15	19	23	29
Plates	3/8	5	7	10	13	16	21
1 and 3	1/2	5	6	7	9	11	16
Thicknesses	5/8	5	5	6	7	9	12
(in.)	3/4	5	5	5	6	7	10
	1	4	5	5	5	6	8

Right-Angle Vibration Transmission Loss (dB)

Plate 2 Thickness (in.)

		1/4	3/8	1/2	5/8	3/4	1
	1/4	7	9	12	15	17	22
Plates	3/8	6	7	8	10	12	16
1 and 3	1/2	7	6	7	8	9	12
Thicknesses	5/8	7	6	6	7	9	12
(in.)	3/4	8	7	6	6	7	8
	1	9	8	7	6	6	7

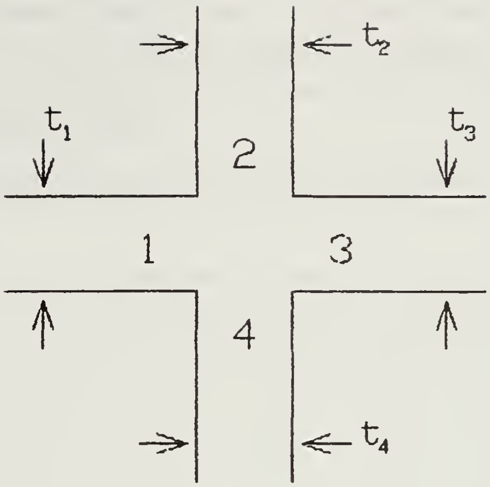

Figure 2 - Cross-Junctions in Ship Structure

Table 4 - Structureborne Noise Transmission Loss for
Cross-Junctions of Steel of Aluminum of
Various Thicknesses (in dB)
This table is taken from reference [7]
page 7-59.

Straight-Through Vibration Transmission Loss (dB)

Plates 2 and 4 Thickness (in.)

		1/4	3/8	1/2	5/8	3/4	1
	1/4	9	15	20	25	22	35
Plates	3/8	6	9	13	17	20	26
1 and 3	1/2	5	7	10	12	15	20
Thicknesses	5/8	5	6	8	10	12	16
(in.)	3/4	5	5	6	8	10	14
	1	4	5	5	6	7	10

Right-Angle Vibration Transmission Loss (dB)

Plates 2 and 4 Thickness (in.)

		1/4	3/8	1/2	5/8	3/4	1
	1/4	9	13	16	20	23	27
Plates	3/8	7	9	12	14	16	21
1 and 3	1/2	7	8	9	11	13	16
Thicknesses	5/8	8	7	8	9	10	14
(in.)	3/4	8	7	8	8	9	12
	1	9	8	7	7	8	8

4.3.2.1.4 Radiation into the Sea

Reference [7] seeks to determine airborne noise. This research seeks to determine noise that is radiated into the sea. Hence, the transfer function which describes the radi-

ation of plate vibrations into the sea is where this research diverges from reference [7]. This research will build on the development of plate radiation into air by reference [7].

Reference [7] develops a transfer function which relates the acceleration level in the structure to the sound power level radiated into the air. This transfer function is shown below.

$$TF = L_W - L_a = 10\log(A_p) + 10\log(\sigma_{rad}) + 10\log(n) - 20\log(f) + 20 \quad dB \qquad \#1$$

L_W is the radiated sound power level. L_a is the acceleration level within the radiating panel. A_p represents the area of a radiating panel. n is the effective number of radiating panels. f is the octave band center frequency. σ_{rad} is the radiation efficiency of the panel.

This transfer function is for a plate radiating into air. This research must adapt this transfer function to predict how vibration levels in a plate will radiate into sea-water.

Adapting the transfer function relationship is accomplished by deriving the sound power level radiated by a vibrating infinite flat plate. Reference [13] gives the expression for the pressure field associated with a vibrating infinite flat plate. This expression is shown below.

$$p(x,z) = \frac{\rho_0 \omega v_0}{\sqrt{k^2 - k_s^2}} \cos(k_s x) e^{i\sqrt{k^2-k_s^2}\,z} e^{-i\omega t} \qquad \#2$$

ρ_0 represents the mass density of sea-water. ω represents the frequency of the vibration. k is the wave number corresponding to the vibration frequency. x represents location along the surface of the plate. z represents distance away from the plate. $v_0\cos(k_s x)$ represents the velocity of the plate surface. k_s is the wave number associated with the deflections of the plate.

This equation points out three different regions of excitation of the plate. Consider the exponential expression describing the z-dependence of the pressure distribution. Of vital importance to the structure of the z-dependence is the value of $\sqrt{k^2 - k_s^2}$.

If $k < k_{mn}$, then the exponential term is raised to a negative real value. This indicates that the pressure field has an amplitude that decays exponentially with distance from the plate. This type of radiation occurs "below coincidence". In this context, "coincidence" refers to the acoustic wavelength being equal to the structural wavelength.

If $k = k_{mn}$, then the exponential term has no z-dependence because it is raised to zero. This indicates that the pressure field has constant magnitude out to infinity.--While this is not physically true, it does indicate an efficient radiation condition. In this context, the acoustic wavelength and structural wavelength are "coincident", meaning equal.

If $k > k_{mn}$, then the exponential term is raised to an imaginary power. This indicates an oscillatory z-dependence. Taken in combination with the time dependence, the pressure field is a travelling wave. This region of radiation is said to be "above coincidence" meaning the acoustic frequency is greater than the structural coincidence (resonance) frequency.

The solution to the radiated pressure field is very different in each of these three regions. Hence, they are treated differently as in references [7] and [13]. The first step to determining which of the three regions is involved is to determine the coincidence frequency of the radiating panel on the ship.

Reference [7] gives an expression for the coincidence frequency of plating. This expression, though, is for a panel vibrating in air. A panel vibrating in water will have a much different structural response. Shown below is the approximate expression for coincidence frequency of a plate in air, from reference [7].

$$f_c = \frac{450}{h} \ Hz \qquad \text{and} \qquad \lambda_c = 2.4h \ \ ft \qquad \#3$$

In this expression, h is the thickness of the panel's plating in inches. Reference [13] gives an approximate expression for the coincidence frequency of steel plating in water. This expression is shown below.

$$f_c = \frac{9300}{h}\ Hz \qquad \text{and} \qquad \lambda_c = 0.529h\ \ ft \tag{#4}$$

h retains the same units (inches) in both expressions. However, the second expression accounts for differences in the contribution to stiffness and damping that the sea-water makes to the structural response of the plating. The second expression also accounts for the difference in the speed of sound in air (330m/s) and the speed of sound in sea-water (1500m/s). In the comparative analysis of this research the second expression, from reference [13], will be used to determine the coincidence frequency of a radiating panel.

Now that the means to identify the three regions of radiation efficiency for radiating panels has been established for radiation into the sea, the development of the other terms of the expression for the radiation transfer function can proceed.

From the expression for the pressure field in equation 2, the acceleration level and sound power level must be extracted. First, though, the pressure expression must be cast into decibel form. This requires using an amplitude for the x and z-dependence of the pressure expression.

$$p(x,z) = \frac{\rho_0 \omega v_0}{k_s\sqrt{\left(\frac{k}{k_s}\right)^2 - 1}} \cos(k_s x) e^{i\sqrt{k^2-k_s^2}\,z} e^{-i\omega t} \tag{#5}$$

The amplitude of the pressure ‘wave’ can be considered to be of the form below.

$$p = \frac{\rho_0 \omega v_0}{k_s\sqrt{\left(\frac{k}{k_s}\right)^2 - 1}} \tag{#6}$$

The mean acoustic intensity, I, is a function of the velocity amplitude and the pressure amplitude. Reference [41] gives an expression for the mean acoustic intensity as a function of the pressure and velocity amplitude. This relationship is shown below.

$$<\underline{I}> = <Re(p)Re(v)> = \frac{\rho_0 \omega v_0^2}{k_s\sqrt{\left(\frac{f}{f_c}\right)^2 - 1}} \tag{#7}$$

The pressure amplitude and velocity amplitude, as described above, are inherently real. The mean acoustic intensity is now used to determined the radiated sound power. Once again, reference [41] provides the tool to evaluate the sound power. In this instance, sound power is the mean sound intensity integrated over the area of its radiation. In this instance, the area is that of a radiating panel.

$$W = \int_S \langle \underline{I} \rangle \cdot \underline{dS} = \frac{\rho_0 \omega \upsilon_0^2}{k_c \sqrt{\left(\frac{f}{f_c}\right)^2 - 1}} \cdot A_p \qquad \#8$$

Now that the power radiated is known, the sound power level can be calculated.

$$L_W = 10\log\left(\frac{\rho_0 \omega \upsilon_0^2 A_p}{k_c \sqrt{\left(\frac{f}{f_c}\right)^2 - 1}} \frac{1}{W_0} \right) \qquad \#9$$

To obtain the transfer function, as described in equation 1, L_a must be extracted from the expression for the sound power level above. To this requires the use of the expression relating acceleration level and velocity level, L_v. This expression is shown below.

$$L_a = L_v + 20\log(f) - 44 \quad dB \;\; re \;\; 10^{-3}\frac{cm}{s^2} \qquad \#10$$

$$L_v = 20\log\left(\frac{\upsilon}{\upsilon_{ref}}\right) \quad dB \;\; re \;\; \upsilon_{ref} \qquad \#11$$

Using the second expression, L_v can be extracted from the expression for the sound power level.

$$L_W = 10\log\left(\frac{A_p}{1\,ft^2}\right) + 10\log\left(\rho_0 c \frac{\frac{f}{f_c}}{\sqrt{\left(\frac{f}{f_c}\right)^2 - 1}} \frac{\upsilon_{ref}^2\, 1\,ft^2}{W_0} \right) + L_v \quad dB \;\; re \;\; W_0 \qquad \#12$$

Next, the acceleration level will be introduced in place of L_v.

$$L_W = 10\log\left(\frac{A_p}{1\,ft^2}\right) + 10\log\left(\frac{\frac{f}{f_c}}{\sqrt{\left(\frac{f}{f_c}\right)^2 - 1}} \right) + 10\log\left(\rho_0 c \frac{\upsilon_{ref}^2\, 1\,ft^2}{W_0} \right) + L_a - 20\log(f) + 44 \quad dB re W_0$$

$$\#13$$

From this expression, the transfer function for the panel radiation can be extracted.

$$TF = L_W - L_a \qquad \#14$$

$$\therefore TF = 10\log\left(\frac{A_p}{1ft^2}\right) + 10\log\left(\frac{\frac{f}{f_c}}{\sqrt{\left(\frac{f}{f_c}\right)^2 - 1}}\right) - 20\log(f) + 10\log\left(\rho_0 c\frac{v_{ref}^2 1ft^2}{W_0}\right) + 44dBreW. \qquad \#15$$

This equation is in the precise form as the transfer function described by reference [7] and given in equation 1. There are several differences to be pointed out, though. The term that accounts for the possibility of there being multiple radiating panels being excited by the vibration is the 10log(n) that appears in equation 1 but not equation 15. Equation 15 is for a single radiating panel.

The term that includes the reference quantities, the fourth term on the right-hand side of equation 15, has a big impact on the use of this equation to determine radiation into water. The reference quantities are there to ensure the dimensionless nature of the logarithmic quantities. The $\rho_0 c$ term characterises the medium into which the panel radiates. For radiation into air, substitution of 347m/s for c and 1.270kg/m^3 for the density of air yields the exact 20 dB constant term that appears in equation 1. This constant changes for panel radiation into sea-water. In the case of radiation into sea-water, the constant term becomes 55.6dB for a c of 1500m/s and a ρ_0 of 1027.6kg/m^3. This represents a much improved transformation of panel acceleration into radiated sound power than for a panel radiating into air.

The final term to be discussed is very important. That term is the radiation efficiency, σ_{rad}. The radiation efficiency appearing in equation 15 is derived from the case of the infinite flat plate. Although it has not been stated explicitly, by using the 'amplitude' of the pressure wave in equation 6 in the derivation of equation 15, radiation above coincidence has been implicitly assumed. This is because 'amplitudes' are meaningful only for periodic, hence oscillatory, functions. Therefore, the radiation efficiency, σ_{rad}, must be considered for the three regions of radiation.

Reference [7] takes the approach of modifying σ_{rad} for the three cases of above, below and near coincidence. The radiation efficiency appearing in equation 15, $\left(\frac{\frac{f}{f_c}}{\sqrt{\left(\frac{f}{f_c}\right)^2-1}}\right)$ does not depend upon the medium into which the panel is radiating except in the determination of the coincidence frequency. Hence, the radiation efficiencies developed in reference [7] need only be slightly adapted to serve as the radiation efficiencies of the panels radiating into the sea.

Above coincidence, the radiation efficiency will be precisely equal to that developed for equation 15.

Slightly below coincidence, the radiation efficiency will be altered to reflect the relative values of k and k_{mn}. This radiation efficiency still has the infinite plate as its physical model. Shown below is the radiation efficiency.

$$\sigma_{rad} = \frac{\frac{f}{f_c}}{\sqrt{1-\left(\frac{f}{f_c}\right)^2}} \qquad \#16$$

Significantly below coincidence, the use of an infinite flat plate as a physical model becomes fallacious. Hence, effects of finite plates enter the radiation efficiencies. Two effects dominate the radiated pressure field, which for an infinite plate diminishes exponentially with distance from the plate. These two effects are edge and corner radiation. Reference [7] provides a means to calculate the effects of edge and corner radiation.

First, the radiation efficiency corresponding to edge radiation will be described. The relationship describing edge radiation is derived from the descriptions given in reference [7], pages 7-63 and 7-65. It is shown in the equation below.

$$\sigma^{e}_{rad} = \frac{P\lambda_c}{A_p}\left(\frac{\sqrt{\frac{f}{f_c}}}{\pi^2\left(1-\frac{f}{f_c}\right)^{\frac{3}{2}}}\right) \qquad \#17$$

Here, P represents the perimeter of the radiating panel. λ_c represents the structural wavelength at coincidence. But for the determination of the wavelength at coincidence, this radiation efficiency is not dependent upon the medium into which the acoustic power is being radiated.

The radiation efficiency corresponding to corner radiation will be described in the equation below. The relationship describing corner radiation is derived from the descriptions given in reference [7], pages 7-63 and 7-66. It is shown in the equation below.

$$\sigma^{c}_{rad} = \frac{\lambda_c^2}{A_p}\left(\frac{1-\frac{f}{f_c}}{4\pi\sqrt{\frac{f}{f_c}}}\right) \qquad \#18$$

The same comments regarding the effect of the medium on the edge radiation efficiency can be made about the corner radiation efficiency. The total radiation efficiency well below coincidence is simply the sum of the edge and corner radiation efficiencies.

$$\sigma_{rad} = \sigma^{e}_{rad} + \sigma^{c}_{rad} \qquad \#19$$

Summary of Radiation of Structureborne Noise into Sea-Water

$$TF = 10\log\left(\frac{A_p}{1\,ft^2}\right) + 10\log(\sigma_{rad}) + 10\log(n) - 20\log(f) + 55.6\,dB \qquad \#20$$

Above Coincidence - $f > f_c$

$$\sigma_{rad} = \left(\frac{\frac{f}{f_c}}{\sqrt{\left(\frac{f}{f_c}\right)^2 - 1}}\right) \qquad \#21$$

Near Coincidence - $0.75f_c < f < f_c$

$$\sigma_{rad} = \left(\frac{\frac{f}{f_c}}{\sqrt{1 - \left(\frac{f}{f_c}\right)^2}}\right) \qquad \#22$$

Below Coincidence - $f < 0.75f_c$

$$\sigma_{rad} = \left[\frac{P\lambda_c}{A_p}\left(\frac{\sqrt{\frac{f}{f_c}}}{\pi^2\left(1 - \frac{f}{f_c}\right)^{\frac{3}{2}}}\right)\right] + \left[\frac{\lambda_c^2}{A_p}\left(\frac{1 - \frac{f}{f_c}}{4\pi\sqrt{\frac{f}{f_c}}}\right)\right] \qquad \#23$$

To determine the coincidence frequency, use the following equation.

$$f_c = \frac{9300}{h}\ Hz \qquad \text{and} \qquad \lambda_c = 0.529h\ \ ft \qquad \#24$$

In equation 20, f refers to the octave band center frequency. See the preceding sections for a discussion of units.

4.3.2.2 Airborne to Structureborne Noise Transmission

Airborne noise can excite structures into vibrating. This can serve as a source of structural acceleration. Hence, the approach developed in reference [7] is used to provide a transfer function describing the vibration of structure in response to airborne vibration.

The transfer function for unwetted steel relates the acceleration level, L_a, to the sound pressure level, L_p, in the compartment under consideration. The expression, equations 7-22 and 7-23 from reference [7], is shown below.

$$TF = -57 - 50\log(h) + 20\log(A_p) + 10\log(f) + 10\log(\sigma_{rad}) - 30\log(a) \quad dB \qquad \#1$$

$$\text{or} \quad TF = 0 \quad dB \ \text{(whichever is smaller)} \qquad \#2$$

h represents the panel thickness in inches. A_p represents the area of a panel in square feet. f is the octave band center frequency. σ_{rad} is the same radiation efficiency calculated in the preceding section. a is the panel length to width ratio. Care must be taken, though, in the computation of f_c. In the case of unwetted steel, the approximate relationship given in reference [7] equations 7-20 and 7-21 must be used.

The transfer function for wetted steel relates the acceleration level, L_a, to the sound pressure level, L_p, in the compartment under consideration. The expression, equation 7-26 from reference [7], is shown below.

$$TF = -62 + 10\log(f) - 20\log(h) + 10\log(A_p) - 20\log(a)$$

$$-10\log\left(h + 12.8\sqrt{\frac{h}{f}}\right) + 10\log\left(1.0 + \left(0.7\sqrt{\frac{A_p}{h}}\right)\right) \quad dB \qquad \#3$$

Given the sound pressure level in a compartment, the structureborne noise that is excited can be computed. This structural acceleration level is combined with the structural accelerations due to other sources of vibration to yield the total structural accelerations. The radiation of this acceleration level is discussed in the preceding section.

4.3.3 Overview of the Models That Will be Compared

In the following chapter, a comparison of different propulsion systems will be performed using the acoustic model developed above. OTHEP will be compared with an electric-motor-driven conventional-propeller propulsion system and a geared, steam turbine driven conventional-propeller propulsion system. As mentioned earlier, only the noise sources associated with these propulsion systems and peculiar to these propulsion systems will be considered. Structural noise sources, flow-induced noise sources and propeller noise sources will not be considered. The discussion of propeller noise in Chapter 1 indicates qualitatively that the OTHEP is potentially quieter than conventional propellers. Quantitative assessment of propeller acoustics is well beyond the scope of this research.

5 Comparative Acoustic Analysis

5.1 Overview of Process

To assess the relative merit of OTHEP, the transfer function analysis developed in the preceding chapter is used to predict radiated noise levels for the propulsion systems of submarine designs which feature OTHEP, electric drive, and geared turbine drive. This chapter presents the three submarine propulsion systems which will be compared, the acoustic sources and paths that will be compared, and the results of the noise radiation predictions.

This comparison of the three propulsion systems depends upon the validity of the acoustic model presented in the preceding chapter. The acoustic model is built upon reference [7]. The source level data, mounting and foundation transfer function data, hull structure data, and radiation data are all taken from reference [7] with the sole exception being the source level information for the OTHEP propulsion motor. The basis of the data presented by reference [7] is empirical.--The measured acoustic data of existing equipment and structures provide the rationale for the relationships offered.

The foregoing discussion is meant to point out that the data in reference [7] provides the means to predict noise radiation. Its accuracy is dependent upon how similar the systems under consideration are to the systems from which the data that was used as the basis of reference [7] was collected. The limits of the accuracy of the relationships offered by reference [7] are not clear. Data pertaining to the acoustic emissions of existing submarines and the equipment in them is classified as a rule. Hence, use of reference [7] may seem questionable. However, the equipment installed on submarines is usually designed and built to very exacting acoustic requirements.--The equipment installed on surface ships is not scrutinised as closely. Reference [7] is based on surface ship data. From this is drawn the conclusion that reference [7] will provide an upper bound on the level of acoustic emissions. Most importantly, reference [7] provides a means to fairly compare alternate designs through its uniform approach to the issues of sources, paths and radiation.

5.1.1 The Acoustic Model

The comparative analysis proceeds in three steps. First, the acoustic source level for specified pieces of equipment is estimated using the model described in Chapter 4. Second, the effect of the path that the acoustic energy takes between the source and the point where it is radiated into the sea is also estimated using Chapter 4. It is important to note that the relevant acoustic paths are not known a priori. Rather, this research adopts the bias that the shortest path to a radiator into the sea will be the dominant path.--This bias is not without basis, reference [7] page 8-42; more importantly though, it reduces the number of required calculations greatly. The third step of the analysis calculates the efficiency of the radiation of the acoustic energy into the sea.

The first step, identifying the acoustic source levels, depends upon the equipment included in the respective designs. The second section of this chapter identifies the design of the enginerooms of the alternative propulsion systems. It specifies the equipment which will act as the acoustic sources for the comparative analysis.

The second step, identification of the relevant acoustic paths and their effect on the transmission of acoustic energy, is also discussed in the second section of this chapter. The bias discussed above indicates which paths of all the possible paths to concentrate upon.

The third step, quantification of radiated acoustic energy, is also derived from the information presented in the second section of this chapter. Of interest, all of the submarine designs being compared possess identical hull structural designs. Hence, any difference in the acoustic radiation characteristics of the different designs will depend upon the physical extent of the acoustic sources. Consequently, the "footprint" of the equipment foundations shown in the engineroom arrangements provide the difference in the radiation transfer functions.

5.1.2 The Comparison

Three submarine propulsion systems are compared. The first is the baseline submarine design featuring OTHEP. The second design features a conventional hub-to-diameter ratio propeller which is driven by an electric motor. The third design features a geared, steam turbine driven propulsion system.

The baseline design is the submarine that has been designed for this research in Chapter 3. The other two submarine designs are modifications of this design. In fact, the alternative propulsion system designs are identical to the baseline submarine design except for the engineroom. Hence, only the engineroom layout of the alternate designs will be provided.

The only equipment that is specified in the three submarine designs being compared is equipment which is peculiar to the particular propulsion system. This restriction ignores a multitude of acoustic sources. Whereas many of these sources are common to all three submarines and their presence only serves to complicate calculations, ignoring them will not invalidate the comparison.

5.1.3 The Method

The comparison proceeds from the identification of the equipments which are the acoustic sources. The airborne and structureborne noise source levels for each equipment is computed. All of the equipment within the engineroom contribute to the reverberant sound pressure level within the engineroom through their airborne noise emissions. This reverberant airborne noise excites vibrations in the hull plating at the boundaries of the engineroom. These vibrations in the hull plating cause acoustic noise to be radiated into the sea. This is the first source of radiated noise to be calculated. Note, only the reverberant sound pressure is considered. Direct path sound fields are ignored to ease calculations.

After computation of the airborne noise-excited radiated noise, the structureborne noise emissions of each piece of source equipment are quantitatively followed from the source equipment, through the equipment mountings, through the equip-

ment foundation (if present), through hull structure (if applicable), and to the hull plating where it is radiated into the sea. Most of the equipment is mounted to foundations which are directly connected to the hull. Hence, the acceleration levels at the base of the foundation form the excitation of the hull which is radiated into the sea.

After the structureborne noise from each piece of equipment is converted to a radiated sound power level, the total radiated sound power level of the submarine design is calculated. The total radiated sound power level is simply taken to be the "logarithmic sum" of all of the radiated sound power levels from every piece of equipment's structureborne noise emissions and the airborne noise-excited radiation from the engineroom boundaries.

5.1.4 The Results

The comparison is carried out for each of the three submarine designs. For each design, four possible mountings of the relevant source equipment are considered. They span the possible noise reduction mountings which are currently in use. All four mounting schemes will be presented.

The calculations which yield the results of the comparison are provided in Appendix B. The subsequent sections of this chapter discuss briefly how those calculations are performed. The table below shows the results of the comparison. These results will be discussed in greater detail in section 5.3.

Table 1 - Radiated Noise Levels of the Propulsion Systems

Octave Band Center Frequency (Hz)

	31.5	63	125	250	500	1000	2000	4000	8000
HM									
OTHEP	166	174	171	161	155	149	147	144	134
ED	166	174	171	161	155	149	143	142	134
GTD	153	160	157	148	143	143	137	132	122
HFM									
OTHEP	166	174	171	162	155	149	146	142	129
ED	166	174	171	162	155	149	142	140	129
GTD	153	160	157	149	143	143	136	130	117
LFM									
OTHEP	163	166	161	150	143	134	130	127	117
ED	163	166	161	150	143	134	126	125	117
GTD	150	152	147	137	131	128	120	115	104
TSM									
OTHEP	151	153	144	129	118	108	128	123	94
ED	151	153	144	129	118	107	99	99	94
GTD	138	139	130	116	106	101	92	91	84

HM = Hard Mounted HFM = High Frequency Isolation Mounting
LFM = Low Frequency Isolation Mounting TSM = Two Stage Isolation Mounting
OTHEP = Outside the Hull Electric Propulsion (Baseline Design)
ED = Electric Drive Variant GTD = Geared Turbine Drive Variant

5.2 Description of the Alternate Propulsion Systems, Acoustic Sources and Paths

5.2.1 OTHEP

5..2.1.1 System Configuration

The design of the baseline submarine is carried out in some degree of detail in Chapter 3 and Appendix A. Hence, this information will not be presented here. Appendix A, Figure 4 is a drawing of the engineroom arrangement of the baseline submarine. Also relevant to the configuration of the baseline submarine is the arrangement of the propulsion motor on the aft end of the pressure hull.

5.2.1.2 Acoustic Sources

The equipment listed below is the equipment that is considered in the comparative analysis for the OTHEP propulsion system.

Propulsion Motor	19.2MW	58.8RPM	sea-water cooling/lubrication
Turbine-Generators (2)	27MW	3600RPM	
Sea-Water Pump	1900gpm	+10psi	centrifugal pump
Pump Drive Motor	188HP	1200rpm	induction motor

5.2.1.3 Acoustic Paths

Two acoustic paths exist for the structureborne noise emitted by the propulsion motor. The first path is through the structure which attaches the rotor core to the structure supporting the propeller hub. This path is handled by treating the connecting structure as a mounting, with the rotor core mounted directly to the hull plating at the propeller hub. The second path conducts the noise emitted by the stator from the stator core to the hull plating just fore and aft of the propulsion motor. The path goes through the mounting which connects the stator to the pressure hull. From the point of connection with the pressure hull, the path continues fore and aft, through intersections with framing, to the first stiffener which extends radially from the pressure hull to the hull envelope plating. See the figure below.

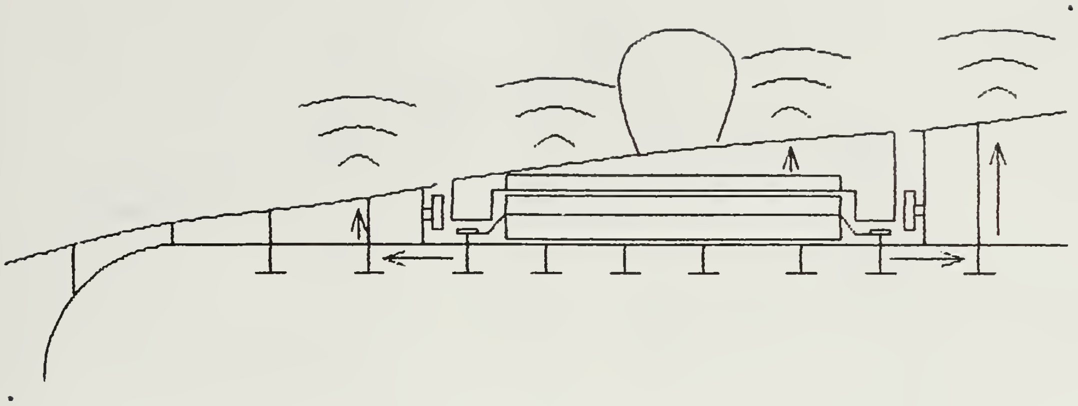

Figure 1 - OTHEP Propulsion Motor Structureborne Noise Paths

The acoustic paths for the structureborne noise emitted by the turbine-generators (2), and the sea-water cooling/lubrication pump unit are similar. The source equipment is attached to its foundation with any of the four mountings shown in the results table above. The acoustic path extends through the mounting and across the foundation to the hull. The sound is radiated from the hull at the location of the foundation's "footprint" on the hull. See the diagram below.

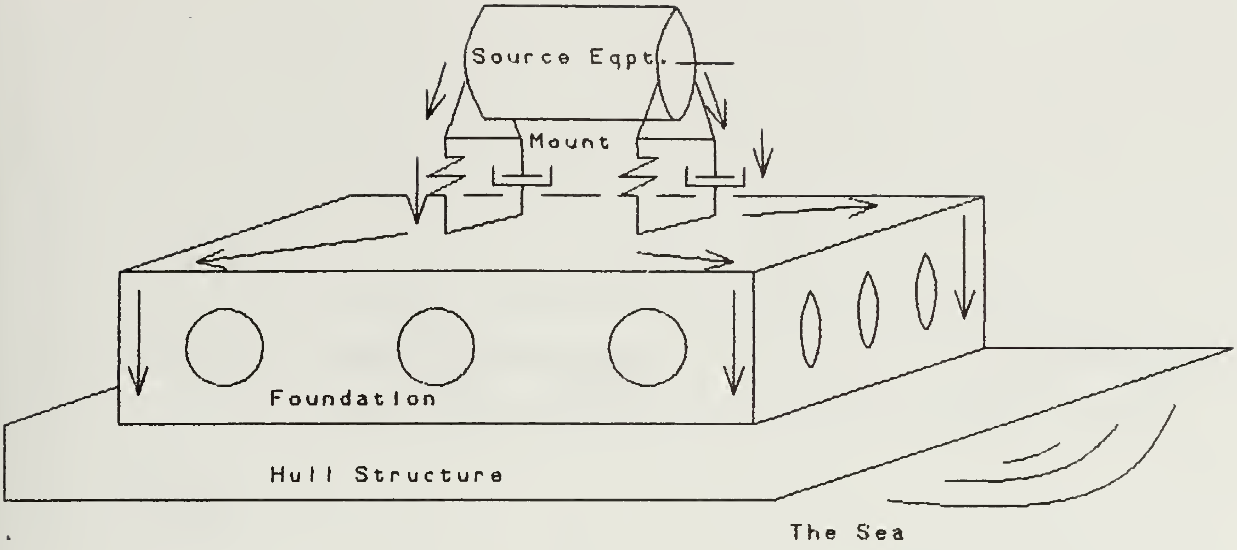

Figure 2 - Source, Mounting, Foundation, Hull Acoustic Path

The only other path to be considered is a partially airborne path. The source equipments emit airborne noise into the engineroom. The reverberant sound pressure level in the engineroom is a function of the room geometry and the airborne sources within the engineroom. The reverberant sound pressure level induces vibrations in the hull structures which form the boundaries of the engineroom. These vibrations, in turn, give rise to acoustic radiation from the hull.

5.2.2 Electric Drive With Conventional Propeller

5.2.2.1 System Configuration

The arrangement drawing below contains the salient aspects of the electric drive propulsion system that is used in the comparison. The hull profile and location of the reactor compartment are the same as the baseline submarine design's. The aft end of the pressure hull is altered to reflect its shape were the electric drive propulsion system to be installed.--The pressure hull displacement is preserved despite the alteration of the shape of the aft end of the pressure hull.

Side View

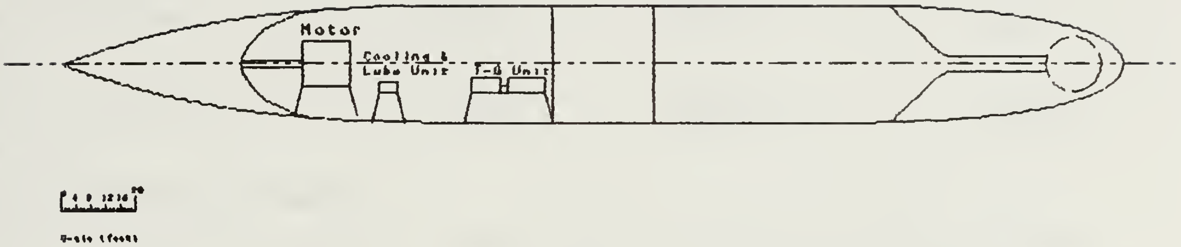

Top View

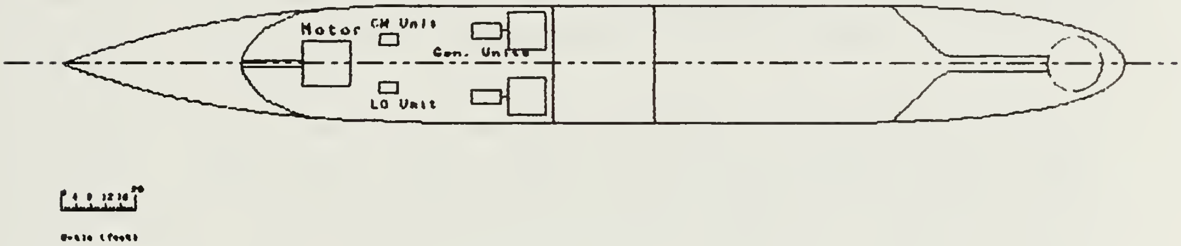

Figure 1 - Electric Drive Engineroom Arrangement

5.2.2.2 Acoustic Sources

The equipment listed below is the equipment that is considered in the comparative analysis for the electric drive propulsion system.

Propulsion Motor	19.2MW	120RPM	freshwater cooled
Turbine-Generators (2)	27MW	3600RPM	
Cooling Water Pump	400gpm	centrifugal pump	
Pump Drive Motor	37.5HP	1200rpm	induction motor
Lube Oil Pump	8gpm	20psi	gear pump
Pump Drive Motor	7.5HP	1200rpm	induction motor

5.2.2.3 Acoustic Paths

The acoustic paths for the structureborne noise emitted by the all of the source equipment of the electric drive submarine design, the propulsion motor, turbine-generators (2), the cooling water pump unit, and the lube oil pump unit, are similar. The source equipment is attached to its foundation with any of the four mountings shown in the results table above. The acoustic path extends through the mounting and across the foundation to the hull. The sound is radiated from the hull at the location of the foundation's "footprint" on the hull. This is the same path that is shown in Figure 5.2.1.3.2.

The only other path to be considered is a partially airborne path. The source equipments emit airborne noise into the engineroom. The reverberant sound pressure level in the engineroom is a function of the room geometry and the airborne sources within the engineroom. The reverberant sound pressure level induces vibrations in the hull structures which form the boundaries of the engineroom. These vibrations, in turn, give rise to acoustic radiation from the hull.

5.2.3 Geared, Steam Turbine Drive

5.2.3.1 System Configuration

The arrangement drawing below contains the salient aspects of the geared turbine drive propulsion system that is used in the comparison. The hull profile and location of the reactor compartment are the same as the baseline submarine

design's. The aft end of the pressure hull is altered to reflect its shape were the electric drive propulsion system to be installed.--The pressure hull displacement is preserved despite the alteration of the shape of the aft end of the pressure hull.

Side View

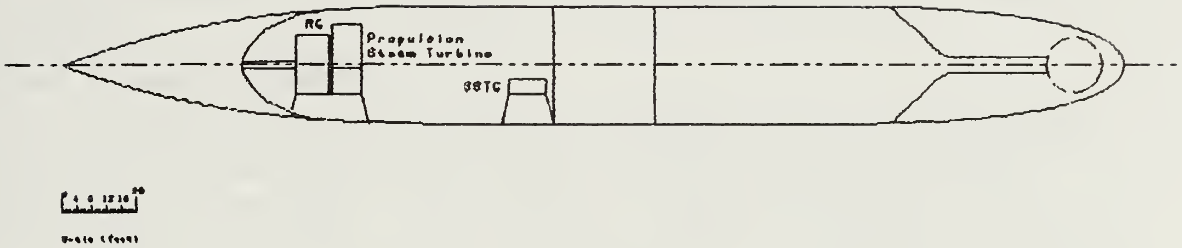

Top View

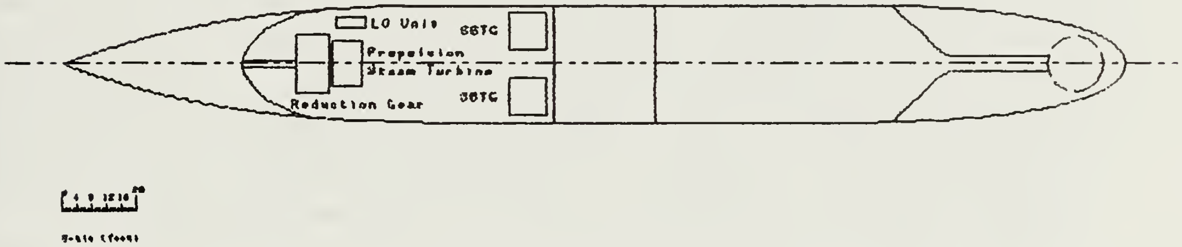

Figure 1 - Geared Turbine Drive Engineroom Arrangement

5.2.3.2 Acoustic Sources

The equipment listed below is the equipment that is considered in the comparative analysis for the geared turbine drive propulsion system.

Propulsion Steam Turbine	19.2MW	3600RPM	
Reduction Gear	19.2MW	120RPM	
Ship's Service Turbine-Generators (2)	1.1MW	3600RPM	
Lube Oil Pump	16gpm	20psi	gear pump
Pump Drive Motor	15HP	1200rpm	induction motor

5.2.3.3 Acoustic Paths

The acoustic paths for the structureborne noise emitted by the all of the source equipment of the geared turbine drive submarine design, the reduction gear, ship service turbine-generators (2), and the lube oil pump unit, are similar. The source equipment is attached to its foundation with any of the four mountings shown in the results table above. The acoustic path extends through the mounting and across the foundation to the hull. The sound is radiated from the hull at the location of the foundation's "footprint" on the hull. This is the same path that is shown in Figure 5.2.1.3.2.

The only other path to be considered is a partially airborne path. The source equipments emit airborne noise into the engineroom. The reverberant sound pressure level in the engineroom is a function of the room geometry and the airborne sources within the engineroom. The reverberant sound pressure level induces vibrations in the hull structures which form the boundaries of the engineroom. These vibrations, in turn, give rise to acoustic radiation from the hull.

5.3 Discussion of Results

5.3.1 Sources That Were Not Considered

Prior to discussing the results of the comparative study it is very important to note the acoustics issues that have been neglected. First of all, structural and mechanical noise sources other than the propulsion system equipment discussed above have been ignored, the propeller shaft for one. Second, all noise created by the propeller has been ignored. These noise sources are very important when comparing propulsion

schemes. Hence, the results presented by this research are only part of the picture. They represent just one portion of the noise emitted by a submarine.

One additional point must be made. Other than the equipment mountings, no noise reduction techniques are considered by this research. Hence, many of the noise sources could be mitigated by proper techniques. This is to say that it should be very possible to improve the noise emission characteristics of any of the three propulsion systems.

5.3.2 Interpretation of Findings

The results presented in the first section of this chapter contain three interesting results. First, perhaps the most salient feature of the comparison is the similarity between the electric drive and OTHEP radiated source levels. This similarity, in view of the disparity in motor source levels, indicates that the turbine-generators are the dominant noise source. Their effect is due to two factors. The turbine-generators have high power ratings. The turbine-generators' foundations cover a large area of hull, thus making a larger, more effective sound radiator.

The most obvious difference between the electric drive and OTHEP radiated noise levels occurs in the 2000Hz octave band. This is the octave band that contains the PWM switching frequency, 2.5kHz. The estimation of the magnitude of the current distortion square wave could be overly conservative,--penalising the OTHEP system as it were. Nonetheless, it points out the need to minimize the PWM distortion of the stator input current. This effect seems to be the only intrusion of the OTHEP propulsion motor into the turbine-generator dominated noise radiation. Without it, the two propulsion systems would be indistinguishable.

The final observation concerns the geared turbine drive source levels. The fact that a mechanical drive appears to be more quiet than an electric drive is counter-intuitive. There are three possible explanations for the geared turbine drive being quieter than the electric drive and OTHEP systems. First, the source levels for the generating plant of the electric drive and OTHEP designs may be too high. Reference [7]

may not provide accurate source levels for motors and generators with ratings as high as 19 and 27MW. This would penalise the electric drive and OTHEP designs. This is the most likely explanation especially when the quality of submarine equipment compared to surface ship equipment is considered.

The second explanation for the disparity of the geared turbine drive source levels and the electric drives source levels is that equipment other than the equipment considered causes geared turbine drives to be less quiet. This explanation is less likely than the one discussed above. The third explanation why the comparative study finds geared turbine drive to be quieter than the electric drives is that, maybe, geared turbine drive is, in reality, quieter than electric drives.

6 Conclusion

6.1 Interpretation of Results

This research produced four items. Each of them is reviewed here.

6.1.1 Feasibility Design

Chapter 3 and Appendix A comprise what is essentially a feasibility design of a submarine which uses the OTHEP concept. The submarine design is balanced and appears to be entirely feasible. The design does possess several characteristics which should be addressed in subsequent design iterations, namely a tendency to be heavy aft and a need for room for crew berthing forward. The inverted geometry, squirrel-cage induction motor appears to also be entirely feasible. Protection of the motor and its components from seawater is a concern, though.

6.1.2 Forces of Electromagnetic Origin

Section 4.2 develops the normal force of electromagnetic origin which acts on the propulsion motor core. The actual relationship is described by equation 4.2.2.18. Evaluating this relationship would be very tedious without using the capabilities of digital computers. For a detailed acoustic analysis of the propulsion motor source level, it would be appropriate to include many of the terms of the series which comprise equation 4.2.2.12. The expression for force on the motor core accounts for conductor width, winding geometry, phase current harmonics, and rotor bar harmonics. The most important assumptions leading to the expression for force concern the permeability of the core material and the 'air'-gap width.

6.1.3 Source Level Estimation

Section 4.2.4 provides an estimation of the propulsion motor source level for use with the TFA method that is developed in section 4.3. The source level estimation found in Table 4.2.4.3 is very approximate. The series expressions for the MMF of the motor were truncated after only a few terms. As a result, the source level for the 8000Hz octave band is zero. The magnitude of the current distortion waveform due to the PWM converter is very conservative. Consequently, the

source level of the octave band which contains the PWM switching frequency is very high, perhaps excessively so. The source level for the propulsion motor is considerably greater than the envelope offered in reference [7] for electric motors. This tends to indicate that reference [7] source levels are only valid for electric machines with power ratings significantly less than the power ratings for the OTHEP machinery. This conclusion must be borne in mind when considering the results of the comparative acoustic analysis.

6.1.4 Acoustic Model Comparative Analysis

The results of the comparative analysis, which uses the acoustic model of section 4.3, of the alternate propulsion systems described in Chapter 5 and calculated in Appendix B indicate that more accurate source levels are needed to assess the acoustic merit of OTHEP. As mentioned in the preceding section, the source levels for the electric motors and generators used with the OTHEP submarine and the electric drive variant are not accurate given the rating of the motors and generators being analysed. Hence, the results of the comparison with the geared, turbine drive variant must be disregarded. However, the comparison between OTHEP and the electric drive variant is meaningful.

Ignoring differences in propeller noise, shaft noise, and other noise sources, the radiated sound power levels of the propulsion machinery of the OTHEP and electric drive designs are virtually identical. The radiated octave band sound power levels are, with one exception, dominated by the generator sound power levels. The single exception is the PWM harmonic of the OTHEP propulsion motor that is mentioned in the preceding section. If the radiated sound power level is, in fact, dominated by the generator noise, then OTHEP's propulsion system acoustic performance will be as good as electric drive acoustic performance. A better idea of the propulsion motor source level for electric drive and OTHEP must be obtained before the preceding statement can be considered to be definitive.

6.2 Fulfillment of Objectives

The principal objective as stated in Chapter 1 is to develop a method to assess the relative acoustic merit of OTHEP. This objective has been fulfilled by the acoustic model of Chapter 4. Two secondary objectives support the principal objective. The first of these is to describe the forces of electromagnetic origin that act on the propulsion motor core. This objective is accomplished through equation 4.2.2.18. The second secondary objective is to compare OTHEP with other submarine propulsion systems. The steps that would have led to the fulfillment of this objective are carried out; however, the results indicate that the source levels for use in the model that fulfills the principal objective are not accurate. Without accurate source level information the second objective cannot be met.

This research has provided a tool that can be used to predict radiated sound power levels. The comparison attempted in this research is a victim of a lack of valid source level information for high-power-rating electric machinery. This lack of source level information does not invalidate the method that has been developed, though. Hopefully, someone with valid source level information could, and would, take the method developed through this research and use the accurate source levels to calculate radiated sound power levels.

6.3 Recommendations for Further Research

This research has uncovered several areas, which if researched, would provide valuable information for the eventual implementation of OTHEP.

6.3.1 Continue Design Process of OTHEP

Further design iterations leading to a detail design of an OTHEP submarine will make OTHEP a legitimate alternative for future submarine designs. Detailed analysis of several design characteristics will have a major impact on the eventual implementation of OTHEP. These characteristics describe integrated electric distribution systems, producibility considerations and adherence to shock criteria. Further design iterations will also improve the quality of arrangements and other naval architectural issues.

6.3.2 Validation of Expression for Electromagnetic Force

In the derivation of the expression which describes the forces of electromagnetic origin which act on the motor core, several assumptions simplify the analysis. A detailed computation using equation 4.2.2.18 to calculate the force on a motor core should be validated by measurements of the force which acts on an actual motor core.

6.3.3 Validation of Source Level Estimation

Ideally, a prototype OTHEP motor or a scaled version of the OTHEP motor would be constructed. The source levels of this motor, when measured, would provide a validation of the octave band source levels provided in Table 4.2.4.3. If the cost of such validation is prohibitive, a FEM analysis of the motor can be performed using the expression developed for the forces of electromagnetic origin. The result of the FEM analysis would provide much more accurate source level information than that provided in Table 4.2.4.3.

6.3.4 Validation of Acoustic Model

A validation of the acoustic model presented in section 4.3 can be performed by comparing the radiated sound power levels calculated using section 4.3 for an existing vessel with actual measured sound power levels for that vessel. This step is extremely vital in view of the derivation of the radiation transfer function, section 4.3.2.1.4, which describes radiation into the sea. This derivation has not been put to the test of predicting actual emissions.

6.4 Recommendations for Supporting Research

The preceding recommendations for further research arise from the raised in this research. Several other design issues relevant to implementation of OTHEP beggar research.

6.4.1 Determination of Propulsive Coefficient of OTHEP Design

The propulsive coefficient of the OTHEP system is estimated in the development of the power versus speed relationship, section 3.1.8. Because the OTHEP configuration is somewhat novel, the propeller efficiency, hull efficiency and relative rotative efficiency are not known with any certainty

at all. Research into the hydrodynamics which dictate these values would provide valuable information characterising the performance of OTHEP.

6.4.2 Design an Optimal Propeller for OTHEP

The propeller design assumed in the submarine design contained in Chapter 3 and Appendix A is the propeller design that Hamner concluded was not optimal. Propeller design is not a simple task. However, a thorough analysis of large hub-to-diameter ratio propellers would provide a more accurate estimation of the open water efficiency of such propellers. A characterisation of the acoustic characteristics of such propellers would also aid in the evaluation of OTHEP's merits. The forces which act on the OTHEP propeller blades will be a deciding factor in the design of the rotating structure which connects the rotor core to the propeller hub.

7 References

1. Hamner, Michael Scott. "A Submarine Electric Propulsion System With Large Hub Propeller." Thesis. M.I.T. 1983.
2. Fox, Robert M. "Bibliography--Tandem Propulsion Systems." Machinery Laboratory Technical Note 117/68. DTRC, April, 1968.
3. "Experimental and Theoretical Research on the Hydrodynamic Characteristics of Large Hub to Diameter Ratio Propellers." Contract No. N 62558-3463. Netherlands Ship Model Basin, Haagstaeg 2, Wageningen, Netherlands, April, 1964.
4. Gerken, T.J. "Feasibility Study, Novel Electric Propulsion System for a Submarine." Electric Machinery Specification U413-61-118. General Dynamics Corporation Electric Boat Division, May 9, 1961.
5. Wiesman, Richard Mark. "Experimental and Analytical Characteristics of Linear Induction Motors for Transportation." Thesis. M.I.T. 1982.
6. Shock and Vibration Information Center. "A Practical Method for Predicting Acoustic Radiation or Shock Excursions of Navy Machinery." Washington, D.C.: U.S. Naval Research Laboratory, December 1964, Bulletin 34, Part 3, pp. 129-138.
7. Design Guide for Shipboard Airborne Noise Control. Society of Naval Architects and Marine Engineers. 1983.
8. Timar, Peregrin L. "Recent Trends in the Noise and Vibration Investigations of Asynchronous Motors." Periodica Polytechnica, Electrical Engineering, v 27, n 3-4, 1983.
9. Timar, Peregrin L. "Influence of Loading on the Sound Power Level Radiated by Induction Motors." Noise Control Engineering Journal, v 31, n 2 (Sep-Oct), 1988. pp. 125-133.
10. Fischer, Raymond W. and Louis M. Petit. "Computer-Assisted Shipboard Noise Predictions." Noise Control Engineering Journal, v 31, n 2 (Sep-Oct), 1988. pp. 111-124.

11. Williams, K., R.K. Singal, and S.P. Vernon. "Vibrations of Long and Short Laminated Stators of Electrical Machines." Journal of Sound and Vibration, v 129, n 1 (Feb 22, 1989). pp. 1-44.

12. Wallace, A.K., Rene Spee, and L.G. Martin. "Current Harmonics and Acoustic Noise in AC Adjustable Speed Drives." Conference Record IAS Annual Meeting, (IEEE Industry Applications Society) Pittsburgh, PA, October 2-7, 1988, v 35, n 6.

13. Blake, W.K. et al. "Elements of Ship Acoustics." (Contains additional notes of D. Ross.) (This is a series of unpublished lecture notes from Draper Laboratory's Professional Summer course, Submarine Observables, Survivability and Control.) July, 1989.

14. Harris, Tedric A. Rolling Bearing Analysis. 2nd ed. New York, NY: John Wiley & Sons, 1984.

15. Wilcock, Donald F., and E. Richard Booser. Bearing Design and Application. New York, NY: McGraw-Hill Book Co., 1957.

16. Constantinescu, Virgiliu Niculae, et al. Sliding Bearings. Trans. A. Nica. New York, NY: Allerton Press, 1985.

17. Krause, Paul C. Analysis of Electric Machinery. New York, NY: McGraw-Hill Book Co., 1986.

18. Fitzgerald, A.E., Charles Kingsley Jr., and Stephan Umans. Electric Machinery. 4th ed. New York, NY: McGraw-Hill Book Co., 1983.

19. Melcher, James R. Continuum Electromechanics. Cambridge, MA: MIT Press, 1981.

20. Beveridge, J.L. "Calculation of Optimum Efficiency for a Series of Large-Hub Propellers for a Submerged Body of Revolution." DTNSRDC Report 1826, August 1964.

21. Denny, S.B., "Measurement of Forces and Spindle Moments on Individual Blades of a Large-Hubbed Propeller." DTNSRDC Report 3252, December 1969.

22. Joosen, W.P.A., J.D. Van Manen and F. Van Der Walle. "Large Hub to Diameter Ratio Propellers with Programmed Blade Control." International Shipbuilding Progress: Shipbuilding and Marine Engineering Monthly, Vol. 10, No. 101, Jan. 1963.

23. "The Tandem Propeller Submarine." Cornell Aeronautical Laboratory, Inc., Cornell University, Buffalo, New York.

24. Izzo, A.J. "Feasibility of a Novel Electric Power Propulsion System (NEPPS) for a Submarine, Vol. III, Hydrodynamic Tests." General Dynamics Corporation, Groton, Connecticut, Electric Boat Division, Contract NOnr 3383 (00), Project NR 097-353, July 31, 1963.

25. Izzo, A.J. "Feasibility of a Novel Electric Power Propulsion System (NEPPS) for a Submarine, Vol. III, Hydrodynamic Tests." General Dynamics Corporation, Groton, Connecticut, Electric Boat Division, AD-342 463/7ST, July 31, 1963.

26. Moore, J.E. Jane's Fighting Ships, 1987-88. New York: Franklin Watts, 1987.

27. Jackson, Harry A. Submarine Design Notes. Course notes, Professional Summer at M.I.T. June 9 - 20, 1986. Revised May 1989.

28. Doerry, Norbert H. SHAPE, Version 1.6. Computer Software. Room 5-309b M.I.T. August 1, 1989.

29. Hottel, Glenn R. SUBLAB, Version 1. Computer Software. M.I.T. August 29, 1988.

30. Doerry, Norbert H. P_HULL, Version 2.0. Computer Software. Room 5-309b M.I.T. July 31, 1989.

31. Newman, J.N. Marine Hydrodynamics. Cambridge, Massachusetts: MIT Press, 1977.

32. Lewis, Edward V. Principles of Naval Architecture, Second Revision. Volume II Resistance, Propulsion and Vibration. Jersey City, NJ: The Society of Naval Architects and Marine Engineers, 1988.

33. "Prediction of Smooth-Water Powering Performance for Surface Displacement Ships." Design Data Sheet 051-1. Washington, D.C.: Naval Sea Systems Command, May 15, 1984.

34. Kirtley, James L. Jr. "Course 6.685 Supplementary Notes, Numbers 1-4." M.I.T. March 1987.

35. Kirtley, James L. Jr. "Application of Superconductors-High T_c and Otherwise-To Electric Power Generators." Electric Machines and Power Systems, 15:121-134, 1988. Hemisphere Publishing Corporation.

36. Matsch, Leander W. *Electromagnetic & Electromechanical Machines*. 2nd ed. New York, NY: Harper & Row, Publishers, Inc., 1977.

37. Sabersky, Rolf H., Allan J. Acosta and Edward G. Hauptmann. *Fluid Flow*. 2nd ed. New York, NY: Macmillan Publishing Co., Inc., 1971.

38. Kassakian, John G., Martin F. Schlect and George C. Verghese. "Principles of Power Electronics." (Unpublished.)

39. Greene, D.L. et al. "Analysis of a High-Power Water-Cooled Electric Propulsion System." *SNAME Transactions*, v 86, 1978. pp. 140-162.

40. Cann, Glenn E. "Submarine Feasibility Design Guide." Department XIII-A, M.I.T. (Unpublished.) 1987. Revised August 1988.

41. Dyer, Ira. "Fundamentals and Applications of Underwater Sound." Course notes, 13.851, M.I.T. Spring 1989.

42. Popov, Egor P. *Introduction to the Mechanics of Solids*. Englewood Cliffs, NJ: Prentice-Hall Inc., 1968.

8 Nomenclature

a	acceleration, panel length-to-width ratio
a_n	Fourier coefficient for MMF series
a_o	reference acceleration
a_{pwm}	Fourier coefficient for current distortion series
A	condition A
A_{cs}	cross sectional area of 'air'-gap
A_m	Fourier coefficient for current distortion series
A_n	Fourier coefficient for MMF series
A_p	radiating panel area
A_{rc}	rotor conductor area
A_s	effective source area
A_{sc}	stator conductor area
A-1	condition A-1
b_p	defined magnetic flux density
b_{pwm}	Fourier coefficient for current distortion series
$\mathbf{B}$	magnetic flux density vector
BHP	brake horsepower
B_i	component of magnetic flux density in i^{th} direction
B_o	magnetic flux density magnitude
B_{sat}	saturation magnetic flux density
C_D	coefficient of drag
C_f	coefficient of frictional drag
C_L	coefficient of lift
CPO	inhabitant of the goat locker
C_r	coefficient of residual drag
C_{rm}	coefficient of residual drag from model test
c_s	rotor sheet-conductor thickness
c_{sw}	speed of sound in sea-water
D	submarine diameter
D_{prop}	propeller diameter
D_{sc}	stator conductor depth

D_{sg}	rotor bar slot gap
D_{si}	stator insulation thickness
D_{ss}	stator slot depth
D_{sw}	stator wedge depth
E	modulus of elasticity
$\mathbf{E}$	electric field intensity vector
$\hat{E}$	electric field intensity complex magnitude
EHP	effective horsepower
f	octave band center frequency
f_c	coincidence frequency
f_i	component of force in i direction
f_{min}	minimum frequency
F	fluid shear force
F_{ai}	component of surface force density in i direction
FF	free flood displacement
F_i	component of force density in i direction
F_L	lift force
F_N	normal force of electromagnetic origin
F_R	resistance force, drag
g	'air'-gap width
h	plate thickness
hp	power rating in horsepower
$\mathbf{H}$	magnetic field intensity vector
HA	"heavy aft" loading condition
HF1	"heavy forward 1" loading condition
H_i	component of magnetic field intensity in i direction
H2	"heavy 2" loading condition
i_{bj}	current in j^{th} rotor bar
i_{bref}	current in reference rotor bar
i_{ra}	a-phase rotor current
i_{sa}	a-phase stator current
I	acoustic intensity

$\underline{I}$	complex current magnitude
$\underline{I}_{bj}$	complex current magnitude for j^{th} rotor bar
I_{core}	motor core moment of inertia
$\underline{I}_{hbj}^{m}$	complex distortion current magnitude of m^{th} harmonic for j^{th} rotor bar
I_p	stator phase current magnitude
I_r	magnitude of balanced rotor currents
$\underline{I}_{ras}$	rotor current with phase angle relative to stator current
I_s	magnitude of balanced stator currents
I_2	referred rotor current from equivalent circuit
$\mathbf{J}$	current density vector
J_m	maximum stator linear current density
k	acoustic wave number
$\overline{k}_c$	average rotor surface-current density
k_{flex}	linearised flexural stiffness of motor core
k_r	rotor winding factor, skew factor
k_s	stator winding factor, plate structural wave number
k_{sb}	stator winding breadth factor
k_{sp}	stator winding pitch factor
k_{spring}	linear stiffness model of sea-water
kW	power rating in kiloWatts
$\underline{K}_{hn}^{m}$	Fourier coefficients of rotor surface current density series
$\underline{K}_n$	Fourier coefficients of rotor surface current density series
$\overline{K}_r$	rotor surface current density
$\overline{K}_r^F$	Fourier series description of rotor surface current density
l	structureborne acoustic path length
L	submarine length, ‘air’-gap length
L_a	acceleration level

L_{aB}	baseline acceleration level
L_{aeff}	effective source level
L_{ag}	'air'-gap length
L_{array}	acoustic array length
L_{A}	length of aft body
LCB	longitudinal center of buoyancy
LCG	longitudinal center of gravity
LEAD	lead ballast displacement
L_{F}	length of fore body
L_{p}	sound pressure level
L_{PMB}	length of parallel mid-body
L_{r}	rotor single phase self-inductance
$\underline{L}_{r}$	rotor winding inductance matrix
L_{ra}	rotor a-phase winding self-inductance
L_{rab}	rotor a- and b-phase mutual inductance
L_{rl}	rotor single phase leakage inductance
$L_{rlbelt5}$	rotor belt leakage inductance, 5th space harmonic
$L_{rlbelt7}$	rotor belt leakage inductance, 7th space harmonic
L_{rlslot}	rotor slot leakage inductance
L_{s}	stator single phase self-inductance
$\underline{L}_{s}$	stator winding inductance matrix
L_{sa}	stator a-phase self inductance
L_{sab}	stator a- and b-phase mutual inductance
L_{sl}	stator single phase leakage inductance
$L_{slbelt5}$	stator belt leakage inductance, 5th space harmonic
$L_{slbelt7}$	stator belt leakage inductance, 7th space harmonic
L_{slr}	stator skew leakage inductance
L_{slslot}	stator slot leakage inductance
L_{slzz}	stator zigzag leakage inductance
L_{sl5}	belt leakage inductance, 5th space harmonic
L_{sl7}	belt leakage inductance, 7th space harmonic
L_{syn}	single phase synchronous inductance
L_{v}	velocity level

L_w	sound power level
L_{wB}	baseline sound power level
L_ϕ	magnetising inductance from equivalent circuit
L2	"light 2" loading condition
m	number of stator turns per phase
m_a	motor core added mass
M	stator a-phase to rotor a-phase mutual inductance, motor core mass
M_{ag}	'air'-gap stator-rotor winding mutual inductance
$\underline{M}_{ag}$	'air'-gap mutual inductance matrix
MBT	main ballast tank and its corresponding displacement
MMF	magneto-motive force
n	number of radiating panels
n_a	aft body paraboloid exponent
n_f	fore body ellipsoid exponent
N	"normal" loading condition
N_r	rotor series turns per phase
N_R	number of rotor bars
N_s	stator series turns per phase
NSC	normal surface condition
N_{SS}	number of stator slots
p	number of pole-pairs, pressure
P	perimeter of radiating panel
PC	propulsive coefficient
P_{diss}	power dissipated by loss mechanisms
P_{in}	electrical real-power input
P_{loss}	stator Ohmic loss
P_{out}	electrical real-power output
P_{rated}	rated power output
q	number of phases
r	distance from center of source area
r_{aft}	aft body hull radius

r_f	distance to boundary of source compartment
$r_{forward}$	fore body hull radius
r_{lim}	limiting acoustic range
rpm	rated speed in rpm
R	‘air’-gap radius, acoustic room constant
R_{ag}	‘air’-gap radius
R_{bar}	resistance of a single rotor bar
Re	Reynolds’ number
R_{OD}	stator outside radius
R_r	rotor inside radius
R_{ra}	resistance of a-phase rotor winding
R_{sa}	resistance of a-phase stator winding
R_{sw}	‘air’-gap resistance
R_1	stator resistance from equivalent circuit
R_2	rotor resistance from equivalent circuit
s_{rated}	rated slip
SHP	shaft horsepower
$SHP_{install}$	installed shaft horsepower
$SHP_{required}$	required shaft horsepower
t	thrust-deduction coefficient, time
t_B	magnetic backing material thickness
TF_{found}	equipment foundation acoustic transfer function
T_i	torque about the i-axis
T_{ij}	component of electromagnetic stress tensor
TF_{mount}	equipment mounting acoustic transfer function
$TF_{radiation}$	into-the-sea acoustic radiation transfer function
T_{rated}	rated torque
$TF_{structure}$	hull structure acoustic transfer function
v	fluid velocity
$\ddot{U}$	acceleration of mid-span of motor core structural model
v_o	acoustic velocity magnitude
V	rotor linear velocity

$\underline{V}$	complex voltage
V_{ag}	induced 'air'-gap voltage
VCB	vertical center of buoyancy
VCG	vertical center of gravity
VL	displacement of variable loads
$\underline{V}_{ras}$	rotor voltage with phase angle relative to stator current
V_{sub}	submarine's velocity
w	wake fraction
W	radiated sound power
W_o	reference sound power
W_{rb}	rotor bar diameter
W_{rh}	rotor hole diameter
W_{rs}	rotor bar slot width
W_{sa}	wetted surface area
W_{sc}	stator conductor width
W_{ss}	stator slot width
W1 - W7	SWBS weight groups 1 - 7
x_a	distance aft along the aft body
x_f	distance forward along the fore body
X_ϕ	magnetising reactance
X_1	stator leakage reactance from equivalent circuit
X_{1slot}	stator slot leakage reactance
X_2	rotor leakage reactance from equivalent circuit
Z_{split}	equivalent circuit current division ratio
Z_{msplit}'	equivalent circuit distortion current division ratio
α	electrical machine empirical constant, winding pitch angle, sea-water acoustic absorption coefficient, angular conductor width
α'	angular conductor width in mechanical radians
β	phase angle of phase currents, acoustic path dissipative loss coefficient

β_r	skew angle
γ	electrical angle between stator turns
ΔC_f	correlation allowance
Δ_{env}	envelope displacement
Δ_{sub}	submerged displacement
Δx	incremental step in x direction
Δy	incremental step in y direction
η_h	hull efficiency
η_M	motor efficiency
η_o	open-water propeller efficiency
η_{rr}	relative-rotative efficiency
η_s	shafting/mechanical transmission efficiency
θ	mechanical angular displacement, stator coordinates
θ'	mechanical angular displacement, rotor coordinates
θ_e	angular displacement in electrical radians, stator coordinates
θ_o	initial rotor position
λ	flux linkage
λ_c	coincidence wavelength
λ_{max}	longest acoustic wavelength
λ_p	circumference-to-slot width ratio, one pole-pair length
λ_{ra}	rotor a-phase winding flux linkage
λ_{sa}	stator a-phase winding flux linkage
$\underline{\Lambda}$	complex flux linkage amplitude
$\underline{\Lambda}_{ras}$	rotor flux linkage amplitude with phase angle relative to stator current
μ	absolute viscosity
μ_o	permeability of free space

ν	kinematic viscosity
ξ_r	rotor current phase angle relative to stator current
ρ	rotor bar resistivity
ρ_{ag}	'air'-gap permeance
ρ_{cond}	conductor resistivity
ρ_o	density of sea-water
ρ_{SW}	resistivity of sea-water, density of sea-water
σ_{rad}	radiation efficiency
τ	fluid shear stress
τ_{ij}	electromagnetic shear stress
ψ'	induced voltage lag angle
ψ'_{msplit}	equivalent circuit rotor distortion current phase angle
ψ_{split}	equivalent circuit rotor current phase angle
ω	stator electrical frequency, acoustic frequency
ω_p	PWM switching frequency
ω_r	rotor electrical frequency
ω_s	stator electrical frequency
ω_{syn}	synchronous frequency
Ω_M	mechanical frequency
∇	hull volume

A Submarine Design Calculations

1.1 Table 1 - Baseline Submarine Design Hull Envelope Offsets

Baseline Submarine Offsets

Distance aft FP. x ft	Hull Radius r ft	Distance aft FP. x ft	Hull Radius r ft
0.00	0.00	126.72	16.00
3.84	5.97	130.56	16.00
7.68	8.01	134.40	16.00
11.52	9.46	138.24	16.00
15.36	10.59	142.08	16.00
19.20	11.51	145.92	16.00
23.04	12.28	149.76	16.00
26.88	12.94	153.60	16.00
30.72	13.51	157.44	16.00
34.56	13.99	161.28	16.00
38.40	14.41	165.12	16.00
42.24	14.76	168.96	16.00
46.08	15.06	172.80	16.00
49.92	15.31	178.56	16.00
53.76	15.52	184.32	15.97
57.60	15.68	190.08	15.91
61.44	15.81	195.84	15.81
65.28	15.90	201.60	15.65
69.12	15.96	207.36	15.42
72.96	15.99	213.12	15.11
76.80	16.00	218.88	14.71
80.64	16.00	224.64	14.22
84.48	16.00	230.40	13.62
88.32	16.00	236.16	12.91
92.16	16.00	241.92	12.07
96.00	16.00	247.68	11.11
99.84	16.00	253.44	10.00

103.68	16.00	259.20	8.75
107.52	16.00	264.96	7.34
111.36	16.00	270.72	5.77
115.20	16.00	276.48	4.02
119.04	16.00	282.24	2.10
122.88	16.00	288.00	0.00

1.2 Table 2 - Combined Structural Design Worksheet

```
Submarine Structural Calculations
(Developed for 13.461 Naval Ship Design by John V. Amv Jr.)

This worksheet is derived from the worksheets contained in the book
Submarine Design Notes by CAPT Harry A. Jackson, Chapter 7.
See this reference for drawings which define the physical significance
of each of the variables.  Go to line 218 for the bulkhead analysis.
Go to line 267 for the end closure analysis.

Input Data:
      Do=       32 ft  This is outside diameter of the submarine's hull.
      OD=     1312 ft  This is the submarine's operating depth.
 Sigma y=    80000 psi This is the yield strength of steel to be used.
       E=29600000 psi This is Young's modulus for the steel to be used.
      nu=     0.35     This is Poisson's ratio for the steel to be used.
       t=     1.75 in  This is the shell plating thickness.*
      Lf=      2.5 ft  This is the frame spacing.*
       b=     0.75 in  This is the frame web thickness.*
      hw=    10.25 in  This is the frame web height.*
     Wfl=     7.25 in  This is the flange width.*
     tfl=    1.375 in  This is the flange thickness.*
      LB=       32 ft  This is length between King frames or bulkheads.*
      bK=     1.25 in  This is the King frame web thickness.*
     hwK=       22 in  This is the King frame web height.*
    WflK=       16 in  This is the King frame flange width.*
    tflK=     1.75 in  This is the King frame flange thickness.*
 test ti=        2 in  This is a tentative King frame insert thickness.*
                     * signifies that these quantities are trial values.

Results of Calculations:
  t init=  2.0992 in  The input value of t should be close to t init.
    hw/b=13.66666     This should be less than or equal to 18.
  Wfl/hw=0.707317     This should be between 0.7 and 0.8.
   tfl/t=0.785714     This should be between 0.75 and 1.
    wt/B=0.183663     This should be close to 0.18.
 sigma 1         0     If this is 1, then shell stresses are too high.
 sigma t=79772.44 psi This should be less than or equal to sigma y.
sigma t<=sigma y ?        1    If this is one, the framing is acceptable.
    Lfeb=28.45688 in  This is the end bay frame spacing.
     AKf=58.74461 in2 This is the King frame flange area. It should be 3
      Af=17.65625 in2 times Af.
     IKf=11968.73 in4 This is the King frame MOI.  It should be 10 times
      If=1336.741 in4 greater than If.
     Pcr=3695.442 psi This is the King frame buckling pressure.  It
 2.25xPc=     1968 psi should be at least 2.25 times greater than Pc.
 calc ti=1.680558 in  This should be close to test ti.  If not, iterate.
sigma tK<sigma yK?        1    If this is one, King frame is acceptable.
```

```
Intermediate Calculations:
      Ds=31.85416 ft  This is the shell diameter.
      Rs=15.92708 ft  This is the shell radius.
       L=  2.4375 ft  This is shell not contiguous to frame's web.
       P=874.6666 psi This is pressure at operating depth, SF=1.5.
      Ro=       16 ft  This is the outer radius of the hull.
  t init=  2.0992 in  This is a first indication of shell thickness.
    t/Ds=0.004578
    L/Ds=0.076520
    hw/b=13.66666
  Wfl/hw=0.707317
   tfl/t=0.785714
      Aw=  7.6875 in2 This is the cross-sectional area of the web.
     Afl= 9.96875 in2 This is the cross-sectional area of the flange.
      Af=17.65625 in2 This is the cross-sectional area of the frame.
      bt=  1.3125 in2
   Af+bt=18.96875 in2
       B=0.069192
   theta=2.058280 rad
sinhtheta3.852407     sinh(theta/2)=1.220672
coshtheta3.980080     cosh(theta/2)=1.577986
       H=-0.68415     These three functions, H, K, and N are auxiliary
       K=0.626888     functions used in Von-Sanden--Gunther formulas.
       N=0.939307
    beta=2.464422 rad
   gamma=0.285932
      n1=0.422512
      n2=0.566994
sinhn1the0.983487          sinn1thet0.764102
coshn1the1.402585          cosn1thet0.645094
sinhn2the1.450581          sinn2thet0.919589
coshn2the1.761870          cosn2thet0.392880
      F1=0.902897
      F2=0.817351
      F3=-1.24511
      F4=0.644585

         Size and Weight of Frames:
      Le=27.15975 in  This is the effective length of the shell.
                  Area in2  Arm in   Moment       d        Ad2        Io
         Plate    47.52956  191.125 9084.088 2.514056 300.4097 12.12994
         Web        7.6875  185.125 1423.148 -3.48594 93.41695 67.30566
         Flange    9.96875 179.3125 1787.521 -9.29844 861.9085 1.570597
         Af       17.65625 SUM  Mom=12294.75 SUM  Ad2=1255.735 1255.735
         At       65.18581                                  If=1336.741
```

```
           y bar =188.6109 in  This is the centroid of the frame.
It has also been chosen to represent the radius to the neutral axis.

              Rna=188.6109 in  This is the same as the centroid.
              Rcg=181.8432 in  This is the centroid of the frame.
               c1=9.985943 in  distance from NA to inner frame surface
               c2=3.389056 in  distance from NA to outer shell surface
                c=9.985943 in  maximum distance from the NA
         A* extrn=19.50469 in2 This is for external frames.
         A* intrn=18.55747 in2 This is for internal frames.
      wt of frame=2.557619 tons  Steel is assumed here.
      wt of shell=7.993134 tons
      frame+shell=10.55075
            wt/B =0.183663     This should roughly be equal to 0.18.

LOBAR Buckling:
     Pcr=2272.144 psi  pressure which hull fails by general instability
     P92=968.3628 psi  These two pressures should be less than
    P92A=866.0425 psi  yield strength.
      P?=1030.186 psi  NOTE - This is a substitute for P92MOD.
       a=0.227581      NOTE - This assumes internal frames.
 sigma u=63975.61 psi
 sigma'u=95526.09 psi  This is an alternate expression.
Shell Stresses:
sigmao/1=45133.72 psi  This is for stress in xm direction.
         18841.89
sigmao/1=13859.29 psi  This is for stress in xf direction.
         50116.32
sigmao/1=54890.71 psi  This is for stress in phim direction.
         49259.73
sigmao/1=43977.36 psi  This is for stress in phif direction.
         54854.47
 sigma a=   60000 psi  This is the maximum allowable stress.

Test to make sure that all stresses are below the allowable stress.
            Test
                0    In these tests, a one indicates that shell stress
                0    is greater than allowable stress.  A zero indicates
                0    that the shell stress is within allowable levels.
                0
                0
                0
                0
                0
                0

General Instability:
```

```
       m=1.563637       m2=2.444963     m2/2=1.222481       m4=5.977844
 Etm4/Rs=1620156.                EI/RsRcg2Lf=208.6920

For n=2:
     Pcr=9863.444 psi
For n=3:
     Pcr=3010.695 psi
For n=4:
     Pcr=3423.932 psi

Frame Analysis:
       F=6.770447
 sigma c=56769.94 psi
      eo=     0.5 in
sigma b1=1304.726 psi  This corresponds to n=2.
sigma b2=14641.37 psi  This corresponds to n=3.
sigma b3=23002.50 psi  This corresponds to n=4.
 sigma b=23002.50 psi  This is the largest buckling stress.
 sigma t=79772.44 psi  This is the total stress.

End Bay Spacing - Here a spacing greater than Lf is used.
    Lfeb=28.45688 in   This uses formula on page 17 of Ch7 of the notes.

King Frame Analysis:       NOTE - This assumes an internal King frame.
     LeK=28.71545 in   This is the effective length of King frame plate.

Item     Area in2   Arm in   Moment     d       Ad2       Io
Plate    50.25204  191.125 9604.421 9.254248 4303.640 12.92474
Web          27.5      179   4922.5 -2.87075 226.6334 1109.166
Flange         28  167.125   4679.5 -14.7457 6086.241 7.145833
Insert   3.244610  190.125 616.8816 8.254248 221.0638 0.015271
     AfK=58.74461 SUM  Mom=19823.30 SUM  Ad2=10839.57 10839.57
     AtK=108.9966                                IfK=11968.73

 y bar K=181.8707 in  centroid of the cross sectional area of King frame
It has also been chosen to represent the radius to the neutral axis.
    ycgK=173.9543 in  radius to the centroid of the web and flange
    RnaK=181.8707 in  This is the same as the centroid.
    RcgK=173.9543 in  This is the same as the web and flange centroid.

1      BK=0.043103 in2 This ignores the area of the insert.
1  betaK=0.450385 rad This ignores the area of the insert.
1 gammaK=2.020600 rad
1 deltaK=3.787397 rad

2      BK=0.040819 in2 This is a second iteration.
2  betaK=0.814460 rad This is a second iteration.
```

```
2 gammaK=0.445961 rad
2 deltaK=1.030730 rad This is the product of onlv two iterations.
 calc ti=1.680558 in  calculated insert thickness. test ti = calc ti?

      c1K=15.62075 in  distance from neutral axis to inner frame surface
      c2K=10.12924 in  distance from neutral axis to outer shell surface
       cK=15.62075 in  maximum distance from the neutral axis
       FK=12.37258
sigma cK=30737.63 psi

Buck Pcr=3695.442 psi  This is for King frame buckling. It should be
                       greater than 2.25 x Pc.
        m=1.563637      m2=2.444963     m2/2=1.222481        m4=5.977844
 Etm4/Rs=1620156.                EI/RsRcg2Lf=2041.880

For n=2:
     Pcr=15363.01 psi
For n=3:
     Pcr=17676.20 psi
For n=4:
     Pcr=30921.76 psi

sigma b1=1383.687 psi  This corresponds to n=2.
sigma b2=3181.826 psi  This corresponds to n=3.
sigma b3=3335.986 psi  This corresponds to n=4.
 sigma b=3335.986 psi  This is the largest buckling stress.
 sigma t=34073.61 psi  This is the total stress.


Bulkhead Analysis
A shear girder arrangement similar to figure 7 - 35 is assumed.
The width of the doubled bulkhead plate is taken to be hwB; it
tapers linearly to tB over a width equal to hwB.  Only one or two
shear girders can be considered.  It is assumed that the shear
girder will act as a deck support, or as part of the deck itself.


Input Values - The same steel as above is assumed.
      tB=       3 in   This is the thickness of the bulkhead plate.
      bB=    2.75 in   This is the thickness of the shear girder web.
Y1 = hwB=      60 in   This is the web height at midspan.
    Wf1B=      32 in   This is the width of the shear girder flange.
    tf1B=       3 in   This is the thickness of the shear girder flange.
      Y0=28.45688 in   This is the girder depth at the shell. It must
       or88.45688 in   equal Lfeb or Lfeb+n*Lf, where n is an integer.
# girder=       2      This is the number of shear girders, 1 or 2.
```

```
Output Values - 3 deck boat and 7' deckheights assumed.
       l=345.2998 in   This is the length of the shear girders.
   Mbmax= 8.9E+08 lbf-in This is max. bending moment on the bulkhead.
  Z reqd=0.000059 in -3  This is the required section modulus.
       c=53.89910 in     This is max. distance from neutral axis.
  Z calc=0.000059 in -3  This is calculated section modulus. It should
                         equal required section modulus. Adjust input
                         until the two are equal. This is midspan.
 bB calc=5.270495 in     This must roughly equal bB, adjust YO and bB.
For stiffener design, see H. Jackson's notes Ch.7 pages 28-30.

The table below is for midspan, at centerline.
         Area in2    Arm in  Moment    d in    A d2       Io
Bulkhead       558     -1.5      -837 10.60089 62707.41    418.5
     Web       165       30      4950 -20.8991 72067.51    49500
  Flange        96     61.5      5904 -49.3991 234266.1       72
  Insert       192    -4.25      -816 13.35089 34223.28      168
     ABf       453  Sum Mom=     9201  Sum Ad2=403264.3 403264.3
     ABT      1011     y bar=9.100890              IBf=906845.6

The table below is for the end, at the shell.
YO is assumed to be Lfeb+Lf.
         Area in2    Arm in  Moment    d in    A d2       Io
Bulkhead       558     -1.5      -837 10.60089 62707.41    418.5
     Web 243.2564 44.22844 10758.85 -35.1275 300165.0 158615.7
  Flange        96     61.5      5904 -49.3991 234266.1       72
  Insert       192    -4.25      -816 19.09654 70018.15      168
     ABf       453  Sum Mom=15009.85  Sum Ad2=667156.7 667156.7
     ABT      1011     y bar=14.84654              IBf=826431.0


End Closure Analysis
  A hemispherical end closure is assumed. A linear relationship
in figure 7-48 is also assumed.  A factor of safety of 1.5 is used
in calculations for yielding and 2.25 in those for buckling.

Input Values
    R1Of=          in  This is outside radius of forward hemisphere.
    R1Oa=    83.75 in  This is outside radius of aft hemisphere.

Output Values
 hemi tf=        0 in  This is thickness of forward hemisphere plate.
 hemi ta=0.740495 in  This is thickness of aft hemisphere plate.


Calculations
  yld tf=        0 in  This accounts for yielding due to pressure.
```

```
buck tf=        0 in  This accounts for buckling due to pressure.
hemi tf=        0 in  This is the larger of the two.
 yld ta= 0.68675 in
buck ta=0.740495 in
hemi ta=0.740495 in
```

```
A1: 'Submarine Structural Calculations
A2: "(Developed for 13.461 Naval Ship Design by John V. Amy Jr.)
A4: 'This worksheet is derived from the worksheets contained in the book
A5: 'Submarine Design Notes by CAPT Harry A. Jackson, Chapter 7.
A6: 'See this reference for drawings which define the physical significance
A7: 'of each of the variables.  Go to line 218 for the bulkhead analysis.
A8: 'Go to line 267 for the end closure analysis.
A10: 'Input Data:
A11: '      Do=
B11: 32
C11: 'ft  This is outside diameter of the submarine's hull.
A12: '      OD=
B12: 1312
C12: 'ft  This is the submarine's operating depth.
A13: ' Sigma y=
B13: 80000
C13: 'psi This is the yield strength of steel to be used.
A14: '       E=
B14: 29600000
C14: 'psi This is Young's modulus for the steel to be used.
A15: '      nu=
B15: 0.35
C15: '    This is Poisson's ratio for the steel to be used.
A16: '       t=
B16: 1.75
C16: 'in  This is the shell plating thickness.*
A17: '      Lf=
B17: 2.5
C17: 'ft  This is the frame spacing.*
A18: '       b=
B18: 0.75
C18: 'in  This is the frame web thickness.*
A19: '      hw=
B19: 10.25
C19: 'in  This is the frame web height.*
A20: '     Wfl=
B20: 7.25
C20: 'in  This is the flange width.*
A21: '     tfl=
B21: 1.375
```

```
C21: 'in  This is the flange thickness.*
A22: '      LB=
B22: 32
C22: 'ft  This is length between King frames or bulkheads.*
A23: '      bK=
B23: 1.25
C23: 'in  This is the King frame web thickness.*
A24: '     hwK=
B24: 22
C24: 'in  This is the King frame web height.*
A25: '    WflK=
B25: 16
C25: 'in  This is the King frame flange width.*
A26: '    tflK=
B26: 1.75
C26: 'in  This is the King frame flange thickness.*
A27: ' test ti=
B27: 2
C27: 'in  This is a tentative King frame insert thickness.*
C28: "* signifies that these quantities are trial values.
A30: 'Results of Calculations:
A31: '  t init=
B31: +$B$53*$B$54*12/$B$13
C31: 'in  The input value of t should be close to t init.
A32: '    hw/b=
B32: +$B$19/$B$18
C32: '    This should be less than or equal to 18.
A33: '  Wfl/hw=
B33: +$B$20/$B$19
C33: '    This should be between 0.7 and 0.8.
A34: '   tfl/t=
B34: +$B$21/$B$16
C34: '    This should be between 0.75 and 1.
A35: '    wt/B=
B35: +$C$108
C35: '    This should be close to 0.18.
A36: ' sigma 1
B36: +$B$139
C36: '    If this is 1, then shell stresses are too high.
A37: ' sigma t=
B37: +$B$160
C37: 'psi This should be less than or equal to sigma y.
A38: 'sigma t<=sigma y ?
C38: @IF($B$160<=$B$13,1,0)
D38: '  If this is one, the framing is acceptable.
A39: '    Lfeb=
B39: +$B$163
```

```
C39: 'in  This is the end bay frame spacing.
A40: '     AKf=
B40: +$B$173
C40: 'in2 This is the King frame flange area. It should be 3
A41: '       Af=
B41: +$C$92
C41: 'in2 times Af.
A42: '      IKf=
B42: +$G$174
C42: 'in4 This is the King frame MOI.  It should be 10 times
A43: '       If=
B43: +$H$93
C43: 'in4 greater than If.
A44: '      Pcr=
B44: +$B$199
C44: 'psi This is the King frame buckling pressure.  It
A45: " 2.25xPc=
B45: 2.25*$B$53
C45: 'psi should be at least 2.25 times greater than Pc.
A46: ' calc ti=
B46: +$B$191
C46: 'in  This should be close to test ti.  If not, iterate.
A47: 'sigma tK<sigma yK?
C47: @IF($B$215<=$B$13,1,0)
D47: '  If this is one, King frame is acceptable.
A49: 'Intermediate Calculations:
A50: '       Ds=
B50: +$B$11-($B$16/12)
C50: 'ft  This is the shell diameter.
A51: '       Rs=
B51: +$B$50/2
C51: 'ft  This is the shell radius.
A52: '        L=
B52: +$B$17-($B$18/12)
C52: 'ft  This is shell not contiguous to frame's web.
A53: '        P=
B53: +$B$12/1.5
C53: 'psi This is pressure at operating depth, SF=1.5.
A54: '       Ro=
B54: +$B$11/2
C54: 'ft  This is the outer radius of the hull.
A55: '  t init=
B55: +$B$53*$B$54*12/$B$13
C55: 'in  This is a first indication of shell thickness.
A56: '    t/Ds=
B56: +$B$16/(12*$B$50)
A57: '    L/Ds=
```

```
B57: +$B$52/$B$50
A58: '     hw/b=
B58: +$B$19/$B$18
A59: '   Wfl/hw=
B59: +$B$20/$B$19
A60: '    tfl/t=
B60: +$B$21/$B$16
A61: '        Aw=
B61: +$B$18*$B$19
C61: 'in2 This is the cross-sectional area of the web.
A62: '       Afl=
B62: +$B$20*$B$21
C62: 'in2 This is the cross-sectional area of the flange.
A63: '        Af=
B63: +$B$61+$B$62
C63: 'in2 This is the cross-sectional area of the frame.
A64: '        bt=
B64: +$B$16*$B$18
C64: 'in2
A65: '    Af+bt=
B65: +$B$63+$B$64
C65: 'in2
A66: '         B=
B66: +$B$64/$B$65
A67: '    theta=
B67: 18.2*$B$52/(@SQRT(100*$B$56)*$B$50)
C67: 'rad
A68: 'sinhtheta
B68: 0.5*(@EXP($B$67)-@EXP(-$B$67))
C68: '     sinh(theta/2)=
E68: 0.5*(@EXP($B$67/2)-@EXP(-$B$67/2))
A69: 'coshtheta
B69: 0.5*(@EXP($B$67)+@EXP(-$B$67))
C69: '     cosh(theta/2)=
E69: 0.5*(@EXP($B$67/2)+@EXP(-$B$67/2))
A70: '         H=
B70: -(3*$E$68*@COS($B$67/2)+$E$69*@SIN($B$67/2))/($B$68+@SIN($B$67))
C70: '     These three functions, H, K, and N are auxiliary
A71: '         K=
B71: ($B$68-@SIN($B$67))/($B$68+@SIN($B$67))
C71: '     functions used in Von-Sanden--Gunther formulas.
A72: '         N=
B72: ($B$69-@COS($B$67))/($B$68+@SIN($B$67))
A73: '     beta=
B73: 1.555*@SQRT($B$51*12*($B$16^3))*$B$72/$B$65
C73: 'rad
A74: '    gamma=
```

```
   B74: ($B$51*12/$B$16)^2*@SQRT(3*(1-$B$15^2))*$B$53/(2*$B$14)
   A75: '       n1=
   B75: 0.5*@SQRT(1-$B$74)
   A76: '       n2=
   B76: 0.5*@SQRT(1+$B$74)
   A77: 'sinhn1the
   B77: 0.5*(@EXP($B$75*$B$67)-@EXP(-$B$75*$B$67))
   D77: 'sinn1thet
   E77: @SIN($B$75*$B$67)
   A78: 'coshn1the
   B78: 0.5*(@EXP($B$75*$B$67)+@EXP(-$B$75*$B$67))
   D78: 'cosn1thet
   E78: @COS($B$75*$B$67)
   A79: 'sinhn2the
   B79: 0.5*(@EXP($B$76*$B$67)-@EXP(-$B$76*$B$67))
   D79: 'sinn2thet
   E79: @SIN($B$76*$B$67)
   A80: 'coshn2the
   B80: 0.5*(@EXP($B$76*$B$67)+@EXP(-$B$76*$B$67))
   D80: 'cosn2thet
   E80: @COS($B$76*$B$67)
   A81: '       F1=
   B81: (4/$B$67)*(($B$78^2-$E$80^2)/(($B$77*$B$78/$B$75)+($E$79*$E$80/$B$76)))
   A82: '       F2=
   B82: ((($B$78*$E$79/$B$76)+($B$77*$E$80/$B$75))/(($B$77*$B$78/$B$75)+($E$79*$E$80

   A83: '       F3=
   B83: @SQRT(3/(1-$B$15^2))*((($E$80*$E$79/$B$76)-($B$77*$B$78/$B$75))/(($B$77*$B$7
$79*$E$80/$B$76)))
   A84: '       F4=
   B84: @SQRT(3/(1-$B$15^2))*((($B$78*$E$79/$B$76)-($B$77*$E$80/$B$75))/(($B$77*$B$7
$79*$E$80/$B$76)))
   B86: 'Size and Weight of Frames:
   A87: '       Le=
   B87: ($B$52*12)*$B$81+$B$18
   C87: 'in  This is the effective length of the shell.
   C88: 'Area in2
   D88: ' Arm in
   E88: ' Moment
   F88: '    d
   G88: '   Ad2
   H88: '    Io
   B89: 'Plate
   C89: +$B$87*$B$16
   D89: +$B$51*12
   E89: +$C89*$D89
   F89: +$D89-$C$95
   G89: +$C89*($F89^2)
   H89: +$B$87*$B$16^3/12
   B90: 'Web
```

```
C90: +$B$19*$B$18
D90: ($B$51*12)-0.5*$B$16-0.5*$B$19
E90: +$C90*$D90
F90: +$D90-$C$95
G90: +$C90*($F90^2)
H90: +$B$18*$B$19^3/12
B91: 'Flange
C91: +$B$20*$B$21
D91: ($B$51*12)-0.5*$B$16-$B$19-0.5*$B$21
E91: +$C91*$D91
F91: +$D91-$C$95
G91: +$C91*($F91^2)
H91: +$B$20*$B$21^3/12
B92: 'Af
C92: +$C$90+$C$91
D92: 'SUM  Mom=
E92: @SUM(E89..E91)
F92: 'SUM  Ad2=
G92: @SUM(G89..G91)
H92: +$G$92
B93: 'At
C93: +$C$89+$C$92
G93: '      If=
H93: @SUM(H89..H92)
B95: '  y bar =
C95: +$E$92/$C$93
D95: 'in  This is the centroid of the frame.
A96: 'It has also been chosen to represent the radius to the neutral axis.
B98: '      Rna=
C98: +$C$95
D98: 'in  This is the same as the centroid.
B99: '      Rcg=
C99: ($E$90+$E$91)/$C$92
D99: 'in  This is the centroid of the frame.
B100: '      c1=
C100: +$C$95-(($B$54*12)-$B$16-$B$19-$B$21)
D100: 'in  distance from NA to inner frame surface
B101: '      c2=
C101: ($B$54*12)-$C$95
D101: 'in  distance from NA to outer shell surface
B102: '       c=
C102: @IF($C$100>=$C$101,$C$100,$C$101)
D102: 'in  maximum distance from the NA
B103: 'A* extrn=
C103: ($B$51*12/$C$99)^2*$C$92
D103: 'in2 This is for external frames.
B104: 'A* intrn=
```

```
C104: ($B$51*12/$C$99)*$C$92
D104: 'in2 This is for internal frames.
A105: '      wt of frame=
C105: 0.0007966*$C$99*$C$92
D105: 'tons  Steel is assumed here.
A106: '      wt of shell=
C106: 0.0007966*$B$51*12*$B$17*12*$B$16
D106: 'tons
A107: '      frame+shell=
C107: +$C$105+$C$106
B108: '   wt/B =
C108: 19251.382*$C$107/(($B$54*12)^2*($B$17*12))
D108: '    This should roughly be equal to 0.18.
A110: 'LOBAR Buckling:
A111: '     Pcr=
B111: 2.6*$B$14*($B$56^2.5)/($B$17/$B$50-0.45*@SQRT($B$56))
C111: 'psi  pressure which hull fails by general instability
A112: '     P92=
B112: 2*$B$13*$B$56/(0.5+1.815*$B$71*(0.85-$B$66)/(1+$B$73))
C112: 'psi  These two pressures should be less than
A113: '    P92A=
B113: 2*$B$13*$B$56/(1+$B$70*(0.85-$B$66)/(1+$B$73))
C113: 'psi  yield strength.
A114: '      P?=
B114: +$B$13*$B$16/($B$51*12*@SQRT(0.75-1.5*$B$115*$B$82+$B$115^2*$B$82^2))
C114: 'psi  NOTE - This is a substitute for P92MOD.
A115: '       a=
B115: (1-0.5*$B$15)/(1+$B$64/$C$104+$B$17*12*$B$16*$B$81/$C$104)
C115: '     NOTE - This assumes internal frames.
A116: ' sigma u=
B116: ($B$12*$B$11*12)/(4.5*$B$16)
C116: 'psi
A117: ' sigma'u=
B117: +$B$53*$B$51*12/$B$16
C117: 'psi  This is an alternate expression.
A118: 'Shell Stresses:
A119: 'sigmao/1=
B119: +$B$116*(0.5+$B$115*$B$81)
C119: 'psi  This is for stress in xm direction.
B120: +$B$116*(0.5-$B$115*$B$81)
A121: 'sigmao/1=
B121: +$B$116*(0.5+$B$115*$B$83)
C121: 'psi  This is for stress in xf direction.
B122: +$B$116*(0.5-$B$115*$B$83)
A123: 'sigmao/1=
B123: +$B$116*(1+$B$115*(-$B$82+0.3*$B$84))
C123: 'psi  This is for stress in phim direction.
```

```
B124: +$B$116*(1+$B$115*(-$B$82-0.3*$B$84))
A125: 'sigmao/1=
B125: +$B$116*(1+$B$115*(-1+0.3*$B$83))
C125: 'psi  This is for stress in phif direction.
B126: +$B$116*(1+$B$115*(-1-0.3*$B$83))
A127: ' sigma a=
B127: 0.75*$B$13
C127: 'psi  This is the maximum allowable stress.
A129: 'Test to make sure that all stresses are below the allowable stress.
B130: '   Test
B131: @IF(B119>$B$127,1,0)
C131: '   In these tests, a one indicates that shell stress
B132: @IF(B120>$B$127,1,0)
C132: '   is greater than allowable stress.  A zero indicates
B133: @IF(B121>$B$127,1,0)
C133: '   that the shell stress is within allowable levels.
B134: @IF(B122>$B$127,1,0)
B135: @IF(B123>$B$127,1,0)
B136: @IF(B124>$B$127,1,0)
B137: @IF(B125>$B$127,1,0)
B138: @IF(B126>$B$127,1,0)
B139: @IF(@SUM(B131..B138)>0,1,0)
A141: 'General Instability:
A142: '        m=
B142: @PI*$B$51/$B$22
C142: '       m2=
D142: +$B$142^2
E142: '     m2/2=
F142: +$D$142/2
G142: '       m4=
H142: +$B$142^4
A143: ' Etm4/Rs=
B143: +$B$14*$B$16*$H$142/($B$51*12)
D143: '       EI/RsRcg2Lf=
F143: +$B$14*$H$93/($B$51*12*($C$99^2)*$B$17*12)
A145: 'For n=2:
A146: '      Pcr=
B146: +$B$143/((3+$F$142)*(4+$D$142)^2)+$F$143*3
C146: 'psi
A147: 'For n=3:
A148: '      Pcr=
B148: +$B$143/((8+$F$142)*(9+$D$142)^2)+$F$143*8
C148: 'psi
A149: 'For n=4:
A150: '      Pcr=
B150: +$B$143/((15+$F$142)*(16+$D$142)^2)+$F$143*15
C150: 'psi
```

```
A152: 'Frame Analysis:
A153: '       F=
B153: +$B$18*(1+0.85*$B$73/$B$66)/(1+$B$73)
A154: ' sigma c=
B154: +$C$99*$B$53*$B$153/$B$65
C154: 'psi
A155: '       eo=
B155: @IF($B$16/2<=0.5,$B$16/2,0.5)
C155: 'in
A156: 'sigma b1=
B156: +$B$14*$B$155*$C$102*3*$B$53/($C$99^2*($B$146-$B$53))
C156: 'psi  This corresponds to n=2.
A157: 'sigma b2=
B157: +$B$14*$B$155*$C$102*8*$B$53/($C$99^2*($B$148-$B$53))
C157: 'psi  This corresponds to n=3.
A158: 'sigma b3=
B158: +$B$14*$B$155*$C$102*15*$B$53/($C$99^2*($B$150-$B$53))
C158: 'psi  This corresponds to n=4.
A159: ' sigma b=
B159: @IF($B$156>=$B$157,@IF($B$156>=$B$158,$B$156,$B$158),@IF($B$157>=$B$158,$B$1

C159: 'psi  This is the largest buckling stress.
A160: ' sigma t=
B160: +$B$159+$B$154
C160: 'psi  This is the total stress.
A162: 'End Bay Spacing - Here a spacing greater than Lf is used.
A163: '     Lfeb=
B163: 1.556*@SQRT($B$51*12*$B$16)
C163: 'in   This uses formula on page 17 of Ch7 of the notes.
A165: 'King Frame Analysis:
D165: 'NOTE - This assumes an internal King frame.
A166: '      LeK=
B166: 2*@SQRT($B$51*12*$B$16)/((3*(1-$B$15^2))^0.25)
C166: 'in   This is the effective length of King frame plate.
A168: 'Item
B168: 'Area in2
C168: '  Arm in
D168: '  Moment
E168: '    d
F168: '   Ad2
G168: '    Io
A169: 'Plate
B169: +$B$166*$B$16
C169: +$B$51*12
D169: +$B169*$C169
E169: +$C169-$B$176
F169: +$B169*($E169^2)
G169: +$B$166*$B$16^3/12
```

```
A170: 'Web
B170: +$B$23*$B$24
C170: ($B$54*12)-$B$27-0.5*$B$24
D170: +$B170*$C170
E170: +$C170-$B$176
F170: +$B170*($E170^2)
G170: +$B$23*$B$24^3/12
A171: 'Flange
B171: +$B$25*$B$26
C171: ($B$54*12)-$B$27-$B$24-0.5*$B$26
D171: +$B171*$C171
E171: +$C171-$B$176
F171: +$B171*($E171^2)
G171: +$B$25*$B$26^3/12
A172: 'Insert
B172: ($B$163/2-$B$23)*($B$27-$B$16)
C172: ($B$54*12)-$B$16-0.5*($B$27-$B$16)
D172: +$B172*$C172
E172: +$C172-$B$176
F172: +$B172*($E172^2)
G172: 2*(($B$163/4-$B$23)*($B$27-$B$16)^3)/12
A173: '    AfK=
B173: @SUM($B170..$B172)
C173: 'SUM  Mom=
D173: @SUM(D169..D172)
E173: 'SUM  Ad2=
F173: @SUM(F169..F172)
G173: +$F$173
A174: '    AtK=
B174: @SUM($B169..$B172)
F174: '    IfK=
G174: @SUM(G169..G173)
A176: ' y bar K=
B176: +$D$173/$B$174
C176: 'in  centroid of the cross sectional area of King frame
A177: 'It has also been chosen to represent the radius to the neutral axis.
A178: '   ycgK=
B178: @SUM($D$170..$D$172)/$B$173
C178: 'in  radius to the centroid of the web and flange
A179: '   RnaK=
B179: +$B$176
C179: 'in  This is the same as the centroid.
A180: '   RcgK=
B180: +$B$178
C180: 'in  This is the same as the web and flange centroid.
A182: '1    BK=
B182: +$B$23*$B$27/($B$23*$B$24+$B$25*$B$26+$B$23*$B$27)
```

```
C182: 'in2 This ignores the area of the insert.
A183: '1  betaK=
B183: 1.555*@SQRT($B$51*12*($B$16^3))/($B$16*$B$17*12+$B$23*$B$24+$B$25*$B$26+$B$2

C183: 'rad This ignores the area of the insert.
A184: '1 gammaK=
B184: 3.632*(0.85-$B$182)/(1+$B$183)
C184: 'rad
A185: '1 deltaK=
B185: 0.25+1.4*$B$184*($B$13/$B$116)
C185: 'rad
A187: "2      BK=
B187: +$B$23*$B$27/($B$173+$B$23*$B$27)
C187: 'in2 This is a second iteration.
A188: "2  betaK=
B188: 1.555*@SQRT($B$11*6*($B$16^3))/($B$173+$B$23*$B$27)
C188: 'rad This is a second iteration.
A189: "2 gammaK=
B189: (0.85-$B$187)/(1+$B$188)
C189: 'rad
A190: "2 deltaK=
B190: 0.25+1.4*$B$189*($B$13/$B$116)
C190: 'rad This is the product of only two iterations.
A191: ' calc ti=
B191: +$B$189*$B$27/($B$190-0.5)
C191: 'in  calculated insert thickness, test ti = calc ti?
A193: '     c1K=
B193: +$B$176-(($B$54*12)-$B$27-$B$24-$B$26)
C193: 'in  distance from neutral axis to inner frame surface
A194: '     c2K=
B194: ($B$54*12)-$B$176
C194: 'in  distance from neutral axis to outer shell surface
A195: '       cK=
B195: @IF($B$193>=$B$194,$B$193,$B$194)
C195: 'in  maximum distance from the neutral axis
A196: '       FK=
B196: +$B$23*(1+0.85*$B$188/$B$187)/(1+$B$188)
A197: 'sigma cK=
B197: +$B$180*$B$53*$B$196/($B$173+$B$23*$B$27)
C197: 'psi
A199: 'Buck Pcr=
B199: 25*$B$14*$G$174/(($B$180*2)^3*2*$B$163)
C199: 'psi  This is for King frame buckling. It should be
C200: '     greater than 2.25 x Pc.
A201: '        m=
B201: @PI*$B$51/$B$22
C201: '       m2=
D201: +$B$142^2
```

```
E201: '    m2/2=
F201: +$D$142/2
G201: '      m4=
H201: +$B$142^4
A202: ' Etm4/Rs=
B202: +$B$14*$B$16*$H$201/($B$51*12)
D202: '      EI/RsRcg2Lf=
F202: +$B$14*$G$174/($B$51*12*($B$180^2)*$B$17*12)
A204: 'For n=2:
A205: '     Pcr=
B205: +$B$202/((3+$F$201)*(4+$D$201)^2)+$F$202*3
C205: 'psi
A206: 'For n=3:
A207: '     Pcr=
B207: +$B$202/((8+$F$201)*(9+$D$201)^2)+$F$202*8
C207: 'psi
A208: 'For n=4:
A209: '     Pcr=
B209: +$B$202/((15+$F$201)*(16+$D$201)^2)+$F$202*15
C209: 'psi
A211: 'sigma b1=
B211: +$B$14*$B$195*$B$155*3*$B$53/($B$180^2*($B$205-$B$53))
C211: 'psi  This corresponds to n=2.
A212: 'sigma b2=
B212: +$B$14*$B$155*$B$195*8*$B$53/($B$180^2*($B$207-$B$53))
C212: 'psi  This corresponds to n=3.
A213: 'sigma b3=
B213: +$B$14*$B$155*$B$195*15*$B$53/($B$180^2*($B$209-$B$53))
C213: 'psi  This corresponds to n=4.
A214: ' sigma b=
B214: @IF($B$211>=$B$212,@IF($B$211>=$B$213,$B$211,$B$213),@IF($B$212>=$B$213,$B$2

C214: 'psi  This is the largest buckling stress.
A215: ' sigma t=
B215: +$B$197+$B$214
C215: 'psi  This is the total stress.
A218: 'Bulkhead Analysis
A219: 'A shear girder arrangement similar to figure 7 - 35 is assumed.
A220: 'The width of the doubled bulkhead plate is taken to be hwB; it
A221: 'tapers linearly to tB over a width equal to hwB.  Only one or two
A222: 'shear girders can be considered.  It is assumed that the shear
A223: 'girder will act as a deck support, or as part of the deck itself.
A226: 'Input Values - The same steel as above is assumed.
A227: '      tB=
B227: 3
C227: 'in   This is the thickness of the bulkhead plate.
A228: '      bB=
B228: 2.75
```

```
  C228: 'in   This is the thickness of the shear girder web.
  A229: 'Y1 = hwB=
  B229: 60
  C229: 'in   This is the web height at midspan.
  A230: '    WflB=
  B230: 32
  C230: 'in   This is the width of the shear girder flange.
  A231: '    tflB=
  B231: 3
  C231: 'in   This is the thickness of the shear girder flange.
  A232: '      YO=
  B232: +$B$163
  C232: 'in   This is the girder depth at the shell. It must
  A233: '        or
  B233: +$B$163+12*$B$17*2
  C233: 'in   equal Lfeb or Lfeb+n*Lf, where n is an integer.
  A234: "# girder=
  B234: 2
  C234: '     This is the number of shear girders, 1 or 2.
  A236: 'Output Values - 3 deck boat and 7' deckheights assumed.
  A237: '        l=
  B237: @IF($B$234=1,$B$11*12-2*$B$16,2*@SQRT(($B$11*6)^2-((0.5*(10+($B$11-10-2*7)/
6)^2))
  C237: 'in   This is the length of the shear girders.
  A238: '   Mbmax=
  B238: ($B$11*12/2-$B$16)^2*$B$237*$B$53/12.223
  C238: 'lbf-in This is max. bending moment on the bulkhead.
  A239: '  Z reqd=
  B239: +$B$13/(1.5*$B$238)
  C239: 'in -3  This is the required section modulus.
  A240: '        c=
  B240: @IF((2*$B$227+$D$254)>=($B$229+$B$231-$D$254),(2*$B$227+$D$254),($B$229+$B23

  C240: 'in     This is max. distance from neutral axis.
  A241: '  Z calc=
  B241: +$B$240/$G$254
  C241: 'in -3  This is calculated section modulus. It should
  C242: '       equal required section modulus. Adjust input
  C243: '       until the two are equal. This is midspan.
  A244: ' bB calc=
  B244: 1.5*@PI*$B$53*($B$11*12/2-$B$16)^2/($B$13*$B$233*4)
  C244: 'in     This must roughly equal bB, adjust YO and bB.
  A245: 'For stiffener design, see H. Jackson's notes Ch.7 pages 28-30.
  A247: 'The table below is for midspan, at centerline.
  B248: 'Area in2
  C248: '   Arm in
  D248: '  Moment
  E248: '   d in
  F248: '  A d2
```

```
G248: '   Io
A249: 'Bulkhead
B249: (30*$B$227+3*$B$230)*$B$227
C249: -0.5*$B$227
D249: +$B249*$C249
E249: +$D$254+0.5*$B$227
F249: +$B249*$E249^2
G249: (30*$B$227+3*$B$230)*$B$227^3/12
A250: '     Web
B250: +$B$228*$B$229
C250: 0.5*$B$229
D250: +$B250*$C250
E250: +$D$254-0.5*$B$229
F250: +$B250*$E250^2
G250: +$B$228*$B$229^3/12
A251: '  Flange
B251: +$B$230*$B$231
C251: +$B$229+0.5*$B$231
D251: +$B251*$C251
E251: +$D$254-$B$229+0.5*$B$231
F251: +$B251*$E251^2
G251: +$B$230*$B$231^3/12
A252: '  Insert
B252: +$B$227*$B$230*2
C252: -$B$227-5*$B$227/12
D252: +$B252*$C252
E252: +$D$254-$C$252
F252: +$B252*$E252^2
G252: +$B$227^3*$B$230/12+2*($B$227^3*$B$230/18)
A253: '     ABf
B253: @SUM($B$250..$B$252)
C253: ' Sum Mom=
D253: @SUM(D249..D252)
E253: ' Sum Ad2=
F253: @SUM(F249..F252)
G253: +$F$253
A254: '     ABT
B254: @SUM($B$249..$B$252)
C254: '   y bar=
D254: +$D$253/$B$254
F254: '     IBf=
G254: @SUM(G249..G253)*$B$234
A256: 'The table below is for the end, at the shell.
A257: 'Y0 is assumed to be Lfeb+Lf.
B258: 'Area in2
C258: '   Arm in
D258: '  Moment
```

```
E258: '   d in
F258: '  A d2
G258: '   Io
A259: 'Bulkhead
B259: (30*$B$227+3*$B$230)*$B$227
C259: -0.5*$B$227
D259: +$B259*$C259
E259: +$D$254+0.5*$B$227
F259: +$B259*$E259^2
G259: (30*$B$227+3*$B$230)*$B$227^3/12
A260: '      Web
B260: +$B$228*$B$233
C260: 0.5*$B$233
D260: +$B260*$C260
E260: +$D$254-0.5*$B$233
F260: +$B260*$E260^2
G260: +$B$228*$B$233^3/12
A261: '  Flange
B261: +$B$230*$B$231
C261: +$B$229+0.5*$B$231
D261: +$B261*$C261
E261: +$D$254-$B$229+0.5*$B$231
F261: +$B261*$E261^2
G261: +$B$230*$B$231^3/12
A262: '  Insert
B262: +$B$227*$B$230*2
C262: -$B$227-5*$B$227/12
D262: +$B262*$C262
E262: +$D$264-$C$262
F262: +$B262*$E262^2
G262: +$B$227^3*$B$230/12+2*($B$227^3*$B$230/18)
A263: '      ABf
B263: @SUM($B$250..$B$252)
C263: ' Sum Mom=
D263: @SUM(D259..D262)
E263: ' Sum Ad2=
F263: @SUM(F259..F262)
G263: +$F$263
A264: '      ABT
B264: @SUM($B$249..$B$252)
C264: '   y bar=
D264: +$D$263/$B$264
F264: '      IBf=
G264: @SUM(G259..G263)
A267: 'End Closure Analysis
A268: '  A hemispherical end closure is assumed. A linear relationship
A269: 'in figure 7-48 is also assumed.  A factor of safety of 1.5 is used
```

```
A270: 'in calculations for yielding and 2.25 in those for buckling.
A272: 'Input Values
A273: '    R10f=
C273: 'in  This is outside radius of forward hemisphere.
A274: '    R10a=
B274: 83.75
C274: 'in  This is outside radius of aft hemisphere.
A276: 'Output Values
A277: ' hemi tf=
B277: +$B$284
C277: 'in  This is thickness of forward hemisphere plate.
A278: ' hemi ta=
B278: +$B$287
C278: 'in  This is thickness of aft hemisphere plate.
A281: 'Calculations
A282: '  yld tf=
B282: +$B$273*(0.75*$B$53/$B$13)
C282: 'in  This accounts for yielding due to pressure.
A283: ' buck tf=
B283: +$B$273*(@SQRT(3*(1-$B$15^2))*$B$53/(2*$B$14))^0.444444
C283: 'in  This accounts for buckling due to pressure.
A284: ' hemi tf=
B284: @IF($B$282>$B$283,$B$282,$B$283)
C284: 'in  This is the larger of the two.
A285: '  yld ta=
B285: +$B$274*(0.75*$B$53/$B$13)
C285: 'in
A286: ' buck ta=
B286: +$B$274*(@SQRT(3*(1-$B$15^2))*$B$53/(2*$B$14))^0.444444
C286: 'in
A287: ' hemi ta=
B287: @IF($B$285>$B$286,$B$285,$B$286)
C287: 'in
```

1.3 Table 3 - Program Output, P_HULL

```
No paper error writing device PRN
Abort, Retry, Ignore?


      Pressure Hull Calculation Program

   COPYRIGHT (C) 1989 by Norbert H. Doerry

   Version 2.0  <> 31 July 1989

   Input File : a:thsbphi9
   Time       : Thu Jan 11 20:25:35 1990

       Segment      :   Fwo    Aft  Length  Surface  Volume   LCB    LCG  Dist
        Type        :  Diam   Diam           Area

  SPHERICAL NOSECAP :   0.00   0.00   0.00       0        0   0.00   0.00   0.0
           CYLINDER :   4.00   4.00  26.92     338      338  13.46  13.46   0.0
 TRANSITION / CONIC :   4.00  31.74  16.00    1189     4819  38.37  36.99  26.9
     ZONE SPHEREOID :  31.74  32.00  12.88    1292    10311  49.38  49.37  42.9
           CYLINDER :  32.00  32.00  96.00    9651    77208 103.80 103.80  55.8
    ZONE PARABOLOID :  32.00  29.56  45.20    4456    34915 173.87 174.14 151.8
 TRANSITION / CONIC :  29.56  13.83   9.00     815     3473 200.46 200.96 197.0
           CYLINDER :  13.83  13.83  37.50    1630     5636 224.75 224.75 206.0
  SPHERICAL TAILCAP :  13.83   0.00   6.92     301      693 246.09 246.96 243.5
              TOTAL :               250.42   19671   137393 123.13 126.80

 TOTAL DISPLACEMENT :  3927.63 LTONS


C>
```

1.4 Figure 1 - Pressure Hull Design Showing Frames and Bulkheads

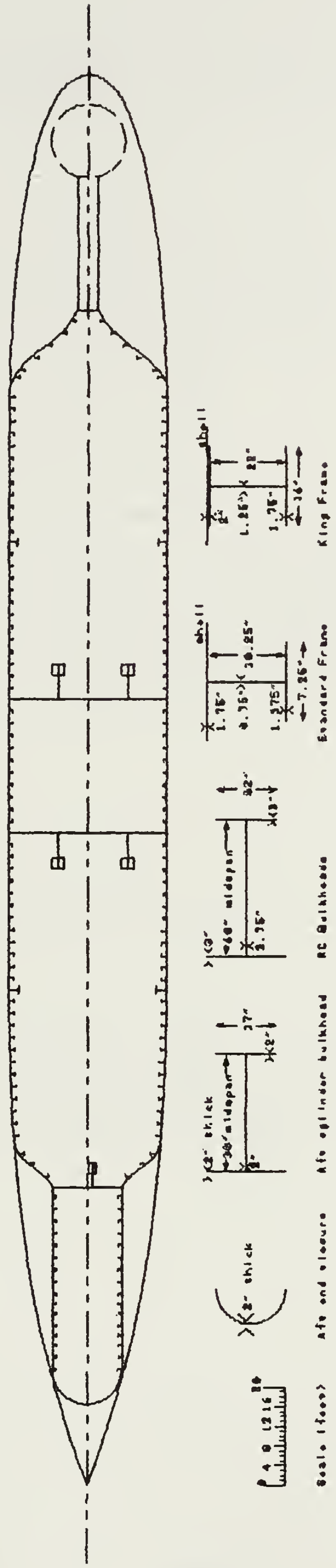

1.5 Table 4 - MBT Size and Location Calculations, Initial Estimate

```
Thesis                                                  John V. Amy Jr.
MBT Calculations                                        05 January 1990

These calculations are peculiar to the pressure hull and envelope
that have been developed thus far.


AFT TANK #1:
  Input
     La=    75.7 ft  This is the distance of aft MBT bulkhead from *
                     the aft end of the PMB at 172.8ft.
     na=    2.75     This is the aft paraboloid exponent.          *
      D=      32 ft  This is the maximum hull diameter.            *
   Laft=   115.2 ft  This is the length of the after body.         *
  Output
     Ro=10.95757 ft  This is the radius at the aft MBT bulkhead.
      L=      20 ft  This is the length of the aft MBT.
  \/aft1= 2231.04 ft3 This is volume of forward segment of tank.
   LCG1=   225.5 ft  This is LCG of forward segment of tank.
  \/aft2=4465.364 ft3 This is volume of aft segment of tank.
   LCG2=   238.5 ft  This is LCG of aft segment of tank.
   \/aft=6696.404 ft3 This is the total volume of the aft tank.
   LCGa=234.1687 ft  This is the LCG of the entire aft tank.



AFT TANK #2:
  Input
    La2=     101 ft  This is the distance of aft bulkhead from PMB. *


  Output
     Ro=4.856812 ft  This is the radius at the aft MBT bulkhead.
      L=     5.3 ft  This is the length of the aft MBT.
   \/a2=851.5330 ft3 This is the volume of the aft aft tank.
  LCG a2=268.6447 ft  This is the LCG of the aft aft tank.
```

```
FWD TANK:
  Input
      Lf=      43 ft  This is the distance of fwd MBT bulkhead from *
                      the fwd end of the PMB at 76.8ft.
      nf=    2.25     This is the fwd ellipsoid exponent.           *
       D=      32 ft  This is the maximum hull diameter.            *
    Lfwd=    76.8 ft  This is the length of the forward body.       *
  Output
      Ro=13.90160 ft  This is the radius at the fwd MBT bulkhead.
       L=    17.2 ft  This is the length of the fwd MBT.
   \/fwd=9578.027 ft3 This is the total volume of the aft tank.
    LCGf=    42.4 ft  This is the LCG of the entire aft tank.
```

```
TOTAL MBT:
  Input
   \/mbt= 17203.8 ft3 This is the required MBT volume.               *
     LCG=  130.82 ft  This is the required MBT LCG.                  *

  Output
   \/sum=17125.96 ft3 This is the sum of the two calculated MBT's.
     LCG=128.6325 ft  This is the two tanks' combined LCG.

  Errors
   %  \/=-0.45242     This is the percent error in volume.
   % LCG=-1.67207     This is the percent error in LCG.
```

```
A1: 'Thesis
G1: 'John V. Amy Jr.
A2: 'MBT Calculations
G2: "05 January 1990
A4: 'These calculations are peculiar to the pressure hull and envelope
A5: 'that have been developed thus far.
A8: 'AFT TANK #1:
A9: '  Input
A10: '      La=
B10: 75.7
C10: 'ft  This is the distance of aft MBT bulkhead from *
C11: '    the aft end of the PMB at 172.8ft.
A12: '      na=
```

```
B12: 2.75
C12: '    This is the aft paraboloid exponent.          *
A13: '       D=
B13: 32
C13: 'ft  This is the maximum hull diameter.           *
A14: '    Laft=
B14: 115.2
C14: 'ft  This is the length of the after body.        *
A15: '  Output
A16: '      Ro=
B16: ($B$13/2)*(1-($B$10/$B$14)^$B$12)
C16: 'ft  This is the radius at the aft MBT bulkhead.
A17: '       L=
B17: +$B$10+172.8-228.5
C17: 'ft  This is the length of the aft MBT.
A18: '  \/aft1=
B18: 2231.04
C18: 'ft3 This is volume of forward segment of tank.
A19: '    LCG1=
B19: 225.5
C19: 'ft  This is LCG of forward segment of tank.
A20: '  \/aft2=
B20: @PI*($B$16^2-49)*$B$17
C20: 'ft3 This is volume of aft segment of tank.
A21: '    LCG2=
B21: ($B$17/2)+228.5
C21: 'ft  This is LCG of aft segment of tank.
A22: '   \/aft=
B22: +$B$18+$B$20
C22: 'ft3 This is the total volume of the aft tank.
A23: '    LCGa=
B23: ($B$18*$B$19+$B$20*$B$21)/$B$22
C23: 'ft  This is the LCG of the entire aft tank.
A28: 'AFT TANK #2:
A29: '  Input
A30: '     La2=
B30: 101
C30: 'ft  This is the distance of aft bulkhead from PMB. *
A33: '  Output
A34: '      Ro=
B34: ($B$13/2)*(1-($B$30/$B$14)^$B$12)
C34: 'ft  This is the radius at the aft MBT bulkhead.
A35: '       L=
B35: +$B$30-95.7
C35: 'ft  This is the length of the aft MBT.
A36: '    \/a2=
B36: (@PI*7*(269.17+163.43+209.74)/12)-2*343*@PI/3+@PI*$B$34^2*$B$35
```

```
 C36: 'ft3 This is the volume of the aft aft tank.
 A37: '  LCG a2=
 B37: (((@PI*7*(269.17+163.43+209.74)/12)-2*343*@PI/3)*266.5+(@PI*$B$34^2*$B$35)*(0
.5))/$B$36
 C37: 'ft  This is the LCG of the aft aft tank.
 A48: 'FWD TANK:
 A49: '  Input
 A50: '      Lf=
 B50: 43
 C50: 'ft  This is the distance of fwd MBT bulkhead from *
 C51: '    the fwd end of the PMB at 76.8ft.
 A52: '      nf=
 B52: 2.25
 C52: '    This is the fwd ellipsoid exponent.           *
 A53: '       D=
 B53: 32
 C53: 'ft  This is the maximum hull diameter.            *
 A54: '    Lfwd=
 B54: 76.8
 C54: 'ft  This is the length of the forward body.       *
 A55: '  Output
 A56: '      Ro=
 B56: ($B$13/2)*((1-($B$50/$B$54)^$B$52)^(1/$B$52))
 C56: 'ft  This is the radius at the fwd MBT bulkhead.
 A57: '        L=
 B57: +$B$50-25.8
 C57: 'ft  This is the length of the fwd MBT.
 A58: '   \/fwd=
 B58: @PI*($B$56^2-16)*$B$57
 C58: 'ft3 This is the total volume of the aft tank.
 A59: '    LCGf=
 B59: 51-($B$57/2)
 C59: 'ft  This is the LCG of the entire aft tank.
 A68: 'TOTAL MBT:
 A69: '  Input
 A70: '   \/mbt=
 B70: 17203.8
 C70: 'ft3 This is the required MBT volume.                *
 A71: '     LCG=
 B71: 130.82
 C71: 'ft  This is the required MBT LCG.                   *
 A73: '  Output
 A74: '   \/sum=
 B74: +$B$22+$B$36+$B$58
 C74: 'ft3 This is the sum of the two calculated MBT's.
 A75: '     LCG=
 B75: ($B$22*$B$23+$B$36*$B$37+$B$58*$B$59)/$B$74
 C75: 'ft  This is the two tanks' combined LCG.
```

```
A77: '  Errors
A78: "   %  \/=
B78: (($B$74/$B$70)-1)*100
C78: '    This is the percent error in volume.
A79: '   % LCG=
B79: (($B$75/$B$71)-1)*100
C79: '    This is the percent error in LCG.
```

1.6 Table 5 - Hull Envelope Wetted Surface Calculations, Program Output, SHAPE 1.6

```
SHAPE

Version 1.6   :  1 August 1989

D =   32.00   nf =    2.25   na =    2.75   v =   34.94
Parameter      Forebody      Midbody    Afterbody    Total Hull
 Length          76.80        96.00       115.20        288.00
 Surf Area     6454.12      9650.97      8563.11      24668.20
 Volume       44019.13     77207.77     57490.09     178716.99
 Displmnt      1259.85      2209.72      1645.39       5114.97
 LCB             46.75       124.80       212.21        133.69
 Cp              0.713        1.000        0.621         0.772
 Cws             0.836        1.000        0.739         0.852
 Cwp             0.819        1.000        0.733         0.845

Tail Cone Angle (Half) (degrees) :   20.90
Percent Parallel Midbody         :   33.33

   Length of Equal Displacement Sub without PMB :     231.84
 Diameter of Equal Displacement Sub without PMB :      38.64
Surf Area of Equal Displacement Sub without PMB :   21895.93

C>
```

1.7 Table 6 - Power versus Speed Calculations

```
Thesis                                                        John V. Amy Jr.
Power versus Speed Calculations                               26 January 1990

 Cd sail=0.009000 Wsa sail=   589.4 ft2       oF=72 nu=1.08E-05 ft2/s
 Cd bpln=0.006200 Wsa bpln=   192.3 ft2                L=      288 ft
 Cd spln=0.006000 Wsa spln=   421.7 ft2       oF=72rho=    1.987 lbfs2/ft4
 Cd rudd=0.006000 Wsa rudd=   305.3 ft2               PC=     0.83
 Cr hull=0.000534 Wsa hull= 24668.2 ft2            eta m=    0.939
Speed kts     Re        Cf        EHP       SHP       BHP
       0         0     ERR          0         0         0
       1  45084299 0.002346 0.711600 0.857350 0.913045
       2  90168598 0.002114 5.296406 6.381213 6.795754
       3   1.4E+08 0.001995 17.18249 20.70179 22.04664
       4   1.8E+08 0.001916 39.64673 47.76714 50.87023
       5   2.3E+08 0.001858 75.88077 91.42262 97.36168
       6   2.7E+08 0.001812 129.0170 155.4422 165.5402
       7   3.2E+08 0.001775 202.1430 243.5458 259.3673
       8   3.6E+08 0.001744 298.3101 359.4097 382.7580
       9   4.1E+08 0.001717 420.5394 506.6740 539.5889
      10   4.5E+08 0.001693 571.8267 688.9478 733.7037
      11   5.0E+08 0.001673 755.1452 909.8135 968.9175
      12   5.4E+08 0.001654 973.4487 1172.829 1249.020
      13   5.9E+08 0.001637 1229.673 1481.534 1577.778
      14   6.3E+08 0.001621 1526.739 1839.444 1958.939
      15   6.8E+08 0.001607 1867.551 2250.062 2396.232
      16   7.2E+08 0.001594 2255.003 2716.871 2893.367
      17   7.7E+08 0.001582 2691.975 3243.343 3454.040
      18   8.1E+08 0.001571 3181.335 3832.934 4081.932
      19   8.6E+08 0.001560 3725.942 4489.087 4780.710
      20   9.0E+08 0.001550 4328.645 5215.235 5554.031
      21   9.5E+08 0.001541 4992.282 6014.797 6405.535
      22   9.9E+08 0.001532 5719.684 6891.185 7338.856
      23   1.0E+09 0.001523 6513.673 7847.799 8357.614
      24   1.1E+09 0.001515 7377.064 8888.029 9465.420
      25   1.1E+09 0.001508 8312.664 10015.25 10665.87
      26   1.2E+09 0.001500 9323.272 11232.85 11962.57
      27   1.2E+09 0.001493 10411.68 12544.19 13359.10
      28   1.3E+09 0.001487 11580.68 13952.62 14859.02
      29   1.3E+09 0.001480 12833.04 15461.50 16465.92
      30   1.4E+09 0.001474 14171.55 17074.16 18183.35
      31   1.4E+09 0.001468 15598.98 18793.95 20014.85
      32   1.4E+09 0.001463 17118.08 20624.19 21963.99
      33   1.5E+09 0.001457 18731.61 22568.21 24034.30
      34   1.5E+09 0.001452 20442.33 24629.32 26229.30
      35   1.6E+09 0.001447 22252.99 26810.83 28552.54
      36   1.6E+09 0.001442 24166.33 29116.06 31007.52
      37   1.7E+09 0.001437 26185.09 31548.30 33597.76
```

```
     38  1.7E+09 0.001433 28312.00 34110.84 36326.77
     39  1.8E+09 0.001428 30549.79 36806.98 39198.06
     40  1.8E+09 0.001424 32901.20 39640.00 42215.12
```

```
A4: ' Cd sail=
B4: (F6) 0.009
C4: 'Wsa sail=
D4: 589.4
E4: 'ft2
F4: 'oF=72 nu=
G4: (S2) 0.000010783
H4: 'ft2/s
A5: ' Cd bpln=
B5: (F6) 0.0062
C5: 'Wsa bpln=
D5: 192.3
E5: 'ft2
F5: '        L=
G5: 288
H5: 'ft
A6: ' Cd spln=
B6: (F6) 0.006
C6: 'Wsa spln=
D6: 421.7
E6: 'ft2
F6: 'oF=72rho=
G6: 1.987
H6: 'lbfs2/ft4
A7: ' Cd rudd=
B7: (F6) 0.006
C7: 'Wsa rudd=
D7: 305.3
E7: 'ft2
F7: '       PC=
G7: 0.83
A8: ' Cr hull=
B8: (F6) 0.000534
C8: 'Wsa hull=
D8: 24668.2
E8: 'ft2
F8: '    eta m=
G8: 0.939
A9: 'Speed kts
B9: '     Re
C9: '     Cf
D9: '    EHP
```

```
E9: '    SHP
F9: '    BHP
A10: 0
B10: 1.688*$A10*$G$5/$G$4
C10: 0.075/((@LOG($B10)-2)^2)
D10: 0
E10: +$D10/$G$7
F10: +$E10/$G$8
A11: 1
B11: 1.688*$A11*$G$5/$G$4
C11: 0.075/((@LOG($B11)-2)^2)
D11: 0.5*$G$6*($A11*1.688)^3*($B$4*$D$4+$B$5*$D$5+$B$6*$D$6+$B$7*$D$7+($B$8+$C11)*

E11: +$D11/$G$7
F11: +$E11/$G$8
```

1.8 Table 7 - Forward Thrust Bearing Calculation, Wilcock Analysis

```
Thesis                                                  John V. Amy Jr.
Thrust Bearing Design                                   1 December 1989

See thesis notes, 30 Nov 89, for development of geometry and sources.

Input:   Center supported, tilting pad thrust bearing is assumed.
       W=277186.6 lbf   This is the ahead thrust load.
        P=       75 psi   This is the stress reacted by lubricant film.
      kg=      0.8        This is actual thrust area fraction.
      D1=    189.6 in     This is the inner diameter.
       N=     58.8 rpm    This is the shaft speed.
      nu=9.14E-06 ft2/s This is the kinematic viscosity of the lubricant
                          at outlet temperature.
     rho=  1.9823 lbf s/ft4 This is density of lubricant at outlet temp.
    Tout=       86 oF     This is the proposed outlet temperature.
      cp=   8.534 Btu/gal-oF This is the heat content of the lubricant.
     Tin=       85 oF     This is the inlet lubricant temperature.

NOTES:
This design is for a saltwater lubricated tilting pad thrust bearing.
The assumptions are for the support to be at 0.58*B; however, the
performance for a center-supported pad can be as good as the 0.58*B
thrust bearing if the pad is not flat, but rounded.
This analysis is based on Wilcock's text.

Output:
     D2'=    213.6 in     This is initial thrust bearing outer diameter.
       U=3103.390 ft/min This is linear velocity of bearing surface.
      b'=       12 in     This is an initial pad width estimate.
ENTRY  Enter the desired pad width.
       b=       12 in     This is the design pad width.
      i'=42.22300         This is the computed number of pads.
ENTRY  Enter the desired # of pads, must be integral and even #.
       i=       42        This is the design number of pads.
      B'=12.06371 in      This is an initial pad length estimate.
ENTRY  Enter the desired pad length.
       B=       12 in     This is the design pad length.
      mu=1.26E-07 reyns This is absolute viscosity of lubricant at
                          outlet temperature.
   Pcalc=45.83111 psi     This is the calculated lubricant pressure.
    op #=1.42E-07         This is the operating number and pad length
     B/b=        1        to width ratio.  These are entering arguments
                          for figure 11-10 of Wilcock.
       q=   0.072         This is a multiplier in the expression for
                          alpha.  This formula for alpha is derived from
   alpha=1.01E-04 rad     Wilcock.
    hmin=0.001213 in      This is the minimum film thickness. It should be
```

```
                        greater than 0.001 inches (for oil).
      q'=    0.01       This formula is developed from Fig. 11-11
       f=0.001011       from Wilcock.
       H=26.36012 HP    This is the power lost due to shear stresses.
       H=19.65674 kW    This is power lost in kW.
       Q=86.54974 in3/s This is the lubricant flow over the pads.
       Q=112.1730 gpm
     /\T=1.167541 oF    This is the tempature rise of the lubricant.

DESIGN GEOMETRY:
      D1=   189.6 in     = 4.815849 m
      D2=   213.6 in     = 5.425450 m
       b=      12 in     = 0.304800 m
       B=      12 in     = 0.304800 m
       i=      42 pads
```

```
A1: 'Thesis
B1: 'John V. Amy Jr.
A2: 'Thrust Bearing Design
B2: "1 December 1989
A4: 'See thesis notes, 30 Nov 89, for development of geometry and sources.
A6: 'Input:
B6: 'Center supported, tilting pad thrust bearing is assumed.
A7: '       W=
B7: 277186.6
C7: 'lbf   This is the ahead thrust load.
A8: '       P=
B8: 75
C8: 'psi   This is the stress reacted by lubricant film.
A9: '      kg=
B9: 0.8
C9: '      This is actual thrust area fraction.
A10: '      D1=
B10: 189.6
C10: 'in    This is the inner diameter.
A11: '       N=
B11: 58.8
C11: 'rpm   This is the shaft speed.
A12: '      nu=
B12: (S2) 0.9142*10^-5
C12: 'ft2/s This is the kinematic viscosity of the lubricant
C13: '      at outlet temperature.
A14: '     rho=
B14: 1.9823
C14: 'lbf s/ft4 This is density of lubricant at outlet temp.
A15: '    Tout=
```

```
B15: 86
C15: 'oF    This is the proposed outlet temperature.
A16: '      cp=
B16: 8.534
C16: 'Btu/gal-oF This is the heat content of the lubricant.
A17: '     Tin=
B17: 85
C17: 'oF    This is the inlet lubricant temperature.
A19: 'NOTES:
A20: 'This design is for a saltwater lubricated tilting pad thrust bearing.
A21: 'The assumptions are for the support to be at 0.58*B; however, the
A22: 'performance for a center-supported pad can be as good as the 0.58*B
A23: 'thrust bearing if the pad is not flat, but rounded.
A24: 'This analysis is based on Wilcock's text.
A26: 'Output:
A27: '     D2'=
B27: 213.6
C27: 'in    This is initial thrust bearing outer diameter.
A28: '       U=
B28: (@PI/24)*($B$10+$B$27)*$B$11
C28: 'ft/min This is linear velocity of bearing surface.
A29: '      b'=
B29: ($B$27-$B$10)/2
C29: 'in    This is an initial pad width estimate.
A30: 'ENTRY  Enter the desired pad width.
A31: '       b=
B31: 12
C31: 'in    This is the design pad width.
A32: '      i'=
B32: (@PI/2)*$B$9*($B$10+$B$27)/$B$31
C32: '      This is the computed number of pads.
A33: 'ENTRY  Enter the desired # of pads, must be integral and even #.
A34: '       i=
B34: 42
C34: '      This is the design number of pads.
A35: '      B'=
B35: (@PI/2)*$B$9*($B$10+$B$27)/$B$34
C35: 'in    This is an initial pad length estimate.
A36: 'ENTRY  Enter the desired pad length.
A37: '       B=
B37: 12
C37: 'in    This is the design pad length.
A38: '      mu=
B38: (S2) +$B$12*$B$14/144
C38: 'reyns This is absolute viscosity of lubricant at
C39: '      outlet temperature.
A40: '   Pcalc=
```

```
B40: +$B$7/($B$34*$B$31*$B$37)
C40: 'psi   This is the calculated lubricant pressure.
A41: '    op #=
B41: (S2) ($B$38*$B$28)/(5*$B$40*$B$37)
C41: '      This is the operating number and pad length
A42: '     B/b=
B42: +$B$37/$B$31
C42: '      to width ratio.  These are entering arguments
C43: '      for figure 11-10 of Wilcock.
A44: '       q=
B44: 0.219*($B$42^1.15)-0.307*$B$42+0.16
C44: '      This is a multiplier in the expression for
C45: '      alpha.  This formula for alpha is derived from
A46: '   alpha=
B46: (S2) @SQRT($B$41*10^6*$B$44)*0.001
C46: 'rad   Wilcock.
A47: '    hmin=
B47: +$B$46*$B$37
C47: 'in    This is the minimum film thickness. It should be
C48: '      greater than 0.001 inches (for oil).
A49: '      g'=
B49: 0.001395*($B$42^2.5)+0.004005*$B$42+0.0046
C49: '      This formula is developed from Fig. 11-11
A50: '       f=
B50: +$B$46*10^3*$B$49
C50: '      from Wilcock.
A51: '       H=
B51: +$B$50*$B$7*$B$28/33000
C51: 'HP    This is the power lost due to shear stresses.
A52: '       H=
B52: +$B$51*0.7457
C52: 'kW    This is power lost in kW.
A53: '       Q=
B53: 0.228*$B$34*$B$46*$B$31*$B$37*$B$28/5
C53: 'in3/s This is the lubricant flow over the pads.
A54: '       Q=
B54: 0.0591*$B$34*$B$46*$B$31*$B$37*$B$28
C54: 'gpm
A55: '     /\T=
B55: 42.4*$B$51/($B$16*$B$54)
C55: 'oF    This is the tempature rise of the lubricant.
A57: 'DESIGN GEOMETRY:
A58: '      D1=
B58: +$B$10
C58: 'in     =
D58: +$B58/39.37
E58: 'm
```

```
A59: '       D2=
B59: +$B$10+2*$B$37
C59: 'in      =
D59: +$B59/39.37
E59: 'm
A60: '         b=
B60: +$B$31
C60: 'in      =
D60: +$B60/39.37
E60: 'm
A61: '         B=
B61: +$B$37
C61: 'in      =
D61: +$B61/39.37
E61: 'm
A62: '         i=
B62: +$B$34
C62: 'pads
```

1.9 Table 8 - Forward Thrust Bearing Calculation, Constantinescu et al Analysis

```
Thesis                                                  John V. Amy Jr.
Thrust Bearing Design                                   4 December 1989
AHEAD, FLOODED, SEA-WATER LUBRICATED, TIN-BRONZE PAD, OTHER BEARING
This thrust bearing design is based on the text, Sliding Bearings
by Constantinescu, et al.  The inputs to this analysis come from
the Wilcock analysis.  Integration of differential equations is
performed using Euler integrations.  A lenticulated rectangular
thrust bearing pad is assumed.
INPUT:  These are results of Wilcock's analysis for flat pads (kg,m,s).
   sigma=2.07E+07 Pa      This is the yield stress of the pad material.
    Davg=   5.121 m       This is the average bearing diameter.
   alpha=1.01E-04 rad     This is the pad tilt from Wilcock.
    hmin=3.08E-05 m       This is Wilcock's minimum film thickness.
       B=  0.3048 m       This is the pad length.
       L=  0.3048 m       This is the pad width.
      nu=9.14E-06 ft2/s  This is lubricant kinematic viscosity at Tamb.
     rho=  1.9823 lbf s2/ft4  This is lubricant density at Tamb.
       N=    58.8 rpm     This is the shaft speed.
       i=      42 pads    This is the number of thrust bearing pads.
    Tamb=      86 oF      This is the ambient lubricant temperature.
  Wtotal= 1233000 N       This is the thrust borne by the bearing.
       P=  316076 Pa      This is the bearing pressure.
     Dph=    4.37 m       This is the runner diameter. (pressure hull)
OUTPUT DATA:
  W brg"= 2463785 N       These are thrusts for each pad times the number
   W brg= 2463785 N       of pads, and should be greater than or equal to
                          equal to W total.  W brg" uses a separation BC
 W total= 1233000 N       in the divergent flow, W brg does not.
       t=0.026421 m       This is the pad thickness.
  Wm bar=0.146731         Non-dimensionalised load, hmin is reference.
  Wp bar=0.184436         Non-dimensionalised load, hp is reference.
      Sp=5.421918         Sommerfeld Number
      Sm=6.815171
  Qx bar=0.565618         Non-dimensionalised lubricant flux rate
  F0 bar=0.905206         Non-dimensionalised friction force at y=0
  Fh bar=0.725564         Non-dimensionalised friction force at y=h
      f0=0.000630         Friction coefficient at y=0
      fh=0.000505         Friction coefficient at y=h
These coefficients can now be compared with experimental values.
See the reference, Constantinescu et al, pages 283..285 and pg 29.
CALCULATIONS       Primes denote initial estimates.
     h1'=7.70E-05 m       This is the inlet film thickness.
     h2'=4.62E-05 m       This is the outlet film thickness.
  delta'=1.91E-05 m       This is the maximum departure from flat plate.
                          Delta/hp is assumed here to be 0.45.
   hmin'=3.94E-05 m       This is to provide estimate of hmin.  It should
                          be greater than 25.4 micrometers.
```

```
      The preceeding values are based on Wilcock's hmin, alpha, B.
ENTRY REQUIRED
   h1=6.60E-05 m      This is the design inlet film thickness.
   h2=3.52E-05 m      This is the design outlet film thickness.
delta=1.57E-05 m      This is design maximum departure from plane.
 hmin=3.11E-05 m      This is the minimun film thickness.
   mu=8.68E-04 kg/m s This is the lubricant absolute viscosity.
    V=15.76633 m/s    This is the bearing linear velocity.
PRESSURE/LOAD CALCULATIONS   ho'=0.000035 m   thickness at pmax
   ho' is assumed to be at 0.6 into the convergent portion of the
   lubricant film.--This is roughly equal to 0.49 x B.
 x/B    hc m       h m      dp/dx    p-pa Pa     W  N     dp/dx    p-pa Pa
    0 0.00E+00 6.60E-05  8.8E+06  0.0E+00          0  8.8E+06  0.0E+00
 0.01 6.22E-07 6.51E-05  8.9E+06  2.7E+04 25.04022  8.9E+06  2.7E+04
 0.02 1.23E-06 6.42E-05  9.0E+06  5.4E+04 50.37355  9.0E+06  5.4E+04
 0.03 1.83E-06 6.32E-05  9.1E+06  8.2E+04 75.98996  9.1E+06  8.2E+04
 0.04 2.41E-06 6.24E-05  9.2E+06  1.1E+05 101.8782  9.2E+06  1.1E+05
 0.05 2.98E-06 6.15E-05  9.3E+06  1.4E+05 128.0259  9.3E+06  1.4E+05
 0.06 3.54E-06 6.06E-05  9.4E+06  1.7E+05 154.4194  9.4E+06  1.7E+05
 0.07 4.09E-06 5.98E-05  9.4E+06  1.9E+05 181.0435  9.4E+06  1.9E+05
 0.08 4.62E-06 5.89E-05  9.5E+06  2.2E+05 207.8817  9.5E+06  2.2E+05
 0.09 5.15E-06 5.81E-05  9.6E+06  2.5E+05 234.9160  9.6E+06  2.5E+05
  0.1 5.65E-06 5.73E-05  9.6E+06  2.8E+05 262.1269  9.6E+06  2.8E+05
 0.11 6.15E-06 5.65E-05  9.7E+06  3.1E+05 289.4932  9.7E+06  3.1E+05
 0.12 6.63E-06 5.57E-05  9.7E+06  3.4E+05 316.9920  9.7E+06  3.4E+05
 0.13 7.11E-06 5.49E-05  9.8E+06  3.7E+05 344.5987  9.8E+06  3.7E+05
 0.14 7.56E-06 5.41E-05  9.8E+06  4.0E+05 372.2870  9.8E+06  4.0E+05
 0.15 8.01E-06 5.34E-05  9.8E+06  4.3E+05 400.0287  9.8E+06  4.3E+05
 0.16 8.44E-06 5.26E-05  9.8E+06  4.6E+05 427.7934  9.8E+06  4.6E+05
 0.17 8.86E-06 5.19E-05  9.8E+06  4.9E+05 455.5493  9.8E+06  4.9E+05
 0.18 9.27E-06 5.12E-05  9.8E+06  5.2E+05 483.2622  9.8E+06  5.2E+05
 0.19 9.67E-06 5.05E-05  9.7E+06  5.5E+05 510.8959  9.7E+06  5.5E+05
  0.2 1.01E-05 4.98E-05  9.7E+06  5.8E+05 538.4125  9.7E+06  5.8E+05
 0.21 1.04E-05 4.91E-05  9.6E+06  6.1E+05 565.7716  9.6E+06  6.1E+05
 0.22 1.08E-05 4.84E-05  9.6E+06  6.4E+05 592.9310  9.6E+06  6.4E+05
 0.23 1.11E-05 4.78E-05  9.5E+06  6.7E+05 619.8464  9.5E+06  6.7E+05
 0.24 1.15E-05 4.72E-05  9.3E+06  7.0E+05 646.4714  9.3E+06  7.0E+05
 0.25 1.18E-05 4.65E-05  9.2E+06  7.2E+05 672.7576  9.2E+06  7.2E+05
 0.26 1.21E-05 4.59E-05  9.1E+06  7.5E+05 698.6547  9.1E+06  7.5E+05
 0.27 1.24E-05 4.53E-05  8.9E+06  7.8E+05 724.1105  8.9E+06  7.8E+05
 0.28 1.27E-05 4.47E-05  8.7E+06  8.1E+05 749.0708  8.7E+06  8.1E+05
 0.29 1.29E-05 4.41E-05  8.5E+06  8.3E+05 773.4798  8.5E+06  8.3E+05
  0.3 1.32E-05 4.36E-05  8.3E+06  8.6E+05 797.2802  8.3E+06  8.6E+05
 0.31 1.34E-05 4.30E-05  8.0E+06  8.8E+05 820.4131  8.0E+06  8.8E+05
 0.32 1.37E-05 4.25E-05  7.8E+06  9.1E+05 842.8182  7.8E+06  9.1E+05
 0.33 1.39E-05 4.20E-05  7.5E+06  9.3E+05 864.4344  7.5E+06  9.3E+05
 0.34 1.41E-05 4.14E-05  7.2E+06  9.5E+05 885.1993  7.2E+06  9.5E+05
```

0.35	1.43E-05	4.09E-05	6.8E+06	9.7E+05	905.0501	6.8E+06	9.7E+05
0.36	1.45E-05	4.04E-05	6.5E+06	9.9E+05	923.9235	6.5E+06	9.9E+05
0.37	1.46E-05	4.00E-05	6.1E+06	1.0E+06	941.7561	6.1E+06	1.0E+06
0.38	1.48E-05	3.95E-05	5.7E+06	1.0E+06	958.4846	5.7E+06	1.0E+06
0.39	1.49E-05	3.90E-05	5.3E+06	1.0E+06	974.0464	5.3E+06	1.0E+06
0.4	1.51E-05	3.86E-05	4.8E+06	1.1E+06	988.3796	4.8E+06	1.1E+06
0.41	1.52E-05	3.82E-05	4.4E+06	1.1E+06	1001.423	4.4E+06	1.1E+06
0.42	1.53E-05	3.78E-05	3.9E+06	1.1E+06	1013.119	3.9E+06	1.1E+06
0.43	1.54E-05	3.74E-05	3.4E+06	1.1E+06	1023.411	3.4E+06	1.1E+06
0.44	1.55E-05	3.70E-05	2.9E+06	1.1E+06	1032.243	2.9E+06	1.1E+06
0.45	1.55E-05	3.66E-05	2.3E+06	1.1E+06	1039.565	2.3E+06	1.1E+06
0.46	1.56E-05	3.62E-05	1.8E+06	1.1E+06	1045.329	1.8E+06	1.1E+06
0.47	1.56E-05	3.59E-05	1.2E+06	1.1E+06	1049.491	1.2E+06	1.1E+06
0.48	1.57E-05	3.55E-05	6.0E+05	1.1E+06	1052.012	6.0E+05	1.1E+06
0.49	1.57E-05	3.52E-05	0.0E+00	1.1E+06	1052.858	0.0E+00	1.1E+06
0.5	1.57E-05	3.49E-05	-6.1E+05	1.1E+06	1051.999	-6.1E+05	1.1E+06
0.51	1.57E-05	3.46E-05	-1.2E+06	1129579	1049.413	-1.2E+06	1.1E+06
0.52	1.57E-05	3.43E-05	-1.8E+06	1.1E+06	1045.082	-1.8E+06	1.1E+06
0.53	1.56E-05	3.40E-05	-2.5E+06	1.1E+06	1038.996	-2.5E+06	1.1E+06
0.54	1.56E-05	3.38E-05	-3.1E+06	1.1E+06	1031.153	-3.1E+06	1.1E+06
0.55	1.55E-05	3.35E-05	-3.7E+06	1.1E+06	1021.558	-3.7E+06	1.1E+06
0.56	1.55E-05	3.33E-05	-4.3E+06	1.1E+06	1010.221	-4.3E+06	1.1E+06
0.57	1.54E-05	3.31E-05	-4.9E+06	1.1E+06	997.1644	-4.9E+06	1.1E+06
0.58	1.53E-05	3.28E-05	-5.5E+06	1.1E+06	982.4159	-5.5E+06	1.1E+06
0.59	1.52E-05	3.26E-05	-6.1E+06	1.0E+06	966.0130	-6.1E+06	1.0E+06
0.6	1.51E-05	3.25E-05	-6.6E+06	1.0E+06	948.0012	-6.6E+06	1.0E+06
0.61	1.49E-05	3.23E-05	-7.2E+06	1.0E+06	928.4347	-7.2E+06	1.0E+06
0.62	1.48E-05	3.21E-05	-7.7E+06	9.8E+05	907.3762	-7.7E+06	9.8E+05
0.63	1.46E-05	3.20E-05	-8.2E+06	9.5E+05	884.8967	-8.2E+06	9.5E+05
0.64	1.45E-05	3.18E-05	-8.6E+06	9.3E+05	861.0753	-8.6E+06	9.3E+05
0.65	1.43E-05	3.17E-05	-9.1E+06	9.0E+05	835.9991	-9.1E+06	9.0E+05
0.66	1.41E-05	3.16E-05	-9.5E+06	8.7E+05	809.7626	-9.5E+06	8.7E+05
0.67	1.39E-05	3.15E-05	-9.8E+06	8.4E+05	782.4672	-9.8E+06	8.4E+05
0.68	1.37E-05	3.14E-05	-1.0E+07	8.1E+05	754.2212	-1.0E+07	8.1E+05
0.69	1.34E-05	3.13E-05	-1.0E+07	7.8E+05	725.1385	-1.0E+07	7.8E+05
0.7	1.32E-05	3.13E-05	-1.1E+07	7.5E+05	695.3385	-1.1E+07	7.5E+05
0.71	1.29E-05	3.12E-05	-1.1E+07	7.2E+05	664.9451	-1.1E+07	7.2E+05
0.72	1.27E-05	3.12E-05	-1.1E+07	6.8E+05	634.0861	-1.1E+07	6.8E+05
0.73	1.24E-05	3.11E-05	-1.1E+07	6.5E+05	602.8924	-1.1E+07	6.5E+05
0.74	1.21E-05	3.11E-05	-1.1E+07	6.2E+05	571.4967	-1.1E+07	6.2E+05
0.75	1.18E-05	3.11E-05	-1.1E+07	5.8E+05	540.0336	-1.1E+07	5.8E+05
0.76	1.15E-05	3.11E-05	-1.1E+07	5.5E+05	508.6377	-1.1E+07	5.5E+05
0.77	1.11E-05	3.12E-05	-1.1E+07	5.1E+05	477.4433	-1.1E+07	5.1E+05
0.78	1.08E-05	3.12E-05	-1.1E+07	4.8E+05	446.5834	-1.1E+07	4.8E+05
0.79	1.04E-05	3.13E-05	-1.1E+07	4.5E+05	416.1888	-1.1E+07	4.5E+05
0.8	1.01E-05	3.13E-05	-1.0E+07	4.2E+05	386.3874	-1.0E+07	4.2E+05
0.81	9.67E-06	3.14E-05	-1.0E+07	3.8E+05	357.3029	-1.0E+07	3.8E+05

```
0.82 9.27E-06 3.15E-05 -9.8E+06  3.5E+05 329.0549 -9.8E+06  3.5E+05
0.83 8.86E-06 3.16E-05 -9.5E+06  3.2E+05 301.7572 -9.5E+06  3.2E+05
0.84 8.44E-06 3.17E-05 -9.1E+06  3.0E+05 275.5162 -9.1E+06  3.0E+05
0.85 8.01E-06 3.18E-05 -8.6E+06  2.7E+05 250.4392 -8.6E+06  2.7E+05
0.86 7.56E-06 3.20E-05 -8.2E+06  2.4E+05 226.6149 -8.2E+06  2.4E+05
0.87 7.11E-06 3.21E-05 -7.7E+06  2.2E+05 204.1323 -7.7E+06  2.2E+05
0.88 6.63E-06 3.23E-05 -7.2E+06  2.0E+05 183.0705 -7.2E+06  2.0E+05
0.89 6.15E-06 3.25E-05 -6.6E+06  1.8E+05 163.5006 -6.6E+06  1.8E+05
 0.9 5.65E-06 3.26E-05 -6.1E+06  1.6E+05 145.4852 -6.1E+06  1.6E+05
0.91 5.15E-06 3.28E-05 -5.5E+06  1.4E+05 129.0786 -5.5E+06  1.4E+05
0.92 4.62E-06 3.31E-05 -4.9E+06  1.2E+05 114.3263 -4.9E+06  1.2E+05
0.93 4.09E-06 3.33E-05 -4.3E+06  1.1E+05 101.2655 -4.3E+06  1.1E+05
0.94 3.54E-06 3.35E-05 -3.7E+06  9.7E+04 89.92505 -3.7E+06  9.7E+04
0.95 2.98E-06 3.38E-05 -3.1E+06  8.6E+04 80.32514 -3.1E+06  8.6E+04
0.96 2.41E-06 3.40E-05 -2.5E+06  7.8E+04 72.47820 -2.5E+06  7.8E+04
0.97 1.83E-06 3.43E-05 -1.8E+06  7.1E+04 66.38877 -1.8E+06  7.1E+04
0.98 1.23E-06 3.46E-05 -1.2E+06  6.7E+04 62.05392 -1.2E+06  6.7E+04
0.99 6.22E-07 3.49E-05 -6.1E+05  6.4E+04 59.46357 -6.1E+05  6.4E+04
   1 0.00E+00 3.52E-05 -1.4E+03  6.3E+04 58.60089 -1.4E+03  6.3E+04
                     pm=625175.9    W pad=53661.55          W pad=
VELOCITY/FLUX CALCULATIONS   ho'=0.000035 m   thickness at pmax
  ho' is assumed to be at 0.6 into the convergent portion of the
  lubricant film.--This is roughly equal to 0.49 x B.
x/B       h m      dp/dx   qx m3/s  du/dy 0  du/dy h    F 0      F h
   0 6.60E-05  8.8E+06 8.46E-05 -5.7E+05  9.5E+04  0.0E+00  0.0E+00
0.01 6.51E-05  8.9E+06 8.46E-05 -5.8E+05  9.1E+04 -4.6E-01  7.7E-02
0.02 6.42E-05  9.0E+06 8.46E-05 -5.8E+05  8.7E+04 -4.6E-01  7.4E-02
0.03 6.32E-05  9.1E+06 8.46E-05 -5.8E+05  8.2E+04 -4.7E-01  7.0E-02
0.04 6.24E-05  9.2E+06 8.46E-05 -5.8E+05  7.7E+04 -4.7E-01  6.6E-02
0.05 6.15E-05  9.3E+06 8.46E-05 -5.9E+05  7.2E+04 -4.7E-01  6.2E-02
0.06 6.06E-05  9.4E+06 8.46E-05 -5.9E+05  6.7E+04 -4.7E-01  5.8E-02
0.07 5.98E-05  9.4E+06 8.46E-05 -5.9E+05  6.1E+04 -4.7E-01  5.4E-02
0.08 5.89E-05  9.5E+06 8.46E-05 -5.9E+05  5.5E+04 -4.7E-01  4.9E-02
0.09 5.81E-05  9.6E+06 8.46E-05 -5.9E+05  4.9E+04 -4.8E-01  4.5E-02
 0.1 5.73E-05  9.6E+06 8.46E-05 -5.9E+05  4.3E+04 -4.8E-01  4.0E-02
0.11 5.65E-05  9.7E+06 8.46E-05 -5.9E+05  3.6E+04 -4.8E-01  3.4E-02
0.12 5.57E-05  9.7E+06 8.46E-05 -6.0E+05  2.9E+04 -4.8E-01  2.9E-02
0.13 5.49E-05  9.8E+06 8.46E-05 -6.0E+05  2.2E+04 -4.8E-01  2.3E-02
0.14 5.41E-05  9.8E+06 8.46E-05 -6.0E+05  1.4E+04 -4.8E-01  1.7E-02
0.15 5.34E-05  9.8E+06 8.46E-05 -6.0E+05  6.1E+03 -4.8E-01  1.1E-02
0.16 5.26E-05  9.8E+06 8.46E-05 -6.0E+05 -2.2E+03 -4.8E-01  4.9E-03
0.17 5.19E-05  9.8E+06 8.46E-05 -6.0E+05 -1.1E+04 -4.8E-01 -1.8E-03
0.18 5.12E-05  9.8E+06 8.46E-05 -6.0E+05 -2.0E+04 -4.8E-01 -8.7E-03
0.19 5.05E-05  9.7E+06 8.46E-05 -6.0E+05 -2.9E+04 -4.8E-01 -1.6E-02
 0.2 4.98E-05  9.7E+06 8.46E-05 -5.9E+05 -3.9E+04 -4.8E-01 -2.3E-02
0.21 4.91E-05  9.6E+06 8.46E-05 -5.9E+05 -4.9E+04 -4.8E-01 -3.1E-02
0.22 4.84E-05  9.6E+06 8.46E-05 -5.9E+05 -5.9E+04 -4.8E-01 -3.7E-02
```

```
0.23 4.78E-05  9.5E+06 8.46E-05 -5.9E+05 -6.9E+04 -4.8E-01 -4.7E-02
0.24 4.72E-05  9.3E+06 8.46E-05 -5.9E+05 -8.0E+04 -4.8E-01 -5.6E-02
0.25 4.65E-05  9.2E+06 8.46E-05 -5.9E+05 -9.2E+04 -4.7E-01 -6.5E-02
0.26 4.59E-05  9.1E+06 8.46E-05 -5.8E+05 -1.0E+05 -4.7E-01 -7.4E-02
0.27 4.53E-05  8.9E+06 8.46E-05 -5.8E+05 -1.2E+05 -4.7E-01 -8.3E-02
0.28 4.47E-05  8.7E+06 8.46E-05 -5.8E+05 -1.3E+05 -4.7E-01 -9.3E-02
0.29 4.41E-05  8.5E+06 8.46E-05 -5.7E+05 -1.4E+05 -4.7E-01 -1.0E-01
 0.3 4.36E-05  8.3E+06 8.46E-05 -5.7E+05 -1.5E+05 -4.6E-01 -1.1E-01
0.31 4.30E-05  8.0E+06 8.46E-05 -5.7E+05 -1.7E+05 -4.6E-01 -1.2E-01
0.32 4.25E-05  7.8E+06 8.46E-05 -5.6E+05 -1.8E+05 -4.6E-01 -1.3E-01
0.33 4.20E-05  7.5E+06 8.46E-05 -5.6E+05 -1.9E+05 -4.5E-01 -1.5E-01
0.34 4.14E-05  7.2E+06 8.46E-05 -5.5E+05 -2.1E+05 -4.5E-01 -1.6E-01
0.35 4.09E-05  6.8E+06 8.46E-05 -5.5E+05 -2.2E+05 -4.4E-01 -1.7E-01
0.36 4.04E-05  6.5E+06 8.46E-05 -5.4E+05 -2.4E+05 -4.4E-01 -1.8E-01
0.37 4.00E-05  6.1E+06 8.46E-05 -5.4E+05 -2.5E+05 -4.4E-01 -1.9E-01
0.38 3.95E-05  5.7E+06 8.46E-05 -5.3E+05 -2.7E+05 -4.3E-01 -2.0E-01
0.39 3.90E-05  5.3E+06 8.46E-05 -5.2E+05 -2.8E+05 -4.3E-01 -2.2E-01
 0.4 3.86E-05  4.8E+06 8.46E-05 -5.2E+05 -3.0E+05 -4.2E-01 -2.3E-01
0.41 3.82E-05  4.4E+06 8.46E-05 -5.1E+05 -3.2E+05 -4.2E-01 -2.4E-01
0.42 3.78E-05  3.9E+06 8.46E-05 -5.0E+05 -3.3E+05 -4.1E-01 -2.6E-01
0.43 3.74E-05  3.4E+06 8.46E-05 -4.9E+05 -3.5E+05 -4.0E-01 -2.7E-01
0.44 3.70E-05  2.9E+06 8.46E-05 -4.9E+05 -3.7E+05 -4.0E-01 -2.8E-01
0.45 3.66E-05  2.3E+06 8.46E-05 -4.8E+05 -3.8E+05 -3.9E-01 -2.9E-01
0.46 3.62E-05  1.8E+06 8.46E-05 -4.7E+05 -4.0E+05 -3.9E-01 -3.1E-01
0.47 3.59E-05  1.2E+06 8.46E-05 -4.6E+05 -4.1E+05 -3.8E-01 -3.2E-01
0.48 3.55E-05  6.0E+05 8.46E-05 -4.6E+05 -4.3E+05 -3.7E-01 -3.3E-01
0.49 3.52E-05  0.0E+00 8.46E-05 -4.5E+05 -4.5E+05 -3.7E-01 -3.5E-01
 0.5 3.49E-05 -6.1E+05 8.46E-05 -4.4E+05 -4.6E+05 -3.6E-01 -3.6E-01
0.51 3.46E-05 -1.2E+06 8.46E-05 -4.3E+05 -4.8E+05 -3.5E-01 -3.7E-01
0.52 3.43E-05 -1.8E+06 8.46E-05 -4.2E+05 -5.0E+05 -3.5E-01 -3.9E-01
0.53 3.40E-05 -2.5E+06 8.46E-05 -4.2E+05 -5.1E+05 -3.4E-01 -4.0E-01
0.54 3.38E-05 -3.1E+06 8.46E-05 -4.1E+05 -5.3E+05 -3.3E-01 -4.1E-01
0.55 3.35E-05 -3.7E+06 8.46E-05 -4.0E+05 -5.4E+05 -3.3E-01 -4.2E-01
0.56 3.33E-05 -4.3E+06 8.46E-05 -3.9E+05 -5.6E+05 -3.2E-01 -4.4E-01
0.57 3.31E-05 -4.9E+06 8.46E-05 -3.8E+05 -5.7E+05 -3.2E-01 -4.5E-01
0.58 3.28E-05 -5.5E+06 8.46E-05 -3.8E+05 -5.8E+05 -3.1E-01 -4.6E-01
0.59 3.26E-05 -6.1E+06 8.46E-05 -3.7E+05 -6.0E+05 -3.0E-01 -4.7E-01
 0.6 3.25E-05 -6.6E+06 8.46E-05 -3.6E+05 -6.1E+05 -3.0E-01 -4.8E-01
0.61 3.23E-05 -7.2E+06 8.46E-05 -3.5E+05 -6.2E+05 -2.9E-01 -4.9E-01
0.62 3.21E-05 -7.7E+06 8.46E-05 -3.5E+05 -6.3E+05 -2.9E-01 -5.0E-01
0.63 3.20E-05 -8.2E+06 8.46E-05 -3.4E+05 -6.4E+05 -2.8E-01 -5.1E-01
0.64 3.18E-05 -8.6E+06 8.46E-05 -3.4E+05 -6.5E+05 -2.8E-01 -5.2E-01
0.65 3.17E-05 -9.1E+06 8.46E-05 -3.3E+05 -6.6E+05 -2.7E-01 -5.3E-01
0.66 3.16E-05 -9.5E+06 8.46E-05 -3.3E+05 -6.7E+05 -2.7E-01 -5.3E-01
0.67 3.15E-05 -9.8E+06 8.46E-05 -3.2E+05 -6.8E+05 -2.6E-01 -5.4E-01
0.68 3.14E-05 -1.0E+07 8.46E-05 -3.2E+05 -6.9E+05 -2.6E-01 -5.5E-01
0.69 3.13E-05 -1.0E+07 8.46E-05 -3.2E+05 -6.9E+05 -2.6E-01 -5.5E-01
```

```
  0.7 3.13E-05 -1.1E+07 8.46E-05 -3.1E+05 -7.0E+05 -2.5E-01 -5.6E-01
 0.71 3.12E-05 -1.1E+07 8.46E-05 -3.1E+05 -7.0E+05 -2.5E-01 -5.6E-01
 0.72 3.12E-05 -1.1E+07 8.46E-05 -3.1E+05 -7.0E+05 -2.5E-01 -5.6E-01
 0.73 3.11E-05 -1.1E+07 8.46E-05 -3.1E+05 -7.0E+05 -2.5E-01 -5.7E-01
 0.74 3.11E-05 -1.1E+07 8.46E-05 -3.1E+05 -7.1E+05 -2.5E-01 -5.7E-01
 0.75 3.11E-05 -1.1E+07 8.46E-05 -3.1E+05 -7.1E+05 -2.5E-01 -5.7E-01
 0.76 3.11E-05 -1.1E+07 8.46E-05 -3.1E+05 -7.0E+05 -2.5E-01 -5.7E-01
 0.77 3.12E-05 -1.1E+07 8.46E-05 -3.1E+05 -7.0E+05 -2.5E-01 -5.7E-01
 0.78 3.12E-05 -1.1E+07 8.46E-05 -3.1E+05 -7.0E+05 -2.5E-01 -5.7E-01
 0.79 3.13E-05 -1.1E+07 8.46E-05 -3.1E+05 -7.0E+05 -2.5E-01 -5.6E-01
  0.8 3.13E-05 -1.0E+07 8.46E-05 -3.2E+05 -6.9E+05 -2.5E-01 -5.6E-01
 0.81 3.14E-05 -1.0E+07 8.46E-05 -3.2E+05 -6.9E+05 -2.5E-01 -5.6E-01
 0.82 3.15E-05 -9.8E+06 8.46E-05 -3.2E+05 -6.8E+05 -2.6E-01 -5.5E-01
 0.83 3.16E-05 -9.5E+06 8.46E-05 -3.3E+05 -6.7E+05 -2.6E-01 -5.5E-01
 0.84 3.17E-05 -9.1E+06 8.46E-05 -3.3E+05 -6.6E+05 -2.6E-01 -5.4E-01
 0.85 3.18E-05 -8.6E+06 8.46E-05 -3.4E+05 -6.5E+05 -2.7E-01 -5.3E-01
 0.86 3.20E-05 -8.2E+06 8.46E-05 -3.4E+05 -6.4E+05 -2.7E-01 -5.3E-01
 0.87 3.21E-05 -7.7E+06 8.46E-05 -3.5E+05 -6.3E+05 -2.8E-01 -5.2E-01
 0.88 3.23E-05 -7.2E+06 8.46E-05 -3.5E+05 -6.2E+05 -2.8E-01 -5.1E-01
 0.89 3.25E-05 -6.6E+06 8.46E-05 -3.6E+05 -6.1E+05 -2.9E-01 -5.0E-01
  0.9 3.26E-05 -6.1E+06 8.46E-05 -3.7E+05 -6.0E+05 -2.9E-01 -4.9E-01
 0.91 3.28E-05 -5.5E+06 8.46E-05 -3.8E+05 -5.8E+05 -3.0E-01 -4.8E-01
 0.92 3.31E-05 -4.9E+06 8.46E-05 -3.8E+05 -5.7E+05 -3.0E-01 -4.7E-01
 0.93 3.33E-05 -4.3E+06 8.46E-05 -3.9E+05 -5.6E+05 -3.1E-01 -4.6E-01
 0.94 3.35E-05 -3.7E+06 8.46E-05 -4.0E+05 -5.4E+05 -3.2E-01 -4.5E-01
 0.95 3.38E-05 -3.1E+06 8.46E-05 -4.1E+05 -5.3E+05 -3.2E-01 -4.4E-01
 0.96 3.40E-05 -2.5E+06 8.46E-05 -4.1E+05 -5.1E+05 -3.3E-01 -4.2E-01
 0.97 3.43E-05 -1.8E+06 8.46E-05 -4.2E+05 -5.0E+05 -3.3E-01 -4.1E-01
 0.98 3.46E-05 -1.2E+06 8.46E-05 -4.3E+05 -4.8E+05 -3.4E-01 -4.0E-01
 0.99 3.49E-05 -6.1E+05 8.46E-05 -4.4E+05 -4.6E+05 -3.5E-01 -3.7E-01
    1 3.52E-05 -1.4E+03 8.46E-05 -4.5E+05 -4.5E+05 -3.5E-01 -3.7E-01
                                      F 0,h=-36.9614 -29.6262
  PAD THICKNESS CALCULATIONS
     D2=  5.4258 m     This is the outer diameter of the bearing.
     D1=  4.8162 m     This is the inner diameter of the bearing.
     Da=    4.37 m     This is the outer diameter of the runner.
sigma ai=20685000 Pa    This is the yield stress of the pad material.
      t=0.026421 m     This is the pad thickness.  A factor of safety
                       of 1.5 is assumed.


A9: 'INPUT:  These are results of Wilcock's analysis for flat pads (kg,m,s).
A10: '   sigma=
B10: (S2) 20685000
C10: 'Pa     This is the yield stress of the pad material.
A11: '    Davg=
B11: 5.121
```

```
C11: 'm      This is the average bearing diameter.
A12: '   alpha=
B12: (S2) 0.000101
C12: 'rad    This is the pad tilt from Wilcock.
A13: '    hmin=
B13: (S2) 30.81*10^-6
C13: 'm      This is Wilcock's minimum film thickness.
A14: '       B=
B14: 0.3048
C14: 'm      This is the pad length.
A15: '       L=
B15: 0.3048
C15: 'm      This is the pad width.
A16: '      nu=
B16: (S2) 0.9142*10^-5
C16: 'ft2/s  This is lubricant kinematic viscosity at Tamb.
A17: '     rho=
B17: 1.9823
C17: 'lbf s2/ft4  This is lubricant density at Tamb.
A18: '       N=
B18: 58.8
C18: 'rpm    This is the shaft speed.
A19: '       i=
B19: 42
C19: 'pads   This is the number of thrust bearing pads.
A20: '    Tamb=
B20: 86
C20: 'oF     This is the ambient lubricant temperature.
A21: '  Wtotal=
B21: 1.233*10^6
C21: 'N      This is the thrust borne by the bearing.
A22: '       P=
B22: 316076
C22: 'Pa     This is the bearing pressure.
A23: '     Dph=
B23: 4.37
C23: 'm      This is the runner diameter. (pressure hull)
A24: 'OUTPUT DATA:
A25: '  W brg"=
B25: (FO) +$I$161*$B$19
C25: 'N      These are thrusts for each pad times the number
A26: '   W brg=
B26: (FO) +$F$161*$B$19
C26: 'N      of pads, and should be greater than or equal to
C27: '       equal to W total.  W brg" uses a separation BC
A28: ' W total=
B28: (FO) +$B$21
```

```
C28: 'N       in the divergent flow, W brg does not.
A29: '        t=
B29: +$B$273
C29: 'm       This is the pad thickness.
A30: '  Wm bar=
B30: ($B$53^2*$F$161)/($B$54*$B$55*$B$15*$B$14^2)
C30: '        Non-dimensionalised load, hmin is reference.
A31: '  Wp bar=
B31: ((($B$50+$B$51)/2-$B$52)^2*$F$161)/($B$54*$B$55*$B$15*$B$14^2)
C31: '        Non-dimensionalised load, hp is reference.
A32: '       Sp=
B32: 1/$B$31
C32: '        Sommerfeld Number
A33: '       Sm=
B33: 1/$B$30
A34: '  Qx bar=
B34: +$D$167/($B$55*$B$15*$B$53)
C34: '        Non-dimensionalised lubricant flux rate
A35: '  F0 bar=
B35: -$G$267*$B$53/($B$54*$B$55*$B$14*$B$15)
C35: '        Non-dimensionalised friction force at y=0
A36: '  Fh bar=
B36: -$H$267*$B$53/($B$54*$B$55*$B$14*$B$15)
C36: '        Non-dimensionalised friction force at y=h
A37: '       f0=
B37: -$G$267/$F$161
C37: '        Friction coefficient at y=0
A38: '       fh=
B38: -$H$267/$F$161
C38: '        Friction coefficient at y=h
A39: 'These coefficients can now be compared with experimental values.
A40: 'See the reference, Constantinescu et al, pages 283..285 and pg 29.
A41: 'CALCULATIONS
C41: 'Primes denote initial estimates.
A42: '      h1'=
B42: (S2) +$B$43+$B$12*$B$14
C42: 'm       This is the inlet film thickness.
A43: '      h2'=
B43: (S2) 1.5*$B$13
C43: 'm       This is the outlet film thickness.
A44: '  delta'=
B44: (S2) ($B$42+$B$43)/(2*(1+1/0.45))
C44: 'm       This is the maximum departure from flat plate.
C45: '        Delta/hp is assumed here to be 0.45.
A46: '   hmin'=
B46: (S2) +$B$43*((($B$42+$B$43)/(2*$B$43))-((($B$42-$B$43)^2)/(16*$B$43*$B$44))-(
))
C46: 'm       This is to provide estimate of hmin.  It should
```

```
C47: '        be greater than 25.4 micrometers.
B48: 'The preceeding values are based on Wilcock's hmin, alpha, B.
A49: '   ENTRY REQUIRED
A50: '       h1=
B50: (S2) 0.000066
C50: 'm       This is the design inlet film thickness.
A51: '       h2=
B51: (S2) +$B$50-$B$12*$B$14
C51: 'm       This is the design outlet film thickness.
A52: '   delta=
B52: (S2) ($B$50+$B$51)/(2*(1+1/0.45))
C52: 'm       This is design maximum departure from plane.
A53: '    hmin=
B53: (S2) +$B$51*(($B$50+$B$51)/(2*$B$51)-($B$50-$B$51)^2/(16*$B$51*$B$52)-$B$52/$

C53: 'm       This is the minimun film thickness.
A54: '       mu=
B54: (S2) 47.8868*$B$16*$B$17
C54: 'kg/m s This is the lubricant absolute viscosity.
A55: '        V=
B55: @PI*$B$11*$B$18/60
C55: 'm/s    This is the bearing linear velocity.
A56: '   PRESSURE/LOAD CALCULATIONS   ho'=
E56: +$C$109
F56: 'm   thickness at pmax
A57: '       ho' is assumed to be at 0.6 into the convergent portion of the
A58: '       lubricant film.--This is roughly equal to 0.49 x B.
A59: '    x/B
B59: '  hc m
C59: '   h m
D59: '  dp/dx
E59: ' p-pa Pa
F59: '   W  N
G59: '  dp/dx
H59: ' p-pa Pa
A60: 0
B60: (S2) +$B$52*(1-4*($A60-0.5)^2)
C60: (S2) +$B$50-($B$50-$B$51)*$A60-$B60
D60: (S1) (6*$B$54*$B$55*(1-$E$56/$C60))/($C60^2)
E60: (S1) 0
F60: 0
G60: (S1) @IF($E60>=0,$D60,0)
H60: (S1) 0
A61: 0.01
B61: (S2) +$B$52*(1-4*($A61-0.5)^2)
C61: (S2) +$B$50-($B$50-$B$51)*$A61-$B61
D61: (S1) (6*$B$54*$B$55*(1-$E$56/$C61))/($C61^2)
E61: (S1) (($D60+$D61)/2)*($A61-$A60)*$B$14+$E60
```

```
F61: +$E61*($A61-$A60)*$B$14*$B$15
G61: (S1) @IF($E61>=0,$D61,0)
H61: (S1) (($G60+$G61)/2)*($A61-$A60)*$B$14+$H60


C161: '      pm=
D161: @SUM(E60..E160)/101
E161: '   W pad=
F161: @SUM(F60..F160)
H161: '   W pad=
A162: '   VELOCITY/FLUX CALCULATIONS   ho'=
E162: +$C$109
F162: 'm   thickness at pmax
A163: '      ho' is assumed to be at 0.6 into the convergent portion of the
A164: '      lubricant film.--This is roughly equal to 0.49 x B.
A165: '   x/B
B165: '   h m
C165: '  dp/dx
D165: ' qx m3/s
E165: ' du/dy 0
F165: ' du/dy h
G165: '   F 0
H165: '   F h
A166: 0
B166: (S2) +$C60
C166: (S1) +$G60
D166: (S2) (0.5*$B$55*$B166-($C166*$B166^3)/(12*$B$54))*$B$15
E166: (S1) -$B166*$C166/(2*$B$54)-$B$55/$B166
F166: (S1) +$B166*$C166/(2*$B$54)-$B$55/$B166
G166: (S1) 0
H166: (S1) 0
A167: 0.01
B167: (S2) +$C61
C167: (S1) +$G61
D167: (S2) (0.5*$B$55*$B167-($C167*$B167^3)/(12*$B$54))*$B$15
E167: (S1) -$B167*$C167/(2*$B$54)-$B$55/$B167
F167: (S1) +$B167*$C167/(2*$B$54)-$B$55/$B167
G167: (S1) +$B$54*$E166*($A167-$A166)*$B$14*$B$15
H167: (S1) +$B$54*$F166*($A167-$A166)*$B$14*$B$15


F267: '   F 0,h=
G267: @SUM(G166..G266)
H267: @SUM(H166..H266)
A268: '   PAD THICKNESS CALCULATIONS
A269: '      D2=
B269: +$B$11+$B$14
```

```
C269: 'm     This is the outer diameter of the bearing.
A270: '      D1=
B270: +$B$11-$B$14
C270: 'm     This is the inner diameter of the bearing.
A271: '      Da=
B271: +$B$23
C271: 'm     This is the outer diameter of the runner.
A272: 'sigma ai=
B272: +$B$10
C272: 'Pa    This is the yield stress of the pad material.
A273: '       t=
B273: @SQRT((3*$F$161*($B$269+$B$270-2*$B$271))/(2*@PI*$B$271*0.6667*$B$272))
C273: 'm     This is the pad thickness.  A factor of safety
C274: '      of 1.5 is assumed.
```

Table 9 - Astern Thrust Bearing Calculation, Wilcock Analysis

```
Thesis
Thrust Bearing Design                                    1 December 1989

See thesis notes, 30 Nov 89, for development of geometry and sources.

Input:    Center supported, tilting pad thrust bearing is assumed.
        W=221749.3 lbf    This is the astern thrust load, 80% x ahead.
         P=       75 psi    This is the stress reacted by lubricant film.
       kg=      0.8         This is actual thrust area fraction.
       D1=    189.6 in      This is the inner diameter.
         N=     58.8 rpm     This is the shaft speed.
       nu=9.14E-06 ft2/s This is the kinematic viscosity of the lubricant
                            at outlet temperature.
      rho=  1.9823 lbf s/ft4 This is density of lubricant at outlet temp.
     Tout=       86 oF      This is the proposed outlet temperature.
       cp=   8.534 Btu/gal-oF This is the heat content of the lubricant.
      Tin=       85 oF      This is the inlet lubricant temperature.

NOTES:
This design is for a saltwater lubricated tilting pad thrust bearing.
The assumptions are for the support to be at 0.58*B; however, the
performance for a center-supported pad can be as good as the 0.58*B
thrust bearing if the pad is not flat, but rounded.
This analysis is based on Wilcock's text.

Output:
      D2'=    209.6 in      This is initial thrust bearing outer diameter.
        U=3072.603 ft/min This is linear velocity of bearing surface.
       b'=       10 in      This is an initial pad width estimate.
ENTRY  Enter the desired pad width.
        b=       10 in      This is the design pad width.
       i'=50.16495          This is the computed number of pads.
ENTRY  Enter the desired # of pads, must be integral and even #.
        i=       50         This is the design number of pads.
       B'=10.03299 in       This is an initial pad length estimate.
ENTRY  Enter the desired pad length.
        B=       10 in      This is the design pad length.
       mu=1.26E-07 reyns This is absolute viscosity of lubricant at
                            outlet temperature.
   Pcalc=44.34986 psi       This is the calculated lubricant pressure.
    op #=1.74E-07           This is the operating number and pad length
      B/b=        1         to width ratio.  These are entering arguments
                            for figure 11-10 of Wilcock.
        q=    0.072         This is a multiplier in the expression for
                            alpha.  This formula for alpha is derived from
   alpha=1.12E-04 rad       Wilcock.
    hmin=0.001120 in        This is the minimum film thickness. It should be
```

```
                               greater than 0.001 inches (for oil).
      q'=     0.01             This formula is developed from Fig. 12-11
       f=0.001120              from Wilcock.
       H=23.13487 HP           This is the power lost due to shear stresses.
       H=17.25167 kW           This is power lost in kW.
       Q=78.49712 in3/s This is the lubricant flow over the pads.
       Q=101.7364 gpm
     /\T=1.129806 oF           This is the tempature rise of the lubricant.

DESIGN GEOMETRY:
      D1=   189.6 in       = 4.815849 m
      D2=   209.6 in       = 5.323850 m
       b=      10 in       = 0.254000 m
       B=      10 in       = 0.254000 m
       i=      50 pads
```

1.11 Table 10 - Astern Thrust Bearing Calculation, Constantinescu et al Analysis

```
Thesis                                                   John V. Amy Jr.
Thrust Bearing Design                                    4 December 1989
ASTERN, FLOODED, SEA-WATER LUBRICATED, TIN-BRONZE PAD, OTHER BEARING
This thrust bearing design is based on the text, Sliding Bearings
by Constantinescu, et al.  The inputs to this analysis come from
the Wilcock analysis.  Integration of differential equations is
performed using Euler integrations.  A lenticulated rectangular
thrust bearing pad is assumed.
INPUT:  These are results of Wilcock's analysis for flat pads (kg,m,s).
   sigma=2.07E+07 Pa      This is the yield stress of the pad material.
    Davg=     5.07 m      This is the average bearing diameter.
   alpha=1.12E-04 rad     This is the pad tilt from Wilcock.
    hmin=2.84E-05 m       This is Wilcock's minimum film thickness.
       B=    0.254 m      This is the pad length.
       L=    0.254 m      This is the pad width.
      nu=9.14E-06 ft2/s   This is lubricant kinematic viscosity at Tamb.
     rho=   1.9823 lbf s2/ft4  This is lubricant density at Tamb.
       N=     58.8 rpm    This is the shaft speed.
       i=       50 pads   This is the number of thrust bearing pads.
    Tamb=       86 oF     This is the ambient lubricant temperature.
  Wtotal=986340.9 N       This is the thrust borne by the bearing.
       P=   305793 Pa     This is the bearing pressure.
     Dph=     4.37 m      This is the runner diameter. (pressure hull)
OUTPUT DATA:
  W brg"= 1749029 N       These are thrusts for each pad times the number
   W brg= 1749029 N       of pads, and should be greater than or equal to
                          equal to W total.  W brg" uses a separation BC
 W total=  986341 N       in the divergent flow, W brg does not.
       t=0.019698 m       This is the pad thickness.
  Wm bar=0.167062         Non-dimensionalised load, hmin is reference.
  Wp bar=0.200926         Non-dimensionalised load, hp is reference.
      Sp=4.976951         Sommerfeld Number
      Sm=5.985796
  Qx bar=0.552806         Non-dimensionalised lubricant flux rate
  F0 bar=0.952153         Non-dimensionalised friction force at y=0
  Fh bar=0.702853         Non-dimensionalised friction force at y=h
      f0=0.000730         Friction coefficient at y=0
      fh=0.000539         Friction coefficient at y=h
These coefficients can now be compared with experimental values.
See the reference, Constantinescu et al, pages 283..285 and pg 29.
CALCULATIONS      Primes denote initial estimates.
     h1'=7.11E-05 m       This is the inlet film thickness.
     h2'=4.27E-05 m       This is the outlet film thickness.
  delta'=1.77E-05 m       This is the maximum departure from flat plate.
                          Delta/hp is assumed here to be 0.45.
   hmin'=3.64E-05 m       This is to provide estimate of hmin.  It should
                          be greater than 25.4 micrometers.
```

```
      The preceeding values are based on Wilcock's hmin, alpha, B.
ENTRY REQUIRED
   h1=6.60E-05 m      This is the design inlet film thickness.
   h2=3.76E-05 m      This is the design outlet film thickness.
delta=1.61E-05 m      This is design maximum departure from plane.
 hmin=3.26E-05 m      This is the minimun film thickness.
   mu=8.68E-04 kg/m s This is the lubricant absolute viscosity.
    V=15.60931 m/s    This is the bearing linear velocity.
PRESSURE/LOAD CALCULATIONS   ho'=0.000035 m   thickness at pmax
   ho' is assumed to be at 0.6 into the convergent portion of the
   lubricant film.--This is roughly equal to 0.49 x B.
 x/B    hc m      h m      dp/dx    p-pa Pa    W  N    dp/dx   p-pa Pa
    0 0.00E+00 6.60E-05  8.5E+06  0.0E+00          0  8.5E+06  0.0E+00
 0.01 6.36E-07 6.51E-05  8.6E+06  2.2E+04 13.97539  8.6E+06  2.2E+04
```

1.12 Table 11 - Journal Bearing Calculation, Wilcock Analysis

```
Thesis                                                  John V. Amy Jr.
Thrust Bearing Design                                   6 December 1989
TILTING PAD, JOURNAL BEARING
See thesis notes, 30 Nov 89, for development of geometry and sources.

Input:   Center supported, tilting pad journal bearing is assumed.
       W=   88500 lbf    This is the thrust load.
       P=      75 psi    This is the stress reacted by lubricant film.
      kg=     0.8        This is actual thrust area fraction.
      D1=   177.2 in     This is the inner diameter.
       N=    58.8 rpm    This is the shaft speed.
      nu=9.04E-06 ft2/s This is the kinematic viscosity of the lubricant
                         at outlet temperature.
     rho=  1.9819 lbf s/ft4 This is density of lubricant at outlet temp.
    Tout=      87 oF     This is the proposed outlet temperature.
      cp=   8.534 Btu/gal-oF This is the heat content of the lubricant.
     Tin=      85 oF     This is the inlet lubricant temperature.

NOTES:
This design is for a saltwater lubricated tilting pad thrust bearing.
The assumptions are for the support to be at 0.58*B; however, the
performance for a center-supported pad can be as good as the 0.58*B
thrust bearing if the pad is not flat, but rounded.
This analysis is based on Wilcock's text.

Output:
     D2'=182.4222 in     This is initial thrust bearing outer diameter.
       U=2767.977 ft/min This is linear velocity of bearing surface.
      b'=2.611112 in     This is an initial pad width estimate.
ENTRY  Enter the desired pad width.
       b=       7 in     This is the design pad width.
      i'=64.55923        This is the computed number of pads.
ENTRY  Enter the desired # of pads, must be integral and even #.
       i=      64        This is the design number of pads.
      B'=7.061165 in     This is an initial pad length estimate.
ENTRY  Enter the desired pad length.
       B=       7 in     This is the design pad length.
      mu=1.24E-07 reyns This is absolute viscosity of lubricant at
                         outlet temperature.
   Pcalc=28.22066 psi    This is the calculated lubricant pressure.
    op #=3.49E-07        This is the operating number and pad length
     B/b=       1        to width ratio.  These are entering arguments
                         for figure 11-10 of Wilcock.
       q=   0.072        This is a multiplier in the expression for
                         alpha.  This formula for alpha is derived from
   alpha=1.58E-04 rad    Wilcock.
    hmin=0.001109 in     This is the minimum film thickness. It should be
```

```
                          greater than 0.001 inches (for oil).
      q'=    0.01         This formula is developed from Fig. 11-11
       f=0.001584         from Wilcock.
       H=11.76092 HP      This is the power lost due to shear stresses.
       H=8.770121 kW      This is power lost in kW.
       Q=62.71234 in3/s This is the lubricant flow over the pads.
       Q=81.27850 gpm
     /\T=0.718917 oF      This is the tempature rise of the lubricant.

DESIGN GEOMETRY:
      D1=   177.2 in      = 4.500889 m
      D2=   191.2 in      = 4.856489 m
       b=       7 in      = 0.177800 m
       B=       7 in      = 0.177800 m
       i=      64 pads
```

1.13 Table 12 - Journal Bearing Calculation, Constantinescu et al Analysis

```
Thesis                                                   John V. Amy Jr.
Thrust Bearing Design                                    6 December 1989
TILTING PAD, LENTICULATED, TIN-BRONZE, SEA WATER FLOODED JOURNAL BEARING
This journal bearing design is based on the text, Sliding Bearings
by Constantinescu, et al.  The inputs to this analysis come from
the Wilcock analysis.  Integration of differential equations is
performed using Euler integrations.  A lenticulated rectangular
journal bearing pad is assumed.
INPUT:  These are results of Wilcock's analysis for flat pads (kg,m,s).
   sigma=2.07E+07 Pa      This is the yield stress of the pad material.
    Davg=      4.5 m      This is the average bearing diameter.
   alpha=1.58E-04 rad     This is the pad tilt from Wilcock.
    hmin=2.82E-05 m       This is Wilcock's minimum film thickness.
       B=   0.1778 m      This is the pad length.
       L=   0.1778 m      This is the pad width.
      nu=9.14E-06 ft2/s  This is lubricant kinematic viscosity at Tamb.
     rho=   1.9823 lbf s2/ft4  This is lubricant density at Tamb.
       N=     58.8 rpm    This is the shaft speed.
       i=       64 pads   This is the number of thrust bearing pads.
    Tamb=       86 oF     This is the ambient lubricant temperature.
  Wtotal=   394600 N      This is the thrust borne by the bearing.
       P=194583.8 Pa      This is the bearing pressure.
     Dph=    4.449 m      This is the runner diameter. (pressure hull)
OUTPUT DATA:
  W brg"=   790218 N      These are thrusts for each pad times the number
   W brg=   790218 N      of pads, and should be greater than or equal to
                          equal to W total.  W brg" uses a separation BC
 W total=   394600 N      in the divergent flow, W brg does not.
       t=0.003130 m       This is the pad thickness.
  Wm bar=0.145644         Non-dimensionalised load, hmin is reference.
  Wp bar=0.183511         Non-dimensionalised load, hp is reference.
      Sp=5.449247         Sommerfeld Number
      Sm=6.866041
  Qx bar=0.566324         Non-dimensionalised lubricant flux rate
  F0 bar=0.902672         Non-dimensionalised friction force at y=0
  Fh bar=0.726785         Non-dimensionalised friction force at y=h
      f0=0.000984         Friction coefficient at y=0
      fh=0.000792         Friction coefficient at y=h
These coefficients can now be compared with experimental values.
See the reference, Constantinescu et al, pages 283..285 and pg 29.
CALCULATIONS        Primes denote initial estimates.
     h1'=7.03E-05 m       This is the inlet film thickness.
     h2'=4.23E-05 m       This is the outlet film thickness.
  delta'=1.75E-05 m       This is the maximum departure from flat plate.
                          Delta/hp is assumed here to be 0.45.
   hmin'=3.60E-05 m       This is to provide estimate of hmin.  It should
                          be greater than 25.4 micrometers.
```

```
      The preceeding values are based on Wilcock's hmin, alpha. B.
ENTRY REQUIRED
   h1=6.00E-05 m       This is the design inlet film thickness.
   h2=3.19E-05 m       This is the design outlet film thickness.
delta=1.43E-05 m       This is design maximum departure from plane.
 hmin=2.82E-05 m       This is the minimun film thickness.
   mu=8.68E-04 kg/m s This is the lubricant absolute viscosity.
    V=13.85442 m/s     This is the bearing linear velocity.
PRESSURE/LOAD CALCULATIONS   ho'=0.000031 m   thickness at pmax
   ho' is assumed to be at 0.6 into the convergent portion of the
   lubricant film.--This is roughly equal to 0.49 x B.
 x/B    hc m       h m      dp/dx   p-pa Pa    W  N     dp/dx   p-pa Pa
    0 0.00E+00 6.00E-05  9.4E+06  0.0E+00          0  9.4E+06  0.0E+00
 0.01 5.65E-07 5.92E-05  9.5E+06  1.7E+04 5.291675  9.5E+06  1.7E+04
```

1.14 Table 13 - ‘Air’-Gap Pressure Force Calculations

Thesis
Support Structure Design - Normal Pressure Force

John V. Amy Jr.
9 February 1990

mu=
tag=
Lag= 102.91 in
phd= 10 psi

Rag= 98.82 in
V=
Q =

2z/L	z	p(z)	F(z)
0.00	0.0000	10	0
0.01	0.5146	9.9	3162.914
0.02	1.0291	9.8	3130.966
0.03	1.5437	9.7	3099.017
0.04	2.0582	9.6	3067.068
0.05	2.5728	9.5	3035.120
0.06	3.0873	9.4	3003.171
0.07	3.6019	9.3	2971.223
0.08	4.1164	9.2	2939.274
0.09	4.6310	9.1	2907.325
0.10	5.1455	9	2875.377
0.11	5.6601	8.9	2843.428
0.12	6.1746	8.8	2811.479
0.13	6.6892	8.7	2779.531
0.14	7.2037	8.6	2747.582
0.15	7.7183	8.5	2715.633
0.16	8.2328	8.4	2683.685
0.17	8.7474	8.3	2651.736
0.18	9.2619	8.2	2619.788
0.19	9.7765	8.1	2587.839
0.20	10.2910	8	2555.890
0.21	10.8055	7.9	2523.942
0.22	11.3201	7.8	2491.993
0.23	11.8347	7.7	2460.044
0.24	12.3492	7.6	2428.096
0.25	12.8638	7.5	2396.147
0.26	13.3783	7.4	2364.198
0.27	13.8929	7.3	2332.250
0.28	14.4074	7.2	2300.301
0.29	14.9220	7.1	2268.353
0.30	15.4365	7	2236.404
0.31	15.9511	6.9	2204.455
0.32	16.4656	6.8	2172.507
0.33	16.9802	6.7	2140.558
0.34	17.4947	6.6	2108.609
0.35	18.0093	6.5	2076.661
0.36	18.5238	6.4	2044.712
0.37	19.0384	6.3	2012.763

```
0.38  19.5529       6.2 1980.815
0.39  20.0675       6.1 1948.866
0.40  20.5820         6 1916.918
0.41  21.0966       5.9 1884.969
0.42  21.6111       5.8 1853.020
0.43  22.1257       5.7 1821.072
0.44  22.6402       5.6 1789.123
0.45  23.1548       5.5 1757.174
0.46  23.6693       5.4 1725.226
0.47  24.1839       5.3 1693.277
0.48  24.6984       5.2 1661.328
0.49  25.2130       5.1 1629.380
0.50  25.7275         5 1597.431
0.51  26.2421       4.9 1565.483
0.52  26.7566       4.8 1533.534
0.53  27.2712       4.7 1501.585
0.54  27.7857       4.6 1469.637
0.55  28.3003       4.5 1437.688
0.56  28.8148       4.4 1405.739
0.57  29.3294       4.3 1373.791
0.58  29.8439       4.2 1341.842
0.59  30.3585       4.1 1309.894
0.60  30.8730         4 1277.945
0.61  31.3876       3.9 1245.996
0.62  31.9021       3.8 1214.048
0.63  32.4167       3.7 1182.099
0.64  32.9312       3.6 1150.150
0.65  33.4458       3.5 1118.202
0.66  33.9603       3.4 1086.253
0.67  34.4749       3.3 1054.304
0.68  34.9894       3.2 1022.356
0.69  35.5040       3.1 990.4076
0.70  36.0185         3 958.4590
0.71  36.5331       2.9 926.5103
0.72  37.0476       2.8 894.5617
0.73  37.5622       2.7 862.6131
0.74  38.0767       2.6 830.6644
0.75  38.5913       2.5 798.7158
0.76  39.1058       2.4 766.7672
0.77  39.6204       2.3 734.8185
0.78  40.1349       2.2 702.8699
0.79  40.6495       2.1 670.9213
0.80  41.1640         2 638.9726
0.81  41.6786       1.9 607.0240
0.82  42.1931       1.8 575.0754
0.83  42.7077       1.7 543.1267
0.84  43.2222       1.6 511.1781
```

```
     0.85  43.7368        1.5 479.2295
     0.86  44.2513        1.4 447.2808
     0.87  44.7659        1.3 415.3322
     0.88  45.2804        1.2 383.3836
     0.89  45.7950        1.1 351.4349
     0.90  46.3095          1 319.4863
     0.91  46.8241        0.9 287.5377
     0.92  47.3386        0.8 255.5890
     0.93  47.8532        0.7 223.6404
     0.94  48.3677        0.6 191.6918
     0.95  48.8823        0.5 159.7431
     0.96  49.3968        0.4 127.7945
     0.97  49.9114        0.3 95.84590
     0.98  50.4259        0.2 63.89726
     0.99  50.9405        0.1 31.94863
     1.00  51.4550  1.7E-18  5.5E-16
                     Sum  F=  158145.7
```

```
A1: 'Thesis
G1: 'John V. Amy Jr.
A2: 'Support Structure Design - Normal Pressure Force
G2: "9 February 1990
A4: '        mu=
D4: '      Rag=
E4: 98.82
F4: 'in
A5: '      tag=
D5: '        V=
A6: '      Lag=
B6: 102.91
C6: 'in
A7: '      phd=
B7: 10
C7: 'psi
D7: '        Q =
A9: '  2z/L
B9: '     z
C9: '    p(z)
D9: '    F(z)
A10: (F2) 0
B10: (F4) +$A10*$B$6/2
C10: +$B$7
D10: 0
A11: (F2) 0.01
B11: (F4) +$A11*$B$6/2
C11: -($B$7*2/$B$6)*A11*$B$6/2+$B$7
```

```
D11: 2*@PI*$E$4*(B11-B10)*C11


C111: 'Sum  F=
D111: @SUM(D10..D110)
```

1.15 Table 14 - Stator Ring Force and Moment Calculations

```
Thesis                                                 John V. Amy Jr.
Support Structure Design   Stator Rings                13 December 1989

This worksheet develops shear and moment diagrams which describe the
shear forces and bending moments which result from the weight of the
stator and the normal forces of EM origin.
   Shear  @ zero-=-0.14286 Avg shear  .00000  Mb @ 2pi 0.00427
   Shear  @  2*pi= 0.14286  @ 2*pi-=-0.14286  Avg Mb =  .00000
 theta       Fbp        Frp      Shear     dx/R      dMb       Mb
 0.0E+00 -0.71429       1.0     0.1429  0.00000  0.00000  0.00427
 3.0E-02  0.00000       0.0     0.1429  0.02992 -0.00427   .00000
 6.0E-02  0.00000       0.0     0.1429  0.02992 -0.00427 -0.00428
 9.0E-02  0.00000       0.0     0.1429  0.02992 -0.00427 -0.00855
 1.2E-01  0.00000       0.0     0.1429  0.02992 -0.00427 -0.01283
 1.5E-01 -0.71429       0.0    -0.5714  0.02992  0.01710  0.00427
 1.8E-01  0.00000       0.0    -0.5714  0.02992  0.01710  0.02137
 2.1E-01  0.00000       1.0     0.4286  0.02992 -0.01282  0.00854
 2.4E-01  0.00000       0.0     0.4286  0.02992 -0.01282 -0.00428
 2.7E-01  0.00000       0.0     0.4286  0.02992 -0.01282 -0.01710
 3.0E-01 -0.71429       0.0    -0.2857  0.02992  0.00855 -0.00855
 3.3E-01  0.00000       0.0    -0.2857  0.02992  0.00855   .00000
 3.6E-01  0.00000       0.0    -0.2857  0.02992  0.00855  0.00854
 3.9E-01  0.00000       0.0    -0.2857  0.02992  0.00855  0.01709
 4.2E-01  0.00000       1.0     0.7143  0.02992 -0.02137 -0.00428
 4.5E-01 -0.71429       0.0      .0000  0.02992   .00000 -0.00428
 4.8E-01  0.00000       0.0      .0000  0.02992   .00000 -0.00428
 5.1E-01  0.00000       0.0      .0000  0.02992   .00000 -0.00428
 5.4E-01  0.00000       0.0      .0000  0.02992   .00000 -0.00428
 5.7E-01  0.00000       0.0      .0000  0.02992   .00000 -0.00428
 6.0E-01 -0.71429       0.0    -0.7143  0.02992  0.02137  0.01709
 6.3E-01  0.00000       1.0     0.2857  0.02992 -0.00855  0.00854
 6.6E-01  0.00000       0.0     0.2857  0.02992 -0.00855   .00000
 6.9E-01  0.00000       0.0     0.2857  0.02992 -0.00855 -0.00855
 7.2E-01  0.00000       0.0     0.2857  0.02992 -0.00855 -0.01710
 7.5E-01 -0.71429       0.0    -0.4286  0.02992  0.01282 -0.00428
 7.8E-01  0.00000       0.0    -0.4286  0.02992  0.01282  0.00854
 8.1E-01  0.00000       0.0    -0.4286  0.02992  0.01282  0.02137
 8.4E-01  0.00000       1.0     0.5714  0.02992 -0.01710  0.00427
 8.7E-01  0.00000       0.0     0.5714  0.02992 -0.01710 -0.01283
 9.0E-01 -0.71429       0.0    -0.1429  0.02992  0.00427 -0.00855
 9.3E-01  0.00000       0.0    -0.1429  0.02992  0.00427 -0.00428
 9.6E-01  0.00000       0.0    -0.1429  0.02992  0.00427   .00000
 9.9E-01  0.00000       0.0    -0.1429  0.02992  0.00427  0.00427
 1.0E+00  0.00000       0.0    -0.1429  0.02992  0.00427  0.00854
 1.0E+00 -0.71429       1.0     0.1429  0.02992 -0.00427  0.00427
 1.1E+00  0.00000       0.0     0.1429  0.02992 -0.00427   .00000
 1.1E+00  0.00000       0.0     0.1429  0.02992 -0.00427 -0.00428
```

```
1.1E+00  0.00000       0.0   0.1429  0.02992 -0.00427 -0.00855
1.2E+00  0.00000       0.0   0.1429  0.02992 -0.00427 -0.01283
1.2E+00 -0.71429       0.0  -0.5714  0.02992  0.01710  0.00427
1.2E+00  0.00000       0.0  -0.5714  0.02992  0.01710  0.02137
1.3E+00  0.00000       1.0   0.4286  0.02992 -0.01282  0.00854
1.3E+00  0.00000       0.0   0.4286  0.02992 -0.01282 -0.00428
1.3E+00  0.00000       0.0   0.4286  0.02992 -0.01282 -0.01710
1.3E+00 -0.71429       0.0  -0.2857  0.02992  0.00855 -0.00855
1.4E+00  0.00000       0.0  -0.2857  0.02992  0.00855   .00000
1.4E+00  0.00000       0.0  -0.2857  0.02992  0.00855  0.00854
1.4E+00  0.00000       0.0  -0.2857  0.02992  0.00855  0.01709
1.5E+00  0.00000       1.0   0.7143  0.02992 -0.02137 -0.00428
1.5E+00 -0.71429       0.0    .0000  0.02992   .00000 -0.00428
1.5E+00  0.00000       0.0    .0000  0.02992   .00000 -0.00428
1.6E+00  0.00000       0.0    .0000  0.02992   .00000 -0.00428
1.6E+00  0.00000       0.0    .0000  0.02992   .00000 -0.00428
1.6E+00  0.00000       0.0    .0000  0.02992   .00000 -0.00428
1.6E+00 -0.71429       0.0  -0.7143  0.02992  0.02137  0.01709
1.7E+00  0.00000       1.0   0.2857  0.02992 -0.00855  0.00854
1.7E+00  0.00000       0.0   0.2857  0.02992 -0.00855   .00000
1.7E+00  0.00000       0.0   0.2857  0.02992 -0.00855 -0.00855
1.8E+00  0.00000       0.0   0.2857  0.02992 -0.00855 -0.01710
1.8E+00 -0.71429       0.0  -0.4286  0.02992  0.01282 -0.00428
1.8E+00  0.00000       0.0  -0.4286  0.02992  0.01282  0.00854
1.9E+00  0.00000       0.0  -0.4286  0.02992  0.01282  0.02137
1.9E+00  0.00000       1.0   0.5714  0.02992 -0.01710  0.00427
1.9E+00  0.00000       0.0   0.5714  0.02992 -0.01710 -0.01283
1.9E+00 -0.71429       0.0  -0.1429  0.02992  0.00427 -0.00855
2.0E+00  0.00000       0.0  -0.1429  0.02992  0.00427 -0.00428
2.0E+00  0.00000       0.0  -0.1429  0.02992  0.00427   .00000
2.0E+00  0.00000       0.0  -0.1429  0.02992  0.00427  0.00427
2.1E+00  0.00000       0.0  -0.1429  0.02992  0.00427  0.00854
2.1E+00 -0.71429       1.0   0.1429  0.02992 -0.00427  0.00427
2.1E+00  0.00000       0.0   0.1429  0.02992 -0.00427   .00000
2.2E+00  0.00000       0.0   0.1429  0.02992 -0.00427 -0.00428
2.2E+00  0.00000       0.0   0.1429  0.02992 -0.00427 -0.00855
2.2E+00  0.00000       0.0   0.1429  0.02992 -0.00427 -0.01283
2.2E+00 -0.71429       0.0  -0.5714  0.02992  0.01710  0.00427
2.3E+00  0.00000       0.0  -0.5714  0.02992  0.01710  0.02137
2.3E+00  0.00000       1.0   0.4286  0.02992 -0.01282  0.00854
2.3E+00  0.00000       0.0   0.4286  0.02992 -0.01282 -0.00428
2.4E+00  0.00000       0.0   0.4286  0.02992 -0.01282 -0.01710
2.4E+00 -0.71429       0.0  -0.2857  0.02992  0.00855 -0.00855
2.4E+00  0.00000       0.0  -0.2857  0.02992  0.00855   .00000
2.5E+00  0.00000       0.0  -0.2857  0.02992  0.00855  0.00854
2.5E+00  0.00000       0.0  -0.2857  0.02992  0.00855  0.01709
2.5E+00  0.00000       1.0   0.7143  0.02992 -0.02137 -0.00428
```

```
2.5E+00 -0.71429      0.0    .0000  0.02992   .00000 -0.00428
2.6E+00  0.00000      0.0    .0000  0.02992   .00000 -0.00428
2.6E+00  0.00000      0.0    .0000  0.02992   .00000 -0.00428
2.6E+00  0.00000      0.0    .0000  0.02992   .00000 -0.00428
2.7E+00  0.00000      0.0    .0000  0.02992   .00000 -0.00428
2.7E+00 -0.71429      0.0  -0.7143  0.02992  0.02137  0.01709
2.7E+00  0.00000      1.0   0.2857  0.02992 -0.00855  0.00854
2.8E+00  0.00000      0.0   0.2857  0.02992 -0.00855   .00000
2.8E+00  0.00000      0.0   0.2857  0.02992 -0.00855 -0.00855
2.8E+00  0.00000      0.0   0.2857  0.02992 -0.00855 -0.01710
2.8E+00 -0.71429      0.0  -0.4286  0.02992  0.01282 -0.00428
2.9E+00  0.00000      0.0  -0.4286  0.02992  0.01282  0.00854
2.9E+00  0.00000      0.0  -0.4286  0.02992  0.01282  0.02137
2.9E+00  0.00000      1.0   0.5714  0.02992 -0.01710  0.00427
3.0E+00  0.00000      0.0   0.5714  0.02992 -0.01710 -0.01283
3.0E+00 -0.71429      0.0  -0.1429  0.02992  0.00427 -0.00855
3.0E+00  0.00000      0.0  -0.1429  0.02992  0.00427 -0.00428
3.1E+00  0.00000      0.0  -0.1429  0.02992  0.00427   .00000
3.1E+00  0.00000      0.0  -0.1429  0.02992  0.00427  0.00427
3.1E+00  0.00000      0.0  -0.1429  0.02992  0.00427  0.00854
3.1E+00 -0.71429      1.0   0.1429  0.02992 -0.00427  0.00427
3.2E+00  0.00000      0.0   0.1429  0.02992 -0.00427   .00000
3.2E+00  0.00000      0.0   0.1429  0.02992 -0.00427 -0.00428
3.2E+00  0.00000      0.0   0.1429  0.02992 -0.00427 -0.00855
3.3E+00  0.00000      0.0   0.1429  0.02992 -0.00427 -0.01283
3.3E+00 -0.71429      0.0  -0.5714  0.02992  0.01710  0.00427
3.3E+00  0.00000      0.0  -0.5714  0.02992  0.01710  0.02137
3.4E+00  0.00000      1.0   0.4286  0.02992 -0.01282  0.00854
3.4E+00  0.00000      0.0   0.4286  0.02992 -0.01282 -0.00428
3.4E+00  0.00000      0.0   0.4286  0.02992 -0.01282 -0.01710
3.4E+00 -0.71429      0.0  -0.2857  0.02992  0.00855 -0.00855
3.5E+00  0.00000      0.0  -0.2857  0.02992  0.00855   .00000
3.5E+00  0.00000      0.0  -0.2857  0.02992  0.00855  0.00854
3.5E+00  0.00000      0.0  -0.2857  0.02992  0.00855  0.01709
3.6E+00  0.00000      1.0   0.7143  0.02992 -0.02137 -0.00428
3.6E+00 -0.71429      0.0    .0000  0.02992   .00000 -0.00428
3.6E+00  0.00000      0.0    .0000  0.02992   .00000 -0.00428
3.7E+00  0.00000      0.0    .0000  0.02992   .00000 -0.00428
3.7E+00  0.00000      0.0    .0000  0.02992   .00000 -0.00428
3.7E+00  0.00000      0.0    .0000  0.02992   .00000 -0.00428
3.7E+00 -0.71429      0.0  -0.7143  0.02992  0.02137  0.01709
3.8E+00  0.00000      1.0   0.2857  0.02992 -0.00855  0.00854
3.8E+00  0.00000      0.0   0.2857  0.02992 -0.00855   .00000
3.8E+00  0.00000      0.0   0.2857  0.02992 -0.00855 -0.00855
3.9E+00  0.00000      0.0   0.2857  0.02992 -0.00855 -0.01710
3.9E+00 -0.71429      0.0  -0.4286  0.02992  0.01282 -0.00428
3.9E+00  0.00000      0.0  -0.4286  0.02992  0.01282  0.00854
```

```
3.9E+00  0.00000       0.0  -0.4286  0.02992  0.01282  0.02137
4.0E+00  0.00000       1.0   0.5714  0.02992 -0.01710  0.00427
4.0E+00  0.00000       0.0   0.5714  0.02992 -0.01710 -0.01283
4.0E+00 -0.71429       0.0  -0.1429  0.02992  0.00427 -0.00855
4.1E+00  0.00000       0.0  -0.1429  0.02992  0.00427 -0.00428
4.1E+00  0.00000       0.0  -0.1429  0.02992  0.00427   .00000
4.1E+00  0.00000       0.0  -0.1429  0.02992  0.00427  0.00427
4.2E+00  0.00000       0.0  -0.1429  0.02992  0.00427  0.00854
4.2E+00 -0.71429       1.0   0.1429  0.02992 -0.00427  0.00427
4.2E+00  0.00000       0.0   0.1429  0.02992 -0.00427   .00000
4.2E+00  0.00000       0.0   0.1429  0.02992 -0.00427 -0.00428
4.3E+00  0.00000       0.0   0.1429  0.02992 -0.00427 -0.00855
4.3E+00  0.00000       0.0   0.1429  0.02992 -0.00427 -0.01283
4.3E+00 -0.71429       0.0  -0.5714  0.02992  0.01710  0.00427
4.4E+00  0.00000       0.0  -0.5714  0.02992  0.01710  0.02137
4.4E+00  0.00000       1.0   0.4286  0.02992 -0.01282  0.00854
4.4E+00  0.00000       0.0   0.4286  0.02992 -0.01282 -0.00428
4.5E+00  0.00000       0.0   0.4286  0.02992 -0.01282 -0.01710
4.5E+00 -0.71429       0.0  -0.2857  0.02992  0.00855 -0.00855
4.5E+00  0.00000       0.0  -0.2857  0.02992  0.00855   .00000
4.5E+00  0.00000       0.0  -0.2857  0.02992  0.00855  0.00854
4.6E+00  0.00000       0.0  -0.2857  0.02992  0.00855  0.01709
4.6E+00  0.00000       1.0   0.7143  0.02992 -0.02137 -0.00428
4.6E+00 -0.71429       0.0    .0000  0.02992   .00000 -0.00428
4.7E+00  0.00000       0.0    .0000  0.02992   .00000 -0.00428
4.7E+00  0.00000       0.0    .0000  0.02992   .00000 -0.00428
4.7E+00  0.00000       0.0    .0000  0.02992   .00000 -0.00428
4.8E+00  0.00000       0.0    .0000  0.02992   .00000 -0.00428
4.8E+00 -0.71429       0.0  -0.7143  0.02992  0.02137  0.01709
4.8E+00  0.00000       1.0   0.2857  0.02992 -0.00855  0.00854
4.8E+00  0.00000       0.0   0.2857  0.02992 -0.00855   .00000
4.9E+00  0.00000       0.0   0.2857  0.02992 -0.00855 -0.00855
4.9E+00  0.00000       0.0   0.2857  0.02992 -0.00855 -0.01710
4.9E+00 -0.71429       0.0  -0.4286  0.02992  0.01282 -0.00428
5.0E+00  0.00000       0.0  -0.4286  0.02992  0.01282  0.00854
5.0E+00  0.00000       0.0  -0.4286  0.02992  0.01282  0.02137
5.0E+00  0.00000       1.0   0.5714  0.02992 -0.01710  0.00427
5.1E+00  0.00000       0.0   0.5714  0.02992 -0.01710 -0.01283
5.1E+00 -0.71429       0.0  -0.1429  0.02992  0.00427 -0.00855
5.1E+00  0.00000       0.0  -0.1429  0.02992  0.00427 -0.00428
5.1E+00  0.00000       0.0  -0.1429  0.02992  0.00427   .00000
5.2E+00  0.00000       0.0  -0.1429  0.02992  0.00427  0.00427
5.2E+00  0.00000       0.0  -0.1429  0.02992  0.00427  0.00854
5.2E+00 -0.71429       1.0   0.1429  0.02992 -0.00427  0.00427
5.3E+00  0.00000       0.0   0.1429  0.02992 -0.00427   .00000
5.3E+00  0.00000       0.0   0.1429  0.02992 -0.00427 -0.00428
5.3E+00  0.00000       0.0   0.1429  0.02992 -0.00427 -0.00855
```

```
 5.4E+00  0.00000      0.0   0.1429  0.02992 -0.00427 -0.01283
 5.4E+00 -0.71429      0.0  -0.5714  0.02992  0.01710  0.00427
 5.4E+00  0.00000      0.0  -0.5714  0.02992  0.01710  0.02137
 5.4E+00  0.00000      1.0   0.4286  0.02992 -0.01282  0.00854
 5.5E+00  0.00000      0.0   0.4286  0.02992 -0.01282 -0.00428
 5.5E+00  0.00000      0.0   0.4286  0.02992 -0.01282 -0.01710
 5.5E+00 -0.71429      0.0  -0.2857  0.02992  0.00855 -0.00855
 5.6E+00  0.00000      0.0  -0.2857  0.02992  0.00855   .00000
 5.6E+00  0.00000      0.0  -0.2857  0.02992  0.00855  0.00854
 5.6E+00  0.00000      0.0  -0.2857  0.02992  0.00855  0.01709
 5.7E+00  0.00000      1.0   0.7143  0.02992 -0.02137 -0.00428
 5.7E+00 -0.71429      0.0    .0000  0.02992   .00000 -0.00428
 5.7E+00  0.00000      0.0    .0000  0.02992   .00000 -0.00428
 5.7E+00  0.00000      0.0    .0000  0.02992   .00000 -0.00428
 5.8E+00  0.00000      0.0    .0000  0.02992   .00000 -0.00428
 5.8E+00  0.00000      0.0    .0000  0.02992   .00000 -0.00428
 5.8E+00 -0.71429      0.0  -0.7143  0.02992  0.02137  0.01709
 5.9E+00  0.00000      1.0   0.2857  0.02992 -0.00855  0.00854
 5.9E+00  0.00000      0.0   0.2857  0.02992 -0.00853   .00000
 5.9E+00  0.00000      0.0   0.2857  0.02992 -0.00855 -0.00855
 6.0E+00  0.00000      0.0   0.2857  0.02992 -0.00855 -0.01710
 6.0E+00 -0.71429      0.0  -0.4286  0.02992  0.01282 -0.00428
 6.0E+00  0.00000      0.0  -0.4286  0.02992  0.01282  0.00854
 6.0E+00  0.00000      0.0  -0.4286  0.02992  0.01282  0.02137
 6.1E+00  0.00000      1.0   0.5714  0.02992 -0.01710  0.00427
 6.1E+00  0.00000      0.0   0.5714  0.02992 -0.01710 -0.01283
 6.1E+00 -0.71429      0.0  -0.1429  0.02992  0.00427 -0.00855
 6.2E+00  0.00000      0.0  -0.1429  0.02992  0.00427 -0.00428
 6.2E+00  0.00000      0.0  -0.1429  0.02992  0.00427   .00000
 6.2E+00  0.00000      0.0  -0.1429  0.02992  0.00427  0.00427
 6.3E+00  0.00000      0.0  -0.1429  0.02992  0.00427  0.00854
 6.3E+00 -0.71429      1.0   0.1429  0.02992 -0.00427  0.00427
                    Avg shear-4.3E-11           Avg Mb =-0.00000
```

```
A1: 'Thesis
G1: 'John V. Amy Jr.
A2: 'Support Structure Design
D2: 'Stator Rings
G2: "13 December 1989
A4: 'This worksheet develops shear and moment diagrams which describe the
A5: "shear forces and bending moments which result from the weight of the
A6: 'stator and the normal forces of EM origin.
A7: '   Shear  @ zero-=
C7: (F5) -0.1428571429
D7: 'Avg shear
E7: (F5) +$D$221
```

```
F7: ' Mb @ 2pi
G7: (F5) +$G$220
A8: '   Shear  @  2*pi=
C8: (F5) +$D$220
D8: ' @ 2*pi-=
E8: (F5) +$D$219
F8: ' Avg Mb =
G8: (F5) +$G$221
A9: ' theta
B9: '   Fbp
C9: '   Frp
D9: '  Shear
E9: '  dx/R
F9: '   dMb
G9: '   Mb
A10: (S1) 0
B10: (F5) -30/42
C10: (F1) 1
D10: (F4) +B10+C10+$C$7
E10: (F5) 0
F10: (F5) -D10*E10
G10: (F5) 0.00427
A11: (S1) 0.02991993
B11: (F5) 0
C11: (F1) 0
D11: (F4) +B11+C11+D10
E11: (F5) (A11-A10)
F11: (F5) -D11*E11
G11: (F5) @SUM($F$10..F11)+$G$10


C221: 'Avg shear
D221: @SUM(D10..D219)/210
F221: ' Avg Mb =
G221: @SUM(G10..G219)/210
```

1.16 Figure 2 - Stator Ring Shear Diagram

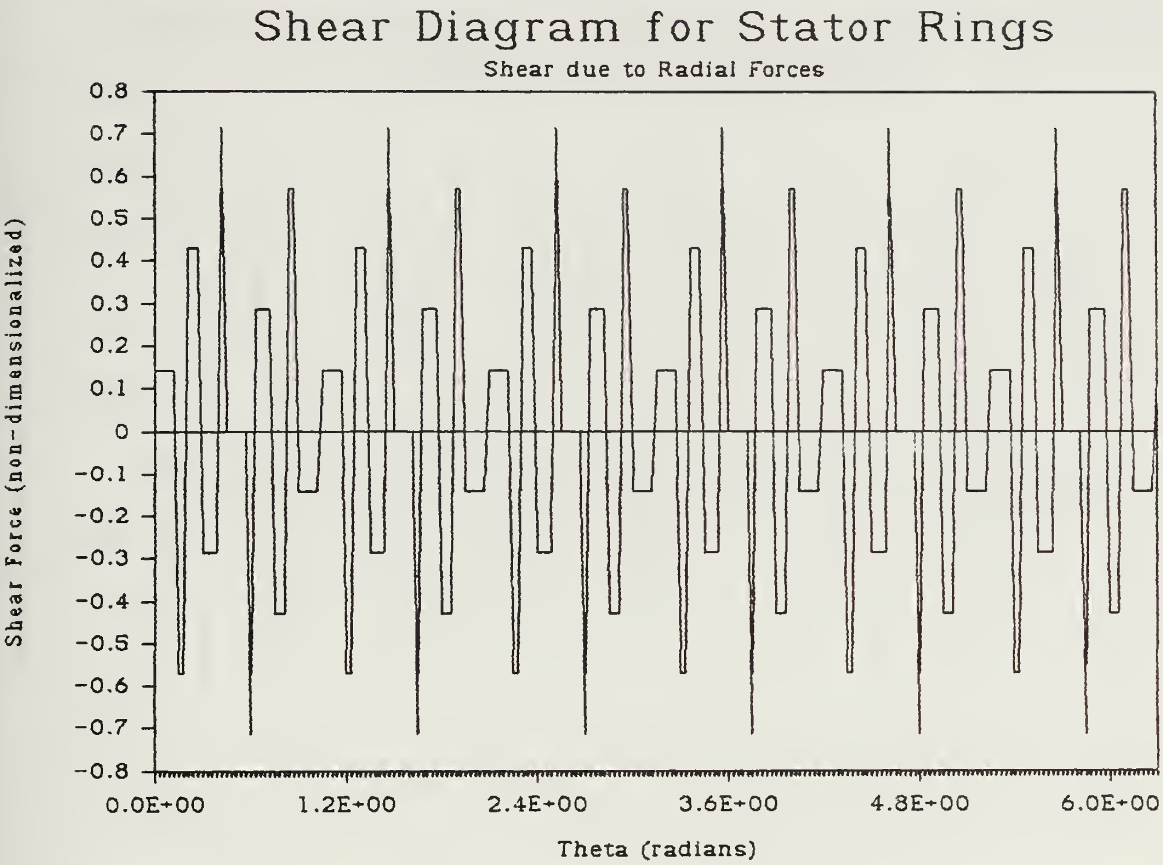

1.17 Figure 3 - Stator Ring Bending Moment Diagram

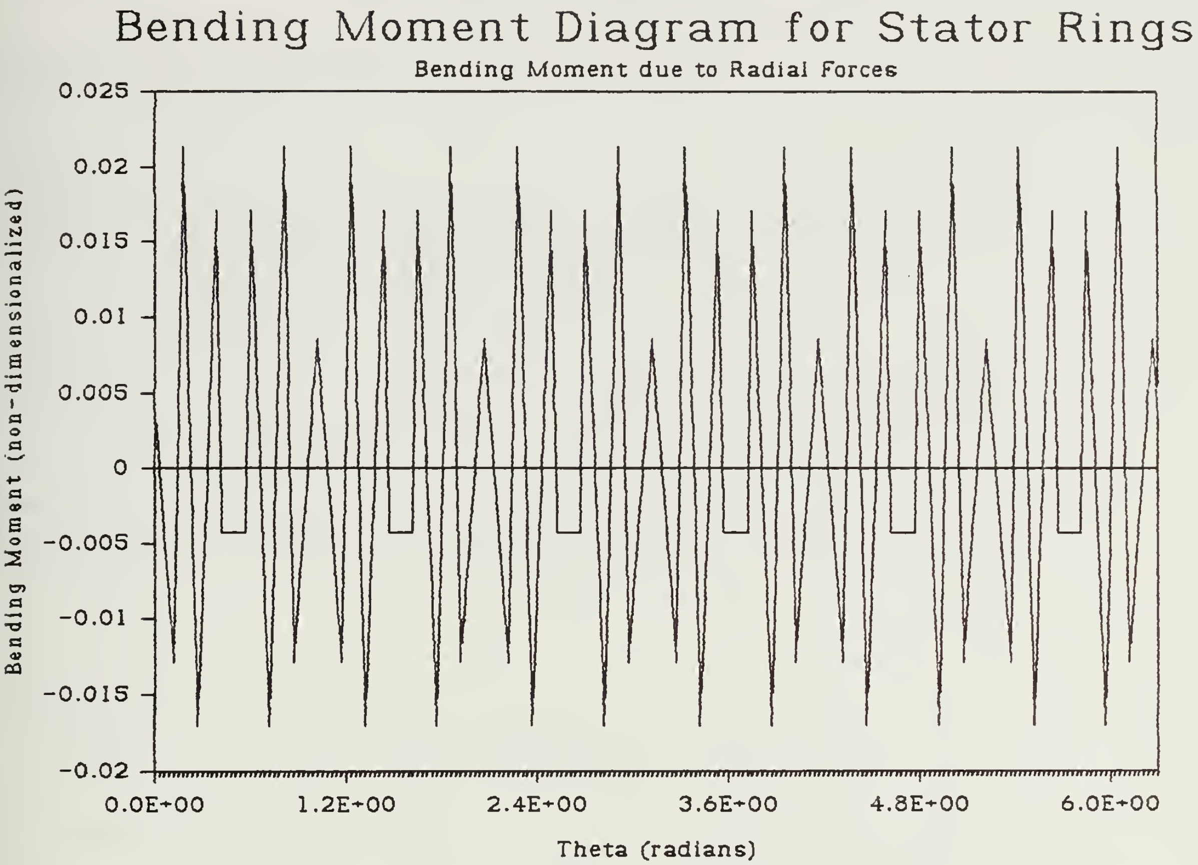

1.18 Table 15 - Combined Stator Support Structure Calculations

```
Thesis                                                     John V. Amy Jr.
Support Structure Design                                   3 March 1990


Inputs:
sigma yp=   80000 psi   This is yield stress of material.
      Wc= 82723.2 lbf   This is weight of stator core.
      Fn=  813120 lbf   This is normal forces.
       F=362725.1 lbf   This is thrust force.
  Pstack= 668.182 psi   This is core stacking stress.
   poles=       60      This is the number of stator poles.
       i=       64      This is number of journal bearing pads.
     rho=   0.283 lbf/in3  This is density of material.

See thesis notes dated 12-14 December 1989 and 19 December 1989 for
definitions of variables and development of relationships.



Core Pins:
     Rcp=    0.32 in2   This is radius of core pin.             *
     FOS=     1.5       This is factor of safety for core pin.  *

     Acp=0.321699 in2   This is cross-sectional area of pin.

 sigma 1= 668.182 psi   This is due to stacking pressure.

 sigma 2=50072.19 psi   This is due to normal, thrust and weight forces.

 sigma 3=       0 psi

sigma vM=49741.47 psi   This is von Mises' stress.

 sigma a=53333.33 psi   This is the allowable stress.

Compare sigma vM with sigma a.  Sigma vM should be less than or equal
to sigma a.  Make it close to save space and weight.  Adjust Rcp to
change design.

Tilters:
      La=     2.6 in    This is the length of the tilter arm.   *
      Lb=   10.35 in    This is the tilter base's length.       *
      ha=       2 in    This is the tilter arm width.           *
      hb=   2.625 in    This is the tilter base width.          *
      tt=       1 in    This is the tilter thickness.           *
     FOS=     1.5       This is factor of safety for tilter.    *
```

```
      W1= 1378.72 lbf   This is the core weight per pole pair.
 sigma 1=11768.56 psi   This is due to thrust force.

 sigma 2=32086.65 psi   This is due to weight and normal forces.

 sigma 3=       0 psi

sigma vM=28111.70 psi   This is von Mises' stress.

 sigma a=53333.33 psi   This is the allowable stress in the structure.
                        Sigma a should be greater than sigma vM.
 Wtilter=10.63195 lbf   This is the weight of a tilter.
Ring Pins:
     Rrp=    0.43 in    This is the radius of ring pin.        *
     FOS=     1.5       This is factor of safety for ring pin. *

     Arp=0.580880 in2   This is cross-sectional area of pin.
      W2=1399.983 lbf   This is weight per pole pair with tilter.

 sigma 1=53302.39 psi   This is due to weight, thrust and normal forces.

 sigma 2=       0 psi   This is due to normal, thrust and weight forces.

 sigma 3=       0 psi

sigma vM=53302.39 psi   This is von Mises' stress.

 sigma a=53333.33 psi   This is the allowable stress.

Compare sigma vM with sigma a.  Sigma vM should be less than or equal
to sigma a.  Adjust Rrp to change design.

Stator Rings:
      Ro=    93.6 in    This is stator ring outer diameter.    *
      Ri=    89.5 in    This is stator ring inner diameter.    *
     tsr=     0.5 in    This is the stator ring thickness.     *
     FOS=    3.75       This is stator ring factor of safety.  *

     Asr=    2.05 in2   This is cross sectional area of a stator ring.
    Asrc=287.6128 in2   This is circumferential area.
      V3=5090.098 lbf   This is shear due to weight, normal forces.
 sigma b=9952.465 psi   This is due to bending.

 sigma 1=2482.975 psi   This is due to V3 shear.

 sigma 2=10267.75 psi   This is due to sigma b and thrust shear.
```

```
 sigma 3=       0 psi

sigma vM=9278.866 psi   This is von Mises' stress.

 sigma a=21333.33 psi   This is the allowable stress.
Axial Beam:
     Wrp=0.328778 lbf   This is weight of a ring pin.
     Wsr=333.7171 lbf   This is weight of stator ring.
      W4=1323.683 lbf   This is weight supported by each beam.
      F4=1416.894 lbf   This is thrust supported by each beam.
     Fp4=14028.68 lbf   This is total normal force, including weight.

    Lbjb= 126.535 in    This is length of axial beam.         *
    hwab=       4 in    This is height of web.                *
     bab=     0.5 in    This is web thickness.                *
   Wflab=       2 in    This is flange width.                 *
   tflab=   0.375 in    This is the flange thickness.         *
 Wflmwab=       1 in    This is mid-web flange width.         *
 tflmwab=   0.375 in    This is mid-web flange thickness.     *
     FOS=    3.75       This is axial beam factor of safety.  *

     Acs=     3.5 in2   This is cross section less mid-web flange.
     Iab=9.861979 in4   This is moment of inertia less mid-web flange.
  tau yz=2004.097 psi   This is the shear stress due to bending.
sigma xx=17634.00 psi   This is normal stress due to bending.
  tau xz=5667.579 psi   This is shear due to twisting in the web.
  tau yz=354.2237 psi   This is also shear from twisting in the web.

 sigma x=23301.58 psi   This is x-directed stress in web.

 sigma y=2358.321 psi   This is y-directed stress in web.

 sigma z=8025.900 psi   This is z-directed stress in web.

sigma vM=18762.84 psi   This is von Mises' stress FOR THE WEB ONLY.

 sigma a=21333.33 psi   This is the allowable stress FOR THE WEB ONLY.

  tau xz=1416.894 psi   This is shear due to twisting in the flange.
  tau yz=3778.386 psi   This is also shear from twisting in the flange.

 sigma x=19050.90 psi   This is x-directed stress in flange.

 sigma y=5782.484 psi   This is y-directed stress in flange.

 sigma z=7199.378 psi   This is z-directed stress in flange.
```

```
sigma vM=12619.77 psi   This is von Mises' stress FOR THE FLANGE ONLY.

 sigma a=21333.33 psi   This is the allowable stress FOR FLANGE ONLY.

 sigma Q=1889.193 psi   This is stress in piece that reacts Q.

sigma F4=7556.772 psi   This is stress in piece that reacts F4.

 sigma a=21333.33 psi   This is allowable stress for Q and F4 pieces.

  tau MW=18704.91 psi   This is shear in mid-web flange, normal forces.

 sigma a=21333.33 psi   This is allowable stress mid-web flange.




Torque Reactors:
     ttr=      0.5 in    This is torque reactor width (=tsr).    *
   tfltr=        1 in    This is piece thickness.                *
     Ltr=       12 in    This is torque reactor length.          *
     htr=        3 in    This is the height of the reactor.      *
     FOS=    2.25        This is torque reactor factor of safety.*

 sigma b=146.1321 psi   This is bending stress in reactor.
  tau TR=2338.113 psi   This is shear stress in reactor.

 sigma 1=146.1321 psi

 sigma 2=2338.113 psi

 sigma 3=        0 psi

sigma vM=2268.580 psi   This is von Mises' stress.

 sigma a=35555.55 psi   This is the allowable stress for the reactor.

Pieces:
     FOS=    3.75        This is factor of safety for cutouts.  *

sigma sr=4545.174 psi   This is the stress in the stator ring piece.

 sigma a=21333.33 psi   This is the allowable stress.

sigma sr=12752.05 psi   This is the stress in the torque reactor piece.
```

```
sigma a=21333.33 psi   This is the allowable stress.
```

```
Geometric Compatibility:

          0.64 in   <=  0.666666 in  This relates core pin thickness
                                     to tilter arm width.

          0.86 in   <=     0.875 in  This relates ring pin thickness
                                     to tilter base width.

          0.86 in   <=     1.025 in  This relates ring pin thickness
                                     to stator ring height.

             3 in   <=     3.075 in  This relates axial beam flange
                                     and tilter base width to stator
                                     ring height.

         0.375 in   <=     1.025 in  This relates axial beam flange
                                     thickness to stator ring height.

        2.2125 in   <=         4 in  This relates the thicknesses
                                     of the stator ring pieces,
                                     mid-web flange thickness, and
                                     axial beam flange thickness.

             2 in   >=     0.375 in  This relates the height of the
                                     torque reactor to the axial beam
                                     flange thickness.
```

```
A1: 'Thesis
G1: 'John V. Amy Jr.
A2: 'Support Structure Design
G2: "3 March 1990
A5: 'Inputs:
A6: 'sigma yp=
B6: (G) 80000
```

```
C6: 'psi   This is yield stress of material.
A7: '      Wc=
B7: (G) 82723.2
C7: 'lbf   This is weight of stator core.
A8: '      Fn=
B8: (G) 813120
C8: 'lbf   This is normal forces.
A9: '       F=
B9: (G) 362725.1
C9: 'lbf   This is thrust force.
A10: (F2) '  Pstack=
B10: (G) 668.182
C10: 'psi   This is core stacking stress.
A11: (F2) '   poles=
B11: 60
C11: '      This is the number of stator poles.
A12: (F2) '       i=
B12: 64
C12: '      This is number of journal bearing pads.
A13: (F2) '     rho=
B13: 0.283
C13: 'lbf/in3  This is density of material.
A15: (F2) 'See thesis notes dated 12-14 December 1989 and 19 December 1989 for
A16: (F2) 'definitions of variables and development of relationships.
A21: (F2) 'Core Pins:
A22: '      Rcp=
B22: 0.32
C22: 'in2   This is radius of core pin.
H22: '*
A23: (F2) '     FOS=
B23: 1.5
C23: '      This is factor of safety for core pin.
H23: '*
A25: '      Acp=
B25: @PI*$B$22^2
C25: 'in2   This is cross-sectional area of pin.
A27: (F2) ' sigma 1=
B27: +$B$10
C27: 'psi   This is due to stacking pressure.
A29: (F2) ' sigma 2=
B29: @SQRT(($B$9/($B$11*$B$25))^2+(($B$7+$B$8)/($B$11*$B$25))^2)
C29: 'psi   This is due to normal, thrust and weight forces.
A31: (F2) ' sigma 3=
B31: 0
C31: 'psi
A33: (F2) 'sigma vM=
B33: @SQRT(0.5*(($B27-$B29)^2+($B29-$B31)^2+($B31-$B27)^2))
```

```
C33: 'psi   This is von Mises' stress.
A35: (F2) ' sigma a=
B35: +$B$6/$B$23
C35: 'psi   This is the allowable stress.
A37: (F2) 'Compare sigma vM with sigma a.  Sigma vM should be less than or equal
A38: (F2) 'to sigma a.  Make it close to save space and weight.  Adjust Rcp to
A39: (F2) 'change design.
A41: 'Tilters:
A42: (F2) '      La=
B42: 2.6
C42: 'in    This is the lengtn of the tilter arm.
H42: '*
A43: (F2) '      Lb=
B43: 10.35
C43: 'in    This is the tilter base's length.
H43: '*
A44: (F2) '      ha=
B44: 2
C44: 'in    This is the tilter arm width.
H44: '*
A45: (F2) '      hb=
B45: 2.625
C45: 'in    This is the tilter base width
H45: '*
A46: (F2) '      tt=
B46: 1
C46: 'in    This is the tilter thickness.
H46: '*
A47: (F2) '     FOS=
B47: 1.5
C47: '      This is factor of safety for tilter.
H47: '*
A49: (F2) '      W1=
B49: +$B$7/$B$11
C49: 'lbf   This is the core weight per pole pair.
A50: (F2) ' sigma 1=
B50: (3*$B$9*$B$42)/($B$11*$B$44^2*$B$46)
C50: 'psi   This is due to thrust force.
A52: (F2) ' sigma 2=
B52: (3*(0.5*$B$49+$B$8/$B$11)*$B$43)/(2*$B$45^2*$B$46)
C52: 'psi   This is due to weight and normal forces.
A54: (F2) ' sigma 3=
B54: 0
C54: 'psi
A56: (F2) 'sigma vM=
B56: @SQRT(0.5*(($B50-$B52)^2+($B52-$B54)^2+($B54-$B50)^2))
C56: 'psi   This is von Mises' stress.
```

```
A58: (F2) ' sigma a=
B58: +$B$6/$B$47
C58: 'psi   This is the allowable stress in the structure.
C59: '      Sigma a should be greater than sigma vM.
A60: (F2) ' Wtilter=
B60: (2*$B$42*$B$44+$B$43*$B$45)*$B$46*$B$13
C60: 'lbf   This is the weight of a tilter.
A61: (F2) 'Ring Pins:
A62: (F2) '      Rrp=
B62: 0.43
C62: 'in    This is the radius of ring pin.
H62: '*
A63: (F2) '      FOS=
B63: 1.5
C63: '      This is factor of safety for ring pin.
H63: '*
A65: '      Arp=
B65: @PI*$B$62^2
C65: 'in2   This is cross-sectional area of pin.
A66: '      W2=
B66: +$B$49+2*$B$60
C66: 'lbf   This is weight per pole pair with tilter.
A68: (F2) ' sigma 1=
B68: @SQRT(($B$9/(0.5*$B$11*$B$65))^2+(($B$8/(0.5*$B$11)+$B$66)/$B$65)^2
C68: 'psi   This is due to weight, thrust and normal forces.
A70: (F2) ' sigma 2=
B70: 0
C70: 'psi   This is due to normal, thrust and weight forces.
A72: (F2) ' sigma 3=
B72: 0
C72: 'psi
A74: (F2) 'sigma vM=
B74: @SQRT(0.5*(($B68-$B70)^2+($B70-$B72)^2+($B72-$B68)^2))
C74: 'psi   This is von Mises' stress.
A76: (F2) ' sigma a=
B76: +$B$6/$B$23
C76: 'psi   This is the allowable stress.
A78: (F2) 'Compare sigma vM with sigma a.  Sigma vM should be less than or equal
A79: (F2) 'to sigma a.  Adjust Rrp to change design.
A81: (F2) 'Stator Rings:
A82: (F2) '       Ro=
B82: 93.6
C82: 'in    This is stator ring outer diameter.
H82: '*
A83: (F2) '       Ri=
B83: 89.5
C83: 'in    This is stator ring inner diameter.
```

```
H83: '*
A84: (F2) '      tsr=
B84: 0.5
C84: 'in    This is the stator ring thickness.
H84: '*
A85: (F2) '      FOS=
B85: 3.75
C85: '       This is stator ring factor of safety.
H85: '*
A87: (F2) '      Asr=
B87: ($B$82-$B$83)*$B$84
C87: 'in2   This is cross sectional area of a stator ring.
A88: '     Asrc=
B88: 2*@PI*(0.5*($B$82+$B$83))*$B$84
C88: 'in2   This is circumferential area.
A89: (F2) '        V3=
B89: 0.7143*(0.25*($B$66+2*$B$8/$B$11))
C89: 'lbf   This is shear due to weight, normal forces.
A90: (F2) ' sigma b=
B90: (6*0.02137*0.5*($B$82+$B$83)*1.4*$B$89)/($B$84*($B$82-$B$83)^2)
C90: 'psi   This is due to bending.
A92: (F2) ' sigma 1=
B92: +$B$89/$B$87
C92: 'psi   This is due to V3 shear.
A94: (F2) ' sigma 2=
B94: (0.25*$B$9/$B$88)+$B$90
C94: 'psi   This is due to sigma b and thrust shear.
A96: (F2) ' sigma 3=
B96: 0
C96: 'psi
A98: (F2) 'sigma vM=
B98: @SQRT(0.5*(($B92-$B94)^2+($B94-$B96)^2+($B96-$B92)^2))
C98: 'psi   This is von Mises' stress.
A100: (F2) ' sigma a=
B100: +$B$6/$B$85
C100: 'psi   This is the allowable stress.
A101: (F2) 'Axial Beam:
A102: '      Wrp=
B102: +$B$13*($B$65*($B$46+2*$B$84))
C102: 'lbf   This is weight of a ring pin.
A103: (F2) '      Wsr=
B103: +$B$13*($B$87*2*@PI*0.5*($B$82+$B$83))
C103: 'lbf   This is weight of stator ring.
A104: (F2) '       W4=
B104: ($B$7+$B$11*($B$60+$B$102)+4*$B$103)/$B$12
C104: 'lbf   This is weight supported by each beam.
A105: (F2) '       F4=
```

```
B105: +$B$9/(4*$B$12)
C105: 'lbf   This is thrust supported by each beam.
A106: (F2) '      Fp4=
B106: +$B$104+$B$8/$B$12
C106: 'lbf   This is total normal force, including weight.
A108: (F2) '     Lbjb=
B108: 126.535
C108: 'in    This is length of axial beam.
H108: '*
A109: (F2) '     hwab=
B109: 4
C109: 'in    This is height of web.
H109: '*
A110: (F2) '      bab=
B110: 0.5
C110: 'in    This is web thickness.
H110: '*
A111: (F2) '    Wflab=
B111: 2
C111: 'in    This is flange width.
H111: '*
A112: '    tflab=
B112: 0.375
C112: 'in    This is the flange thickness.
H112: '*
A113: ' Wflmwab=
B113: 1
C113: 'in    This is mid-web flange width.
H113: '*
A114: ' tflmwab=
B114: 0.375
C114: 'in    This is mid-web flange thickness.
H114: '*
A115: '      FOS=
B115: 3.75
C115: '       This is axial beam factor of safety.
H115: '*
A117: '      Acs=
B117: +$B$109*$B$110+2*$B$111*$B$112
C117: 'in2   This is cross section less mid-web flange.
A118: '      Iab=
B118: ($B$110*$B$109^3)/12+2*(($B$111*$B$112^3)/12+$B$111*$B$112*(0.5*($B$109+$B$1

C118: 'in4   This is moment of inertia less mid-web flange.
A119: '  tau yz=
B119: (0.5*$B$106)/$B$117
C119: 'psi   This is the shear stress due to bending.
A120: 'sigma xx=
```

```
B120: (0.04125*$B$106*$B$108)*0.5*($B$109+2*$B$112)/$B$118
C120: 'psi   This is normal stress due to bending.
A121: '  tau xz=
B121: +$B$105/($B$110*$B$84)
C121: 'psi   This is shear due to twisting in the web.
A122: '  tau yz=
B122: ($B$105*2*$B$112)/($B$109*$B$84*($B$111-$B$110))
C122: 'psi   This is also shear from twisting in the web.
A124: ' sigma x=
B124: +$B$120+$B$121
C124: 'psi   This is x-directed stress in web.
A126: ' sigma y=
B126: +$B$119+$B$122
C126: 'psi   This is y-directed stress in web.
A128: ' sigma z=
B128: +$B$119+$B$121+$B$122
C128: 'psi   This is z-directed stress in web.
A130: (F2) 'sigma vM=
B130: @SQRT(0.5*(($B124-$B126)^2+($B126-$B128)^2+($B128-$B124)^2))
C130: 'psi   This is von Mises' stress FOR THE WEB ONLY.
A132: (F2) ' sigma a=
B132: +$B$6/$B$115
C132: 'psi   This is the allowable stress FOR THE WEB ONLY.
A134: '  tau xz=
B134: +$B$105/($B$111*$B$84)
C134: 'psi   This is shear due to twisting in the flange.
A135: '  tau yz=
B125: 2*$B$105/($B$84*($B$111-$B$110))
C135: 'psi   This is also shear from twisting in the flange.
A137: ' sigma x=
B137: +$B$120+$B$134
C137: 'psi   This is x-directed stress in flange.
A139: ' sigma y=
B139: +$B$119+$B$135
C139: 'psi   This is y-directed stress in flange.
A141: ' sigma z=
B141: +$B$119+$B$134+$B$135
C141: 'psi   This is z-directed stress in flange.
A143: (F2) 'sigma vM=
B143: @SQRT(0.5*(($B137-$B139)^2+($B139-$B141)^2+($B141-$B137)^2))
C143: 'psi   This is von Mises' stress FOR THE FLANGE ONLY.
A145: (F2) ' sigma a=
B145: +$B$6/$B$115
C145: 'psi   This is the allowable stress FOR FLANGE ONLY.
A147: ' sigma Q=
B147: +$B$105*(4*$B$112/(($B$111-$B$110)^2*$B$84))
C147: 'psi   This is stress in piece that reacts Q.
```

```
A149: 'sigma F4=
B149: +$B$105/($B$84*$B$112)
C149: 'psi   This is stress in piece that reacts F4.
A151: ' sigma a=
B151: +$B$6/$B$115
C151: 'psi   This is allowable stress for Q and F4 pieces.
A153: '  tau MW=
B153: +$B$106/(2*$B$113*$B$114)
C153: 'psi   This is shear in mid-web flange, normal forces.
A155: ' sigma a=
B155: +$B$6/$B$115
C155: 'psi   This is allowable stress mid-web flange.
A161: 'Torque Reactors:
A162: '     ttr=
B162: 0.5
C162: 'in    This is torque reactor width (=tsr).
H162: '*
A163: '   tfltr=
B163: 1
C163: 'in    This is piece thickness.
H163: '*
A164: '     Ltr=
B164: 12
C164: 'in    This is torque reactor length.
H164: '*
A165: '     htr=
B165: 3
C165: 'in    This is the height of the reactor.
H165: '*
A166: '     FOS=
B166: 2.25
C166: '      This is torque reactor factor of safety.*
A168: ' sigma b=
B168: +$B$106*2*$B$112/($B$162*$B$164^2)
C168: 'psi   This is bending stress in reactor.
A169: '  tau TR=
B169: +$B$106/($B$162*$B$164)
C169: 'psi   This is shear stress in reactor.
A171: ' sigma 1=
B171: +$B$168
C171: 'psi
A173: ' sigma 2=
B173: +$B$169
C173: 'psi
A175: ' sigma 3=
B175: 0
C175: 'psi
```

```
A177: 'sigma vM=
B177: @SQRT(0.5*(($B171-$B173)^2+($B173-$B175)^2+($B175-$B171)^2))
C177: 'psi   This is von Mises' stress.
A179: ' sigma a=
B179: +$B$6/$B$166
C179: 'psi   This is the allowable stress for the reactor.
A181: 'Pieces:
A182: '      FOS=
B182: 3.75
C182: '        This is factor of safety for cutouts.
H182: '*
A184: 'sigma sr=
B184: 12*$B$105*$B$112/($B$84*(0.5*($B$82-$B$83)-$B$112)^2)
C184: 'psi   This is the stress in the stator ring piece.
A186: ' sigma a=
B186: +$B$6/$B$182
C186: 'psi   This is the allowable stress.
A188: 'sigma sr=
B188: 12*$B$105*$B$112/($B$162*$B$163^2)
C188: 'psi   This is the stress in the torque reactor piece.
A190: ' sigma a=
B190: +$B$6/$B$182
C190: 'psi   This is the allowable stress.
A201: 'Geometric Compatibility:
B203: 2*$B$22
C203: 'in   <=
D203: +$B$44/3
E203: 'in  This relates core pin thickness
E204: '    to tilter arm width.
B206: 2*$B$62
C206: 'in   <=
D206: +$B$45/3
E206: 'in  This relates ring pin thickness
E207: '    to tilter base width.
B209: 2*$B$62
C209: 'in   <=
D209: 0.25*($B$82-$B$83)
E209: 'in  This relates ring pin thickness
E210: '    to stator ring height.
B212: +$B$45+$B$112
C212: 'in   <=
D212: [illegible]5*($B$82-$B$83)
E212: 'in  This relates axial beam flange
E213: '    ard tilter base width to stator
E214: '    ring height.
B216: +$B$112
C216: 'in   <=
```

```
D216: 0.25*($B$82-$B$83)
E216: 'in  This relates axial beam flange
E217: '    thickness to stator ring height.
B219: +$B$163+$B$114+0.5*(0.5*($B$82-$B$83)-$B$112)
C219: 'in   <=
D219: +$B$109
E219: 'in  This relates the thicknesses
E220: '    of the stator ring pieces,
E221: '    mid-web flange thickness, and
E222: '    axial beam flange thickness.
B224: +$B$165-$B$163
C224: 'in   >=
D224: +$B$112
E224: 'in  This relates the height of the
E225: '    torque reactor to the axial beam
E226: '    flange thickness.
```

1.19 Figure 4 - Arrangement Drawings, Deck Plans

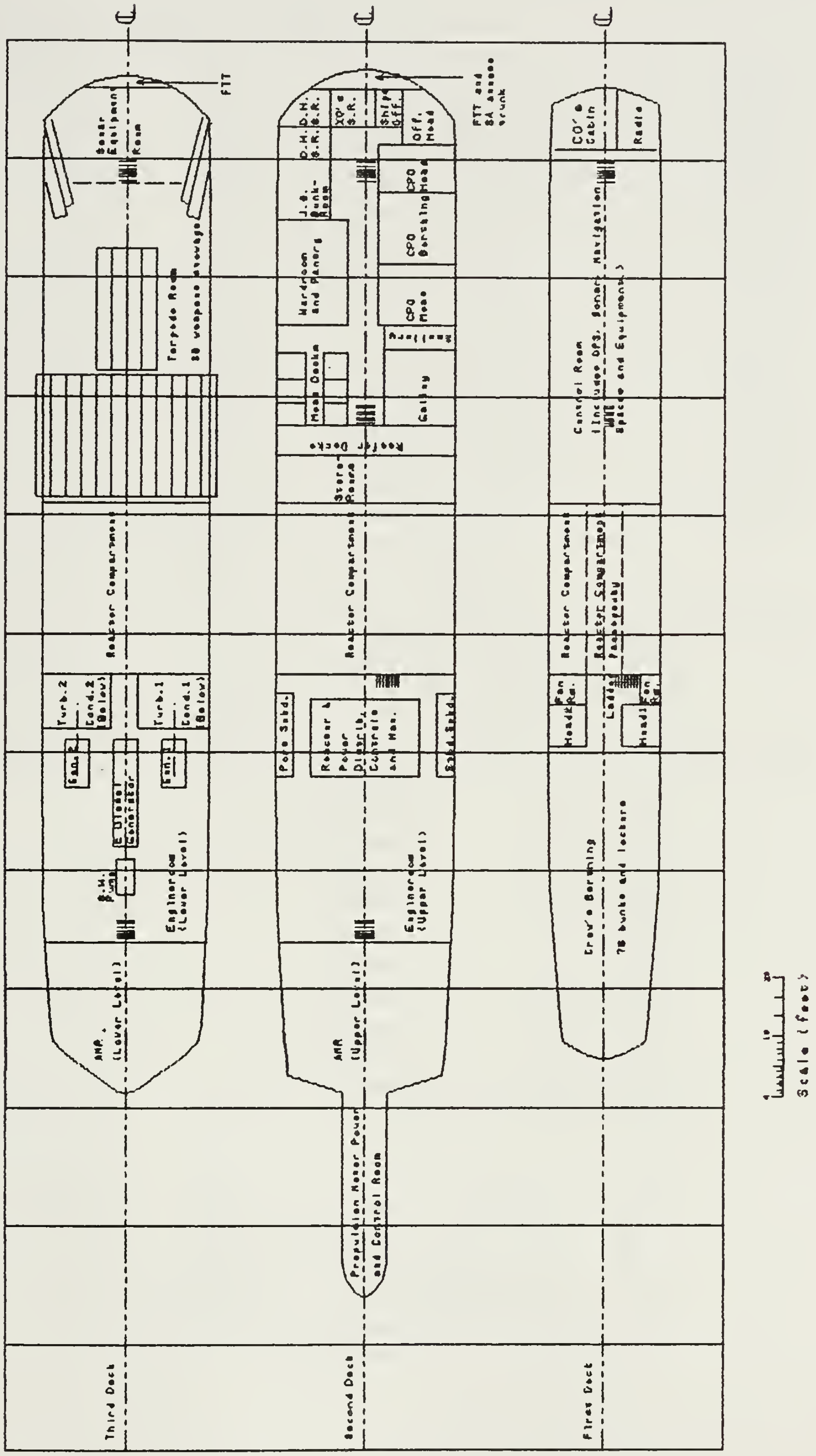

1.20 Table 16 - Weight Report and Weight Balancing Calculations

```
Thesis                                                         John V. A
Baseline Design - Weight Balance                               17 Januar
All weights are assumed to be in long tons.
WEIGHT SUMMARY:       VCG                 LCG                   % of A-1
 Group 1= 1687.10 15.96750 ft + base137.6334 ft - FP  0.470213
 Group 2=  786.96     13.40 ft + base  156.95 ft - FP  0.219334
 Group 3=  236.90     10.61 ft + base  149.04 ft - FP  0.066027
 Group 4=  219.89     20.35 ft + base   75.82 ft - FP  0.061284
 Group 5=  421.27     15.60 ft + base  209.85 ft - FP  0.117412
 Group 6=  130.83     20.59 ft + base  123.84 ft - FP  0.036463
 Group 7=  105.00     13.00 ft + base   68.00 ft - FP  0.029264
 Cond A1= 3587.95 15.35709 ft + base144.7744 ft - FP         1
    Lead=  358.80      13.3 ft + base101.1421 ft - FP  0.100001
  Cond A= 3946.75 15.17008 ft + base140.8077 ft - FP  1.100001
Var Load=  274.37 8.862505 ft + base109.3004 ft - FP  0.076469
     NSC= 4221.12 14.76009 ft + base138.7598 ft - FP  1.176471
     MBT=  527.63        16 ft + base124.7595 ft - FP  0.147055
   /\sub= 4748.75 14.89786 ft + base137.2042 ft - FP  1.323527
      FF=  357.43 16.11768 ft + base56.93094 ft - FP  0.099620
   /\env= 5106.18 14.98325 ft + base133.6851 ft - FP  1.423147
GROUP 1:  WEIGHT      VCG                 LCG
     Wep= 448.784    16.000 ft + base 135.860 ft - FP  1" over a
    Wphp= 333.102    16.000 ft + base 154.540 ft - FP  ph plate-
     Wfr= 186.671    16.000 ft + base 148.074 ft - FP
     Wkf=  17.910    16.000 ft + base 142.000 ft - FP
     Wbh= 148.952    15.632 ft + base 145.276 ft - FP
    Wrem= 551.682    16.000 ft + base 123.130 ft - FP  phull lcb
                            ft + base         ft - FP
                            ft + base         ft - FP
                            ft + base         ft - FP
                            ft + base         ft - FP
                            ft + base         ft - FP
                            ft + base         ft - FP
                            ft + base         ft - FP
                            ft + base         ft - FP
                            ft + base         ft - FP
                            ft + base         ft - FP
                            ft + base         ft - FP
      W1=1687.101    15.968 ft + base 137.633 ft - FP

GROUP 2:  WEIGHT      VCG                 LCG
     Wrx= 392.890    14.667 ft + base 141.250 ft - FP
   Wshld= 238.120    11.000 ft + base 141.250 ft - FP
    Waux=  66.670    11.000 ft + base 175.000 ft - FP
    Wmtr=  84.010    16.000 ft + base 254.230 ft - FP
   Wprop=   5.270    16.000 ft + base 257.870 ft - FP
                            ft + base         ft - FP
```

```
                           ft + base         ft - FP
                           ft + base         ft - FP
                           ft + base         ft - FP
                           ft + base         ft - FP
                           ft + base         ft - FP
                           ft + base         ft - FP
                           ft + base         ft - FP
                           ft + base         ft - FP
                           ft + base         ft - FP
                           ft + base         ft - FP
                           ft + base         ft - FP
      W2= 786.960   13.398 ft + base 156.951 ft - FP

GROUP 3:  WEIGHT     VCG               LCG
    Wbat=  61.622     4.000 ft + base 111.500 ft - FP
    Wtur=  69.210    12.000 ft + base 160.250 ft - FP
    Wgen=  44.930    12.000 ft + base 171.750 ft - FP
   Wegen=  20.000    12.000 ft + base 177.500 ft - FP
    Wdis=  41.140    16.000 ft + base 147.800 ft - FP
                           ft + base         ft - FP
                           ft + base         ft - FP
                           ft + base         ft - FP
                           ft + base         ft - FP
                           ft + base         ft - FP
                           ft + base         ft - FP
                           ft + base         ft - FP
                           ft + base         ft - FP
                           ft + base         ft - FP
                           ft + base         ft - FP
                           ft + base         ft - FP
                           ft + base         ft - FP
      W3= 236.902   10.614 ft + base 149.045 ft - FP

GROUP 4:  WEIGHT     VCG               LCG
     Wll=  57.873    11.500 ft + base  64.000 ft - FP
     Wsa=  27.612    16.000 ft + base  13.500 ft - FP
     Wfc=   5.511    14.500 ft + base  34.460 ft - FP
     Wul= 128.889    25.500 ft + base  96.250 ft - FP
                           ft + base         ft - FP
                           ft + base         ft - FP
                           ft + base         ft - FP
                           ft + base         ft - FP
                           ft + base         ft - FP
                           ft + base         ft - FP
                           ft + base         ft - FP
                           ft + base         ft - FP
                           ft + base         ft - FP
```

```
                           ft + base         ft - FP
                           ft + base         ft - FP
                           ft + base         ft - FP
                           ft + base         ft - FP
      W4= 219.885   20.347 ft + base  75.822 ft - FP

GROUP 5:  WEIGHT     VCG               LCG
    Wpfr=  13.354   25.500 ft + base 157.750 ft - FP
    Wsft=   8.340   25.500 ft + base 157.750 ft - FP
    Wedg=  30.037   10.500 ft + base 178.000 ft - FP
    Wll1=  46.340   11.500 ft + base 221.000 ft - FP
    Wll2= 115.639   11.500 ft + base 211.500 ft - FP
     Wul= 207.560   18.500 ft + base 216.500 ft - FP
                           ft + base         ft - FP
                           ft + base         ft - FP
                           ft + base         ft - FP
                           ft + base         ft - FP
                           ft + base         ft - FP
                           ft + base         ft - FP
                           ft + base         ft - FP
                           ft + base         ft - FP
                           ft + base         ft - FP
                           ft + base         ft - FP
                           ft + base         ft - FP
      W5= 421.270   15.599 ft + base 209.852 ft - FP

GROUP 6:  WEIGHT     VCG               LCG
     Wd2=  82.470   18.000 ft + base  93.750 ft - FP
     Wd1=  43.583   25.000 ft + base 187.500 ft - FP
     Wco=   4.777   25.000 ft + base  62.500 ft - FP
                           ft + base         ft - FP
                           ft + base         ft - FP
                           ft + base         ft - FP
                           ft + base         ft - FP
                           ft + base         ft - FP
                           ft + base         ft - FP
                           ft + base         ft - FP
                           ft + base         ft - FP
                           ft + base         ft - FP
                           ft + base         ft - FP
                           ft + base         ft - FP
                           ft + base         ft - FP
                           ft + base         ft - FP
                           ft + base         ft - FP
      W6= 130.830   20.587 ft + base 123.840 ft - FP

GROUP 7:  WEIGHT     VCG               LCG
```

```
    Wtt= 105.000   13.000 ft + base  68.000 ft - FP
                          ft + base         ft - FP
                          ft + base         ft - FP
                          ft + base         ft - FP
                          ft + base         ft - FP
                          ft + base         ft - FP
                          ft + base         ft - FP
                          ft + base         ft - FP
                          ft + base         ft - FP
                          ft + base         ft - FP
                          ft + base         ft - FP
                          ft + base         ft - FP
                          ft + base         ft - FP
                          ft + base         ft - FP
                          ft + base         ft - FP
                          ft + base         ft - FP
                          ft + base         ft - FP
     W7= 105.000   13.000 ft + base  68.000 ft - FP

LEAD:     WEIGHT     VCG               LCG
   STAB= 107.640    7.000 ft + base  17.000 ft - FP
    MAR= 251.160   16.000 ft + base 137.203 ft - FP
                          ft + base         ft - FP
                          ft + base         ft - FP
                          ft + base         ft - FP
                          ft + base         ft - FP
                          ft + base         ft - FP
                          ft + base         ft - FP
                          ft + base         ft - FP
                          ft + base         ft - FP
                          ft + base         ft - FP
                          ft + base         ft - FP
                          ft + base         ft - FP
                          ft + base         ft - FP
                          ft + base         ft - FP
                          ft + base         ft - FP
                          ft + base         ft - FP
   LEAD= 358.800   13.300 ft + base 101.142 ft - FP

VAR. LD.: WEIGHT     VCG               LCG
   Wrfw=  33.748    4.000 ft + base 156.500 ft - FP  *SUBLAB d
  Wprov=  17.834   18.500 ft + base 117.000 ft - FP  *SUBLAB d
  Wstor=  12.621   18.500 ft + base 123.500 ft - FP  *SUBLAB d
    Wfo=  55.697    4.000 ft + base  70.000 ft - FP  *SUBLAB d
  Wtorp=  31.004    9.000 ft + base 110.267 ft - FP  *SUBLAB d
  Wvbal=  49.935    4.000 ft + base  90.000 ft - FP  This from
   Wrmw=  11.798   16.000 ft + base 124.760 ft - FP  Adjust LC
```

```
     Wpw=  12.072    4.000 ft + base  80.000 ft - FP  *SUBLAB d
    Wrem=  49.661   16.000 ft + base 137.182 ft - FP  Adjust th
                           ft + base         ft - FP
                           ft + base         ft - FP
                           ft + base         ft - FP
                           ft + base         ft - FP
                           ft + base         ft - FP
                           ft + base         ft - FP
                           ft + base         ft - FP
                           ft + base         ft - FP
          274.370    8.863 ft + base 109.300 ft - FP

MBT:      WEIGHT     VCG                 LCG
  MBTfwd= 275.794   16.000 ft + base  30.851 ft - FP
  MBTaft= 251.835   16.000 ft + base 227.602 ft - FP
                           ft + base         ft - FP
                           ft + base         ft - FP
                           ft + base         ft - FP
                           ft + base         ft - FP
                           ft + base         ft - FP
                           ft + base         ft - FP
                           ft + base         ft - FP
                           ft + base         ft - FP
                           ft + base         ft - FP
                           ft + base         ft - FP
                           ft + base         ft - FP
                           ft + base         ft - FP
                           ft + base         ft - FP
                           ft + base         ft - FP
                           ft + base         ft - FP
     MBT= 527.629   16.000 ft + base 124.760 ft - FP

FREE FLD: WEIGHT     VCG                 LCG
   Wfwd1= 141.487   16.000 ft + base  13.820 ft - FP
     Wmt=  82.381   16.000 ft + base 273.641 ft - FP
     Weh=   2.901   30.500 ft + base 149.125 ft - FP
   Wfwd2= 130.664   16.000 ft + base  47.000 ft - FP
                           ft + base         ft - FP
                           ft + base         ft - FP
                           ft + base         ft - FP
                           ft + base         ft - FP
                           ft + base         ft - FP
                           ft + base         ft - FP
                           ft + base         ft - FP
                           ft + base         ft - FP
                           ft + base         ft - FP
                           ft + base         ft - FP
```

```
                          ft + base          ft - FP
                          ft + base          ft - FP
                          ft + base          ft - FP
    FF= 357.433   16.118 ft + base  86.931 ft - FP


A1: 'Thesis
G1: 'John V. Amy Jr.
A2: 'Baseline Design - Weight Balance
G2: "17 January 1990
A3: 'All weights are assumed to be in long tons.
A4: 'WEIGHT SUMMARY:
C4: '    VCG
E4: '    LCG
G4: ' % of A-1
A5: ' Group 1=
B5: (F2) +$B$39
C5: +$C$39
D5: 'ft + base
E5: +$E$39
F5: 'ft - FP
G5: +$B5/$B$12
A6: ' Group 2=
B6: (F2) +$B$59
C6: (F2) +$C$59
D6: 'ft + base
E6: (F2) +$E$59
F6: 'ft - FP
G6: +$B6/$B$12
A7: ' Group 3=
B7: (F2) +$B$79
C7: (F2) +$C$79
D7: 'ft + base
E7: (F2) +$E$79
F7: 'ft - FP
G7: +$B7/$B$12
A8: ' Group 4=
B8: (F2) +$B$99
C8: (F2) +$C$99
D8: 'ft + base
E8: (F2) +$E$99
F8: 'ft - FP
G8: +$B8/$B$12
A9: ' Group 5=
B9: (F2) +$B$119
C9: (F2) +$C$119
D9: 'ft + base
```

```
E9: (F2) +$E$119
F9: 'ft - FP
G9: +$B9/$B$12
A10: ' Group 6=
B10: (F2) +$B$139
C10: (F2) +$C$139
D10: 'ft + base
E10: (F2) +$E$139
F10: 'ft - FP
G10: +$B10/$B$12
A11: ' Group 7=
B11: (F2) +$B$159
C11: (F2) +$C$159
D11: 'ft + base
E11: (F2) +$E$159
F11: 'ft - FP
G11: +$B11/$B$12
A12: ' Cond A1=
B12: (F2) @SUM($B$5..$B$11)
C12: ($B$5*$C$5+$B$6*$C$6+$B$7*$C$7+$B$8*$C$8+$B$9*$C$9+$B$10*$C$10+$B$11*$C$11)/$

D12: 'ft + base
E12: ($B$5*$E$5+$B$6*$E$6+$B$7*$E$7+$B$8*$E$8+$B$9*$E$9+$B$10*$E$10+$B$11*$E$11)/$

F12: 'ft - FP
G12: +$B12/$B$12
A13: '    Lead=
B13: (F2) +$B$179
C13: +$C$179
D13: 'ft + base
E13: +$E$179
F13: 'ft - FP
G13: +$B13/$B$12
A14: '  Cond A=
B14: (F2) +$B$12+$B$13
C14: ($B$12*$C$12+$B$13*$C$13)/$B$14
D14: 'ft + base
E14: ($B$12*$E$12+$B$13*$E$13)/$B$14
F14: 'ft - FP
G14: +$B14/$B$12
A15: 'Var Load=
B15: (F2) +$B$199
C15: +$C$199
D15: 'ft + base
E15: +$E$199
F15: 'ft - FP
G15: +$B15/$B$12
A16: '     NSC=
B16: (F2) +$B$14+$B$15
```

```
C16: ($B$14*$C$14+$B$15*$C$15)/$B$16
D16: 'ft + base
E16: ($B$14*$E$14+$B$15*$E$15)/$B$16
F16: 'ft - FP
G16: +$B16/$B$12
A17: '      MBT=
B17: (F2) +$B$219
C17: +$C$219
D17: 'ft + base
E17: +$E$219
F17: 'ft - FP
G17: +$B17/$B$12
A18: '   /\sub=
B18: (F2) +$B16+$B$17
C18: ($3$16*$C$16+$B$17*$C$17)/$B$18
D18: 'ft + base
E18: ($B$16*$E$16+$B$17*$E$17)/$B$18
F18: 'ft - FP
G18: +$B18/$B$12
A19: '       FF=
B19: (F2) +$B$239
C19: +$C$239
D19: 'ft + base
E19: +$E$239
F19: 'ft - FP
G19: +$B19/$B$12
A20: '   /\env=
B20: (F2) +$B$18+$B$19
C20: ($B$18*$C$18+$B$19*$C$19)/$B$20
D20: 'ft + base
E20: ($B$18*$E$18+$B$19*$E$19)/$B$20
F20: 'ft - FP
G20: +$B20/$B$12
A21: 'GROUP 1:
B21: ' WEIGHT
C21: '   VCG
E21: '   LCG
A22: '      Wep=
B22: (F3) 448.784
C22: (F3) 16
D22: 'ft + base
E22: (F3) 135.86
F22: 'ft - FP
G22: "1" over all env
A23: '     Wphp=
B23: (F3) 333.102
C23: (F3) 16
```

```
D23: 'ft + base
E23: (F3) 154.54
F23: 'ft - FP
G23: 'ph plate-env
A24: '      Wfr=
B24: (F3) 186.671
C24: (F3) 16
D24: 'ft + base
E24: (F3) 148.074
F24: 'ft - FP
A25: '      Wkf=
B25: (F3) 17.91
C25: (F3) 16
D25: 'ft + base
E25: (F3) 142
F25: 'ft - FP
A26: '      wbh=
B26: (F3) 148.952
C26: (F3) 15.632
D26: 'ft + base
E26: (F3) 145.276
F26: 'ft - FP
A27: '     Wrem=
B27: (F3) 551.682
C27: (F3) 16
D27: 'ft + base
E27: (F3) 123.13
F27: 'ft - FP
G27: 'phull lcb
D28: 'ft + base
F28: 'ft - FP
D29: 'ft + base
F29: 'ft - FP
D30: 'ft + base
F30: 'ft - FP
D31: 'ft + base
F31: 'ft - FP
D32: 'ft + base
F32: 'ft - FP
D33: 'ft + base
F33: 'ft - FP
D34: 'ft + base
F34: 'ft - FP
D35: 'ft + base
F35: 'ft - FP
D36: 'ft + base
F36: 'ft - FP
```

```
D37: 'ft + base
F37: 'ft - FP
D38: 'ft + base
F38: 'ft - FP
A39: '        W1=
B39: (F3) @SUM($B22..$B38)
C39: (F3) +$I39/$B39
D39: 'ft + base
E39: (F3) +$J39/$B39
F39: 'ft - FP
```

1.21 Figure 5 - Inboard Profile, Showing Some External Features

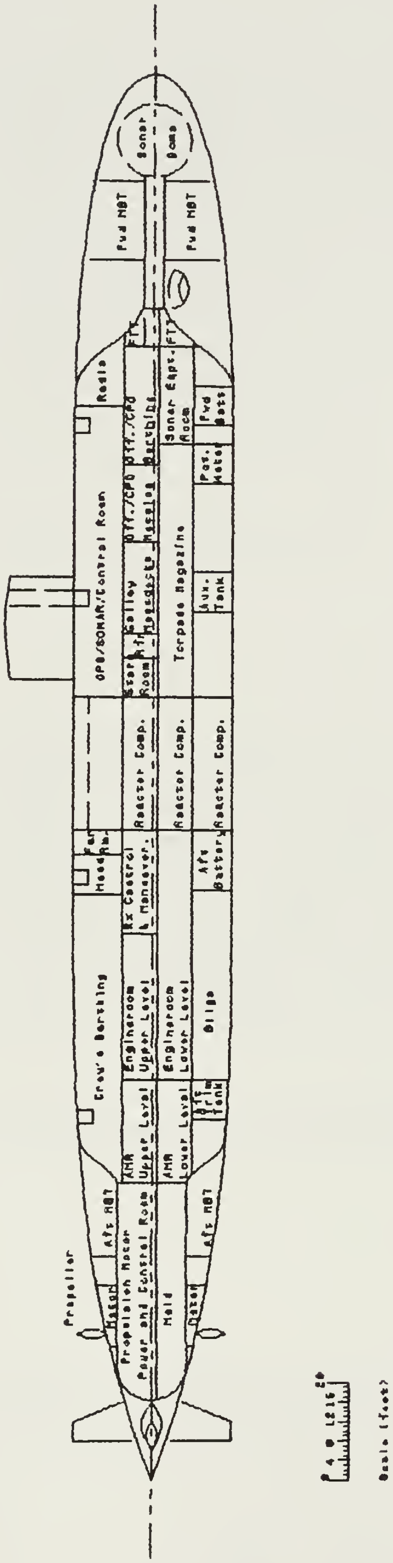

1.22 Table 17 - MBT Size and Location Calculations, Refined Solution

```
Thesis                                                 John V. Amy Jr.
MBT Calculations                                       06 January 1990

AFT MBT:
    Laft=   242.5 ft   This is location of aft bulkhead.   *
    Daft=23.96389 ft   This is diameter at aft bulkhead.
     Lap=    45.5 ft   This is length of aft paraboloid.
    \/ap=10945.52 ft3  This is volume of aft paraboloid.
   LCGap=256.7187 ft   This is LCG of aft paraboloid.
     Lac=    15.5 ft   This is length of aft cylinder.
    \/ac=2386.039 ft3  This is volume of aft cylinder.
   LCGac=  234.75 ft   This is LCG of aft cylinder.
 \/trans=    3473 ft3  This is volume of transition.       *
LCGtrans=  221.46 ft   This is LCG of transition.          *
    \/fp=25618.78 ft3  This is volume of large aft paraboloid.  *
   LCGfp= 239.875 ft   This is LCG of large aft paraboloid.*

   \/aft=8814.219 ft3  This is volume of aft MBT.
  LCGaft=227.6016 ft   This is LCG of aft MBT.



FWD MBT:
    Lfwd=      22 ft   This is location of fwd bulkhead.       *
    Laft=  38.244 ft   This is location of aft bulkhead.       *
    Dfwd=24.17433 ft   This is diameter at fwd bulkhead.
    Daft=26.78228 ft   This is diameter at aft bulkhead.
   \/lps=16588.69 ft3  This is volume of large prolate spheroid.
  LCGlps= 23.9025 ft   This is LCG of large prolate spheroid.
   \/sps=6731.789 ft3  This is volume of small prolate spheroid.
  LCGsps=   13.75 ft   This is LCG of small prolate spheroid.
    \/fc=204.1281 ft3  This is volume of forward cylinder.
   LCGfc=  30.122 ft   This is LCG of forward cylinder.

   \/fwd=9652.782 ft3  This is volume of forward MBT.
  LCGfwd=30.85126 ft   This is LCG of forward MBT.



MBT BALANCE:
   \/req= 17203.8 ft3  This is required volume of all MBT.    *
  LCGreq=  130.82 ft   This is required LCG of all MBT.       *
```

```
 \/mbt=18467.00 ft3  This is calculated MBT volume.
LCGmbt=124.7593 ft   This is calculated MBT LCG.

%   \/=7.342573      This is percent error in volume.
%  LCG=-4.63279      This is percent error in LCG.
```

B Comparative Acoustic Analysis Calculations

2.1 OTHEP

2.1.1 OTHEP Sources

Based on the description of the OTHEP propulsion system in section 5.2.1, the sources listed below will cause the vibrations leading to radiated noise.

2.1.1.1 Rotor Source

In the instance of OTHEP, the rotor is not rigidly connected to the stator, or to a motor casing as in conventional geometry electric motors. Instead, rotor vibrations are transmitted to that portion of the hull contiguous with the propeller hub. This portion of the hull then radiates into the sea-water. Hence, the rotor and its mounting to the propeller hub structure will act as an acoustic source with a path separate from the rest of the equipment which is rigidly connected to the pressure hull.

It is a simplification to say that equilibrium of forces requires that the forces which act on the stator are the forces that act on the rotor, only in the opposite direction. Hence, the total source level for an electric motor will be equally divided between the rotor and the stator in this instance, recognizing that this is quite a simplification.

Whereas the rotor is outside of the pressure hull, only structureborne noise will be considered. The structureborne source level for the rotor is given by the table shown below. The values in the table are taken from Table 3 of section 4.2.4. The values are adjusted to reflect the rotor source level by subtracting 6dB from the values in that table. For acceleration levels, subtracting 6dB corresponds to halving the magnitude of the acceleration.

Table 1 - Propulsion Motor Rotor
Structureborne Noise Source Levels
(in dB re 10^{-3} cm/s^2)

Octave Band Center Frequency (Hz)

31.5	63	125	250	500	1000	2000	4000	8000
8	55	68	83	98	105	138	131	0

2.1.1.2 Stator Source

Since the stator is also outside of the pressure hull, only the structureborne noise source levels of the stator will be considered. The same method as used for the rotor in the preceeding section is used here for the stator. Whereas the rotor is mounted to the propeller hub and is considered separately from the rest of the submarine, the stator is connected to the pressure hull and its interaction with the hull must be considered.

Table 1 – Propulsion Motor Stator
Structureborne Source Noise Levels
(in dB re 10^{-3} cm/s^2)

Octave Band Center Frequency (Hz)

31.5	63	125	250	500	1000	2000	4000	8000
8	55	68	83	98	105	138	131	0

2.1.1.3 Generator Steam Turbine Sources

The equation below shows the baseline airborne noise source level radiated by the steam turbine which drives the generator. This equation is taken from equation 4.3.1.3.1.

$$L_{WBturbine} = 60 + 10\log(27{,}000kW) = 104.3 \quad dB \ \ re \ \ 10^{-12}W \qquad \#1$$

There are two such 27MW turbine-generators in the plant. Hence, this source level applies to each turbine-generator. The octave band adjustments to this baseline airborne source level are taken from Table 1 of section 4.3.1.3. The table shown below provides the octave band airborne source levels for the turbines. Note, a static exciter is assumed for the generator.

Table 1 – Turbine Generator
Airborne Noise Source Levels
(in dB re 10^{-12} W)

Octave Band Center Frequency (Hz)

31.5	63	125	250	500	1000	2000	4000	8000
106	111	112	116	114	114	115	110	109

As discussed in section 4.3.1.3, the structureborne source level for the turbine generators is dominated by the generator itself. See the following section.

2.1.1.4 Generator Sources

The equation below shows the baseline airborne noise source level radiated by the generators. This equation is taken from equation 4.3.1.5.1.1.

$$L_{WBgen}=34+10\log(27{,}000kW)+7\log(3600rpm)=103.2 \quad dB \ re \ 10^{-12}W \qquad \#1$$

The octave band adjustments to this baseline airborne source level are taken from Table 1 of section 4.3.1.5.1. The table shown below provides the octave band airborne source levels for the generator.

Table 1 - Generator
Airborne Noise Source Levels
(in dB re 10^{-12} W)

Octave Band Center Frequency (Hz)

31.5	63	125	250	500	1000	2000	4000	8000
111	114	115	116	116	113	111	108	103

The equation below shows the baseline structureborne noise source level radiated by the generator. This equation is taken from equation 4.3.1.5.1.2.

$$L_{aBgen}=42+10\log(27{,}000kW)+7\log(3600rpm)=111.2 \quad dB \ re \ 10^{-3}\frac{cm}{s^2} \qquad \#2$$

The octave band adjustments to this baseline structureborne source level are taken from Table 2 of section 4.3.1.5.1. The table shown below provides the octave band structureborne source levels for the generator.

Table 2 - Generator
Structureborne Noise Source Levels
(in dB re 10^{-3} cm/s^2)

Octave Band Center Frequency (Hz)

31.5	63	125	250	500	1000	2000	4000	8000
111	122	125	125	127	128	129	129	129

2.1.1.5 Sea-Water Cooling/Lubrication Pump

The equation below shows the baseline airborne noise source level radiated by the sea-water cooling/lubrication pump. This equation is taken from equation 4.3.1.4.1.

$$L_{WBpump}=15+10\log(187.7HP)+15\log(1200rpm)=83.9 \quad dB \ \ re \ \ 10^{-12}W \qquad \#1$$

The octave band adjustments to this baseline airborne source level are taken from Table 1 of section 4.3.1.4. The table shown below provides the octave band airborne source levels for the pump. A centrifugal pump is assumed.

Table 1 - Sea-Water Cooling/Lubrication Pump
Airborne Noise Source Levels
(in dB re 10^{-12} W)

Octave Band Center Frequency (Hz)

31.5	63	125	250	500	1000	2000	4000	8000
109	109	110	110	111	113	110	107	102

The equation below shows the baseline structureborne noise source level radiated by the sea-water cooling/lubrication pump. This equation is taken from equation 4.3.1.4.2.

$$L_{aBpump}=60+10\log(187.7HP)=82.7 \quad dB \ \ re \ \ 10^{-3}\frac{cm}{s^2} \qquad \#2$$

The octave band adjustments to this baseline structureborne source level are taken from Table 2 of section 4.3.1.4. The table shown below provides the octave band structureborne source levels for the sea-water cooling/lubrication pump.

Table 2 - Sea-Water Cooling/Lubrication Pump
Structureborne Noise Source Levels
(in dB re 10^{-3} cm/s^2)

Octave Band Center Frequency (Hz)

31.5	63	125	250	500	1000	2000	4000	8000
83	91	104	102	106	107	103	107	106

The equation below shows the baseline airborne noise source level radiated by the sea-water cooling/lubrication

pump drive motor. An induction motor is assumed to be the pump's drive motor. This equation is taken from equation 4.3.1.5.2.1.

$$L_{WBdmtr}=5+13\log(187.7HP)+15\log(1200rpm)=80.8 \quad dB\ re\ 10^{-12}W \qquad \#3$$

The octave band adjustments to this baseline airborne source level are taken from Table 1 of section 4.3.1.5.2. The table shown below provides the octave band airborne source levels for the pump drive motor.

Table 3 - Sea-Water Cooling/Lubrication Pump Drive Motor
Airborne Noise Source Levels
(in dB re 10^{-12} W)

Octave Band Center Frequency (Hz)

31.5	63	125	250	500	1000	2000	4000	8000
76	77	81	85	86	86	85	79	72

The structureborne noise source level for electric motors are taken from Table 2 of section 4.3.1.5.2. The table shown below provides the octave band structureborne source levels for the sea-water cooling/lubrication pump drive motor.

Table 4 - Sea-Water Cooling/Lubrication Pump Drive Motor
Structureborne Noise Source Levels
(in dB re 10^{-3} cm/s^2)

Octave Band Center Frequency (Hz)

31.5	63	125	250	500	1000	2000	4000	8000
92	92	92	92	92	92	92	92	92

Whereas the pump and its drive motor are essentially a single unit and will be mounted as a single unit, the source level of the entire unit will be the "logarithmic sum" of the source levels of the pump and its drive motor. The "logarithmic sum" refers to the computation involved in combining source levels that are given in decibels. For example, the combined acceleration level of a 12dB source and a 15dB source is not 27dB. Rather, the magnitude of the two accelerations must be added, then the logarithm of that sum multiplied by 20 will yield the correct acceleration level, 19.7dB. This combination of accelerations followed by the

computation of the acceleration level in decibels of the combined accelerations will be refered to as "logarithmic addition." The tables below show the airborne and structure-borne noise source levels for the complete pump unit.

Table 5 - Sea-Water Cooling/Lubrication Pump Unit
Airborne Noise Source Levels
(in dB re 10^{-12} W)

Octave Band Center Frequency (Hz)

31.5	63	125	250	500	1000	2000	4000	8000
109	109	110	110	111	113	110	107	101

Table 6 - Sea-Water Cooling/Lubrication Pump Unit
Structureborne Noise Source Levels
(in dB re 10^{-3} cm/s^2)

Octave Band Center Frequency (Hz)

31.5	63	125	250	500	1000	2000	4000	8000
95	97	106	104	107	108	105	108	107

2.1.2 OTHEP Paths

2.1.2.1 Structureborne Noise Excited by Airborne Noise

The airborne noise within the engineroom can excite vibrations in the hull. Hence, the sound pressure level within the engineroom must be computed. This requires two calculations. First, the "room constant" must be calculated in accordance with section 7.2.2 of reference [7]. Second, the sound pressure level within the space, due to the equipment operating within the space, must be calculated.

Based on the arrangement drawings of the baseline submarine and the methods of section 7.2.2 of reference [7], the room constant for the baseline submarine's main engineroom is shown in the table below. No acoustic damping materials will be considered in the comparative analysis.

Table 1 - OTHEP Engineroom Room Constants - R
(in ft^2)

Octave Band Center Frequency (Hz)

31.5	63	125	250	500	1000	2000	4000	8000
1163	1300	1265	1060	1026	1060	1060	923	787

The next step is to calculate the reverberant sound pressure level in the space. Note, direct field sound pressure levels will not be computed. Only the revereberant field will be computed. To find the reverberant sound pressure level, the equation below must be used. The equation is taken from reference [7] section 7.2.2.

$$L_p = L_W - 10\log(R) + 16 \quad dB\ re\ 20\mu Pa \qquad \#1$$

In this expression, L_p represents the reverberant sound pressure level. L_w represents the sound power level which is the "logarithmic sum" of all of the airborne noise sources in the space. R represents the room constant. The table below shows the resultant sound power level due to the turbines, generators and sea-water cooling/lubrication pump located in the baseline submarine's engineroom.

Table 2 - OTHEP Engineroom Reverberant
Sound Power Levels, L_w
(in dB re 10^{-12}W)

Octave Band Center Frequency (Hz)

31.5	63	125	250	500	1000	2000	4000	8000
116	119	120	123	122	121	120	116	114

These values for L_w and the values for R in Table 1 are substituted into equation 1 to yield the sound pressure levels shown in the table below.

Table 3 - OTHEP Engineroom Reverberant
Sound Pressure Levels, L_P
(in dB re 20 microPa)

Octave Band Center Frequency (Hz)

31.5	63	125	250	500	1000	2000	4000	8000
102	104	105	108	108	106	106	102	101

Knowing the reverberant sound pressure level, L_P, permits calculation of the structural vibrations excited by the airborne noise. First, though, the transfer function described in section 4.3.2.2 must be calculated. In this instance, the pressure hull is the structure being excited into vibration. Hence, it is a "wetted" structure.

The area of a panel is taken to be a square whose side equals the pressure hull frame spacing, 2.5ft in this case (Appendix A). Hence, the area of a panel, A_p, is 6.25ft^2. The panel length to width ratio, a, is 1 in this case. Equation 4.3.2.2.3 provides the transfer function for wetted steel using the panel characteristics listed here. The table below shows the transfer function.

Table 4 - OTHEP Engineroom Airborne-to-Structureborne
Transfer Function (in dB)

Octave Band Center Frequency (Hz)

31.5	63	125	250	500	1000	2000	4000	8000
-47	-43	-39	-36	-32	-29	-26	-22	-19

From the reverberant sound pressure level and the transfer function, the excited structural vibration level can be calculated.

$$L_{aex} = L_p + TF \quad dB \ re \ 10^{-3}\frac{cm}{s^2} \qquad \#2$$

Using the relationship in equation 2, the table shown below is the acceleration level in the pressure hull due to airborne noise-excited vibrations.

Table 5 - OTHEP Engineroom Airborne Noise-Excited
Structureborne Noise Levels
(in dB re $10^{-3} cm/s^2$)

Octave Band Center Frequency (Hz)

31.5	63	125	250	500	1000	2000	4000	8000
55	61	66	73	75	78	80	80	81

These structureborne noise levels must be included as if they were noise generated by a separate source.

2.1.2.2 Rotor Source Structureborne Noise

From the rotor configuration described in Chapter 3, the precise mounting of the rotor core to the rotor structure has not been described. Hence, hard mounting, low frequency isolation mounting and high frequency isolation mounting will be considered. It seems most likely, though, that hard mounting would be implemented in light of the canned-rotor solution to the sea-water protection problem.

Furthermore, the rotor structure is both the foundation and the hull structure as far as the rotor structureborne noise source is concerned. Hence, the vibration level at the top of the rotor foundation will be taken as the vibration level for the radiating panels. This implies that the foundation transfer function will not be used, $TF_{foundation} = 0dB$.

The rotor qualifies as a Class III (over 10,000lbs) piece of machinery. The rotor structure would qualify as a Type B foundation. The vibration levels in the rotor's portion of hull are calculated using the structureborne noise source levels in section B.2.1.1.1 and the machinery attachment transfer functions from section 4.3.2.1.1.

$$L_{ahull} = L_{artr} - TF_{mount} \qquad \#1$$

Table 1 - OTHEP Hull Acceleration Levels
in the Rotor Segment
(in dB re 10^{-3} cm/s^2)

Octave Band Center Frequency (Hz)

	31.5	63	125	250	500	1000	2000	4000	8000
HM	3	51	65	80	95	102	135	128	0
HFM	3	51	65	81	95	102	134	126	0
LFM	0	43	55	69	83	87	118	111	0

HM = Hard Mount HFM = High Frequency Isolation Mount
LFM = Low Frequency Isolation Mount

2.1.2.3 Stator Source Structureborne Noise

The stator configuration is similar to the rotor; however, there are some important differences. These differences lie chiefly in the path from the source to the sea. In the rotor, there is essentially only the mounting between the source and the panel which vibrates into the sea. With the stator, the vibrations must travel along hull structure before being radiated into the sea.

The stator qualifies as a Class III (over 10,000lbs) piece of machinery. The pressure hull structure to which the stator is mounted would qualify as a Type B foundation. Using the structureborne noise source levels in section B.2.1.1.2 and the machinery attachment transfer functions from section 4.3.2.1.1, the vibration levels at the stator's mounting to the pressure hull are calculated using the equation shown below.

$$L_{amount} = L_{astator} - TF_{mount} \qquad \#1$$

The stator is mounted directly to the pressure hull. Hence, no foundation transfer function is called for, $TF_{foundation}$ = 0dB. The most important path of the structureborne noise will be axially along the pressure hull to the hull envelope plating.

The path consists of a right angle from the stator mounting into the pressure hull plating. The pressure hull plating is followed for one frame spacing before the next intersection.--It continues through a "T"-junction at a

pressure hull frame before continuing for one frame spacing to a "Cross" junction. At this cross junction, a pressure hull frame lies radially inward and an MBT stiffener lies radially outward. The path makes a right angle turn into the stiffener and so continues to the hull envelope plating. All of the structure along this path is "wetted".

The transfer function for this path through the structure is calculated using the method described in section 4.3.2.1.3. The equation below shows the transfer function calculation for the path described above. The pressure hull plating will be taken as being one inch thick, the framing and stiffener at 0.75 inches thick.

$$TF_{structure} = 8 + \beta \cdot L_f + 6 + \beta \cdot L_f + 8 + \beta \cdot (R_{env} - R_{ph}) = 24.4 \quad dB \qquad \#2$$

For a dissipative loss coefficient of 0.3dB/ft, a frame spacing of 2.5ft, an envelope radius of 10ft, and a pressure hull radius of 7 feet, the entire structure transfer function becomes 24dB. This leads to the hull vibration levels at the aft end of the aft MBT shown in the table below.

Table 1 - OTHEP Hull Acceleration Levels
At Aft MBT Due to Stator Source
(in dB re 10^{-3} cm/s^2)

Octave Band Center Frequency (Hz)

	31.5	63	125	250	500	1000	2000	4000	8000
HM	-21	26	40	56	71	78	111	104	0
HFM	-21	26	40	57	71	78	110	102	0
LFM	-24	18	30	45	59	63	94	87	0

HM = Hard Mount HFM = High Frequency Isolation Mount
LFM = Low Frequency Isolation Mount

2.1.2.4 Turbine-Generator Structureborne Noise

From the arrangement drawing of the baseline design in Appendix A, the turbine-generator unit is seen to be mounted on a common foundation. In this configuration, all four of the machinery attachments discussed in section 4.3.2.1.1 could be used. Furthermore, the foundation is attached directly to the pressure hull. Hence, the vibration level at

the bottom of the foundation will be taken to be the hull vibration level. Therefore, no structure transfer function will be used, $TF_{structure}$ = 0dB.

The turbine-generator unit is taken to be a Class III machinery (over 10,000lbs). It will sit on a Type B foundation. To find the hull acceleration levels due to the turbine-generator unit, the mounting and foundation transfer functions are simply subtracted from the generator source level. This source level is the source level given in Table 2 of section B.2.1.1.4.

The table shown below represents the hull acceleration levels due to the turbine-generators.

Table 1 - OTHEP Hull Acceleration Levels
Due to Turbine Generator
(in dB re 10^{-3} cm/s^2)

Octave Band Center Frequency (Hz)

	31.5	63	125	250	500	1000	2000	4000	8000
HM	119	134	138	135	134	133	131	128	126
HFM	119	134	138	136	134	133	130	126	121
LFM	116	126	128	124	122	118	114	111	109
TSM	104	113	111	103	97	91	84	81	79

HM = Hard Mount HFM = High Frequency Isolation Mount
LFM = Low Frequency Isolation Mount TSM = Two-Stage Mount

2.1.2.5 Sea-Water Cooling/Lubrication Pump Structureborne Noise

From the arrangement drawing of the baseline design in Appendix A, the sea-water cooling/lubrication pump unit is seen to be mounted on a common foundation. In this configuration, all four of the machinery attachments discussed in section 4.3.2.1.1 could be used. Furthermore, the foundation is attached directly to the pressure hull. Hence, the vibration level at the bottom of the foundation will be taken to be the hull vibration level. Therefore, no structure transfer function will be used, $TF_{structure}$ = 0dB.

The sea-water cooling/lubrication pump unit is a Class II machinery (over 1000lbs and under 10,000lbs). It will sit on a Type B foundation. To find the hull acceleration levels due to the pump unit, the mounting and foundation transfer functions are simply subtracted from the sea-water cooling/lubrication pump unit structureborne source level. This source level is the source level given in Table 6 of section B.2.1.1.5.

The table shown below represents the hull acceleration levels due to the sea-water cooling/lubrication pump unit.

Table 1 - OTHEP Hull Acceleration Levels
Due to Sea-Water Cooling/Lubrication Pump Unit
(in dB re 10^{-3} cm/s^{2})

Octave Band Center Frequency (Hz)

	31.5	63	125	250	500	1000	2000	4000	8000
HM	99	106	116	112	112	111	105	105	102
HFM	99	106	115	111	109	108	101	100	97
LFM	96	97	102	94	92	91	85	85	82
TSM	86	83	87	77	72	68	60	60	57

HM = Hard Mount HFM = High Frequency Isolation Mount
LFM = Low Frequency Isolation Mount TSM = Two-Stage Mount

2.1.3 OTHEP Radiation

Now that all of the hull accelerations due to the equipment being studied have been calculated, the amount of acoustic energy radiated into the sea-water must be found. Hence, the transfer function developed in section 4.3.2.1.4 will be used. First, though, the coincidence frequency must be calculated.

Using equations 4.3.2.1.4.24 as shown below, the coincidence frequency and wavelength can be determined.

$$f_c=\frac{9300}{1.75\text{in.}}=5314\ Hz \qquad \lambda_c=0.529\cdot 1.75\text{in.}=0.93\ ft \qquad \#1$$

Based on this calculation, the octave bands whose center frequencies are 31.5, 63, 125, 250, 500, 1000, and 2000Hz will all be below coincidence and use the radiation efficiency given by equation 4.3.2.1.4.23. (P is taken to be 10ft, 4 x

2.5ft.) The octave band whose center frequency is 4000Hz will lie within the coincidence range and use the radiation efficiency given by equation 4.3.2.1.4.22. Lastly, the octave band whose center frequency is 8000Hz will lie above the coincidence range and use the radiation efficiency given by equation 4.3.2.1.4.21. Ten times the log of these radiation efficiencies are shown in the table below.

Table 1 - OTHEP Radiation Efficiencies
(in dB)

Octave Band Center Frequency (Hz)

31.5	63	125	250	500	1000	2000	4000	8000
-8	-9	-10	-11	-11	-10	-7	1	1

These values of ten times the log to the base ten of the radiation efficiency must be added to the remainder of the expression for the radiation transfer function, equation 4.3.2.1.4.20. All of the alternative propulsion systems have the same hull, hence, the area of a radiating panel will be the same throughout this comparative study. The potential change in the radiation transfer function comes in the number of panels excited by the different pieces of equipment and the different propulsion systems. In the case of the sound radiated by the OTHEP rotor, roughly 88 panels will be exicited. The resulting radiation transfer function is shown below.

Table 2 - OTHEP Rotor Segment
Radiation Transfer Function
(in dB)

Octave Band Center Frequency (Hz)

31.5	63	125	250	500	1000	2000	4000	8000
45	38	31	24	18	13	10	12	6

When this radiation transfer function is applied to the acceleration levels in the rotor segment, Table 1 in section B.2.1.2.2, the sound power level radiated by the rotor segment into the sea results. This is shown below.

Table 3 - OTHEP Rotor
Radiated Sound Power Levels
(in dB re 10^{-12} W)

Octave Band Center Frequency (Hz)

	31.5	63	125	250	500	1000	2000	4000	8000
HM	48	88	95	105	114	116	145	140	0
HFM	48	88	95	106	114	116	144	138	0
LFM	45	80	85	94	102	101	128	123	0

HM = Hard Mount HFM = High Frequency Isolation Mount
LFM = Low Frequency Isolation Mount

When determining the radiation transfer function for the stator structureborne noise, roughly 45 panels will radiate sound. When the resultant radiation transfer function is applied to the acceleration levels at the aft MBT, Table 1 in section B.2.1.2.3, the sound power levels radiated into the sea by stator structureborne noise result. These sound power levels are shown below.

Table 4 - OTHEP Stator
Radiated Sound Power Levels
(in dB re 10^{-12} W)

Octave Band Center Frequency (Hz)

	31.5	63	125	250	500	1000	2000	4000	8000
HM	21	61	68	77	86	88	118	113	0
HFM	21	61	68	78	86	88	117	111	0
LFM	18	53	58	66	74	73	101	96	0

HM = Hard Mount HFM = High Frequency Isolation Mount
LFM = Low Frequency Isolation Mount

When determining the radiation transfer function for the turbine-generator structureborne noise, roughly 69 panels will radiate sound. When the resultant radiation transfer function is applied to the acceleration levels arising from the turbine-generator vibrations, Table 1 in section B.2.1.2.4, the sound power levels radiated into the sea by the turbine-generator structureborne noise result. These sound power levels are shown below.

Table 5 - OTHEP Turbine-Generator
Radiated Sound Power Levels
(in dB re 10^{-12} W)

Octave Band Center Frequency (Hz)

	31.5	63	125	250	500	1000	2000	4000	8000
HM	163	171	168	158	152	146	140	139	131
HFM	163	171	168	159	152	146	139	137	126
LFM	160	163	158	147	140	131	123	122	114
TSM	148	150	141	126	115	104	93	92	84

HM = Hard Mount HFM = High Frequency Isolation Mount
LFM = Low Frequency Isolation Mount TSM = Two-Stage Mount

When determining the radiation transfer function for the sea-water cooling pump unit structureborne noise, roughly 17 panels will radiate sound. When the resultant radiation transfer function is applied to the acceleration levels arising from the sea-water cooling pump unit vibrations, Table 1 in section B.2.1.2.5, the sound power levels radiated into the sea by the sea-water cooling pump unit structureborne noise result. These sound power levels are shown below.

Table 6 - OTHEP Sea-Water Cooling Pump Unit
Radiated Sound Power Levels
(in dB re 10^{-12} W)

Octave Band Center Frequency (Hz)

	31.5	63	125	250	500	1000	2000	4000	8000
HM	136	137	139	129	124	118	108	110	101
HFM	136	137	138	128	121	115	104	105	96
LFM	133	128	125	111	104	98	88	90	81
TSM	123	114	110	94	84	75	63	65	56

HM = Hard Mount HFM = High Frequency Isolation Mount
LFM = Low Frequency Isolation Mount TSM = Two-Stage Mount

When determining the radiation transfer function for the airborne noise induced structureborne noise, roughly 314 panels will radiate sound. When the resultant radiation transfer function is applied to the acceleration levels arising from the airborne noise induced structural vibrations, Table 5 in

section B.2.1.2.1, the sound power levels radiated into the sea by the airborne noise induced structureborne noise result. These sound power levels are shown below.

Table 7 - OTHEP Airborne Noise-Excited
Radiated Sound Power Levels
(in dB re 10^{-12} W)

Octave Band Center Frequency (Hz)

31.5	63	125	250	500	1000	2000	4000	8000
105	104	102	102	99	97	96	97	93

HM = Hard Mount HFM = High Frequency Isolation Mount
LFM = Low Frequency Isolation Mount TSM = Two-Stage Mount

To find the total radiated sound power level, the "logarithmic sum" of all of the radiated sound power levels must be computed. When this is done, the total radiated sound power level for the OTHEP propulsion system is found. The total radiated sound power level is shown below.

Table 8 - OTHEP Total
Radiated Sound Power Level
(in dB re 10^{-12} W)

Octave Band Center Frequency (Hz)

	31.5	63	125	250	500	1000	2000	4000	8000
HM	166	174	171	161	155	149	147	144	134
HFM	166	174	171	162	155	149	146	142	129
LFM	163	166	161	159	143	134	130	127	117
TSM	151	153	144	129	118	108	128	123	94

HM = Hard Mount HFM = High Frequency Isolation Mount
LFM = Low Frequency Isolation Mount TSM = Two-Stage Mount

It is important to note that in this result, the stator and rotor of the propulsion motor are assumed to be mounted by only the first three means shown above. It does not seem possible to used two-stage mounting in the motor configuration that has been developed. This is not to say that it is impossible to use a two-stage mount, but, rather, without embarking on a feasibility study of such a mount, its use will be discounted.

One additional note, two turbine-generator units are included in the calculation of both the airborne noise level and the structureborne noise level.

2.2 Electric Drive With Conventional Propeller

2.2.1 Electric Drive Sources

Based on the description of the electric drive with conventional hub-to-diameter ratio propeller propulsion system in section 5.2.2, the sources listed below will cause the vibrations leading to radiated noise.

2.2.1.1 Propulsion Motor Source

In contrast with OTHEP, the propulsion motor is located within the pressure hull, inside the engine room. It is mounted on a foundation that sits on the pressure hull. The motor is connected to a rotating shaft.

The equation below shows the baseline airborne noise source level radiated by the electric drive propulsion motor. An AC motor is assumed to be the propulsion motor. Its speed is taken to be 120rpm. This equation is taken from equation 4.3.1.5.2.1.

$$L_{WBedMTR}=5+13\log(25{,}750HP)+15\log(120rpm)=93.5 \quad dB \ re \ 10^{-12}W \qquad \#1$$

The octave band adjustments to this baseline airborne source level are taken from Table 1 of section 4.3.1.5.2. The table shown below provides the octave band airborne source levels for the electric drive propulsion motor.

Table 1 - Electric Drive Propulsion Motor
Airborne Noise Source Levels
(in dB re 10^{-12} W)

Octave Band Center Frequency (Hz)

31.5	63	125	250	500	1000	2000	4000	8000
89	90	94	98	99	99	98	92	85

The structureborne noise source level for electric motors is taken from Table 2 of section 4.3.1.5.2. The table shown below provides the octave band structureborne source levels for the electric drive propulsion motor.

Table 2 - Electric Drive Propulsion Motor
Structureborne Noise Source Levels
(in dB re 10^{-3} cm/s^{2})

Octave Band Center Frequency (Hz)

31.5	63	125	250	500	1000	2000	4000	8000
92	92	92	92	92	92	92	92	92

2.2.1.2 Generator Steam Turbine Sources

The equation below shows the baseline airborne noise source level radiated by the steam turbines which drive the electric drive generators. This equation is taken from equation 4.3.1.3.1.

$$L_{WBedturb} = 60 + 10\log(27{,}000\,kW) = 104.3 \quad dB \ re \ 10^{-12} W \qquad \#1$$

There are two such 27MW turbine-generators in the plant. Hence, this source level applies to each turbine-generator. The octave band adjustments to this baseline airborne source level are taken from Table 1 of section 4.3.1.3. The table shown below provides the octave band airborne source levels for the electric drive turbines. Note, a static exciter is assumed for the generators. This is the same electrical generation plant as the OTHEP plant.

Table 1 - Electric Drive Turbine-Generator
Airborne Noise Source Levels
(in dB re 10^{-12} W)

Octave Band Center Frequency (Hz)

31.5	63	125	250	500	1000	2000	4000	8000
106	111	112	116	114	114	115	110	109

As discussed in section 4.3.1.3, the structureborne source level for the electric drive turbine-generators is dominated by the generator itself. See the following section.

2.2.1.3 Generator Sources

The equation below shows the baseline airborne noise source level radiated by the electric drive generators. This equation is taken from equation 4.3.1.5.1.1.

$$L_{WBedgen} = 34 + 10\log(27{,}000kW) + 7\log(3600rpm) = 103.2 \quad dB \ \ re \ \ 10^{-12}W \qquad \#1$$

The octave band adjustments to this baseline airborne source level are taken from Table 1 of section 4.3.1.5.1. The table shown below provides the octave band airborne source levels for the electric drive generators.

Table 1 - Electric Drive Generator
Airborne Noise Source Levels
(in dB re 10^{-12} W)

Octave Band Center Frequency (Hz)

31.5	63	125	250	500	1000	2000	4000	8000
111	114	115	116	116	113	111	108	103

The equation below shows the baseline structureborne noise source level radiated by the electric drive generators. This equation is taken from equation 4.3.1.5.1.2.

$$L_{aBedgen} = 42 + 10\log(27{,}000kW) + 7\log(3600rpm) = 111.2 \quad dB \ \ re \ \ 10^{-3}\frac{cm}{s^2} \qquad \#2$$

The octave band adjustments to this baseline structureborne source level are taken from Table 2 of section 4.3.1.5.1. The table shown below provides the octave band structureborne source levels for the electric drive generators.

Table 2 - Electric Drive Generator
Structureborne Noise Source Levels
(in dB re 10^{-3} cm/s^2)

Octave Band Center Frequency (Hz)

31.5	63	125	250	500	1000	2000	4000	8000
111	122	125	125	127	128	129	129	129

2.2.1.4 Propulsion Motor Cooling Water Pump

The equation below shows the baseline airborne noise source level radiated by the electric drive propulsion motor cooling water pump. This equation is taken from equation 4.3.1.4.1.

$$L_{WBedpmp} = 15 + 10\log(37.5HP) + 15\log(1200rpm) = 76.9 \quad dB \ \ re \ \ 10^{-12}W \qquad \#1$$

The octave band adjustments to this baseline airborne source level are taken from Table 1 of section 4.3.1.4. The table shown below provides the octave band airborne source levels for the electric drive propulsion motor cooling water pump. A centrifugal pump is assumed.

Table 1 - Electric Drive Propulsion Motor Cooling Water Pump
Airborne Noise Source Levels
(in dB re 10^{-12} W)

Octave Band Center Frequency (Hz)

31.5	63	125	250	500	1000	2000	4000	8000
102	102	103	103	104	106	103	100	95

The equation below shows the baseline structureborne noise source level radiated by the electric drive propulsion motor cooling water pump. This equation is taken from equation 4.3.1.4.2.

$$L_{aBedpmp} = 60 + 10\log(37.5HP) = 75.7 \quad dB \ \ re \ \ 10^{-3}\frac{cm}{s^2} \qquad \#2$$

The octave band adjustments to this baseline structureborne source level are taken from Table 2 of section 4.3.1.4. The table shown below provides the octave band structureborne source levels for the electric drive propulsion motor cooling water pump.

Table 2 - Electric Drive Propulsion Motor Cooling Water Pump
Structureborne Noise Source Levels
(in dB re 10^{-3} cm/s^{2})

Octave Band Center Frequency (Hz)

31.5	63	125	250	500	1000	2000	4000	8000
76	84	97	95	99	100	96	100	99

The equation below shows the baseline airborne noise source level radiated by the electric drive propulsion motor cooling water pump drive motor. An induction motor is assumed to be the pump's drive motor. This equation is taken from equation 4.3.1.5.2.1.

$$L_{WBedcwpdmtr} = 5 + 13\log(37.5HP) + 15\log(1200rpm) = 71.7 \quad dB \ \ re \ \ 10^{-12}W \qquad \#3$$

The octave band adjustments to this baseline airborne source level are taken from Table 1 of section 4.3.1.5.2. The table shown below provides the octave band airborne source levels for the electric drive propulsion motor cooling water pump drive motor.

Table 3 - Electric Drive Propulsion Motor
Cooling Water Pump Drive Motor
Airborne Noise Source Levels
(in dB re 10^{-12} W)

Octave Band Center Frequency (Hz)

31.5	63	125	250	500	1000	2000	4000	8000
67	68	72	76	77	77	76	70	63

The structureborne noise source level for electric motors are taken from Table 2 of section 4.3.1.5.2. The table shown below provides the octave band structureborne source levels for the electric propulsion motor cooling water pump drive motor.

Table 4 - Electric Drive Propulsion Motor
Cooling Water Pump Drive Motor
Structureborne Noise Source Levels
(in dB re 10^{-3} cm/s^2)

Octave Band Center Frequency (Hz)

31.5	63	125	250	500	1000	2000	4000	8000
92	92	92	92	92	92	92	92	92

Whereas the pump and its drive motor are essentially a single unit and will be mounted as a single unit, the source level of the entire unit will be the "logarithmic sum" of the source levels of the pump and its drive motor. The tables below show the airborne and structureborne noise source levels for the complete pump unit.

Table 5 - Electric Drive Propulsion Motor
Cooling Water Pump Unit
Airborne Noise Source Levels
(in dB re 10^{-12} W)

Octave Band Center Frequency (Hz)

31.5	63	125	250	500	1000	2000	4000	8000
102	102	103	103	104	106	103	100	95

Table 6 - Electric Drive Propulsion Motor
Cooling Water Pump Unit
Structureborne Noise Source Levels
(in dB re 10^{-3} cm/s^2)

Octave Band Center Frequency (Hz)

31.5	63	125	250	500	1000	2000	4000	8000
93	95	101	100	102	103	100	103	102

2.2.1.5 Propulsion Motor Lubrication Oil Pump

The equation below shows the baseline airborne noise source level radiated by the propulsion motor lubrication oil pump. This equation is taken from equation 4.3.1.4.1.

$$L_{WBedlopmp} = 15 + 10\log(7.4HP) + 15\log(1200rpm) = 69.9 \quad dB \ \ re \ \ 10^{-12}W \qquad \#1$$

The octave band adjustments to this baseline airborne source level are taken from Table 1 of section 4.3.1.4. The table shown below provides the octave band airborne source levels for the electric drive propulsion motor lubrication oil pump. A gear pump is assumed.

Table 1 - Electric Drive Propulsion Motor
Lubrication Oil Pump
Airborne Noise Source Levels
(in dB re 10^{-12} W)

Octave Band Center Frequency (Hz)

31.5	63	125	250	500	1000	2000	4000	8000
105	105	106	106	107	109	106	103	98

The equation below shows the baseline structureborne noise source level radiated by the electric drive propulsion motor lubrication oil pump. This equation is taken from equation 4.3.1.4.2.

$$L_{aBedlopmp} = 60 + 10\log(7.4HP) = 68.7 \quad dB \;\; re \;\; 10^{-3}\frac{cm}{s^2} \qquad \#2$$

The octave band adjustments to this baseline structureborne source level are taken from Table 2 of section 4.3.1.4. The table shown below provides the octave band structureborne source levels for the electric drive propulsion motor lubrication pump.

Table 2 - Electric Drive Propulsion Motor
Lubrication Oil Pump
Structureborne Noise Source Levels
(in dB re 10^{-3} cm/s^2)

Octave Band Center Frequency (Hz)

31.5	63	125	250	500	1000	2000	4000	8000
79	90	103	101	106	107	103	113	114

The equation below shows the baseline airborne noise source level radiated by the electric drive propulsion motor lubrication oil pump drive motor. An induction motor is assumed to be the pump's drive motor. This equation is taken from equation 4.3.1.5.2.1.

$$L_{WBedlopdmtr} = 5 + 13\log(7.4HP) + 15\log(1200rpm) = 62.5 \quad dB \;\; re \;\; 10^{-12}W \qquad \#3$$

The octave band adjustments to this baseline airborne source level are taken from Table 1 of section 4.3.1.5.2. The table shown below provides the octave band airborne source levels for the electric drive propulsion motor lubrication oil pump drive motor.

Table 3 - Electric Drive Propulsion Motor
Lubrication Oil Pump Drive Motor
Airborne Noise Source Levels
(in dB re 10^{-12} W)

Octave Band Center Frequency (Hz)

31.5	63	125	250	500	1000	2000	4000	8000
58	59	63	67	68	68	67	61	54

The structureborne noise source level for electric motors are taken from Table 2 of section 4.3.1.5.2. The table shown below provides the octave band structureborne source levels for the electric propulsion motor lubrication oil pump drive motor.

Table 4 - Electric Drive Propulsion Motor
Lubrication Oil Pump Drive Motor
Structureborne Noise Source Levels
(in dB re 10^{-3} cm/s^2)

Octave Band Center Frequency (Hz)

31.5	63	125	250	500	1000	2000	4000	8000
92	92	92	92	92	92	92	92	92

Whereas the pump and its drive motor are essentially a single unit and will be mounted as a single unit, the source level of the entire unit will be the "logarithmic sum" of the source levels of the pump and its drive motor. The tables below show the airborne and structureborne noise source levels for the complete pump unit.

Table 5 - Electric Drive Propulsion Motor
Lubrication Oil Pump Unit
Airborne Noise Source Levels
(in dB re 10^{-12} W)

Octave Band Center Frequency (Hz)

31.5	63	125	250	500	1000	2000	4000	8000
105	105	106	106	107	109	106	103	98

Table 6 - Electric Drive Propulsion Motor
Lubrication Oil Pump Unit
Structureborne Noise Source Levels
(in dB re 10^{-3} cm/s^2)

Octave Band Center Frequency (Hz)

31.5	63	125	250	500	1000	2000	4000	8000
94	97	105	103	107	108	105	114	114

2.2.2 Electric Drive Paths and Radiation

2.2.2.1 Airborne Noise-Excited Structureborne Noise

The airborne noise within the engineroom can excite vibrations in the hull. Hence, the sound pressure level within the engineroom must be computed. This requires two calculations. First, the "room constant" must be calculated in accordance with section 7.2.2 of reference [7]. Second, the sound pressure level within the space, due to the equipment operating within the space, must be calculated.

The room constant for the baseline submarine, OTHEP, will be the same for the electric drive variant and the geared-turbine drive variant. This is because the enginerooms are precisely the same. Based on the arrangement drawings of the baseline submarine and the methods of section 7.2.2 of reference [7], the room constant for the baseline submarine's main engineroom is shown in the table below. No acoustic damping materials are allowed in the comparative analysis.

Table 1 - Electric Drive Engineroom Room Constants - R
(in ft^2)

Octave Band Center Frequency (Hz)

31.5	63	125	250	500	1000	2000	4000	8000
1163	1300	1265	1060	1026	1060	1060	923	787

The next step is to calculate the reverberant sound pressure level in the space. Note, direct field sound pressure levels will not be computed. Only the reverberant field will be computed. To find the reverberant sound pressure level, the equation below must be used. The equation is taken from reference [7] section 7.2.2.

$$L_P = L_W - 10\log(R) + 16 \quad dB\ re\ 20\mu Pa \qquad \#1$$

In this expression, L_P represents the reverberant sound pressure level. L_W represents the sound power level resulting from the "logarithmic sum" of all of the airborne noise sources in the space. R represents the room constant. The table below shows the resultant sound power level due to the propulsion motor, turbines, generators and sea-water cooling/lubrication pump located in the electric drive submarine's engineroom.

Table 2 - Electric Drive Engineroom
Reverberant Sound Power Level
(in dB re 10^{-12}W)

Octave Band Center Frequency (Hz)

31.5	63	125	250	500	1000	2000	4000	8000
116	119	120	122	122	120	120	116	114

These values for L_W and the values for R in Table 1 are substituted into equation 1 to yield the sound pressure levels shown in the table below.

Table 3 - Electric Drive Engineroom
Reverberant Sound Pressure Levels
(in dB re 20 microPa)

Octave Band Center Frequency (Hz)

31.5	63	125	250	500	1000	2000	4000	8000
101	104	105	108	108	106	106	102	101

Knowing the reverberant sound pressure level, L_P, permits calculation of the structural vibrations excited by the airborne noise. First, though, the transfer function described in section 4.3.2.2 must be calculated. In this instance, the pressure hull is the structure being excited into vibration. Hence, it is a "wetted" structure.

The area of a panel is taken to be a square whose side equals the pressure hull frame spacing, 2.5ft in this case (Appendix A). Hence, the area of a panel, A_p, is $6.25ft^2$. The panel length to width ratio, a, is 1 in this case. Equation 4.3.2.2.3 provides the transfer function for wetted

steel using the panel characteristics listed here. The table below shows the transfer function. Note, this is the same as that of the baseline submarine, OTHEP.

Table 4 - Electric Drive Engineroom
Airborne-to-Structureborne Transfer Function (in dB)

Octave Band Center Frequency (Hz)

31.5	63	125	250	500	1000	2000	4000	8000
-47	-43	-39	-36	-32	-29	-26	-22	-19

From the reverberant sound pressure level and the transfer function, the airborne noise-excited structural vibration level can be calculated.

$$L_{aex} = L_p + TF \quad dB \ re \ 10^{-3}\frac{cm}{s^2} \qquad \#2$$

Using the relationship in equation 2, the table shown below is the acceleration level in the pressure hull due to airborne noise-excited vibrations.

Table 5 - Electric Drive Engineroom
Airborne Noise-Excited Structureborne Noise Levels
(in dB re 10^{-3}cm/s^{2})

Octave Band Center Frequency (Hz)

31.5	63	125	250	500	1000	2000	4000	8000
54	61	66	73	75	77	80	80	81

These structureborne noise levels must be included as if they were noise generated by a separate source.

When determining the radiation transfer function for the airborne noise-excited structureborne noise, roughly 314 panels will radiate sound. When the resultant radiation transfer function is applied to the acceleration levels arising from the airborne noise-excited vibrations, Table 5 above, the sound power levels radiated into the sea by the airborne noise-excited structureborne noise result. These sound power levels are shown below.

Table 6 - Electric Drive Airborne Noise-Excited
Structureborne Noise Radiated Sound Power Levels
(in dB re 10^{-12} W)

Octave Band Center Frequency (Hz)

31.5	63	125	250	500	1000	2000	4000	8000
105	104	102	102	99	96	96	97	93

2.2.2.2 Propulsion Motor Structureborne Noise

The propulsion motor qualifies as a Class III (over 10,000lbs) piece of machinery. The motor's foundation would certainly qualify as a Type B foundation. Using the structureborne noise source levels in section B.2.2.1.1, the machinery attachment transfer functions from section 4.3.2.1.1, the foundation transfer functions from section 4.3.2.1.2, and an appropriate radiation transfer function, the radiated sound power level for the electric drive propulsion motor can be computed.

When determining the radiation transfer function for the electric drive propulsion motor structureborne noise, roughly 88 panels will radiate sound. Using the resultant radiation transfer function yields the sound power levels radiated into the sea by the propulsion motor structureborne noise. These sound power levels are shown below.

Table 1 - Electric Drive Propulsion Motor
Radiated Sound Power Levels
(in dB re 10^{-12} W)

Octave Band Center Frequency (Hz)

	31.5	63	125	250	500	1000	2000	4000	8000
HM	145	142	136	126	117	110	104	103	95
HFM	145	142	136	127	117	110	103	101	90
LFM	142	134	126	115	105	95	87	86	78
TSM	130	121	109	94	80	68	57	56	48

HM = Hard Mount HFM = High Frequency Isolation Mount
LFM = Low Frequency Isolation Mount TSM = Two-Stage Mount

2.2.2.3 Turbine-Generator Structureborne Noise

From the arrangement drawing of the electric drive submarine design in section 5.2.2, the turbine-generator unit is seen to be mounted on a common foundation. In this configuration, all four of the machinery attachments discussed in section 4.3.2.1.1 could be used. Furthermore, the foundation is attached directly to the pressure hull. Hence, the vibration level at the bottom of the foundation will be taken to be the hull vibration level. Therefore, no structure transfer function will be used, $TF_{structure}$ = 0dB.

The turbine-generator unit is a Class III machinery (over 10,000lbs). It will sit on a Type B foundation. To find the hull acceleration levels due to the turbine-generator unit, the mounting and foundation transfer functions are simply subtracted from the generator source level. This source level is the source level given in Table 2 of section B.2.2.1.3.

Using the structureborne noise source levels in section B.2.2.1.3, the machinery attachment transfer functions from section 4.3.2.1.1, the foundation transfer functions from section 4.3.2.1.2, and the appropriate radiation transfer function, the radiated sound power level for the electric drive turbine-generator can be computed. Note, this is the same turbine-generator unit that is used in the OTHEP design.

When determining the radiation transfer function for the electric drive turbine-generator structureborne noise, roughly 69 panels will radiate sound. Using the resultant radiation transfer function yields the sound power levels radiated into the sea by the turbine-generator structureborne noise. These sound power levels are shown below.

Table 1 - Electric Drive Turbine-Generator
Radiated Sound Power Levels
(in dB re 10^{-12} W)

Octave Band Center Frequency (Hz)

	31.5	63	125	250	500	1000	2000	4000	8000
HM	163	171	168	158	152	146	140	139	131
HFM	163	171	168	159	152	146	139	137	126
LFM	160	163	158	147	140	131	123	122	114
TSM	148	150	141	126	115	104	93	92	84

HM = Hard Mount HFM = High Frequency Isolation Mount
LFM = Low Frequency Isolation Mount TSM = Two-Stage Mount

2.2.2.4 Propulsion Motor Cooling Water Pump Unit Structureborne Noise

From the arrangement drawing of the electric drive submarine design in section 5.2.2, the propulsion motor cooling water pump unit is seen to be mounted on a common foundation. In this configuration, all four of the machinery attachments discussed in section 4.3.2.1.1 could be used. Furthermore, the foundation is attached directly to the pressure hull. Hence, the vibration level at the bottom of the foundation will be taken to be the hull vibration level. Therefore, no structure transfer function will be used, $TF_{structure}$ = 0dB.

The cooling water pump unit is a Class II machinery (over 1000lbs and under 10,000lbs). It will sit on a Type B foundation. To find the hull acceleration levels due to the cooling water pump unit, the mounting and foundation transfer functions are simply subtracted from the cooling water pump unit source level. This source level is the source level given in Table 6 of section B.2.2.1.4.

Using the structureborne noise source levels in section B.2.2.1.4, the machinery attachment transfer functions from section 4.3.2.1.1, the foundation transfer functions from section 4.3.2.1.2, and the appropriate radiation transfer function, the radiated sound power level for the electric drive propulsion motor cooling water pump unit can be computed.

When determining the radiation transfer function for the electric drive propulsion motor cooling water pump unit structureborne noise, roughly 16 panels will radiate sound. Using the resultant radiation transfer function yields the sound power levels radiated into the sea by the propulsion motor cooling water pump unit structureborne noise. These sound power levels are shown below.

Table 1 - Electric Drive Propulsion Motor
Cooling Water Pump Unit
Radiated Sound Power Levels
(in dB re 10^{-12} W)

Octave Band Center Frequency (Hz)

	31.5	63	125	250	500	1000	2000	4000	8000
HM	135	134	134	124	118	112	103	104	96
HFM	135	134	133	123	115	109	99	99	91
LFM	132	125	120	106	98	92	83	84	76
TSM	122	111	105	89	78	69	58	59	51

HM = Hard Mount HFM = High Frequency Isolation Mount
LFM = Low Frequency Isolation Mount TSM = Two-Stage Mount

2.2.2.5 Propulsion Motor Lubrication Oil Pump Unit Structureborne Noise

From the arrangement drawing of the electric drive design in section 5.2.2, the lubrication oil pump unit is seen to be mounted on a common foundation. In this configuration, all four of the machinery attachments discussed in section 4.3.2.1.1 could be used. Furthermore, the foundation is attached directly to the pressure hull. Hence, the vibration level at the bottom of the foundation will be taken to be the hull vibration level. Therefore, no structure transfer function will be used, $TF_{structure}$ = 0dB.

The lubrication oil pump unit is a Class I machinery (under 1000lbs). It will sit on a Type B foundation. To find the hull acceleration levels due to the pump unit, the mounting and foundation transfer functions are simply subtracted from the propulsion motor lubrication oil pump unit structureborne source level. This source level is the source level given in Table 6 of section B.2.2.1.5.

Using the structureborne noise source levels in section B.2.2.1.5, the machinery attachment transfer functions from section 4.3.2.1.1, the foundation transfer functions from section 4.3.2.1.2, and the appropriate radiation transfer function, the radiated sound power level for the electric drive propulsion motor lubrication oil pump unit can be computed.

When determining the radiation transfer function for the electric drive propulsion motor lubrication oil pump unit structureborne noise, roughly 16 panels will radiate sound. Using the resultant radiation transfer function yields the sound power levels radiated into the sea by the propulsion motor lubrication oil pump unit structureborne noise. These sound power levels are shown below.

Table 1 - Electric Drive Propulsion Motor
Lubrication Oil Pump Unit
Radiated Sound Power Levels
(in dB re 10^{-12} W)

Octave Band Center Frequency (Hz)

	31.5	63	125	250	500	1000	2000	4000	8000
HM	131	133	136	127	122	116	107	114	107
HFM	131	132	135	125	118	107	98	105	98
LFM	124	118	114	103	98	92	83	90	83
TSM	119	110	104	88	78	72	63	70	63

HM = Hard Mount HFM = High Frequency Isolation Mount
LFM = Low Frequency Isolation Mount TSM = Two-Stage Mount

2.2.3 Electric Drive Total Radiated Sound Power Level

To find the total radiated sound power level, the "logarithmic sum" of all of the radiated sound power levels must be computed. When this is done, the total radiated sound power level for the electric drive propulsion system is found. The total radiated sound power level is shown below.

Table 1 - Electric Drive Total
Radiated Sound Power Level
(in dB re 10^{-12} W)

Octave Band Center Frequency (Hz)

	31.5	63	125	250	500	1000	2000	4000	8000
HM	166	174	171	161	155	149	143	142	134
HFM	166	174	171	162	155	149	142	140	129
LFM	163	166	161	150	143	134	126	125	117
TSM	151	153	144	129	118	107	99	99	94

HM = Hard Mount HFM = High Frequency Isolation Mount
LFM = Low Frequency Isolation Mount TSM = Two-Stage Mount

Of note, two turbine-generator units are included in the calculation of both the airborne noise level and the structureborne noise level.

2.3 Geared, Steam Turbine Drive

2.3.1 Geared Drive Sources

Based on the description of the geared, steam turbine drive with conventional hub-to-diameter ratio propeller propulsion system in section 5.2.3, the sources listed below will cause the vibrations leading to radiated noise.

2.3.1.1 Propulsion Steam Turbine

The table below shows the baseline airborne noise source level radiated by the propulsion steam turbines which drive the geared turbine drive's reduction gear, shaft, and, hence, propeller . These source levels are taken from Table 1 of section 4.3.1.1.

Table 1 - Geared Turbine Drive Propulsion Steam Turbine
Airborne Noise Source Levels
(in dB re 10^{-12} W)

Octave Band Center Frequency (Hz)

31.5	63	125	250	500	1000	2000	4000	8000
90	95	97	93	93	93	91	90	87

The structureborne noise source level for the propulsion steam turbine is dominated by the reduction gear to which it is attached, section 4.3.1.1. Hence, no structureborne noise source level will be developed for the propulsion steam turbine.

2.3.1.2 Reduction Gear

The equation below shows the baseline airborne noise source level radiated by the reduction gear which drives the geared turbine drive's shaft. This equation is taken from equation 4.3.1.2.1.

$$L_{WBrg} = 69 + 3.4\log(25{,}750HP) + 3.4\log(120rpm) = 91.1 \quad dB \ \ re \ \ 10^{-12}W \qquad \#1$$

The octave band adjustments to this baseline airborne source level are taken from Table 1 of section 4.3.1.2. The table shown below provides the octave band airborne source levels for the geared turbine drive reduction gear.

Table 1 - Geared Turbine Drive Reduction Gear
Airborne Noise Source Levels
(in dB re 10^{-12} W)

Octave Band Center Frequency (Hz)

31.5	63	125	250	500	1000	2000	4000	8000
99	100	101	103	105	106	107	103	91

The equation below shows the baseline structureborne noise source level radiated by the geared turbine drive reduction gear. This equation is taken from equation 4.3.1.2.2.

$$L_{aBrg} = 47 + 10\log(25{,}750HP) = 91.1 \quad dB \ \ re \ \ 10^{-3}\frac{cm}{s^2} \qquad \#2$$

The octave band adjustments to this baseline structureborne source level are taken from Table 2 of section 4.3.1.2. The table shown below provides the octave band structureborne source levels for the geared turbine drive reduction gear.

Table 2 - Geared Turbine Drive Reduction Gear
Structureborne Noise Source Levels
(in dB re 10^{-3} cm/s^{2})

Octave Band Center Frequency (Hz)

31.5	63	125	250	500	1000	2000	4000	8000
91	100	94	99	114	124	124	119	109

2.3.1.3 Turbine-Generator Source Level

The equation below shows the baseline airborne noise source level radiated by the steam turbines which drive the geared turbine drive ship's service generators. This equation is taken from equation 4.3.1.3.1.

$$L_{WBgtturb} = 60 + 10\log(1100kW) = 90.4 \quad dB \ re \ 10^{-12} W \qquad \#1$$

There are two such 1.1MW turbine-generators in the plant. Hence, this source level applies to each turbine-generator. The octave band adjustments to this baseline airborne source level are taken from Table 1 of section 4.3.1.3. The table shown below provides the octave band airborne source levels for the geared turbine drive ship's service turbine-generator turbines. Note, a static exciter is assumed for the generators.

Table 1 - Geared Turbine Drive Turbine-Generator
Airborne Noise Source Levels
(in dB re 10^{-12} W)

Octave Band Center Frequency (Hz)

31.5	63	125	250	500	1000	2000	4000	8000
92	97	98	102	100	100	101	96	95

As discussed in section 4.3.1.3, the structureborne source level for the geared turbine drive ship's service turbine generators is dominated by the generator itself. See the following section.

2.3.1.4 Turbine-Generator Generator Source Levels

The equation below shows the baseline airborne noise source level radiated by the geared turbine drive ship's service generators. This equation is taken from equation 4.3.1.5.1.1.

$$L_{WBgtgen} = 34 + 10\log(1100kW) + 7\log(3600rpm) = 89.3 \quad dB \;\; re \;\; 10^{-12}W \qquad \#1$$

The octave band adjustments to this baseline airborne source level are taken from Table 1 of section 4.3.1.5.1. The table shown below provides the octave band airborne source levels for the geared turbine drive ship's service generators.

Table 1 - Geared Turbine Drive Ship's Service Generator
Airborne Noise Source Levels
(in dB re 10^{-12} W)

Octave Band Center Frequency (Hz)

31.5	63	125	250	500	1000	2000	4000	8000
97	100	101	102	102	99	97	94	89

The equation below shows the baseline structureborne noise source level radiated by the geared turbine drive ship's service generators. This equation is taken from equation 4.3.1.5.1.2.

$$L_{aBgtgen} = 42 + 10\log(1100kW) + 7\log(3600rpm) = 97.3 \quad dB \;\; re \;\; 10^{-3}\frac{cm}{s^2} \qquad \#2$$

The octave band adjustments to this baseline structureborne source level are taken from Table 2 of section 4.3.1.5.1. The table shown below provides the octave band structureborne source levels for the geared turbine drive ship's service generators.

Table 2 - Geared Turbine Drive Ship's Service Generator
Structureborne Noise Source Levels
(in dB re 10^{-3} cm/s^2)

Octave Band Center Frequency (Hz)

31.5	63	125	250	500	1000	2000	4000	8000
97	108	111	111	113	114	115	115	115

2.3.1.5 Reduction Gear Lubrication Oil Pump

The equation below shows the baseline airborne noise source level radiated by the geared turbine drive reduction gear lubrication oil pump. This equation is taken from equation 4.3.1.4.1.

$$L_{WBrglopmp} = 15 + 10\log(14.8HP) + 15\log(1200rpm) = 72.9 \quad dB \ re \ 10^{-12}W \qquad \#1$$

The octave band adjustments to this baseline airborne source level are taken from Table 1 of section 4.3.1.4. The table shown below provides the octave band airborne noise source levels for the geared turbine drive reduction gear lubrication oil pump. A gear pump is assumed.

Table 1 - Geared Turbine Drive Reduction Gear
Lubrication Oil Pump
Airborne Noise Source Levels
(in dB re 10^{-12} W)

Octave Band Center Frequency (Hz)

31.5	63	125	250	500	1000	2000	4000	8000
108	108	109	109	110	112	109	106	101

The equation below shows the baseline structureborne noise source level radiated by the geared turbine drive reduction gear lubrication oil pump. This equation is taken from equation 4.3.1.4.2.

$$L_{aBrglopmp} = 60 + 10\log(14.8HP) = 71.7 \quad dB \ re \ 10^{-3}\frac{cm}{s^2} \qquad \#2$$

The octave band adjustments to this baseline structureborne source level are taken from Table 2 of section 4.3.1.4. The table shown below provides the octave band structureborne source levels for the geared turbine drive reduction gear lubrication oil pump.

Table 2 - Geared Turbine Drive Reduction Gear
Lubrication Oil Pump
Structureborne Noise Source Levels
(in dB re 10^{-3} cm/s^2)

Octave Band Center Frequency (Hz)

31.5	63	125	250	500	1000	2000	4000	8000
82	93	106	104	109	110	106	116	117

The equation below shows the baseline airborne noise source level radiated by the geared turbine drive reduction gear lubrication oil pump drive motor. An induction motor is assumed to be the pump's drive motor. This equation is taken from equation 4.3.1.5.2.1.

$$L_{WBrglopdmtr} = 5 + 13\log(14.8HP) + 15\log(1200rpm) = 66.4 \quad dB\ re\ 10^{-12}W \qquad \#3$$

The octave band adjustments to this baseline airborne source level are taken from Table 1 of section 4.3.1.5.2. The table shown below provides the octave band airborne source levels for the geared turbine drive reduction gear lubrication oil pump drive motor.

Table 3 - Geared Turbine Drive Reduction Gear
Lubrication Oil Pump Drive Motor
Airborne Noise Source Levels
(in dB re 10^{-12} W)

Octave Band Center Frequency (Hz)

31.5	63	125	250	500	1000	2000	4000	8000
61	62	66	70	71	71	70	64	57

The structureborne noise source level for electric motors are taken from Table 2 of section 4.3.1.5.2. The table shown below provides the octave band structureborne source levels for the geared turbine drive reduction gear lubrication oil pump drive motor.

Table 4 - Geared Turbine Drive Reduction Gear
Lubrication Oil Pump Drive Motor
Structureborne Noise Source Levels
(in dB re 10^{-3} cm/s^2)

Octave Band Center Frequency (Hz)

31.5	63	125	250	500	1000	2000	4000	8000
92	92	92	92	92	92	92	92	92

Whereas the pump and its drive motor are essentially a single unit and will be mounted as a single unit, the source level of the entire unit will be the "logarithmic sum" of the source levels of the pump and its drive motor. The tables below show the airborne and structureborne noise source levels for the complete pump unit.

Table 5 - Geared Turbine Drive Reduction Gear
Lubrication Oil Pump Unit
Airborne Noise Source Levels
(in dB re 10^{-12} W)

Octave Band Center Frequency (Hz)

31.5	63	125	250	500	1000	2000	4000	8000
108	108	109	109	110	112	109	106	101

Table 6 - Geared Turbine Drive Reduction Gear
Lubrication Oil Pump Unit
Structureborne Noise Source Levels
(in dB re 10^{-3} cm/s^2)

Octave Band Center Frequency (Hz)

31.5	63	125	250	500	1000	2000	4000	8000
94	98	107	106	110	111	107	116	117

2.3.2 Geared Turbine Drive Paths and Radiation

2.3.2.1 Airborne Noise-Excited Structureborne Noise

The airborne noise within the engineroom can excite vibrations in the hull. Hence, the sound pressure level within the engineroom must be computed. This requires two calculations. First, the "room constant" must be calculated

in accordance with section 7.2.2 of reference [7]. Second, the sound pressure level within the space, due to the equipment operating within the space, must be calculated.

The room constant for the baseline submarine, OTHEP, will be the same as the electric drive variant and the geared-turbine drive variant. This is because the enginerooms are precisely the same. Based on the arrangement drawings of the baseline submarine and the methods of section 7.2.2 of reference [7], the room constant for the baseline submarine's main engineroom is shown in the table below. No acoustic damping materials are allowed in the comparative analysis.

Table 1 - Geared Turbine Drive Engineroom Room Constants - R (in ft^2)

Octave Band Center Frequency (Hz)

31.5	63	125	250	500	1000	2000	4000	8000
1163	1300	1265	1060	1026	1060	1060	923	787

The next step is to calculate the reverberant sound pressure level in the space. Note, direct field sound pressure levels will not be computed. Only the reverberant field will be computed. To find the reverberant sound pressure level, the equation below must be used. The equation is taken from reference [7] section 7.2.2.

$$L_p = L_W - 10\log(R) + 16 \quad dB\ re\ 20\mu Pa \qquad \#1$$

In this expression, L_P represents the reverberant sound pressure level. L_W represents the sound power level resulting from the "logarithmic sum" of all of the airborne noise sources in the space. R represents the room constant. The table below shows the resultant sound power level due to the propulsion steam turbine, reduction gear, turbines, generators and reduction gear lubrication oil pump located in the geared turbine drive submarine's engineroom.

Table 2 - Geared Turbine Drive Engineroom
Reverberant Sound Power Level
(in dB re $10^{-12}W$)

Octave Band Center Frequency (Hz)

31.5	63	125	250	500	1000	2000	4000	8000
109	110	111	112	113	114	112	109	104

These values for L_w and the values for R in Table 1 are substituted into equation 1 to yield the sound pressure levels shown in the table below.

Table 3 - Geared Turbine Drive Engineroom
Reverberant Sound Pressure Levels
(in dB re 20 microPa)

Octave Band Center Frequency (Hz)

31.5	63	125	250	500	1000	2000	4000	8000
95	95	96	98	99	100	98	95	91

Knowing the reverberant sound pressure level, L_p, permits calculation of the structural vibrations excited by the airborne noise. First, though, the transfer function described in section 4.3.2.2 must be calculated. In this instance, the pressure hull is the structure being excited into vibration. Hence, it is a "wetted" structure.

The area of a panel is taken to be a square whose side equals the pressure hull frame spacing, 2.5ft in this case (Appendix A). Hence, the area of a panel, A_p, is 6.25ft^2. The panel length to width ratio, a, is 1 in this case. Equation 4.3.2.2.3 provides the transfer function for wetted steel using the panel characteristics listed here. The table below shows the transfer function. Note, this is the same as that of the baseline submarine, OTHEP.

Table 4 - Geared Turbine Drive Engineroom
Airborne-to-Structureborne Transfer Function (in dB)

Octave Band Center Frequency (Hz)

31.5	63	125	250	500	1000	2000	4000	8000
-47	-43	-39	-36	-32	-29	-26	-22	-19

From the reverberant sound pressure level and the transfer function, the airborne noise-excited structural vibration level can be calculated.

$$L_{aex}=L_p+TF \quad dB \ re \ 10^{-3}\frac{cm}{s^2} \qquad \#2$$

Using the relationship in equation 2, the table shown below is the acceleration level in the pressure hull due to airborne noise-excited vibrations.

Table 5 - Geared Turbine Drive Engineroom
Airborne Noise-Excited Structureborne Noise Levels
(in dB re 10^{-3}cm/s^{2})

Octave Band Center Frequency (Hz)

31.5	63	125	250	500	1000	2000	4000	8000
48	52	57	62	66	71	73	73	72

These structureborne noise levels must be included as if they were noise generated by a separate source.

When determining the radiation transfer function for the airborne noise-excited structureborne noise, roughly 314 panels will radiate sound into the sea. When the resultant radiation transfer function is applied to the acceleration levels arising from the airborne noise-excited vibrations, Table 5 above, the sound power levels radiated into the sea by the airborne noise-excited structureborne noise result. These sound power levels are shown below.

Table 6 – Geared Turbine Drive Airborne Noise-Excited
Structureborne Noise Radiated Sound Power Levels
(in dB re 10^{-12} W)

Octave Band Center Frequency (Hz)

31.5	63	125	250	500	1000	2000	4000	8000
98	95	93	92	90	90	88	90	83

2.3.2.2 Reduction Gear Structureborne Noise

The reduction gear qualifies as a Class III (over 10,000lbs) piece of machinery. The reduction gear's foundation would certainly qualify as a Type B foundation. Using the structureborne noise source levels in section B.2.3.1.2, the machinery attachment transfer functions from section 4.3.2.1.1, the foundation transfer functions from section 4.3.2.1.2, and an appropriate radiation transfer function, the radiated sound power level for the electric drive propulsion motor can be computed.

When determining the radiation transfer function for the electric drive propulsion motor structureborne noise, roughly 88 panels will radiate sound. Using the resultant radiation transfer function yields the sound power levels radiated into the sea by the reduction gear structureborne noise. These sound power levels are shown below.

Table 1 – Geared Turbine Drive Reduction Gear
Radiated Sound Power Levels
(in dB re 10^{-12} W)

Octave Band Center Frequency (Hz)

	31.5	63	125	250	500	1000	2000	4000	8000
HM	144	150	138	133	140	143	136	130	112
HFM	144	150	138	134	140	143	135	128	107
LFM	141	142	128	122	128	128	119	113	95
TSM	129	129	111	101	103	101	89	83	65

HM = Hard Mount HFM = High Frequency Isolation Mount
LFM = Low Frequency Isolation Mount TSM = Two-Stage Mount

2.3.2.3 Turbine-Generator Structureborne Noise

From the arrangement drawing of the electric drive submarine design in section 5.2.3, the turbine-generator unit is seen to be mounted on a common foundation. In this configuration, all four of the machinery attachments discussed in section 4.3.2.1.1 could be used. Furthermore, the foundation is attached directly to the pressure hull. Hence, the vibration level at the bottom of the foundation will be taken to be the hull vibration level. Therefore, no structure transfer function will be used, $TF_{structure}$ = 0dB.

The turbine-generator unit is a Class III machinery (over 10,000lbs). It will sit on a Type B foundation. To find the hull acceleration levels due to the turbine-generator unit, the mounting and foundation transfer functions are simply subtracted from the generator source level. This source level is the source level given in Table 2 of section B.2.3.1.4.

Using the structureborne noise source levels in section B.2.3.1.4, the machinery attachment transfer functions from section 4.3.2.1.1, the foundation transfer functions from section 4.3.2.1.2, and the appropriate radiation transfer function, the radiated sound power level for the geared turbine drive turbine-generator can be computed. Note, this is the same turbine-generator unit that is used in the OTHEP design.

When determining the radiation transfer function for the geared turbine drive turbine-generator structureborne noise, roughly 69 panels will radiate sound. Using the resultant radiation transfer function yields the sound power levels radiated into the sea by the turbine-generator structureborne noise. These sound power levels are shown below.

Table 1 - Geared Turbine Drive Turbine-Generator
Radiated Sound Power Levels
(in dB re 10^{-12} W)

Octave Band Center Frequency (Hz)

	31.5	63	125	250	500	1000	2000	4000	8000
HM	149	157	154	145	138	132	126	125	118
HFM	149	157	154	146	138	132	125	123	113
LFM	146	149	144	134	126	117	109	108	101
TSM	134	136	127	113	101	90	79	78	71

HM = Hard Mount HFM = High Frequency Isolation Mount
LFM = Low Frequency Isolation Mount TSM = Two-Stage Mount

2.3.2.4 Reduction Gear Lubrication Oil Pump Unit Structure-borne Noise

From the arrangement drawing of the geared turbine submarine design in section 5.2.3, the lubrication oil pump unit is seen to be mounted on a common foundation. In this configuration, all four of the machinery attachments discussed in section 4.3.2.1.1 could be used. Furthermore, the foundation is attached directly to the pressure hull. Hence, the vibration level at the bottom of the foundation will be taken to be the hull vibration level. Therefore, no structure transfer function will be used, $TF_{structure}$ = 0dB.

The lubrication oil pump unit is a Class II machinery (over 1000lbs under 10,000lbs). It will sit on a Type B foundation. To find the hull acceleration levels due to the pump unit, the mounting and foundation transfer functions are simply subtracted from the reduction gear lubrication oil pump unit structureborne source level. This source level is the source level given in Table 6 of section B.2.3.1.5.

Using the structureborne noise source levels in section B.2.3.1.5, the machinery attachment transfer functions from section 4.3.2.1.1, the foundation transfer functions from section 4.3.2.1.2, and the appropriate radiation transfer function, the radiated sound power level for the geared turbine drive reduction gear lubrication oil pump unit can be computed.

When determining the radiation transfer function for the geared turbine drive reduction gear lubrication oil pump unit structureborne noise, roughly 16 panels will radiate sound. Using the resultant radiation transfer function yields the sound power levels radiated into the sea by the reduction gear lubrication oil pump unit structureborne noise. These sound power levels are shown below.

Table 1 - Geared Turbine Drive Reduction Gear
Lubrication Oil Pump Unit
Radiated Sound Power Levels
(in dB re 10^{-12} W)

Octave Band Center Frequency (Hz)

	31.5	63	125	250	500	1000	2000	4000	8000
HM	136	138	141	131	126	120	110	117	111
HFM	136	138	140	130	123	117	106	112	106
LFM	133	129	128	113	106	100	90	97	91
TSM	123	115	112	96	86	77	65	72	66

HM = Hard Mount HFM = High Frequency Isolation Mount
LFM = Low Frequency Isolation Mount TSM = Two-Stage Mount

2.3.3 Geared Turbine Drive Total Radiated Sound Power Level

To find the total radiated sound power level, the "logarithmic sum" of all of the radiated sound power levels must be computed. When this is done, the total radiated sound power level for the geared turbine drive propulsion system is found. The total radiated sound power level is shown below.

Table 1 - Geared Turbine Drive Total
Radiated Sound Power Level
(in dB re 10^{-12} W)

Octave Band Center Frequency (Hz)

	31.5	63	125	250	500	1000	2000	4000	8000
HM	153	160	157	148	143	143	137	132	122
HFM	153	160	157	149	143	143	136	130	117
LFM	150	152	147	137	131	128	120	115	104
TSM	138	139	130	116	106	101	92	91	84

HM = Hard Mount HFM = High Frequency Isolation Mount
LFM = Low Frequency Isolation Mount TSM = Two-Stage Mount

Of note, two turbine-generator units are included in the calculation of both the airborne noise level and the structureborne noise level.

614-583

Thesis
A43855 Amy
c.1 Outside the Hull Electric Propulsion for a submarine.

Thesis
A43855 Amy
c.1 Outside the Hull Electric Propulsion for a submarine.

thesA43855
Outside the Hull Electric Propulsion for
3 2768 000 89148 5
DUDLEY KNOX LIBRARY